Lecture Notes in Electrical Engineering 1041

Suryanarayana Doolla
Zakir Hussain Rather
Venkatasailanathan Ramadesigan *Editors*

Advances in Renewable Energy and Its Grid Integration

Proceedings of ICAER 2022

Springer

Lecture Notes in Electrical Engineering

Volume 1041

The book series *Lecture Notes in Electrical Engineering* (LNEE) publishes the latest developments in Electrical Engineering—quickly, informally and in high quality. While original research reported in proceedings and monographs has traditionally formed the core of LNEE, we also encourage authors to submit books devoted to supporting student education and professional training in the various fields and applications areas of electrical engineering. The series cover classical and emerging topics concerning:

- Communication Engineering, Information Theory and Networks
- Electronics Engineering and Microelectronics
- Signal, Image and Speech Processing
- Wireless and Mobile Communication
- Circuits and Systems
- Energy Systems, Power Electronics and Electrical Machines
- Electro-optical Engineering
- Instrumentation Engineering
- Avionics Engineering
- Control Systems
- Internet-of-Things and Cybersecurity
- Biomedical Devices, MEMS and NEMS

For general information about this book series, comments or suggestions, please contact leontina.dicecco@springer.com.

To submit a proposal or request further information, please contact the Publishing Editor in your country:

China

Jasmine Dou, Editor (jasmine.dou@springer.com)

India, Japan, Rest of Asia

Swati Meherishi, Editorial Director (Swati.Meherishi@springer.com)

Southeast Asia, Australia, New Zealand

Ramesh Nath Premnath, Editor (ramesh.premnath@springernature.com)

USA, Canada

Michael Luby, Senior Editor (michael.luby@springer.com)

All other Countries

Leontina Di Cecco, Senior Editor (leontina.dicecco@springer.com)

**** This series is indexed by EI Compendex and Scopus databases. ****

Suryanarayana Doolla · Zakir Hussain Rather ·
Venkatasailanathan Ramadesigan
Editors

Advances in Renewable Energy and Its Grid Integration

Proceedings of ICAER 2022

Springer

Editors
Suryanarayana Doolla
Department of Energy Science
and Engineering
Indian Institute of Technology Bombay
Mumbai, Maharashtra, India

Zakir Hussain Rather
Department of Energy Science
and Engineering
Indian Institute of Technology Bombay
Mumbai, Maharashtra, India

Venkatasailanathan Ramadesigan
Department of Energy Science
and Engineering
Indian Institute of Technology Bombay
Mumbai, Maharashtra, India

ISSN 1876-1100 ISSN 1876-1119 (electronic)
Lecture Notes in Electrical Engineering
ISBN 978-981-99-2282-6 ISBN 978-981-99-2283-3 (eBook)
https://doi.org/10.1007/978-981-99-2283-3

This Springer imprint is published by the registered company Springer Nature Singapore Pte Ltd.
The registered company address is: 152 Beach Road, #21-01/04 Gateway East, Singapore 189721, Singapore

Preface I

The Department of Energy Science and Engineering (DESE) at IIT Bombay is a leading interdisciplinary energy education and research center. DESE has developed several novel education programs focusing on the application of science and engineering to problems in energy. Keeping the vision of the department "To develop sustainable energy systems and solution for the future" in mind, there is a strong need of providing a common platform to the researchers in the field of energy and allied domains. DESE has been organizing the biennial conference International Conference on Advances in Energy Research since 2007 which serves as an excellent forum to present new findings, exchange novel ideas, discuss new developments, and reflect on the challenges that lie ahead.

This book is a compendium of all the papers of the submissions accepted at the 8th International Conference on Advances in Energy Research (ICAER 2022), organized from July 7 to 9, 2022. After a rigorous peer-review process, about 97 papers have been accepted for the proceedings of the conference.

Various aspects of energy research including, but not limited to, conventional energy, renewable energy, grid integration of renewables, electric mobility, energy storage, energy policy and economics, and energy education were covered in the conference. This conference threw light on various recent accomplishments by researchers worldwide in the areas of solar thermal, thermal storage, solar PV with new materials, novel batteries, biofuels-based transportation, and rural energy needs, to name a few. The conference also included a special session on "Industry innovations in energy" where leading experts from industry were invited to present innovative case studies from their respective industries.

Mumbai, India

Prof. Suryanarayana Doolla
Prof. Zakir Hussain Rather
Prof. Venkatasailanathan Ramadesigan

Preface II

The 8th International Conference on Advances in Energy Research (ICAER 2022) was organized by the Department of Energy Science and Engineering, Indian Institute of Technology Bombay, between July 7 and 9, 2022, virtually in Mumbai, India. The conference received around 250 submissions. Of these, around 120 submissions were accepted for oral presentation after a rigorous peer-review. The conference was attended by over 300 participants. This book is a compendium of selected papers presented at the conference. The Springer Nature Publications sponsored three best paper awards and seven consolation prizes. The conference hosted 10 invited lectures and presentations by academics and industry personnel from all over the world. Two special sessions on "Industry innovations in energy" and "Energy education" were also organized.

Mumbai, India

Prof. Zakir Hussain Rather
Prof. Suryanarayana Doolla
Prof. Venkatasailanathan Ramadesigan

Acknowledgments We would like to sincerely thank Indian Institute of Technology Bombay for organizing the 8th edition of International Conference on Advances in Energy Research (ICAER 2022) in the Department of Energy Science and Engineering. We would also like to thank Prof. Suneet Singh (Head of the Department) for his constant support and valuable suggestions in organizing this conference. We would also like to thank all the invited speakers, delegates, sponsors, the members of the organizing and advisory committee, and most importantly the student organizing committee, student volunteers, and staff of the Department of Energy Science and Engineering for their dedicated efforts in organizing this conference.

Contents

About the Editors

Suryanarayana Doolla is currently a professor at the Indian Institute of Technology Bombay, where he teaches and directs research in power electronics and power systems as a faculty member of the Energy Science and Engineering Department. He received the B.Tech. degree in electrical engineering from the Nagarjuna University in 2000, M.Tech. degree in Energy Systems Engineering from IIT Bombay, and Ph.D. degrees in Power Systems from IIT Delhi, India, in 2002 and 2007, respectively. He was with Power Research and Development Consultants (2009), Bangalore, and Machine 2 Machine (2006–2008), Hyderabad, before joining IIT Bombay.

Dr. Zakir Hussain Rather is an electrical engineer by training, with Ph.D. from Aalborg University, Denmark. He has been working in renewable energy (RE) and electric mobility sector for past 12 years, with around 4 years of RE industry experience in Europe. He, in close collaboration with the Danish National transmission system operator, Energinet.dk, has extensively worked on the Danish grid. He is currently working as an associate professor with the Department of Energy Science and Engineering, Indian Institute of Technology (IIT) Bombay, where the focus of his work continues to be on grid integration of renewables, grid integration of Electric Vehicles (EVs), power system operation under high penetration of renewable generation and EVs. He is an editor of *IEEE Transactions on Sustainable Energy*, editor of *IETE Technical Review*, guest editor of *International Journal of Power and Energy Systems*, and a senior member of IEEE, IEEE Power and Energy Society, IEEE Smart Grid Community, IEEE Industrial Electronics Society, and Danish Smart Grid Research Forum. He is also involved in various BIS committees on EV charging infrastructure. His areas of research interest include grid and system integration of wind and solar power, power system dynamics, EV charging infrastructure and EV grid integration, smart and micro-grids, and WAMPACS.

He is the recipient of 'IREDA-NIWE Award for Best Research Work in Wind Energy'. He is a registered expert in Joint Research Centre (JRC) European Commission. He is also the recipient of Young Faculty Award, IIT Bombay, and several best paper and industry awards.

Venkatasailanathan Ramadesigan is an associate professor in the Department of Energy Science and Engineering at the Indian Institute of Technology Bombay. He received his B.Tech. in Chemical and Electrochemical engineering from the Central Electrochemical Research Institute (CECRI), Tamil Nadu, and obtained his M.S. in Chemical Engineering at the University of South Carolina, Columbia, USA. He received his Ph.D. in Energy, Environmental and Chemical Engineering at Washington University in St. Louis, Missouri, USA. His research interests broadly include modelling and simulation of electrochemical energy storage and conversion systems, nonlinear parameter estimation, model-based optimization and design, advanced battery management systems, system integration, and large-scale energy storage. His current research involves modelling, simulation and optimization of lithium-ion and other metal-ion batteries, redox flow batteries, fuel cells, modelling and control of hybrid renewable energy-battery systems, advanced battery management systems, and battery recycling.

Smart Algorithm for Optimal Energy Utilization in EV Charging Stations

Yashodhan Jaltare, Sakshi Kulkarni, Sumeet Gawande, and Meera Murali

1 Introduction

The growing number of electric vehicles poses a challenge to existing infrastructure. Undersized connection lines and a lack of charging stations raise the concern of satisfying EV charging demands which leads to the approach of coordinated or "smart" charging. In other words, our aim is to introduce an algorithm that helps us decide which electric vehicle can charge at which charging station and at which current during which time periods. Flexibility in planning arises from the length of stay, the available electrical supply cost of the units, and the mode of charging (conventional or fast).

We present a smart charging algorithm that schedules electric vehicles to maximize revenue and coordinates electric vehicle charging to reduce load peaks and maximize infrastructure usage. The algorithm uses input parameters of the desired SoC, the duration of charging, and the mode of charging. With this information the model calculates and allocates the charging load for each time interval, with the primary objective of reducing cost per EV charge. We compare the smart charging scenario to a naive charging scenario to evaluate the potential of smart charging. The algorithm we present has the following benefits: Maximum use of existing infrastructure, Fair share maximization, Profit maximization, Integrated mode of charging.

2 Literature Survey

Grid-orientated smart charging involves scheduling the power supplied to electric vehicles based on the state of charge (SoC) in that instance and the time left to charge.

Y. Jaltare (✉) · S. Kulkarni · S. Gawande · M. Murali
College of Engineering, Pune, Wellesley Road, Shivajinagar, Pune, Maharashtra 411005, India
e-mail: jaltareyr18.elec@coep.ac.in
URL: https://www.coep.org.in/

S. Doolla et al. (eds.), *Advances in Renewable Energy and Its Grid Integration*,
Lecture Notes in Electrical Engineering 1041,
https://doi.org/10.1007/978-981-99-2283-3_1

It ensures that the parametric constraints of the power capacity of the EVCS and the individual EV are not violated and allows for an efficacious distribution of charging capacity amongst the EV. This is particularly beneficial when multiple heterogeneous electric vehicles that have different charging times are connected to the EVCS.

Research on the vehicle-grid interaction has been conducted in the year of 2016 [1, 2] to ensure maintaining a demand and supply balance. Many charging methodologies have been developed with consumer-centered applications. These smart charging methodologies are divided into two types: time-based scheduling and power based scheduling. Vehicles can be charged according to a predefined priority criterion [3] by Kumar et al. For example, vehicles that require fast charging will be charged with a higher kWh capacity.

Frendo et al. [4] present an algorithm for smart charging that uses machine learning to determine the demand for electric vehicles. The algorithm depends on the prediction of the SoC of the vehicles. Since it is bound to vary in practice, an online algorithm that minimizes energy cost without knowing future information [5] is an efficient alternative to regular offline or day-to-day planning algorithms.

Research [6] done in the year of 2021 introduces an algorithm which schedules heterogeneous fleets of vehicles for charging with fair share maximization as the top priority. Cao et al. [7] present an algorithm that schedules loads while reducing charging costs and managing load peaks. The above examples are an example of time-based scheduling.

An approach by Frendo et al. [8] for heterogeneous charging of vehicles in a parking lot demonstrates the real-time feasibility of smart charging. This has been achieved by generating charge profiles of electric vehicles based on the car model and its SoC. This approach has been demonstrated for slow charging and uses machine learning to determine the future requirement. Charging vehicles with a pre-computed user-defined schedule will help an EVCS prioritize consumers according to their wait time.

Paper published in 2019 [9] presents power-based scheduling algorithms for solving mixed integer problems modeled by an EVCS whereas Alonso et al. [10] present a Genetic Algorithm for the same. We present an algorithm that combines the advantages offered by online and offline algorithms.

3 Necessity of Smart Charging

When a battery is connected to a charging system, charging occurs in constant current, constant voltage (CC-CV) mode. During CC mode, the battery draws constant current from the power supply until the voltage at the battery terminals reaches the rated voltage. When the rated voltage is reached, the battery runs in CV mode. In CV mode, the voltage across the battery remains constant and whereas the current drawn by the battery reduces drastically. Figure 1 shows a typical battery behavior in CC-CV mode.

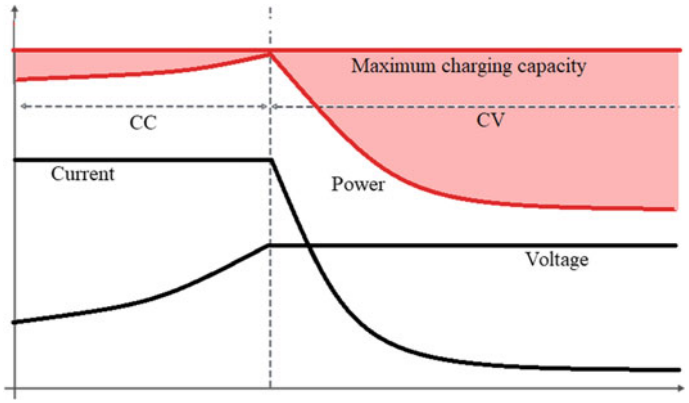

Fig. 1 EV battery charging profile

Therefore, there is great potential for a smart charging algorithm that controls the amount of power that goes out of a charging point and the remaining power can be channelled through other charging points without the risk of system overloading.

4 Overview of the Smart Charging Algorithm

The algorithm commences with the arrival of an Electric Vehicle. The system checks if the EV was scheduled for the time-slot in the EVCS. The scheduled EV is directed to its assigned charging point via a communication system. The pre-scheduling of the EVs will take place before the day commences. The system schedules the EVs accordingly based on markers: cumulative profits for the station, sum of planned powers, EV load during the period (Fig. 2).

IF the EV is not scheduled, users will fill in the required SoC, their car model, their arrival time, and their tentative desired charging duration as well as the mode of charging (fast or conventional).

The power distribution is calculated and reallocated to the electric vehicles based on the new addition. For better control over power slots and allocation, our goal is to calculate the allocation after every 15 min based on the following priority marks: item mode of charging, expected departure time, current SoC of the EV, desired SoC of the EV.

Charging is stopped once the desired power is supplied. The algorithm can be split into 2 parts, namely the schedule guided heuristic (day-ahead scheduling and real time) and power scheduling. The parts have been discussed in detail in the following sections.

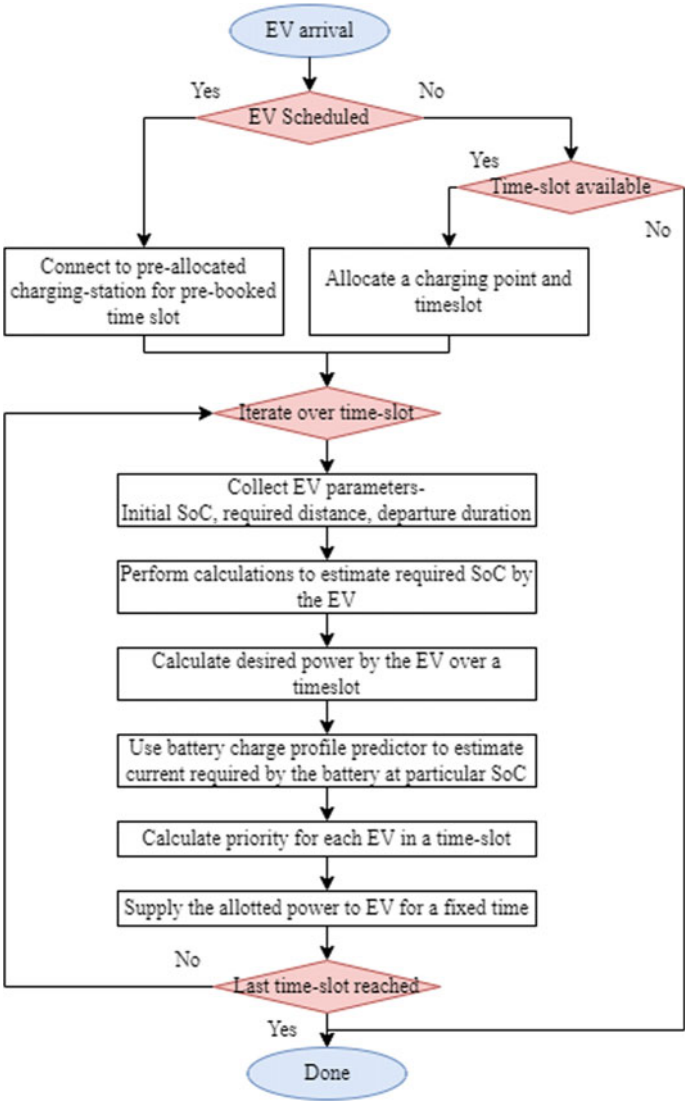

Fig. 2 Smart charging algorithm

4.1 Day Ahead Scheduling

Day ahead or offline scheduling of EVs on a daily basis is beneficial for the EVCS operator, as an optimized schedule can be created to maximize profits. The aim of a scheduling algorithm for the next day is to achieve an economically rewarding operation while adjusting for the load on the power network. We get the details from

a user for pre-scheduling a vehicle. The user can only schedule the vehicle for the next day.

The user selects a time slot from a total of 8 time slots. Each of the time slots is 3 h long, starting from 12 am to 11:59 pm. Suppose the user selects the time slot from 6 am to 9 am. After selecting the slot, the algorithm assigns the vehicle to the available charging station present in the slot from 6 am to 9 am. Whenever a different user enters his details for pre-scheduling in the same time slot, the algorithm first checks if the user can be accommodated in the particular time slot; else asks the user to choose a different time slot. In case the user can be accommodated, the algorithm creates an optimized schedule for the time slot with the new addition and previous users present in the database. The schedule is filled by selecting time-slots for charging which can fit in optimum number of EVs with the constrained power requirement and first come-first serve basis. For the day-ahead scheduling, creating and optimizing schedules is done via a greedy filling technique which is based on a set of mathematically calculated priorities. The order of the cars is determine according to the desired duration of charging the vehicle, the priority given to each vehicle and in a way that maximum cars can be fit in the schedule. The schedule is optimized after every entry.

4.2 Real Time Algorithm

Real time algorithms usually focus on power allocation and management based on profit maximization. When an unscheduled EV arrives at the station, the user enters his details and requirements, the algorithm checks if there is any station available for the desired duration of charging given by the user, with an acceptable difference of 15 min. If a charging station is available, the car is assigned to the station and the schedule is updated.

4.3 Power Scheduling of EVs

A EV battery's charging profile is shown in Fig. 1. Normally, a fixed amount of power is allocated to all electric vehicles, but this leads to the waste of infrastructure capacity during CV mode. We calculate the power required by the vehicle, by calculating the magnitude of the current that is to be supplied to the vehicle. This helps us estimate the power requirement, and we can allocate unused power to other stations. The power scheduling algorithm works as follows:

The system collects the data of all cars connected to the charging station, which are represented as (x_k) every 15 min. The power (w_k) to be provided is calculated based on the current and voltage at the time. For real time application, the voltage will be measured at the charging station, in our application we predict the voltage using the battery charge profile prediction discussed in the section above.

Data: Car Details, Schedule
Calculate SoC_{final}
while $Schedule \neq None$ **do**
  for *All Cars in current TimeSlot* **do**
    Calculate Priority for Car Calculate Power required for Car
  end
  Define Constraints $Maximize : \sum_{k \epsilon I} p_k * x_k$
  Subject To (f): $\sum_{k \epsilon I} w_k * x_k \leq c$ where, $I \epsilon \{0, 1\} \; \forall \; k \; \epsilon \; I$
  Create a tree of possible subproblems S
  $Solution \; \widehat{x} \; \epsilon \; \{x \; \epsilon \; S | \; f(x) <= f(\widehat{x})\}$
  if *S cannot be pruned* **then**
    Partition S into $S_1, S_2 \ldots S_n$ Check Solution for Subproblem
  end
  $Return \; \widehat{x}$
end

Algorithm 1: Power scheduling

We estimate the charging current on the basis of the current and final SoC. This method is known as the Coulomb counting method. Mathematically, it is calculated as follows, where (i) is the magnitude of the current:

$$SoC_{final} = SoC_{current} + \int_{current\ time}^{end\ time} i * dt \tag{1}$$

Priority p_k for each car is calculated based on various factors that will be discussed below the scenario is modeled as a linear integer problem (LIP), where the constraints are defined as follows:

$$Maximize : \sum_{k \epsilon I} p_k * x_k \tag{2}$$

$$Subject\ To : \sum_{k \epsilon I} w_k * x_k \leq c \; where, \; I \epsilon \{0, 1\} \; \forall \; k \; \epsilon \; I \tag{3}$$

This LIP is modeled as a fractional knapsack problem. Suppose that we have k number of cars items, each one with a required power magnitude of w_k and estimated priority p_k, we want to select a subset with maximum priority such that the summation of the current magnitudes of the selected cars is less or equal to the EVCS maximum power capacity c. We consider a set of continuous variables $(x_k | k \epsilon N)$ that receive the value 1 if the kth item is selected and 0 if it is not, and a fraction if it is partially selected. This is solved as a feasibility problem and is NP-complete. Now, we try all possible combinations of x_k to solve this problem. This is a tedious task which is time consuming and a naive approach to the problem. Instead, we use the branch-

and-bound technique, a greedy algorithm that tries to find a limit number of solution sets.

In this technique, a tree of solutions is created. Each node in the rooted tree is considered as a new problem. Also, a bounding function is used to limit the search space. On the basis of the solution of the optimal solution, each branch is checked. The branch is discarded if it does not produce a better solution than that found by the algorithm in the previous step. For the optimization step we have used the COIN-OR Linear Programming Solver (CLP) as our primary solver. We create a mathematical model of the fractional knapsack with the bounds and constraints and use the MIP solver to find the optimal solution.

Priorities for Power Scheduling For the LIP modeled below,

$$Maximize : \sum_{k \epsilon I} p_k * x_k$$

we calculate priorities of EVs using a priority function. We have a dynamic priority function that has four weighted components, where z_i is the component and w_i is the weight of each component.

$$p = z_1 * w_1 + z_2 * w_2 + z_3 * w_3 + z_4 * w_4$$

– Component 1: This objective component is calculated for the fair share maximization. Its goal is to minimize the number of EVs that are below a minimum predetermined SOC threshold.

$$z_1 = \frac{SOC_{min} - SOC_{current}}{t * i_{max\ of\ CS}} \quad if \quad SOC_{min} > SOC_{current}$$

– Component 2: The component is calculated with respect to the desired departure time of the user. The goal of the component is to prioritise the charging of EVs that are due for departure over the ones that are due later on. We get the final value as a percentage of the time that is left before the user wants to depart. This component helps us differentiate between fast and slow charging, while giving preference to users whose departure time is near.

$$z_3 = \frac{desired\_departure\_time - present\_time)}{desired\_departure\_duration} * 100$$

– Component 3: This subjective component is calculated based on the current SOC of the vehicle and the desired final SOC of the vehicle, where ϵ is a constant factor used to adjust the units of output

$$z_3 = (SOC_{final} - SOC_{current}) * \epsilon$$

– Component 4: This component is based on the mode of charging of the vehicle. Its goal is to prioritize electric vehicles that have opted for fast charging. The component serves two purposes: maximization of profits by encouraging fast charging and timely delivery of the charged vehicle

$$z_4 = \frac{SOC_{desired} - SOC_{current}}{t * \epsilon},$$

where ϵ is a constant factor used to adjust the units of output.

The weights of each priorities are determined by the order of preference and and impact on the scheduling as well as the magnitude of the output.

5 Test Problem and Results

The smart charging algorithm is tested based on a specific situation mentioned as follows—A charging station available can charge maximum of 5 electric vehicles at a time with maximum charging power of 7.5 kW. A sixth charging point has been added to the existing charging station having no dedicated power supply, which creates an unstable system and hence is susceptible to overloading. The smart charging algorithm is active on this station hence it is called as **Smart charging station**.

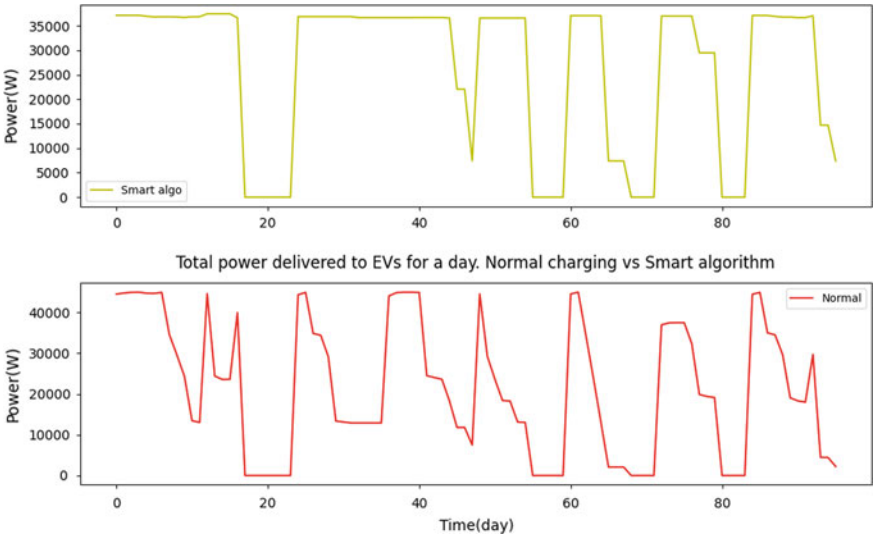

Fig. 3 The smart charging algorithm makes use of available power more effectively than normal charging. For one day, 15 min of time intervals are plotted on x axis

A different charging station is considered called **Naive charging station** in which 6 charging points with a dedicated power supply exist. All charging points can charge an EV with maximum power of 7.5 kW.

EV users can plugin their vehicle to any charging point provided the point is not busy. EV charging slot booking can be done through a graphic user interface. Results are obtained with same set of electric vehicles fed to both the systems. A simulation was carried out to test both the algorithms with same sets of inputs.

Input data to the algorithm consists a schedule of electric vehicles requesting parameters—arrival time, departure time, requested kilometers.

Figure 3 shows that the smart charging algorithm can optimize the use of the infrastructure and its capacity to a greater extent. The smart algorithm was allocated a maximum capacity of 37.5 kW while the normal charging facility runs at a maximum charging capacity of 45 kW. It is observed that smart charging algorithm delivered 26.64 kW power to the vehicles, whereas naive charging algorithm delivered 21.48 kW power for same time duration.

6 Conclusions

Power utilization is increased by application of smart charging algorithm, when the smart charging algorithm was compared with the normal mode of charging with specific sets of electric vehicles available in the market.

The smart algorithm shows that the installation of an additional 7.5 kW charging point can be eliminated without the risk of overloading of the charging station.

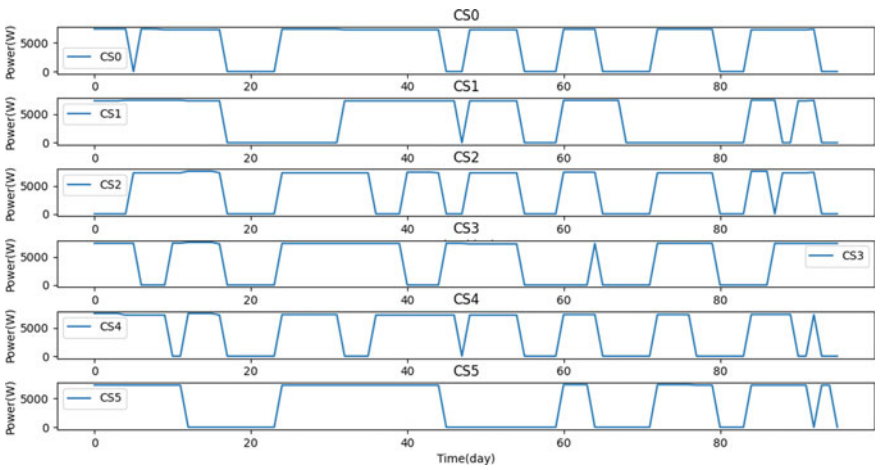

Fig. 4 Power output at each station, controlled by the smart algorithm. For one day, 15 min of time intervals are plotted on x axis

The smart charging algorithm presented in this paper is a general approach and hence can further be extended to any types of electric vehicles by simple improvements to the data set. It can be concluded that the proposed smart charging algorithm uses the EVCS infrastructure more efficiently than under normal charging conditions. The additional charging point can be added to the station capacity by integrating a smart charging algorithm to extend the charging capacity of any EVCS service without overloading the network. The algorithm reduces the power output to the maximum capacity of the charging station, eliminating the risk of completely overloading the grid. The smart algorithm enables for a quick increase in the charging capacity of any EVCS. Therefore, a smart algorithm can be a key to meeting the growing demand for charging electric vehicles in the future without an immediate additional investment in infrastructure and electrical power. When the increase in daily power usage is 23% assuming that the same set of electric vehicles is charged at a charging station, the profits earned by the charging station increase dramatically.

Figure 4 demonstrates the power allocation to each charging point in a Smart charging station based on priority markers.

References

1. Mukherjee J, Gupta A (2015) A review of charge scheduling of electric vehicles in smart grid. IEEE Syst J 9(4):1541–1553
2. Wang Q, Liu X, Du J, Kong F (2016) Smart charging for electric vehicles: a survey from the algorithmic perspective. IEEE Commun Surv Tutor 18(2):1500–1517
3. Kumar K, Sivaneasan B, So P (2015) Impact of priority criteria on electric vehicle charge scheduling. IEEE Trans Transp Electrification 1(3):200–210
4. Frendo O, Gaertner N, Stuckenschmidt H (2019) Real-time smart charging based on precomputed schedules. IEEE Trans Smart Grid 10(6):6921–6932
5. Tang W, Bi S, Zhang Y (2014) Online coordinated charging decision algorithm for electric vehicles without future information. IEEE Trans Smart Grid 5(6):2810–2824
6. Frendo O, Gaertner N, Stuckenschmidt H (2021) Open source algorithm for smart charging of electric vehicle fleets. IEEE Trans Ind Inform 17(9):6014–6022
7. Cao Y, Wang H, Li D, Zhang G (2021) Smart online charging algorithm for electric vehicles via customized actor-critic learning. IEEE Internet Things J 1
8. Frendo O, Graf J, Gaertner N, Stuckenschmidt H (2020) Data-driven smart charging for heterogeneous electric vehicle fleets. Energy AI 1:100007
9. Mao T, Zhang X, Zhou B (2019) Intelligent energy management algorithms for EV-charging scheduling with consideration of multiple EV charging modes. Energies 12(2):265
10. Alonso M, Amaris H, Germain J, Galan J (2014) Optimal charging scheduling of electric vehicles in smart grids by heuristic algorithms. Energies 7(4):2449–2475

Real Power Loss Minimisation and Energy Cost Saving with DG and Capacitor Using JAYA Algorithm in Radial Distribution System

Atul Kumar Dev and Ashwani Kumar

1 Introduction

Optimizing network configuration is a trending topic in research because power loss is a major concern for the network. However, there is a shift in old distribution network to active network from passive and low-carbon distribution systems which creates opportunities with shift of planning issues and the regulatory framework, having the integration of renewable energy sources and distributed generations (DGs). Distribution network operators (DNO) is facing new challenges due to addition of DG as to create sustainability of DG by lowering loss for operational profit and making financial benefit [1]. The unbundling rules in restructured electricity markets with proper planning of DGs and their location and sizes to promote third-party investment in DGs which can lead to economical, technical as well as favorable locations [2]. From last decade researchers are trying to optimally place the DG of suitable size to get minimal losses. Thus, the sizing and siting of DGs along with reactive power management is an optimization problem that needs to be solved for proper planning of the distribution systems. Many authors have applied different heuristics techniques to solve the minimization problem of power loss and reactive power management.

The interconnected system's important components are generation, transmission and distribution system. In distribution network due to higher R/X ratio it has higher loss, also because of its complex network power loss, system reliability, voltage profile drop etc. are some basic issues [3]. For proper utilization of distribution system

A. K. Dev (✉)
National Institute of Technology, Kurukshetra, India
e-mail: atul_32014304@nitkkr.ac.in

A. Kumar
Department of Electrical Engineering, National Institute of Technology, Kurukshetra, India
e-mail: ashwani.k.sharma@nitkkr.ac.in

S. Doolla et al. (eds.), *Advances in Renewable Energy and Its Grid Integration*,
Lecture Notes in Electrical Engineering 1041,
https://doi.org/10.1007/978-981-99-2283-3_2

and its expansion optimally planning of distribution system is essential. Shunt capacitor are equipped to inject reactive power in radial network to address the issues of power saving, cost reduction, power quality, increased reliability [4]. In recent years, Distributed Generation (DG) positioning is becoming trending area of research. With addition of DG it offers advantages i.e. good voltage profile, increased stability and lower power loss [5]. Using capacitor and DG at same time can reduce power losses and increase voltage level, if these are positioned correctly with optimum size [6].

Several optimization techniques have been introduced for dealing with problem of correctly placing the DGs and capacitor in RDS. Genetic Algorithms (GA), Particle Swarm Optimization (PSO), and multi objective algorithms are the most widely used for solving the optimization problem [7]. In recent years, researchers have proposed different meta-heuristic-based intelligent techniques to address the DG and shunt capacitor placement problems. The Artificial Bee Colony (ABC) algorithm has been used in [8] for optimizing installation of DGs in distribution system. GA is used in [9] to identify the optimum position and sizing under load uncertainty for fixed and switched capacitors. In [10] simultaneous placement is done by GA for minimizing the total cost of system considering several practical constraints. Plant Growth Simulation Algorithm (PGSA) is used in [11] for reducing power loss and improvement in voltage profile using capacitor only. For minimizing power losses using Adaptive Quantum Inspired Evolutionary Algorithm (AQIEA) is illustrated in [12]. The drawback of previous algorithms is that these algorithms have specific algorithm based parameters which should be tuned properly because it results in slow convergence rate and non optimal solution and it should be mentioned at the initial stage of optimization algorithms.

In 2016 a new population-based JAYA algorithm is introduced, is used in this study [17]. For obtaining global solution or near to global solution JAYA algorithm does not require tuning of any parameter which is an advantage for it. The simple working of JAYA can be understood as every member in population tries to improve themselves by following the best member and trying to escape worst member and JAYA is easy to implement also [18]. So, in this work active power loss is minimized using JAYA algorithm as it does not require tuning of parameter.

In this work, location of DGs and capacitors are obtained using two different techniques, the first one by using JAYA itself another one by using voltage stability index (VSI) whereas the sizes are determined using JAYA algorithm for both cases. The load growth factor, essential for the planning issues and impact on the losses is considered. The results have been obtained on standard test system 34-bus RDS.

The paper summary after this section is as follows: Sect. 2 outlines the problem formulation in which objective function, operating constraints, load flow and other important terms are discussed. In Sect. 3 JAYA algorithm and in Sect. 4 results and discussion are presented and in Sect. 5 conclusion is mentioned.

2 Problem Formulation

2.1 Objective Function

Objective is to minimize active power loss by addition of DG and capacitor in distribution system. Mathematical representation is given in (1):

$$P_{loss} = \sum_{i=1}^{n} R_i |I_i|^2 \tag{1}$$

2.2 Operating Constraints

Bus voltage constraint

Each bus's voltage must be varied in its acceptable limits between minimum and maximum.

$$V^{\min} \leq V_i \leq V^{\max} \tag{2}$$

For i = 1, 2…n, for total n nodes.

Capacitor size constraint

$$Q_{\min} \leq Q_{Cap,j} \leq Q_{\max} \tag{3}$$

where $Q_{Cap,j}$ is reactive power compensation at j.

Capacitor size should be in the minimum and maximum allowed range.

Total Reactive Power constraint

The sum of injected reactive power by capacitor should be less than total load of reactive power.

$$Q_{Cap}^{T} \leq Q_{load}^{T} \tag{4}$$

where Q_{Cap}^{T} is total capacitor reactive power, Q_{load}^{T} is total sum of load's reactive power

DG capacity limit

The total active power generation of integrated DG unit must be lower than the total active power load of network.

$$P_{DG}^{total} \leq P_{Load}^{total} \tag{5}$$

2.3 Load Flow

For analysis of distribution network traditional methods are not providing good results but for analysis of transmission network traditional methods of load flow i.e. Newton Raphson and its modifications, FDLF methods are good. BIBC load flow and Backward forward sweep load flow (BFSLF) are used generally for distribution network. In this paper direct load flow (DLF) using BIBC is utilized. In comparison to traditional methods, this technique is more robust and efficient [13].

2.4 Voltage Stability Index

A quadratic equation is developed for bus voltage using active and reactive power demand. Equating roots for real value a voltage stability index (VSI) is developed for that specific node [14]. VSI is mathematically represented in (6);

$$VSI = \frac{4X}{Vi}\left(\frac{P_{eff,i}^2 + Q_{eff,i}^2}{Q_{eff,i}^2}\right) \leq 1 \tag{6}$$

$P_{eff,i}$ is effective real power demand for node i, $Q_{eff,i}$ is effective reactive power demand for ith node.

VSI value approaches to zero then system is more stable and if VSI value is high, the system is likely to be instable. For placement of capacitor/DG bus having high VSI value is selected.

2.5 Voltage Stability Margin

When the system cannot provide the desired power to loads then condition of voltage instability arises. The nodes that have probability to collapse can be identified using voltage stability margin (VSM). For each bus VSM is evaluated using (7), weak node is treated which have minimum VSM [15].

$$\begin{aligned} VSM(rr_i) =& V(ss_i)^4 - 4(P_i \times x_i - Q_i \times r_i)^2 \\ & - 4V(ss_i)^2(P_i \times r_i + Q_i \times x_i) \end{aligned} \tag{7}$$

where rr_i is receiving end and ss_i is sending end, for bus i.

2.6 Various Costs

Energy loss cost [16]

It is the annual energy loss cost is represented in (8)

$$C_{EL} = TPL * Ec * T \tag{8}$$

where Ec is energy rate and T is duration in hour having value 0.06 $/kWh and 8760 h respectively.

Capacitor cost for Reactive Power [17]

$$C_{cap} = K_{ci} + K_c * Q_{Cap}^{Total} \tag{9}$$

where $K_{ci} = 1000$ $ is installation cost in $ for capacitor, $K_c = 3$ $/kVAr: is purchase cost for capacitor

Cost of active power of DG [18]

$$Cost_{PDGt} = a.P_{DGt}^2 + b.P_{DGt} + c\ \$/\text{MWh} \tag{10}$$

where the coefficient of cost is taken as, a = 0, b = 20, c = 0.25.

2.7 Model of Load Growth [19]

The load growth modelling is important for distribution system planning and its expansion in future. In this work, load growth's effect on losses, its voltage profile, and system's requirement of reactive power as well as the VSI has also been studied. Mathematically LG is modelled as;

$$load_i = load(1 + gr)^{pp} \tag{11}$$

where gr is growth rate while pp is span of planning period.

Statistical data is typically used to select the rate of load growth for distribution system. In this work, the load growth rate is estimated to be 8.48% over a five-year planning period. The value is taken from [22].

3 JAYA Algorithm

Venkata Rao et al. firstly presents the JAYA optimization algorithm [20]. The thing which stands apart JAYA is that it does not require any parameter tuning apart from

common controlling such as the population size and iterations. JAYA solves problems by moving through the best solution and escaping the worst solution. JAYA derives its name from a Sanskrit word that means "victory". By initialising population size, design variable and iteration the algorithm is set to begin. In this algorithm generally termination criteria is number of iterations.

Steps involved in solution of optimal allocation of DG and capacitor problem using JAYA algorithm

Step 1: Set the population size, design variables, termination criteria i.e. maximum iteration and lower and upper bounds.
Step 2: Call the DLF.
Step 3: Initial population is generated and objective function is evaluated.
JAYA Algorithm starts.
Step 4: Value of objective function is sorted as best and worst solution and their positions also.
Step 5: Modify the solution using

$$Z'_{j,k,i} = Z_{j,k,i} + rand_{1,j,i} \times \left(Z_{j,\text{best},i} - \left|Z_{j,k,i}\right|\right) - rand_{2,j,i} \times \left(Z_{j,\text{worst},i} - \left|Z_{j,k,i}\right|\right)$$

Step 6: Run the DLF, accept the modified solution if it's better than old one otherwise retains the old solution.
Step 7: If stopping criteria is satisfied then give the output results otherwise repeat step 4 to step 6.

4 Results and Discussion

In this work, results are determined for standard 34-bus RDS for minimizing the real power loss. Voltage profile, voltage stability margin (VSM), total real power loss (TPL), total reactive power loss (TQL), energy loss cost and feeder capacity reduction are calculated. The results are obtained by two methods, (i) using JAYA algorithm both location and size is determined. (ii) hybrid method that comprises using VSI as a parameter for location, and sizes are determined by JAYA. Furthermore, two conditions are considered, first is the base case without considering the load growth, second one by considering the load growth model. In this work, unity power factor DG i.e. type 1 DG have been considered. Furthermore, various capacitor and DG combinations are tested, and the best combination is used.

4.1 IEEE 34-Bus Test System

Line and load data for 34 bus system is taken from [4]. The result is calculated for standard 34 bus RDS. In this it has been assumed that base MVA is 100 and base kV is 11 [4]. The results for 34-bus system is summarized in Table 1.

Using JAYA method without Load Growth

With addition of DG and capacitor of optimal sizes of 2985 kW, 1090 kVAr and 1185 kVAr are positioned at optimal buses 21.8 and 23 respectively, the percentage reduction in TPL is 81.94% and saving in energy loss cost is 95506.77 $/year. Voltage profile and loss curve is plotted in Fig. 1.

Using VSI method without Load Growth

By adding DG and capacitor of optimal size of 2301 kW, 799 kVAr and 1598 kVAr are positioned at optimal buses 24.9 and 19 respectively, the percentage reduction in TPL is 76.56% and saving in cost of energy loss is 89231.11 $/year. The improvement in VSM is shown in Fig. 2.

Using JAYA Method with Load Growth

By using LG model losses increased and severe drop in voltage profile. By addition of DG and capacitor of optimal size of 4477 kW, 1481 kVAr and 1867 kVAr at optimal buses 21.9 and 23 respectively, the percentage reduction in TPL is 82.63% and saving in cost of energy loss is 228935.60 $/year. The results considering LG is presented in Table 1.

Using VSI Method with Load Growth

With addition of DG and capacitor of optimal size of 3490 kW, 1201 and 2411 kVAr at optimal buses 24.9 and 19 respectively, the percentage reduction in TPL is 77.39% and saving in cost of energy loss is 214439.54 $/year. The voltage profile and VSM is plotted in Fig. 3 and convergence curve is shown in Fig. 4.

5 Conclusions

In this paper minimization of power loss and energy loss cost is obtained with optimal DG and Capacitor placement using JAYA algorithm and in the second method hybrid technique is used with stability index as a sensitivity approach for optimal location and size is obtained with JAYA. The results have been tested on standard test system IEEE-34 bus RDS. So, JAYA produces better results i.e., reduction of power loss, improvement of voltage profile and enhancement of stability margin with capacitor and DG placement in comparison to hybrid technique. The cost of capacitor, cost of DG, feeder released capacity is also evaluated.

Table 1 Results summary for IEEE 34 bus

34 Bus	Without LG				With LG		
Description	Base Case	JAYA	VSI	Fuzzy-EP[21]	Base case	JAYA	VSI
TPL (kW)	221.75	40.04	51.98	62.13	527.15	91.58	119.16
% TPL Reduction (kW)	–	81.94	76.55	71.98	–	82.62	77.39
TQL (kVAr)	65.15	9.13	12.8	–	154.65	21.03	29.26
% TQL (kVAr)	–	85.98	80.35	–	–	86.40	81.07
Minimum Voltage (p.u.)/bus	0.9417 (27)	0.9832 (34)	0.9796 (34)	0.9808 (12)	0.9098 (27)	0.9741 (34)	0.9691 (34)
Power factor	0.85	0.9402	0.9798	0.7223	0.85	0.9595	0.98
Optimal location and size capacitor(kVAr)	–	8 (1090)	9 (799)	1 (408)	–	9 (1481)	9 (1201)
		23 (1185)	19 (1598)	21 (317.8)		23 (1867)	19 (2411)
				30 (128.9)			
Total Capacitor power (kVAr)	–	2285	2397	854.6		3348	3612
Optimal location and size DG (kW)	–	21 (2985)	24 (2301)	21 (1020.6)	–	21 (4477)	24 (3490)
				27 (1036.3)			
				33 (470.8)			
Annual Cost of energy loss($/year)	116,551.8	21,045.02	27,320.68	–	277,070.04	48,134.44	62,630.49
Saving in cost of energy loss($/year)	–	95,506.776	89,231.112		–	228,935.592	214,439.544
Total Capacitor cost($)	–	7855	8191		–	11,044	11,836
Total DG cost($/h)	–	59.95	46.27		–	89.79	70.05
Total real load (kW)	4363.5	4363.5	4363.5		6965.28	6965.28	6965.28
Total reactive load (kVAr)	2873.5	2873.5	2873.5		4316.77	4316.77	4316.77
Pinput (kW)	4585.25	1418.54	2114.48		7492.43	2579.86	3594.44

(continued)

Table 1 (continued)

34 Bus	Without LG				With LG		
Description	Base Case	JAYA	VSI	Fuzzy-EP[21]	Base case	JAYA	VSI
Qinput (kVAr)	2938.65	597.63	489.3		4471.42	989.8	734.03
Feeder capacity(kVA)	5446.11	1539.29	2170.35		8725.25	2763.21	3668.62
Released feeder capacity(kVA)	–	3906.82	3275.76		–	5962.03	5056.63

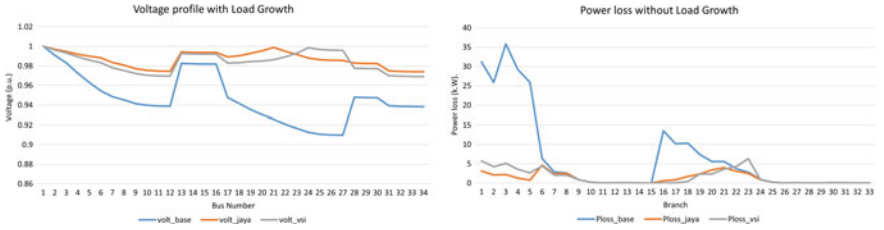

Fig. 1 Voltage profile and loss curve for 34 bus without LG

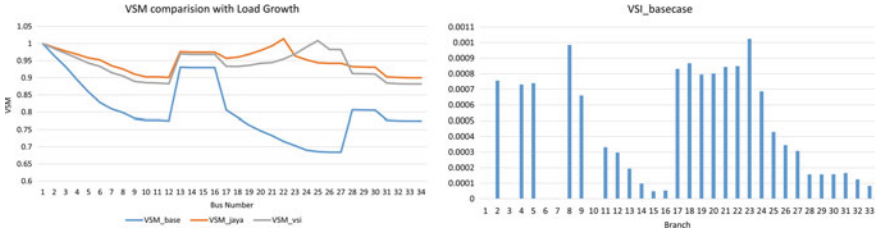

Fig. 2 VSM and VSI for 34 bus without LG

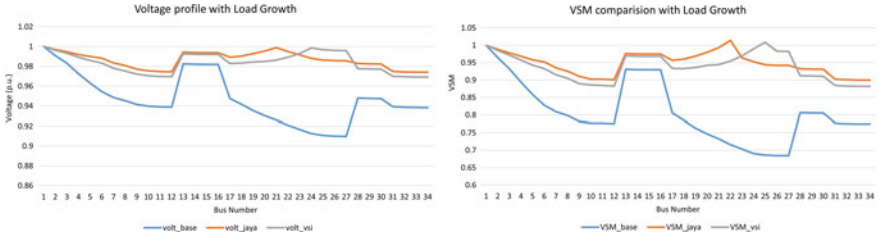

Fig. 3 Voltage profile and VSM for 34 bus with LG

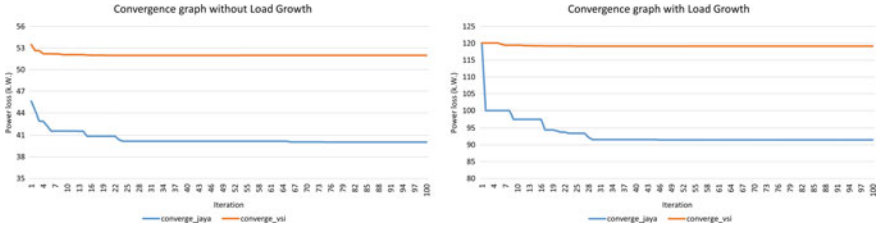

Fig. 4 Convergence curve for 34 bus

References

1. Ochoa LF, Harrison GP (2011) Minimizing energy losses: optimal accommodation and smart operation of renewable distributed generation. IEEE Trans Power Syst 26(1):198–205. https://doi.org/10.1109/TPWRS.2010.2049036
2. Mohanty PK, Lal DK (2021) Effects of load models and load growth in distribution system in presence of distributed generator. https://doi.org/10.1109/ICPEE50452.2021.9358482
3. Kashyap M, Kansal S, Singh BP (2020) Optimal installation of multiple type DGs considering constant, ZIP load and load growth. Int J Ambient Energy 41(14):1561–1569. https://doi.org/10.1080/01430750.2018.1517688
4. Prakash DB, Lakshminarayana C (2017) Optimal siting of capacitors in radial distribution network using whale optimization algorithm. Alex Eng J 56(4):499–509. https://doi.org/10.1016/j.aej.2016.10.002
5. El-Khattam W, Salama MMA (2004) Distributed generation technologies, definitions and benefits. Electric Power Syst Res 71(2):119–128. https://doi.org/10.1016/j.epsr.2004.01.006
6. Dixit M, Kundu P, Jariwala HR (2017) Incorporation of distributed generation and shunt capacitor in radial distribution system for techno-economic benefits. Eng Sci Technol Int J 20(2):482–493. https://doi.org/10.1016/j.jestch.2017.01.003
7. Almabsout EA, El-Sehiemy RA, An ONU, Bayat O (2020) A hybrid local search-genetic algorithm for simultaneous placement of dg units and shunt capacitors in radial distribution systems. IEEE Access 8:54465–54481. https://doi.org/10.1109/ACCESS.2020.2981406
8. Abu-Mouti FS, El-Hawary ME (2011) Optimal distributed generation allocation and sizing in distribution systems via artificial bee colony algorithm. IEEE Trans Power Delivery 26(4):2090–2101. https://doi.org/10.1109/TPWRD.2011.2158246
9. Haghifam MR, Malik OP (2007) Genetic algorithm-based approach for fixed and switchable capacitors placement in distribution systems with uncertainty and time varying loads. IET Gener Transm Distrib 1(2):244–252. https://doi.org/10.1049/iet-gtd:20045267
10. Rahmani-Andebili M (2016) Simultaneous placement of DG and capacitor in distribution network. Electric Power Syst Res 131:1–10. https://doi.org/10.1016/j.epsr.2015.09.014
11. Rao RS, Narasimham SVL, Ramalingaraju M (2011) Optimal capacitor placement in a radial distribution system using plant growth simulation algorithm. Int J Electr Power Energy Syst 33(5):1133–1139. https://doi.org/10.1016/j.ijepes.2010.11.021
12. Manikanta G, Mani A, Singh HP, Chaturvedi DK (2019) Simultaneous placement and sizing of DG and capacitor to minimize the power losses in radial distribution network. Adv Intell Syst Comput 742:605–618. https://doi.org/10.1007/978-981-13-0589-4_56
13. Teng JH (2003) A direct approach for distribution system load flow solutions. IEEE Trans Power Delivery 18(3):882–887. https://doi.org/10.1109/TPWRD.2003.813818
14. Murty VVSN, Kumar A (2015) Optimal placement of DG in radial distribution systems based on new voltage stability index under load growth. Int J Electr Power Energy Syst 69:246–256. https://doi.org/10.1016/j.ijepes.2014.12.080
15. Polisetti K, Kumar A (2016) Comparative analysis of sensitivity based methods for optimal location of capacitor considering optimal power flow formulation. https://doi.org/10.1109/ICPES.2016.7584079.
16. Chalapathi B, Agrawal D, Murty VVSN, Kumar A (2016) Optimal placement of distribution generation in weakly meshed distribution network for energy efficient operation. In: 2015 conference on power, control, communication and computational technologies for sustainable growth, PCCCTSG 2015, pp 150–155. https://doi.org/10.1109/PCCCTSG.2015.7503896.
17. Murty VVSN, Kumar A (2015) Capacitor allocation in radial distribution system with time varying ZIP load model and energy savings. Procedia Comput Sci 70:377–383. https://doi.org/10.1016/j.procs.2015.10.039
18. Suresh MCA, Belwin EJ (2018) Optimal DG placement for benefit maximization in distribution networks by using Dragonfly algorithm. Renew Wind Water Solar 5(1). https://doi.org/10.1186/s40807-018-0050-7

19. Murty VVSN, Kumar A (2013) Comparison of optimal capacitor placement methods in radial distribution system with load growth and ZIP load model. Frontiers Energy 7(2):197–213. https://doi.org/10.1007/s11708-013-0249-7
20. Rao VR (2016) Jaya: a simple and new optimization algorithm for solving constrained and unconstrained optimization problems. Int J Ind Eng Comput 7(1), 19–34. https://doi.org/10.5267/j.ijiec.2015.8.004
21. Ramalakshmi SS (2011) Optimal siting and sizing of distributed generation using fuzzy-EP. In: 2011 international conference on recent advancements in electrical, electronics and control engineering, IConRAEeCE'11—Proceedings, pp 470–477. https://doi.org/10.1109/ICONRAEeCE.2011.6129770
22. https://powermin.gov.in/en/content/power-sector-glance-all-india. Last accessed 04 Apr 2022

Design and Analysis of Grid-Connected 10 kW Solar Photovoltaic (SPV) Power Plant

Divanshi Gupta, Sudhir Kumar Pathak, Sanjeev Anand, V. V. Tyagi, Amit Verma, and Sharan Gupta

1 Introduction

For the development of any country, requires increased industrial production and this in turn requires increased energy consumption [1]. India is among the countries with fastest growing economies in the world and in order to maintain economic growth, India needs to ensure security of energy. Energy sector in India is facing unpredictable challenges. The main reasons for these challenges are the dependence upon imported fuel and its rapidly growing prices [2]. The consumption of various conventional energy resources like fossil fuels has lead to an increase in the amount of environmental pollutants [3]. Most of our daily range of energy requirements can be met by the various renewable energy sources. Renewable energy is most important substitute of energy produced by combusting fuels to meet the increased rate of consumption of energy without harming the environment. Sun is the only form of renewable energy that is clean and abundantly available [4]. India is the tropical country and lies within the latitude of 8 °N to 37 °N. It has approximately 300 clear, sunny days annually which offers good potential for application of solar energy [5]. One of the most promoting ways of utilizing solar energy is through the application of photovoltaic technology [6]. Photovoltaic technology uses sunlight to generate electricity without emitting pollutants [7]. Solar photovoltaic modules are built up of many photovoltaic cells joined in series. When appreciable numbers of SPV modules are connected together, the resultant installation is known as solar photovoltaic power plant [2]. The various advantages of SPV system are reliability, good performance, noiseless and clean energy production, low maintenance and a long-life span of around 25 years. The performance of photovoltaic power plant can

D. Gupta (✉) · S. K. Pathak · S. Anand · V. V. Tyagi · A. Verma · S. Gupta
School of Energy Management, Shri Mata Vaishno Devi University, Jammu and Kashmir, Kakryal, Katra, India
e-mail: divyanshi07.dg@gmail.com

S. Doolla et al. (eds.), *Advances in Renewable Energy and Its Grid Integration*,
Lecture Notes in Electrical Engineering 1041,
https://doi.org/10.1007/978-981-99-2283-3_3

be analyzed through parameters like capacity utilization factor (CUF), performance ratio (PR), specific production etc. [8]. To efficiently capture the sunlight and change it into electrical energy is the main problem of solar photovoltaic system. When SPV module is made to operate in actual environment, its output characteristic differs as compared to that at STC [9].

There are many factors that have great impact on performance of SPV plant such as geographical factors, environmental factors and type of technology used. When orientation of module is made to vary continuously with respect to change in position of sun is known as sun tracking or solar tracking. This tracking system brings prominent increase in performance of plant as compared to single axis tracking that brings about small gain in output over fixed tilt system. Installation of tracking system can be complex and expensive. Tracking system also requires maintenance. Thus, fixed systems are preferred for large scale photovoltaic plant [10]. In most of the cases, it is optimum to set the tilt angle approximately equal to the site latitude to get the maximum output [11]. Technical design and environmental analysis for 100 kW photovoltaic plant situated at north-western Iran was given by Ghadim et al. Different factors like tilt angle, azimuth angle and technical specifications of inverter have been taken into consideration [12]. Performance of solar photovoltaic plant is also dependent on ambient conditions i.e. solar radiation, temperature and humidity. Chattopadhyay and Rajavel performed a comparative study on 10 kW photovoltaic plant in three regions i.e. coastal, urban and rural area with almost similar radiation. This study was performed in India using PVsyst software. It was observed that Solar panels perform well in rural areas because of low humidity and temperature conditions as compared to urban and coastal areas [13]. Sohaib and Hakan designed at 1 MW solar photovoltaic power plant for Sudan using PVsyst software. The designed photovoltaic power would reduce carbon emissions up to 18 million tons per year. Many losses like array loss, efficiency loss due to temperature, ohmic wiring loss were also taken into consideration [14]. However, there is no comprehensive study accounting design of cables for right sizing of solar photovoltaic power plant. Cables act as medium to transfer electrical energy from one module to another module or modules to inverter. Selection and sizing of cable is very important aspect for the design of solar photovoltaic plant [15]. Two main types of conductors which can be used in solar photovoltaic system i.e. copper (Cu) and aluminium (Al). Aluminium has lower conductivity as compared to copper. Therefore, current carrying capacity of copper is greater than aluminium at same cross-sectional area and length. If solar cables are too small sized, they may lead to overheating and loss of energy. On other hand, if solar cables are too large sized, this leads to wastage of money. Determination of correct size of cable is the essential aspect of designing solar photovoltaic plant. The aim of this study is to discusses the sizing of PV array and effect of different parameters like tilt angle, cable sizing and type of cable material on solar PV system of 10 kW situated at Shri Mata Vaishno Devi University, Jammu. Firstly, geographical specification of the selected region has been specified. Next, photovoltaic power plant design parameters are discussed thoroughly. After that, simulation results have been analyzed and compared with each other. Finally, specified conclusions and future recommendations for the design and development of solar PV plant are discussed.

Table 1 GHI, GDI and average temp data from meteo file Meteonorm 7.2

Month	Global horizontal (kWh/m^2)	Diffused horizontal (kWh/m^2)	Temp. (°C)
January	89.2	33.6	9.8
February	89.8	43.1	13.5
March	142.9	61.0	19.0
April	164.2	74.0	24.1
May	201.8	81.5	29.8
June	195.7	93.5	30.8
July	174.6	91.2	30.0
August	154.7	85.0	28.9
September	165.4	58.1	26.8
October	148.1	43.3	22.7
November	111.0	30.5	16.0
December	85.5	35.3	11.7

2 Site Details

Geographical site of Shri Mata Vaishno Devi (Katra), J&K for 10 MW solar power plant, having the latitude of 32.94 °N, the longitude of 74.95 °E and altitude of 676 m is considered to study different design aspects for the design optimization. It receives ample amount of solar radiation and do not suffer extreme of temperature. Amount of solar radiation varies monthly for a particular site and hence ambient temperature also varies. The Table 1 shows different amount of solar insolation received monthly and monthly temperature for site of SMVDU.

3 Performance Indices

The solar PV plant characteristic parameters comprises of energy efficiency, performance ratio (PR), PV system yield (Y_f) and capacity utilization factor. Performances of solar photovoltaic plants vary with regard to different locations and configurations. Performance of different SPV plants can be easily compared by assessing their performance indices. It tells about the performance of a solar photovoltaic power plant and helps us to make comparative study among different parameters of design for a solar photovoltaic plant.

3.1 PV System Yield (Y_f)

Photovoltaic system yield (y_f) is the result obtained by dividing total output of energy (E_o) to nameplate DC power (P_{dc}) of SPV array installed. In other words, it is the time that solar photovoltaic plant takes to operate at name plate power to generate E_o. The unit of PV system yield is hours.

$$\mathbf{Y_f} = \frac{\mathbf{E_o}}{\mathbf{P_{dc}}} \tag{1}$$

3.2 Reference Yield (Y_r)

Reference Yield (Y_r) defined as the result determined by dividing total in plane solar irradiance (H_T) and reference irradiance (G).

$$Y_r = \frac{H_T}{G} \tag{2}$$

If the value of G is equal to 1 kW/m^2, then value of Y_r will represent the number of peak sunshine hours. The units of reference yield is hours per day.

3.3 Performance Ratio (PR)

Performance ratio (PR) is most important parameter in order to evaluate the efficiency of solar Photovoltaic plant. It is defined as the result obtained by dividing energy produced by solar photovoltaic power plant in terms of kWh during the time of evaluation and estimated nominal SPV plant output in terms of kWh for that particular time of evaluation.

Value of performance ratio helps us to find out whether the PV system is operating as estimated or not. The smaller value of performance ratio (PR) indicates the presence of some problem in SPV plant.

$$PR = \frac{\text{Energy produced by Plant for partiular time of evaluation (kWh)}}{\text{Determined nominal plant output for paticular time of evaluation (kWh)}} \tag{3}$$

3.4 Capacity Utilization Factor

Capacity Utilization Factor is the way for representing energy that is delivered by the generation system. It is known as the result obtained by dividing actual AC energy output (E_{ac}) by the amount of energy that would be produced by PV system if operated at nominal power (P_{nom}). Unity value of CUF denotes that the system is capable of delivering full rated power continuously.

$$\text{CUF} = \frac{E_{ac}}{P_{nom} * 8760} \tag{4}$$

3.5 Energy Loss

Energy generated by solar PV plant is always less when compared to rated energy. This is due to many losses occurs during conversion of energy delivered by sun into electricity through PV modules. There are many losses that add up to the system during its operation such as losses due to elevation in cell temperature, optical reflective losses, Losses due to effect of shadow, losses that occur as a result of non-continuous operation of inverter or due to its failure etc.

4 Methodology

4.1 Simulation Software

To efficiently employ the solar resource, it is required to simulate and size SPV system parameters properly. The size of SPV system required and quantum of energy yield can be determined accurately by using simulation software. There are number of softwares like HOMER, RETScreen, Helioscope, PVsyst etc. are available for the design of SPV power plant (Fig. 1).

PVSyst is perceived as the most extensively used software for designing and simulation of solar photo-voltaic power plant. Numbers of simulation software have been developed. One of the user friendly and convenient tools is PVSYST for design of solar photovoltaic power plant. PVSyst is simulation and solar photovoltaic design software. PVSyst is one of the modeling tools, used to estimate the energy yield of a potential project site. It is used for data analysis, sizing and study of absolute SPV power plant. It is used for designing various sorts of solar application systems such as stand-alone, grid connected, DC pumping systems and DC grid system. It includes meteorological data of numerous sites all around. Data of sites which is not covered by software can also be manually inserted in PVsyst. It provides results in

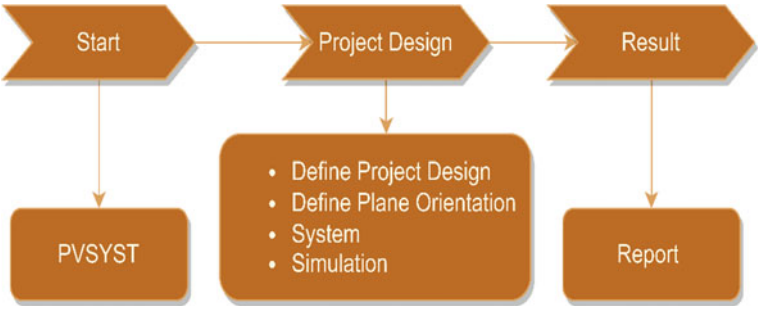

Fig. 1 Methodology for PVSyst. software

the form of report that includes graphs and tables in it. Sharma et al., [16] analyzed the performance of 190 kW connected SPV plant in India using PVsyst and need for optimizing tilt angle for solar modules was also emphasized to maximize the energy output. Okello et al. simulated and estimated performance of grid-tied SPV system. Actual measured parameters and parameters analyzed through PVsyst were compared by him [17]. Ashwini et al. analyzed the architecture of photovoltaic plant and scrutinized its design using PVsyst [18].

4.2 Description of Solar PV Power Plant

Total of 76 Si-poly modules are used having 19 modules in series and 4 strings in parallel. Each unit of module has 160 W of nominal power rating. Total of 4 units of solar inverters are used, each having nominal power rating of 2.5 kW. No 3D scenes are defined and effect of shading is not considered in the project. The detailed specification of PV plant and inverter are presented in Tables 2 and 3.

Table 2 PV array characteristics

Type of module	Si-poly
Manufacturer of module	Trina solar
Modules in series	19
Modules in parallel	04
Module area	125 m^2
Cell area	74 m^2

Table 3 Inverter specifications

Model	Solar inverter Solivia
Manufacturer	Delta energy
Unit nominal power	2.50 kWac
No. of inverters	4
Total power	10 Wac

4.3 Procedure

For performance analysis of 10 kWp grid-connect solar photovoltaic plant situated SMVDU, katra, simulations were performed using software PVsyst. Different design parameters like tilt angle, azimuth angle, cable cross-sectional area and type of conductor material used in DC cables are analysed using PVSyst software. Performance indices such as performance ratio and annual system production are used to study the effect of variation of different design parameters on the system performance. Simulations were done and results were given in the form of reports by PVsyst (Fig. 2).

Design Parameters: Different design parameters like tilt angle, cable cross-sectional area, and type of conductor material used in DC cables are considered.

Tilt Angle and Orientation-Tilt angle is represented as the angle formed between surface of inclined plane and the horizontal. Tilt analysis for the 10 kW solar power plant in SMVDU, Katra is done in order to select an optimum tilt for the project. Tilting of SPV plant plays a crucial role for having maximum generation and a good performance ratio of solar power plant. A system is designed in the PVsyst by selecting geographical location of SMVDU, Katra. In orientation section of software, there is the option of selecting tilt, azimuth etc.

Cable sizing and type of cable conductor-Using PVsyst software, effect of different cable sizing on performance of 10 kW solar photovoltaic plant at SMVDU is studied.

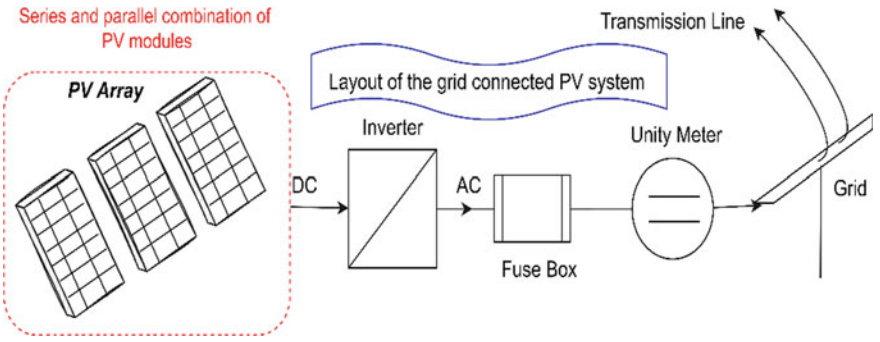

Fig. 2 Layout of grid connected photovoltaic system

Different cross-sectional areas i.e. 2.5 mm^2, 4 mm^2 and 6 mm^2 were selected for both Cu and Al conductors. Different cross-sectional areas of cables lead to different global array resistance and thus ohmic wiring loss changes accordingly. In this simulation software, type of conductor materials and cross- sectional area of conductor wire is chosen easily under the category of detailed losses.

Global Array Resistance and Ohmic Wiring Loss-The ohmic wiring resistance (R_w) results in loss of power which is produced from the modules and reaches the terminals of array. The parameter that is responsible for these losses is R_w which is defined as the global array resistance. The value of R_w is dependent on structure of array. Array resistance (R_w) depends on three factors:

- Resistivity of material used i.e., Al or Cu
- Length of cable wire
- Cross sectional area of cable.

Ohmic resistance can be calculated according to the formula

$$R_w = \frac{\rho l}{a} \tag{5}$$

where, ρ = resistivity of material, l = length of cable, a = cross sectional area of cable.

Global array resistance is calculated by PVsyst and is shown in figure. Ohmic resistance induces losses in the photovoltaic system known as ohmic loss. Ohmic wiring loss can be calculated by using formula given below:

$$P_{loss} = R_w I_{arr}^2 \tag{6}$$

where, I_{arr} = current flowing through the array of modules

The ohmic wiring loss is usually about 60% of the total loss fraction of PV system at STC. From Eq. (5) it is understood that global array resistance and thus ohmic wiring loss are different at different cross-sectional areas, length of cables and cable material used.

5 Results and Discussion

This section focuses on the results of the simulations carried to study the impact of various design parameters on the performance of 10 kW solar photovoltaic plant situated at SMVDU, Katra and hence, obtain an optimal design of SPV plant.

5.1 Effect of Different Types of Conductor Material Used in Cables on Performance of 10 kW SPV Plant

Two types of conductor material i.e., copper (Cu) and aluminium (Al) are considered for the analysis using PVsyst. Copper and aluminium produce different values of global array resistance at particular value of tilt angle and cross-sectional area. Tilt angle is taken equal to 30° and cross-sectional area of 2.5 mm^2 is considered.

It was observed that when types of conductor material changes, global array resistance of SPV plant also changes. Thus, causes change in percent of ohmic wiring loss. Figures 3 and 4 represents the variation in array resistance and ohmic wiring loss with respect to different conductor materials graphically. From the graph above, it is observed that plant using aluminium as conductor material has more array resistance than plant using copper as conductor material. Plant with copper has array resistance equal to 21 mohm and plant using aluminium conductor material has array resistance equal to 35 mohm. This is due to the fact that copper has more conductivity than aluminium.

Similarly, ohmic wiring loss also changes with regard to change in type of conductor material. Value of ohmic wiring loss for 10 kw plant considering copper as cable conductor material is 0.39% and for aluminium conductor material is 0.49%. These changes in value of losses causes change in annual system production and thus causing performance ratio of plant to change. Figures 5 and 6 illustrates the changes in annual system generation and performance ratio with respect to change in type of conductor material graphically.

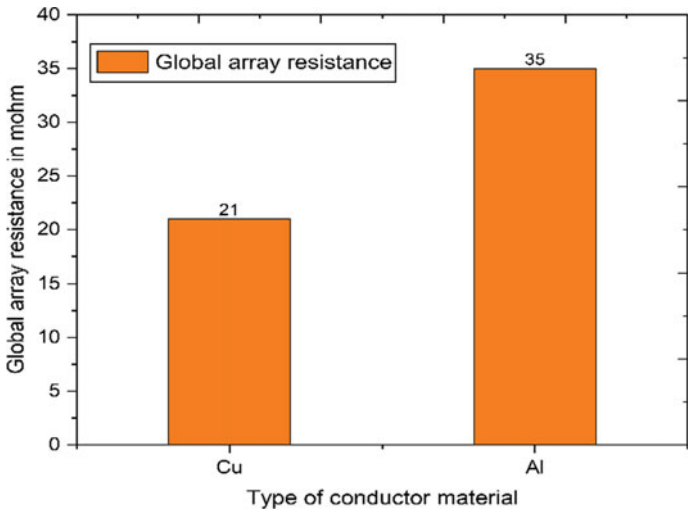

Fig. 3 Variation in global array resistance with respect to change in conductor material

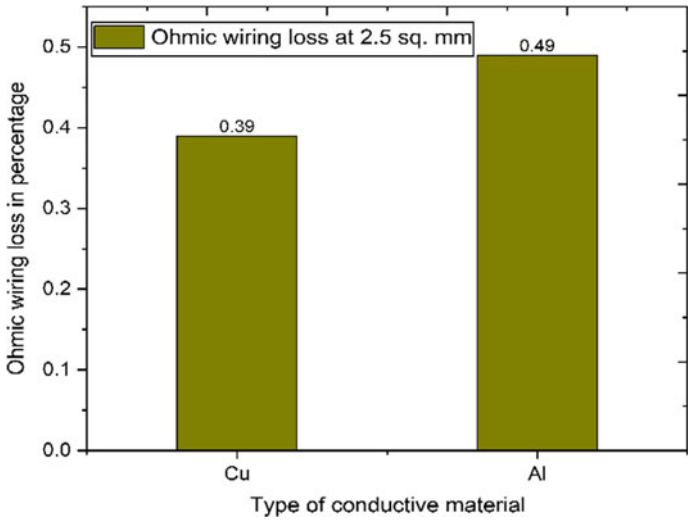

Fig. 4 Variation in ohmic wiring loss with respect to change in conductor material

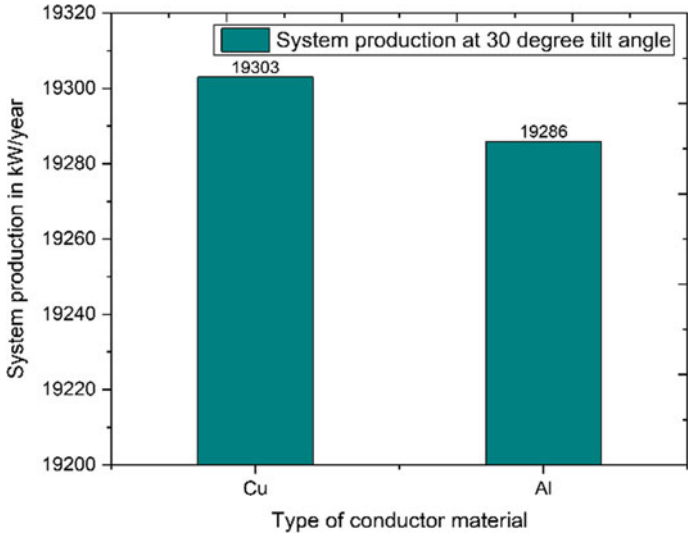

Fig. 5 Variation in system energy production with respect to change in conductor material

5.2 Effect of Variation in Cross-Sectional Area of Cable on Performance of 10 kW SPV Plant

Three cable sizes that are 2.5 mm^2, 4 mm^2 and 6 mm^2 are considered in this analysis. Simulations were performed considering different cable sizes for both aluminium

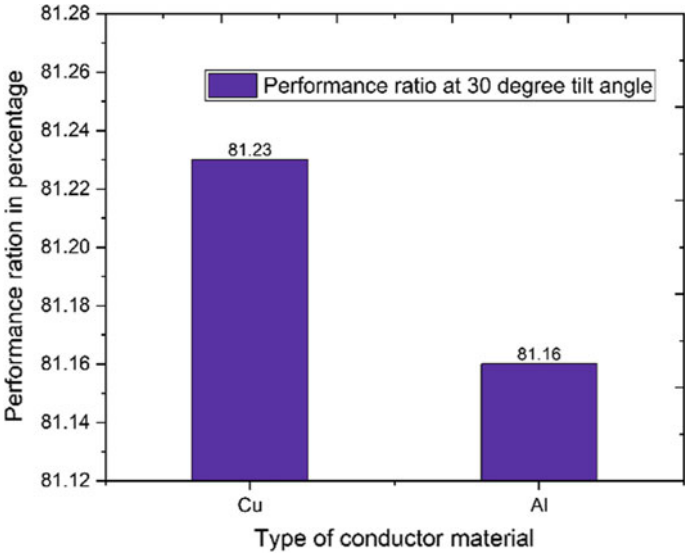

Fig. 6 Variation in performance ratio with respect to change in conductor material

and copper as conductor material. For 10 kW SPV plant, considering tilt of 30° and azimuth of 0° analysis was made by varying the cross- sectional area of cable. Figure 7a represents the variation in array resistance with respect to variation in cross-sectional area of cable graphically for both copper and aluminium conductor materials. Maximum array resistance i.e. 35 mohm is obtained when plant uses cable of aluminium material and cross-section of 2.5 mm^2. Minimum array resistance i.e. 8.6 mohm is obtained when plant uses cable of copper material and cross-section of 6 mm^2.

Similarly, variation in ohmic wire losses is studied for different cross-sectional areas for both aluminium and copper conductor material. The Fig. 7b graphically represents the variation in ohmic wiring loss for 10 kW SPV plant. Maximum ohmic wiring loss i.e. 0.49% is obtained when plant uses cable of aluminium material and cross-section of 2.5 mm^2. Minimum ohmic wiring loss i.e. 0.31% is obtained when plant uses cable of copper material and cross-section of 6 mm^2.

The variation in cross-sectional area of cable wire also causes variation in performance of a SPV plant. The variation in performance of SPV plant can be analyzed by Fig. 8a, b.

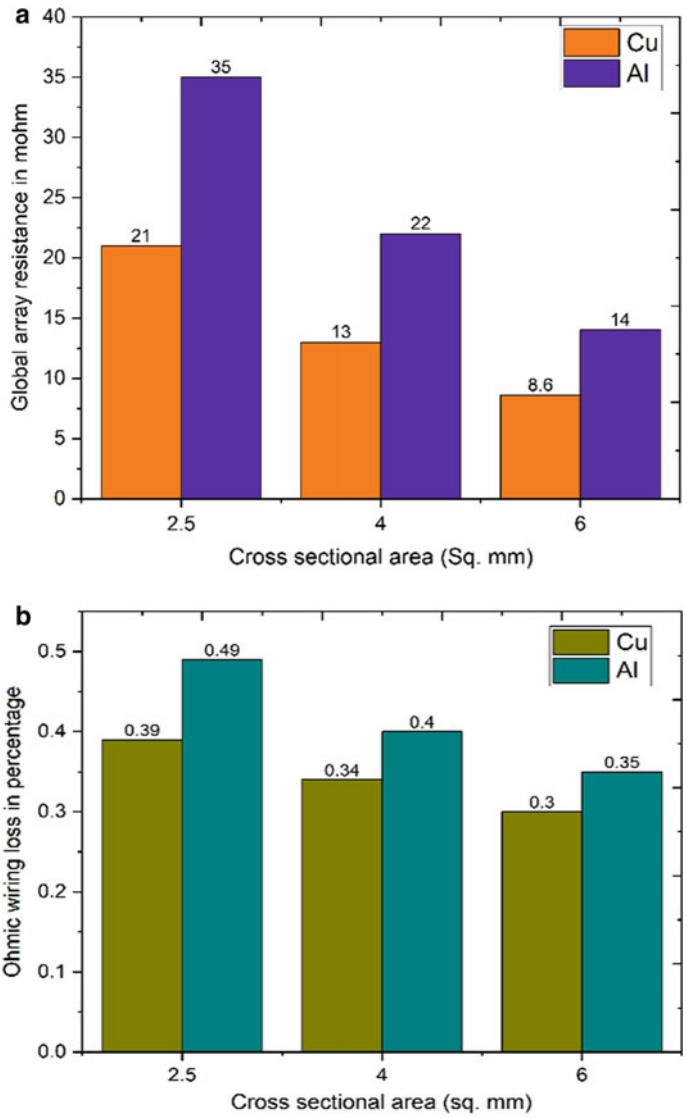

Fig.7 **a** Variation in array resistance material with variation in size of cable for both type of conductor material **b** Variation in ohmic wiring loss with variation in size of cable for both type of conductor material

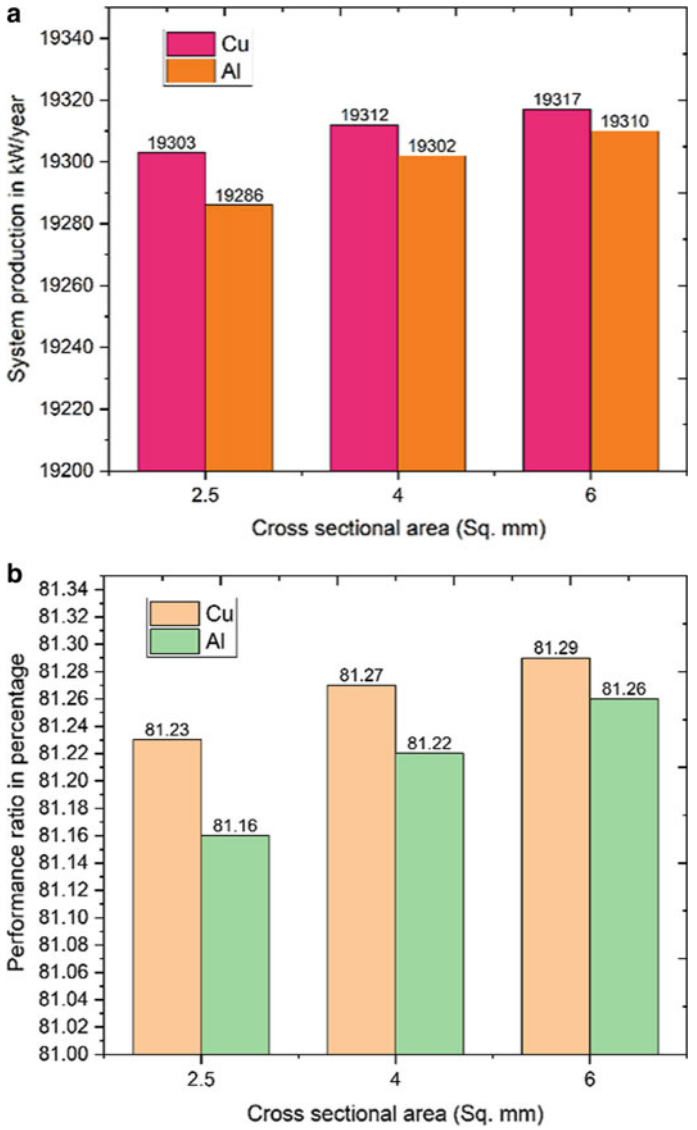

Fig. 8 **a** Variation in system energy production with change in cross-section area of cable for both copper and aluminium **b** performance ratio with change in cross-section area of cable for both copper and aluminium

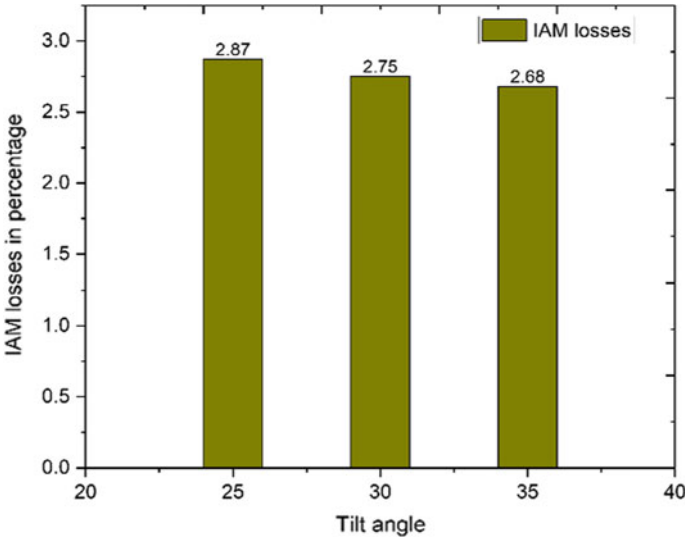

Fig. 9 Impact of tilt angle variation on IAM losses

5.3 Effect of Variation in Tilt Angle on Performance of 10 kW SPV Plant

Tilt analysis for the 10 kW solar PV plant is done in order to select an optimum tilt for the plant. For this power plant, three tilts are considered for tilt analysis. The tilts selected are 25°, 30° and 35°. Different values of tilt were chosen around the site latitude i.e. 32.94° N. From results obtained in PVsyst, it is observed that as angle of tilt changes, I_{am} (Incidence Angle Modifier) losses or array incidence loss changes. These losses increase when value tilt angle moves far from site latitude. Figure 9 graphically represents the variation in array incidence loss with regard to change in tilt angle.

Figure 10a, b represents the effect of variation in tilt angle on output and performance of SPV plant respectively. From the graph above, it observed that system performs best at tilt angle of 35° and using copper as cable conductor with cross-sectional area of 6 mm^2.

6 Conclusion

Performance of solar PV plant depends upon different factors and their effect has been analyzed. The effect of variation in different parameters of design on performance of SPV plant is discussed in detail in this paper and following conclusions are made:

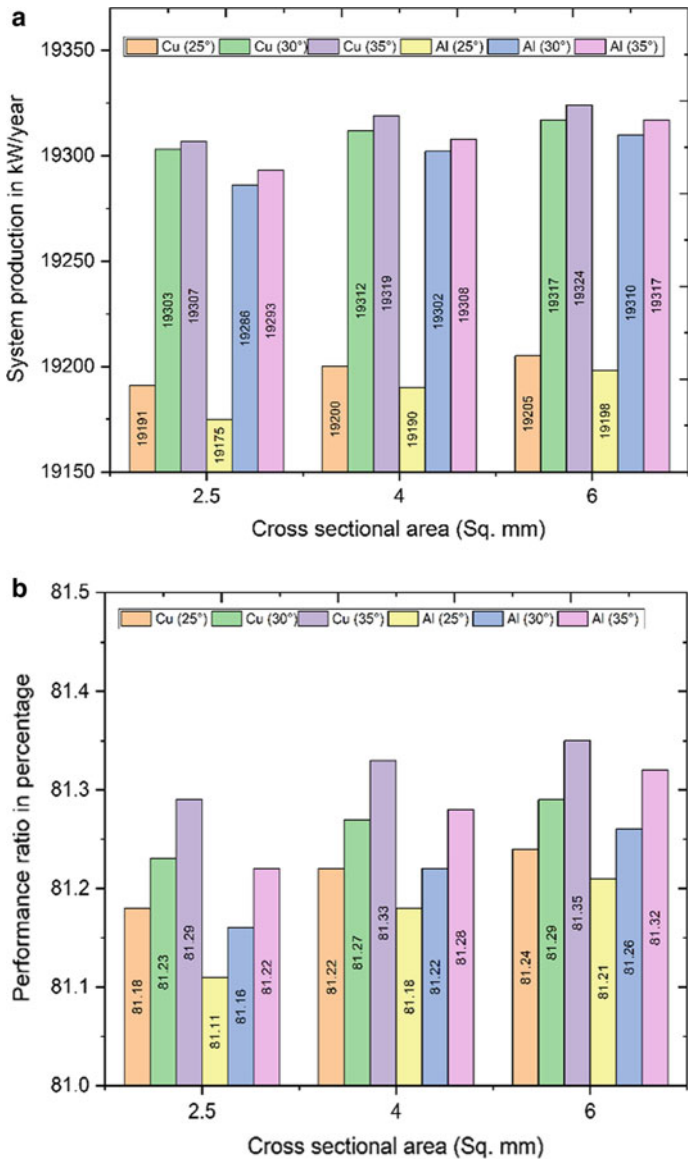

Fig. 10 **a** Effect of variation in tilt angle on output of SPV plant **b** effect of variation in tilt angle on performance ratio

Two types of conductors that are aluminium and copper were selected for the design of 10 kW SPV plant. Due to lower conductivity of aluminium than copper, aluminium produces high array resistance and ohmic wiring loss in SPV plant which results in poor performance of plant. Therefore, the plant which uses copper as conductor material for cable has better performance than plant which uses aluminium as conductor material for cable. Three cross-sectional areas of cables that are 2 mm^2, 4 mm^2 and 6 mm^2 were selected using PVsyst and it was found that higher the cross-sectional area lower is the ohmic wire loss. Therefore, higher is the performance of SPV plant. Effect of different tilt angles on the performance of SPV plant was studied. It was concluded that tilt angle near site latitude generates maximum output. Output decreases as move far from optimum value of tilt angle. For 10 kW power plant at SMVDU with site latitude 32.94°, three angles were taken for study that is 25°, 30° and 35°. Maximum output yielded by plant was at 35° tilt.

From the results, it is clearly observed that maximum energy produced by system i.e. 19,324 kWh/year is at tilt angle of 35°, when cross-sectional area of cable used in plant is 6 mm^2 and copper is used as conductor material in cables. It is also observed that minimum energy is produced when aluminium is used conductor material for cable with cross-sectional area is 2.5 mm^2 and system is at tilt angle of 25°. Also, it observed that system performs best at tilt angle of 35° and using copper as cable conductor with cross-sectional area of 6 mm^2. Therefore, maximum performance ratio of 10 kW SPV plant is 81.35%. Minimum performance ratio i.e., 81.11% is observed at tilt of 25° and by using aluminium as cable conductor with cross-sectional area of 2.5 mm^2.

7 Future Recommendations

Moreover, elaborated study can be done to analyze photovoltaic system using various technologies such as mono-crystalline, amorphous, etc. that can help to identify suitable solar PV technology for the design of SPV plant. Shading analysis could also be done to study the design aspect of SPV plant in detail. Lastly, economic analysis could also be done to achieve such a design of SPV plant that is both technically and economically viable.

References

1. Cubukcu M, Gumus H (2020) Performance analysis of a grid-connected photovoltaic plant in eastern Turkey. Sustain Energy Technol Assess 39:100724
2. Berwala AK, Kumarb S, Kumaria N, Kumara V, Haleemc A (2017) Design and analysis of rooftop grid tied 50 kW capacity solar photovoltaic (SPV) power plant. Renew Sustain Energy Rev
3. Sundaram S, Babu JC (2015) Performance evaluation and validation of 5 MWp grid connected solar photovoltaic plant in South India. Energy Convers Manage 100:429–439

4. Hernández-Callejoa L, Gallardo-Saavedraa S, Alonso-Gómez V (2019) A review of photovoltaic systems: design, operation and maintenance. Sol Energy 188:426–440
5. Bibekbandyopadhyay B, Gupta MK, Vashishtha RD (2011) Solar radiation assessment over India, book on solar future for India. In: Pillai GM (ed) WISE 2011, isbn:81-902925-2-8, pp 349–363
6. Sharma S, Kurian CP, Paragond LS (2018) Solar PV system design using PVsyst: a case study of an academic institute. In: International conference on control, power, communication and computing technologies (ICCPCCT), IEEE
7. EminMeral M, Dincer F (2011) A review of the factors affecting operation and efficiency of photovoltaic based electricity generation systems. Renew Sustain Energy Rev, 2176–2184
8. Sritakaew P, Sangswang A (2006) On the reliability improvement of distribution system using PV grid connected systems. In: Proceedings of the IEEE Asia Pacific
9. Yadav SK, Bajpai U (2018) Performance evaluation of a rooftop solar photovoltaic power plant in Northern India. Energy Sustain Dev 43:130–138
10. Babatunde AA, Abbasoglu S, Senol M (2018) Analysis of the impact of dust, tilt angle and orientation on performance of PV Plants. Renew Sustain Energy Rev 90:1017–1026
11. Hideki W, Fumio Y, Kenji U, Toshiyuki Y (2011) Generation characteristics of 100 kW PV system with various tilt angle and direction arrays. Elsevier J Sol Energy Mater Sol Cells, 382–5
12. Bentouba S, Bourouis M, Zioui N, Pirashanthan A, Velauthapillai D (2021) Performance assessment of a 20 MW photovoltaic power plant in a hot climate using real data and simulation tools. Energy Reports 7:7297–7314
13. HadiVatankhahGhadim JF (2022) Technical design and environmental analysis of 100-kWp on-grid photovoltaic power plant in north-western Iran. Clean Energy 6(2):362–371
14. Chattopadhyay M, Rajavel R (2018) A comparative study on performance of a grid connected solar PV system installed in the urban, rural and coastal region of India. In: 2nd international conference on inventive systems and control (ICISC), Coimbatore, India, pp 131–135
15. Abdalla SNM, Özcan H (2021) Design and simulation of a 1-GWp solar photovoltaic power station in Sudan. Clean Energy 5(1):57–78
16. Sharma V, Chandel SS (2013) Performance analysis of a 190 kWp grid interactive solar photovoltaic power plant in India. Energy 55:476–485
17. Okello D, van Dyk EE, Vorster FJ (2015) Analysis of measured and simulated performance data of a 3.2 kWp grid-connected PV system in Port Elizabeth, South Africa. Energy Convers Manage 100:10–15
18. Ashwini K, Raj A, Gupta M (2016) Performance assessment and orientation optimization of 100 kWp Grid connected solar PV system in Indian scenario. In: IEEE international conference on recent advances and innovations in engineering (ICRAIE-2016), Jaipur, India

Fault Classification of Dry Type Transformer Using Pattern Recognition Neural Network

Pankaj Kumar and Piush Verma

1 Introduction

Dry type transformer has benefits of fireproof, convenient maintenance, burning isolation and dustproofing. The temperature has a significant impact on the dry transformer's failure. The winding insulations breaks down whenever there is surpassing of insulation bearing temperature, which is the main cause of the transformer failure. Therefore, real time monitoring will help in maintaining the windings temperature within the permissible limits, which improves its reliability and working service life.

The process of manufacturing cast resin transformer involves complex pouring process of the winding insulation which can be avoided by designing and manufacturing of the transformer using silicone insulated rubber [1]. The designers of transformer generally use some design curve patterns or thermal analysis method to predict the temperature rise in the windings of the transformer.

To understand the thermal stress effectively different temperature locations and distribution need to be analyzed in different operating conditions. The temperature distribution of windings is not uniformly distributed, the temperature at the lower surface is cooler than the upper [2]. The inside part average temperature rise is higher than the outside part and its good for depicting the hot spot of the temperature rise of LV winding. The internal temperature variable is the one of the most important design parameters of the dry transformer which directly affects its working life [3].

To identify the effect of temperature in the DTT previously partial discharge localization with multiple sensors technique was popular [4]. Then mathematically modelled were used to analyze the temperature distribution in DTT proposed by Rahimpour [5]. Eslamian [6] presented a thermal model of the non-uniform power losses temperature distribution using foil windings for ventilated DTT.

P. Kumar (✉) · P. Verma
National Institute of Technical Teachers and Research, Chandigarh 160019, India
e-mail: pankaj.elect2019@nitttrchd.ac.in

S. Doolla et al. (eds.), *Advances in Renewable Energy and Its Grid Integration*,
Lecture Notes in Electrical Engineering 1041,
https://doi.org/10.1007/978-981-99-2283-3_4

For the analysis of the temperature of the LV and HV windings using simulation software's Finite Element Method (FEM) [7, 8], SOLIDWORKS using COSMOL [9], LabVIEW [10] were used. Aksu [11] presented new optimization methods Invasive Weed Optimization (IWO) and the Firefly Algorithm (FA) for the reduction in weight and losses. Wang [12] presented the model to analyze the hotspot temperature rise and insulation life loss of the transformer. Ebenezer [13] determine the winding temperature and thermal stress points using soft computing techniques.

For conditioning monitoring several literatures have investigated their results and some are discussed further. Srinivasan [14] presented low-cost digital measurement system for measuring temperature rise in 3 phase transformers. Khandait [15] used IoT with embedded system to remotely control management of the temperature of dry transformer. Finocchio [16] applied the neural network to the data collected for the 300 dry transformers of the same manufacturer to identify the which internal variables directly affects the lifetime of the dry transformer. Kumar [17] reviewed condition monitoring of oil filled distribution transformers and dry transformers. IoT has gained the lot of attention of the researchers to analyze the real time data more of oil filled transformers then dry type transformers [18–21]. Due to oil transformers extensive usage in the distribution its research is gaining more attraction. Different sensor in combination of microcontrollers like NodeMCU, Arduino, Arduino nano etc. has been used to gather real time data [22]. ANN used for the fault diagnosis of the power transformer using MATLAB software and health index described in [23, 24].

The implementation of a Feed-forward Back Propagation Neural Network (FFBPNN) for identifying and diagnosing various DTT failures scenarios is explained in this research article. For classification of DTT faults, Pattern-Recognition Neural Network (PatternNet), which is a form of FFBPNN is used to recognize patterns. The Pattern-Recognition Neural Network (PatternNet), a form of ANN, is designed to detect input data that corresponds to distinct classes. In FFBPNN supervised learning method is used to train, where the dataset consists of binary values of 1's symbolizes the inherit class and 0's for other class. The different tests time domain parameters of the DTT were extracted and used as input for the neural network.

The two training functions '**trainlm**' and '**trainscg**' of ANN were used to train the network with different layers of neurons. Their results, comparison and performance for each case is presented.

2 Artificial Neural Network (ANN)

ANN is clone of the human brain which consists of group of nodes called neurons. In ANN there are 3 layers- Input layer, Multiple layers (Hidden layers) and Output layer. The fundamental construction of an ANN is shown in Fig. 1, which comprises of neurons, linking weights, and biases. The three layers are connected through

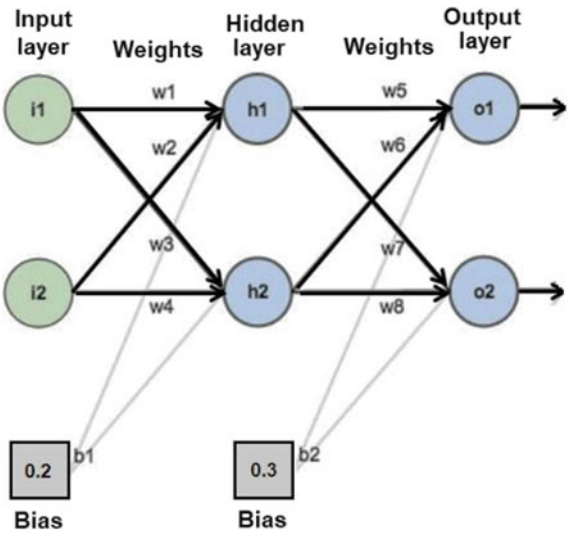

Fig. 1 Basic structure of artificial neural network

connection weights shown by arrows, the circular nodes represent the Artificial neurons.

The most widely used ANN is multi-layered feed forward back propagation neural network (FFBPNN) which uses the backpropagation technique for training. With backpropagation (BP), the ANN performance comes out to be best after determining the appropriate number of hidden layer of neurons. Basically, if the network is small then it is not able to learn and if the network is large then it will have poor generalization. With a large training dataset, the ANN's performance increases but this required more training time. As a result, a variety of BP training algorithms are utilized to increase performance with less training time.

While training the BP algorithm, it adjusts the weights to the steepest descent (i.e., adverse gradient). This path does not guarantee the quickest convergence due to the degradation of the performance function very fast. For faster convergence, conjugate gradient (CG) based training method is used. When using CG based training methods, the search is done in conjugate directions, which usually results in a faster convergence than the steepest descent path. In CG algorithm, the step size is changed for each iteration. In CG direction search is performed to find the step size for which the performance function is least for a specific search path.

Trainscg is a backpropagation training technique that uses the Scaled Conjugate Gradient (SCG) algorithm to update network weights and biases. The **trainlm** method is the fastest for training networks of medium size network. **Trainlm** is the most generally suggested and utilized training technique for achieving greater classification accuracies, but using more memory than other training methods. It is based on the Levenberg–Marquardt (LM) backpropagation algorithm, which is one of the most efficient backpropagation algorithms for neural network training.

3 Experimental Setup and Data Collection

The experimental setup consists of a 1-ϕ 1 KVA, 50 Hz 220/110 step down dry transformer connected with Single Phase Variable Transformer (1-ϕ Variac). The DTT primary terminal connected to the 1-ϕ Varic and it is connected to the single-phase ac supply of 240 V. In the Fig. 2 shows the experimental setup of the online monitoring of DTT, data acquisition using sensors, acquiring data on IoT cloud platform. To acquire the real-time values of temperature measurement two temperature sensors (MAX6675) one for core and other for winding temperature measurement, for current measurement current sensor (ACS712), for voltage measurement voltage sensor (ZMPT101B) is used. All the sensors were interfaced with Arduino Uno board through jumper wires and board connected to the personal computer via USB interface.

ESP8266 Wi-Fi module is used to send the data obtained by Arduino's flash memory to the IoT cloud platform ThingSpeak. The personal computer used the serial monitor software of the Arduino IDE. ThingSpeak platform shows the real time data of the different parameters of DTT. Tables 1 and 2 provide the technical specs of the DTT and other hardware materials employed.

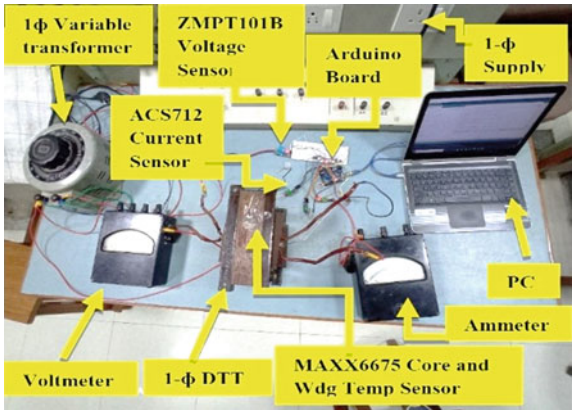

Fig. 2 Lab setup of dry type transformer fault detection

Table 1 Specifications of dry type transformer

Parameters	Value
Transformer type	1-phase, dry type transformer
Power rating	1 KVA
Frequency	50 Hz ± 3%
Current	4.20 A
Cooling type	Dry type/air cooled
Voltage ratio	220/110 V
Winding material	Copper

Table 2 Hardware components specifications

Materials	Specifications
Current sensor	ACS712 current sensor
	Supply voltage—5 V
	Sensitivity—100 mV/A
	Range—20 A AC/DC
Arduino Uno	Microcontroller: ATmega328P
	Digital I/O pins: 14 (with 6 PWM output)
	Operating voltage: 5 V
	Analog input pins: 6
	Voltage (input)—7 to 12 V
	Memory: 32 KB flash memory, 2 KB SRAM, 1 KB EEPROM
Personal computer	Processor—Intel(R) Core (TM) i3-7th Gen
	Processor speed—2.40 GHz
	RAM—8 GB
	Hard disk—512 SSD
	Windows—windows 7 home
Voltage sensor	ZMPT101B digital voltage sensor
	Range—0–1000 V
	Sampling resistor-100 Ω
	Rated input/output current—2 mA
	Turn ratio-1000:1000
	Operating temp—40 °C ~+ 60 °C
	Isolation voltage—4000 V
Temperature sensor	Max6675-Digital K-type thermocouple
	Temperature measuring range—0–1024 °C
	Operating temperature range—20–85 °C
	Resolution—0.25 °C
	Supply voltage—3–5 V

Online data was collected through sensors on the IoT cloud platform software ThingSpeak for 60 runs for each test was acquired. The TX and RX pins of the Arduino used for transferring the data from the board to personal computer via USB serial port having 9600 baud rate.

4 Proposed Work

In this proposed work real time data of the DTT parameters of fault conditions were recorded from the sensors are collected over the IoT cloud platform Thingspeak as shown in Fig. 3a-c.

In Fig. 4. Warning alert message for winding temperature limit exceeding above 32 °C is shown as per the DTT datasheet. The cast resin DTT was operated under different test conditions and its parameters like temperature, voltage and current has acquired using the IoT based data acquisition system.

Artificially different fault conditions are induced in the DTT and the real time data is collected for each fault one by one. Below are the various DTT conditions that are taken into account:

1. Healthy DTT (HEALTHY)
2. Open Circuit Fault (OCF)
3. Overload Fault (OLF)
4. Short Circuit Fault (SCF).

Pre-processing and feature extraction steps followed by data acquisition, when the data obtained from IoT cloud platform. The real time data is checked for the time domain features and meaningful values are retrieved, respectively.

Fig. 3 **a** Open circuit fault data on IoT platform **b** short circuit fault data on IoT platform **c** overload fault data on IoT platform

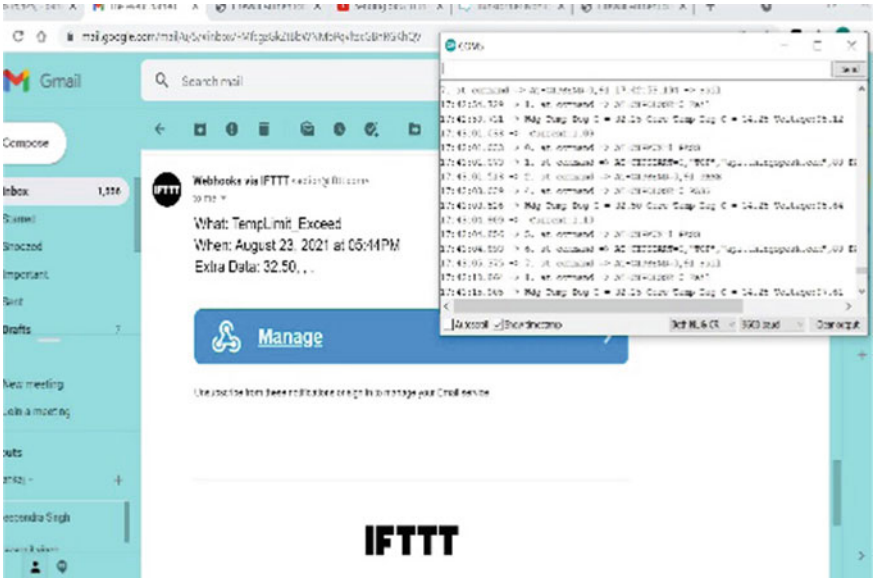

Fig. 4 Waring alert message for temperature limit exceeding

Before feeding the real time data to ANN as an input for training and testing, its features were scaled (normalized) within boundaries of [0 1]. This stage assures that all the features (ANN inputs) were assigned equivalent weights. The above process is followed to enhance classification results and remove any unnecessary bias toward any one trait. The input feature matrix has 432 rows which are feature vectors and 4 columns of features, equivalent to 27 runs for 4 DTT conditions, which were collected by measuring winding temperature, core temperature, voltage and current, resulting in a total of 432 feature vectors. The pattern recognition neural network's output feature matrix was chosen in the manner mentioned below:

$$\text{HEALTHY} : \begin{bmatrix} 1 & 0 & 0 & 0 \end{bmatrix}^{\mathrm{T}}$$

$$\text{OCF} : \begin{bmatrix} 0 & 1 & 0 & 0 \end{bmatrix}^{\mathrm{T}}$$

$$\text{SCF} : \begin{bmatrix} 0 & 0 & 1 & 0 \end{bmatrix}^{\mathrm{T}}$$

$$\text{OLF} : \begin{bmatrix} 0 & 0 & 0 & 1 \end{bmatrix}^{\mathrm{T}}$$

The input feature matrix was divided into two datasets: Training (302) and Testing (130), with 65 validation samples and 65 testing samples for DTT condition. Using two different algorithms (**trainlm** and **trainscg**) PatternNet was trained. By changing the different numbers of hidden layers of neurons the performance of the PattenNet was checked to see how well it performed and whether it was suitable for the given classification challenge. The best result (classification accuracy) is achieved after

training and testing of each network eight times with the same dataset. To obtain best validation overall performance for different network configurations, Mean Square Error (MSE), total number of epochs, and classification accuracy of testing dataset were selected.

5 Results and Discussion

Tables 3 demonstrate the results achieved for multiple hidden layers of neurons using scaled conjugate gradient and Table 4 demonstrate the results achieved for multiple hidden layers of neurons using Levenberg–Marquardt training algorithms. Also, using the **trainscg** and **trainlm** training algorithms, the network with 8 hidden layer neurons achieves the maximum testing accuracy, 76.6% and 92.2%, respectively. As a result, it is evident that both training algorithms work best for the 8 hidden layers of neurons, for the classification of the faults conditions of DTT in the given task.

According to the obtained results for **trainlm** function, the training validation error and testing performance (MSE) for different number of hidden layers of neuron is

Table 3 Results with **trainscg** training function

No. of hidden layers of neurons	Training		Testing	
	Validation performance (MSE)	Epochs	Testing performance (MSE)	Classification accuracy (%)
2	0.0909	32	0.1017	56.2
4	0.1201	25	0.1074	59.4
6	0.1136	16	0.1073	67.2
8	0.0968	28	0.0975	76.6
10	0.0676	39	0.0853	67.2
12	0.0891	36	0.0933	71.9

Table 4 Results with **trainlm** training function

No. of hidden layers of neurons	Training		Testing	
	Validation performance (MSE)	Epochs	Testing performance (MSE)	Classification accuracy (%)
2	0.0787	33	0.0875	73.4
4	0.0753	18	0.0726	70.3
6	0.0590	15	0.0543	86.9
8	0.0521	14	0.0483	92.2
10	0.0920	21	0.0691	85.2
12	0.0687	18	0.0597	78.1

least than for **trainscg** function. The number of epochs is less (14 epochs) for **trainlm** than for **trainscg** (28 epochs). This demonstrates that, when compared both training functions **trainscg** (PatternNet's default training function) and **trainlm**, the **trainlm** completes training fast and provides more accurate outcomes for pattern recognition neural networks.

For **trainscg** function the validation performance (MSE) and epochs of the training reduces as the number of hidden layers are increasing to a point (28 for 8 hidden layer neurons). As the number of hidden layers are increasing testing performance (MSE) is decreases and classification accuracy increases. On the other hand, the obtained results for **trainlm** function achieved best for eight hidden layers of neurons for validation performance (MSE), testing performance (MSE), and classification accuracy.

The plot of classification outputs and target output of **trainscg** function and **trainlm** function of PatternNet for 8 hidden layer neurons for different DTT conditions are shown in Fig. 5a, b. The target output and output points overlap each other are accurately identified testing samples. Therefor it is evident that **trainlm** provides the less number of incorrect classifications.

The confusion matrix was shown in the Fig. 6a for the **trainscg** function for 8 hidden layers of neuron in which out of 31 training samples 6 samples of HEALTHY class were misclassified as OLF, SCF, OCF (i.e. 19.4% inter-class misclassification). In OCF out 12 training samples 2 were misclassified as Healthy (i.e. 16.7% inter-class misclassification). In SCF misclassification is 21.4% and for OLF its 25.0%. Overall, using the **trainscg** function 76.6% samples were accurately classified and 23.4% were misclassified. In the case of **trainlm**, however, no such occurrence was found. The confusion matrix for **trainlm** function accurately recognized OCF, SCF, and HEALTHY situations with a 100% classification rate for 8 hidden layers of neurons as shown in Fig. 6b. Overall **Trainlm** function accurately classify 92.2% samples and 7.8% samples were misclassified. **Trainlm** function achieves higher classification accuracy overall (both inter-class and intra-class) than **trainscg**.

6 Conclusion and Future Scope

The experimental work in this research is done for the categorization of various DTT faults. The PatternNet NN was built with a customizable number of hidden layers of neurons using two different training algorithms for categorization of DTT errors. **Trainlm**'**s** overall classification results are substantially better than **trainscg's**. The **trainlm** method's analysis outputs efficiently classify DTT states with high accuracy (92.2%). This demonstrates that the proposed approach is effective in detecting DTT

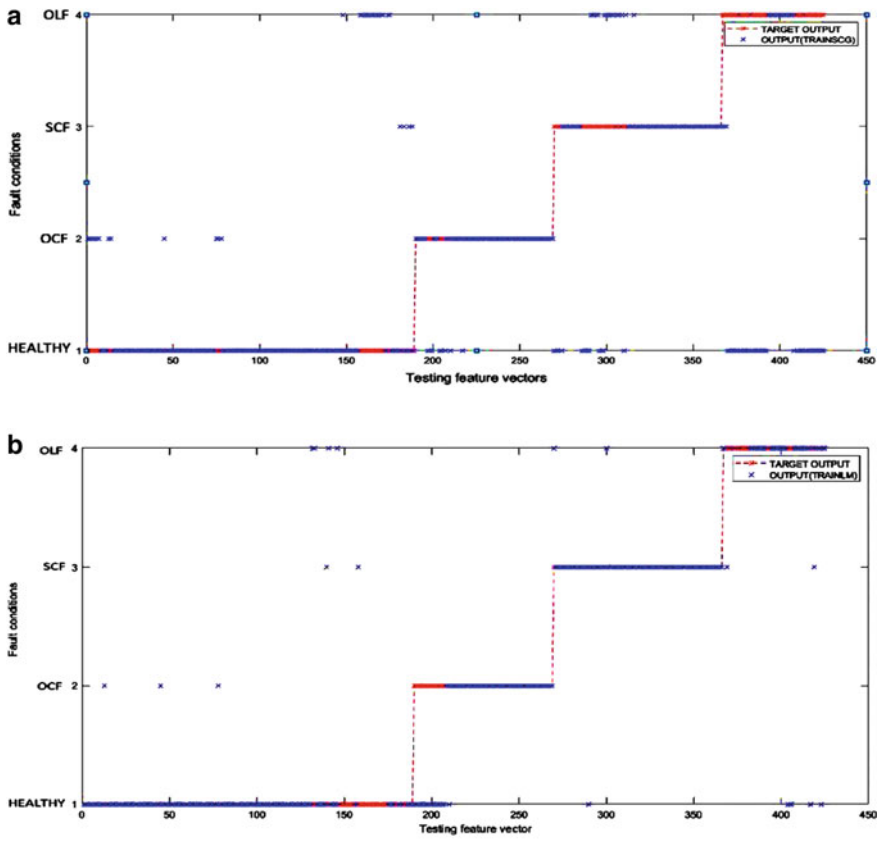

Fig. 5 **a** Plot of PatternNet target and actual outputs using **trainscg** function **b** plot of PatternNet target and actual outputs using **trainlm** function

defects. This work might be expanded by approaching new algorithms machine learning classification techniques, regression, clustering and others can be explored to improve the efficiency of the current work's classification performance.

For categorization purposes, a larger number of DTT defects, such as magnetizing inrush current, operating noises, and so on, can be considered.

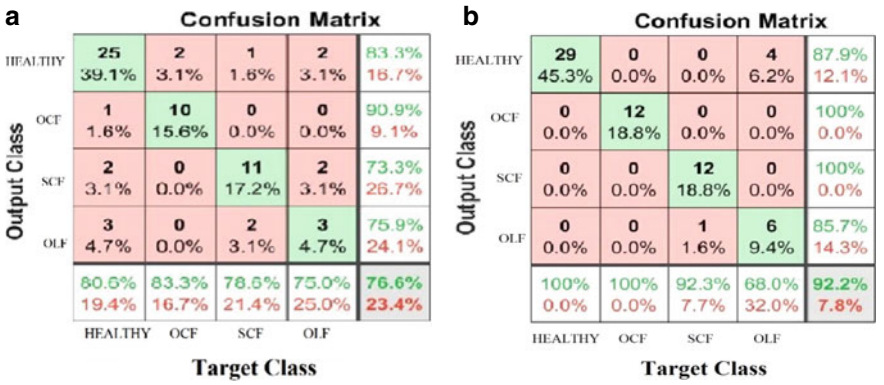

Fig. 6 **a** Confusion matrix for **trainscg** function with 8 hidden layers of neurons **b** confusion matrix for **trainlm** function with 8 hidden layers of neurons

References

1. Institute of Electrical and Electronics Engineers, ITEC 2016 (2016) IEEE transportation electrification conference and expo, Asia-Pacific : (ITEC Asia-pacific): June 1–4, 2016, BEXCO, Busan, Korea
2. Lee M, Abdullah HA, Jofriet JC, Patel D (2010) Temperature distribution in foil winding for ventilated dry-type power transformers. Electric Power Syst Res 80(9):1065–1073. https://doi.org/10.1016/j.epsr.2010.01.013
3. Jahromi A (2009) Power transformer asset management using health index
4. Thungsuk N et al (2022) The investigation of detect position of partial discharge in cast-resin transformer using high-frequency current transformer sensor and acoustic emission sensor. Appl Sci (Switzerland) 12(3). https://doi.org/10.3390/app12031310
5. Rahimpour E, Azizian D (2007) Analysis of temperature distribution in cast-resin dry-type transformers. Electr Eng 89(4):301–309. https://doi.org/10.1007/s00202-006-0008-4
6. Eslamian M, Vahidi B, Eslamian A (2011) Thermal analysis of cast-resin dry-type transformers. Energy Convers Manage 52(7):2479–2488. https://doi.org/10.1016/j.enconman.2011.02.006
7. Ning W, Ding X (2012) Three-dimensional finite element analysis on fluid thermal field of dry-type transformer. In: Proceedings of the 2012 2nd international conference on instrumentation and measurement, computer, communication and control, IMCCC 2012, pp 516–519. https://doi.org/10.1109/IMCCC.2012.128
8. Torin LR, Medina DOG, Sousa T (2019) Dry-type power transformers thermal analysis with finite element method. Int J Adv Eng Res Sci 6(3):159–165. https://doi.org/10.22161/ijaers.6.3.19
9. Ding X, Ning W (2012) Analysis of the dry-type transformer temperature field based on fluid-solid coupling. In: Proceedings of the 2012 2nd international conference on instrumentation and measurement, computer, communication and control, IMCCC 2012, pp 520–523. https://doi.org/10.1109/IMCCC.2012.129.
10. LabVIEW with Fuzzy Logic Controller dry type muhammud 2008
11. Aksu İÖ, Demirdelen T (2018) A comprehensive study on dry type transformer design with swarm-based metaheuristic optimization methods for industrial applications. Energy Sources Part A Recovery Utilization Environ Effects 40(14):1743–1752. https://doi.org/10.1080/15567036.2018.1486908

12. Quan YS, Fang LJ, Wang ZJ, Shi PX (2014) Study of the winding temperature distribution for distribution transformers. Appl Mech Mater 672–674:1380–1383. https://doi.org/10.4028/www.scientific.net/AMM.672-674.1380
13. Determination of winding temperature of a distribution transformer using soft computing techniques
14. Srinivasan M, Paramasivam S, Krishnan A (2011) Low cost digital measurement system for determination of temperature rise in dry type transformer
15. Khandait AP, Kadaskar S, Thakare G, Professor A, Scholar U (2017) Real time monitoring of transformer using IOT." [Online]. Available www.ijert.org
16. Finocchio MAF, Lopes JJ, de França JA, Piai JC, Mangili JF (2017) Neural networks applied to the design of dry-type transformers: an example to analyze the winding temperature and elevate the thermal quality. Int Trans Electr Energy Syst 27(3). https://doi.org/10.1002/etep.2257
17. Kumar P, Verma P (2021) Review paper on diagnostics study of dry transformer
18. Sejdiu B, Ismaili F, Ahmedi L (2020) Integration of semantics into sensor data for the IoT: A systematic literature review. Int J Semantic Web Inf Syst 16(4). IGI Global, pp 1–25. https://doi.org/10.4018/IJSWIS.2020100101
19. Soppimath VM, Sheeri P, Kalakaraddi R, Kumar CS, Kumar CS (2018) Monitoring and control of operational parameters of distribution transformer using IoT technology distribution transformer using IoT technology. Int J Adv Sci Eng 5(1):871. https://doi.org/10.29294/ijase.5.1.2018.871-878
20. Bethalsha C (2020) Real-time transformer health monitoring using IOT. Int J Res Appl Sci Eng Technol 8(9):521–526. https://doi.org/10.22214/ijraset.2020.31512
21. Vinoth MD, Ganapathi R, Dineshkumar C, Sathish C International Journal of Advanced Research in Electrical, Electronics and Instrumentation Engineering IOT Based Distribution Transformer Monitoring System. [Online]. Available www.ijareeie.com
22. Professor A Design and implementation of real-time transformer health monitoring system using Raspberry-Pi." [Online]. Available www.ijert.org
23. Kumari P, Kaur K, Singh J (2016) Condition monitoring of power transformer using ANN for IEC based on DGA
24. Doğuş Üniversites Istanbul (2011) International symposium on innovations in intelligent systems and applications 2011.06.15–18 Istanbul, and INISTA 2011.06.15–18 Istanbul. International symposium on innovations in intelligent systems and applications (INISTA), 2011 15–18 June 2011, Istanbul, Turkey

Design and Development of Emulated Fuel Cell Based Hierarchical Controlled DC Microgrid System

Ameya Thale, Udayraj Tawde, Avinash Saruk, Shreyas Sarnaik, and Sushil Thale

1 Introduction

With a critical need to reduce dependency on fossil fuels, significant research has been carried out in electricity generation using renewable energy sources (RES) such as solar, wind, tidal energy and many more. However, due to the intermittent nature of RES, the grid stability gets challenged. Hence, integration of various RES along with energy storage system (ESS) interfaced to a AC or a DC microgrid can be a solution to the above-mentioned problem which can control power sharing during unpredictable load demands using a communication interface. Use of a DC microgrid is preferred over AC microgrid because of its several advantages such as reduced cost and size of microgrid along with higher efficiency. Since the ratio of DC loads to AC loads is increasing, the requirement of number of power electronics convertor is reduced which eventually increases the efficiency.

Use of CAN communication in the system facilitates a better control for power sharing among the microgrid sources and to have better bus voltage regulation. To have a balanced and stable DC microgrid system, it is required to control the power flow of the microgrid under various scenarios to which the system may be subjected to during the course of its operation.

This research work essentially involves up-gradation of existing DC microgrid in the lab. The existing microgrid has two Solar Photovoltaic sources (SPV—each 1 kW) interfaced with DC-DC boost convertors and a Distributed Battery Energy Storage (DBES) system connected to the Microgrid DC Bus of 48 V. DBES system is interfaced with a bi-directional converter to maintain charge and discharge of DBES. An emulated Fuel Cell source is interfaced with the existing DC microgrid to study

A. Thale · U. Tawde · A. Saruk · S. Sarnaik · S. Thale (✉)
Department of Electrical Engineering, Fr. Conceicao Rodrigues Institute of Technology, Navi Mumbai, Maharashtra, India
e-mail: sushil.thale@fcrit.ac.in

S. Doolla et al. (eds.), *Advances in Renewable Energy and Its Grid Integration*,
Lecture Notes in Electrical Engineering 1041,
https://doi.org/10.1007/978-981-99-2283-3_5

and verify the system performance improvement. Various simulations of voltage and current controlled loops were carried out. DSP control board TMS320F28379D was programmed and interfaced with the power converters in order to control their operation and allow proper load sharing during unpredictable load demands. CAN communication protocol was implemented in order to establish communication between the DSP controllers to ensure load sharing and regulation of MG bus voltage.

The paper presents some insights into the design, development and testing of low power low voltage autonomous DC microgrid with hierarchical control. Each power converter is interfaced with a local controller, and these local controllers are linked with a supervisory controller which eventually controls the operation of each local controller. Thus, two-level hierarchical control strategy was implemented.

2 Literature Review

2.1 DC Microgrid

In a DC microgrid, ESS plays a significant role in storing the excess energy generated and supplying it to the loads to bridge the demand supply gap. The batteries are preferred for ESS due to their high energy density and low cost. The Ultracapacitors are preferred for fulfilling the transient load requirements due its fast dynamic response and high power density [1, 2].

The hierarchical control is adopted for reliable and optimize operation of a standalone dc microgrid. The hierarchical control is typically composed of multi-layers or multi-level control. The primary control formulates as first layer directly acting on the power converters to provide high speed controls. The higher-layer controls provide functionalities like bus voltage control ensuring optimized microgrid operations. This control strategy is a combined form of Decentralized (Only Local controllers) and Centralized control (Master–Slave configuration) [1].

The different types of power converters used for controlling the power delivered or absorbed by the DC microgrid resources. Typically, buck converter, boost converter and bidirectional converter (BDC) are used [3].

2.2 Microgrid Power Management

The power management in a microgrid is the optimal administration of total power generated and demanded. This involves source optimization, ESS management, power import/export and stability of microgrid bus voltage. The dispatchable sources like battery or fuel cell operate typically as voltage sources whereas the non-dispatchable sources like SPV or wind operate as current sources [4]. In decentralized control strategy, the droop control is used for the microgrid sources [5]. The main

disadvantage of droop control is its poor dynamic response. As reported in [6], the proposed hybrid control scheme, with average current and voltage controllers are employed in each converter to enhance current sharing accuracy and retain the bus voltage simultaneously.

2.3 Fuel Cell as Microgrid Source

A Fuel Cell (FC) produces current based on chemical reaction facilitated by the mixture of reactants, electrolyte and catalyst. Thus, it's dynamic response is slow compared to that of a battery. Additionally, there is a huge voltage drop from no load to full load condition for a fuel cell. But still FC is very useful DC microgrid source being dispatchable and long-term availability point of view. In this research work, the fuel cell (FC) characteristic as shown in Fig. 1 that is similar to the Ballard 'Nexa' PEMFC model is emulated. The Nexa PEMFC has a capacity of 1.2 kW, output voltage of 24 V. The FC output is then boosted to 48 V with the help of a boost converter. The boost converter provides 48 V and 21 A which is equivalent to 1KW of power drawn from the Fuel Cell. As load changes the output voltage changes exponentially, while the rise in temperature and humidity also affects the curve. Increasing stack temperature generally causes an increase in output voltage, i.e., it shifts the I-V curve upward.

3 System Description

The existing microgrid lab setup had two Solar Photovoltaic sources (SPV) each interfaced with DC-DC boost converters and one Battery based source all of which were interfaced to the DC microgrid bus of 48 V. The battery source is interfaced

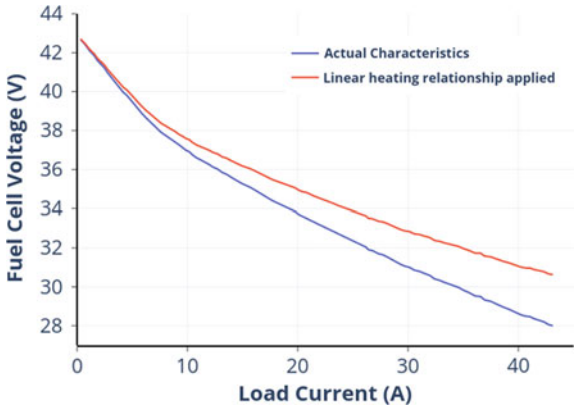

Fig. 1 Characteristics to be emulated fuel cell

with a bi-directional converter to facilitate the charge and discharge operation. The microgrid was built for total capacity of 3 kW with 840 Whr battery ESS. The local controllers select appropriate mode of operation viz. Current Mode control (CMC), Voltage Mode control (VMC) or Maximum power extraction mode based on the communication received from the supervisory control. The SPV power converters are designed to operate in all 3 modes. While BDC for ESS are designed to operate in VMC and CMC mode.

3.1 Boost Converter and Fuel Cell Emulation

The primary physical modification in the DC microgrid is that of an emulated Fuel Cell stack (FCS), proposed to be interfaced with the DC bus through a Boost converter. Following section will highlight the design considerations for the boost converter and steps taken to emulate the FCS source.

Boost Converter Calculations

1. The input voltage range of Boost converter is considered as,

   Input voltage at No Load ($V_{\text{in(max)}}$ at NL) = 48 V
   Input voltage at Full Load ($V_{\text{in(min)}}$ at FL) = 24 V

2. The maximum output voltage of boost converter (V_o) = 48 V
3. The maximum output current

$$I_{\text{out}} = \frac{\text{P}_{\text{out}}}{\text{V}_{\text{o}}} = 21\,\text{A}$$

4. The Duty cycle(D) of converter is calculated from the following formula

$$D = \frac{\text{Vo}}{V_{\text{in(min)}}} = 0.5 \tag{1}$$

5. Selection of Inductor-

Often data sheets give a range of recommended inductor values. If this is the case, it is recommended to choose an inductor from this range. The higher the inductor value, the higher is the maximum output current because of the reduced ripple current. The lower the inductor value, smaller is the solution size. Note that the inductor must always have a higher current rating than the maximum current because the current increases with decreasing inductance.

First, a minimum value of Inductor is calculated which also requires calculation of minimum input current $I_{\text{in(min)}}$. In a Boost Converter, this taken as 5–10% of maximum load current (drawn by the dummy load).

$$I_{\text{in(min)}} = 10\% \times 21 = 2.1\,A$$

Input voltage V_{in} or the nominal input voltage is taken as 36 V (between 24 V and 48 V).

$$L_{\text{min}} = \frac{D_{\text{min}} \times V_{\text{in}}}{2 * I_{\text{in(min)}} \times fs} = 0.143\,\text{mH} \tag{2}$$

While the calculated L_{min} value is 143 uH, the actual inductor L_{act} to be used is 5 to 10 times this value.

$$L_{\text{act}} = 5 \times L_{\text{min}} = 715\ \text{uH} \tag{3}$$

We had a readily available 500 uH/50 A inductor available in the lab, so it was selected for the physical implementation of the converter.

6. Selection of Capacitor-

The following formula was used for calculation of output capacitor, taking 1% ripple in the output voltage

$$C_{\text{out(min)}} = \frac{\text{Io(min)} \times \text{D}}{\text{fs} \times \Delta \text{V}_{\text{out}}} = 1500\ \text{uF} \tag{4}$$

We had a readily available 2000 uF/450 V capacitor available in the lab, so it was selected for the physical implementation of the converter.

FC Emulation. The FC emulation was done using the LabVIEW platform, with a Programmable DC source (PDCS). The voltage output of the PDCS modified to track the set FC VI characteristics for a given load condition. Figure 2 shows boost converter setup and FC emulation screenshot.

By using the LabVIEW, the voltage of the DC source was set according to the Fuel Cell characteristics for which the data points were collected from the VI characteristic graph plot. The LabView VI developed was able to mimic the characteristics of

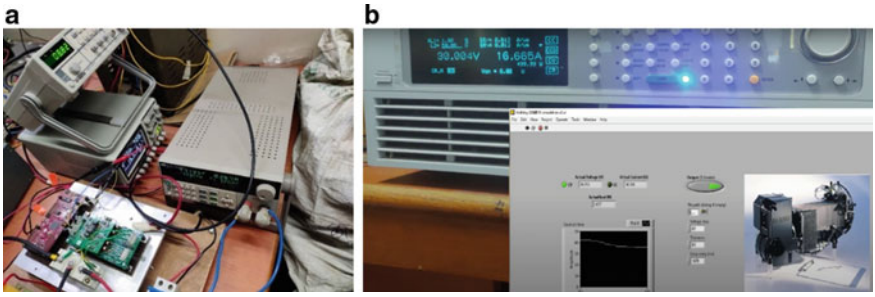

Fig. 2 **a** Boost converter setup **b** FC emulation using LabVIEW and electronic load

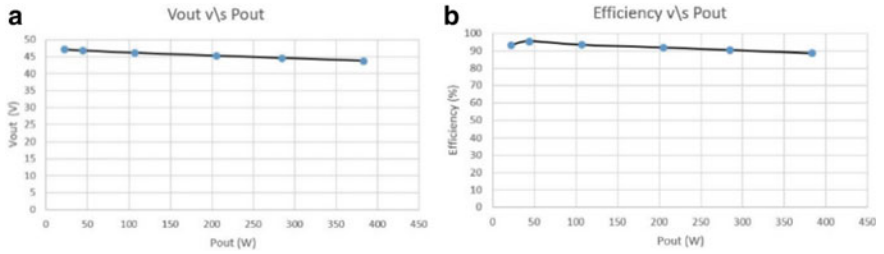

Fig. 3 FC emulation graphs-load variation **a** V_{out} versus P_{out}; **b** efficiency versus P_{out}

Emulated Fuel Cell source, while tracking the input side voltage, current and actual load connected to the microgrid. Figure 3 shows the FC emulation graphs obtained with hardware setup. Also, a provision was made to add a delay to the response of the emulated FC which could be arbitrarily control using some variables. The PI controller was implemented in digital form using the DSP board in TI's Code Composer Studio.

For giving the analog voltage to the DSP, a simple voltage divider attenuator was made. The pulses generated by the DSP were given to the gate driver (SKYPER32R) for the IGBT (SKM145GB066D) after appropriate voltage level shifting.

3.2 Hierarchical Control Strategy

The Fig. 3 shows the schematic block diagram representation of the DC microgrid under study. The hierarchical control is implemented through TI DSP TMS 320F28379D controller boards interfaced with each other on CAN communication.

Local Control: This level of control is basically required for generating the switching pulses for the converters used for all the sources. Each of the sources will be configured in various modes as per their expected function in the control strategy.

1. **SPV**—MPPT mode
2. **FCS**—Current control mode, Voltage control mode
3. **Battery**—Current control mode, Charging mode.

Supervisory Control: By using CAN communication, coordination for the power sharing between each source is achieved. Supervisory control makes decisions as per the situation demands [7]. Both of the control layers above will be implemented in the form of code using Texas Instruments' TMS320F28379D DSP development board.

Testing Scenarios: The microgrid is bound to encounter various different scenarios with respect to variable parameters like solar insolation, Hydrogen availability (fuel for FC), SOC of battery and load demand at that particular instant. Operation has to be carried out while keeping the DC bus voltage within permitted limits and at the same

time ensuring power is taken from the appropriate source. For instance, management of battery SOC is important, as it has a limited number of charge discharge cycles which have to be effectively utilized in order to prolong battery life. Thus, following scenarios/setups will be considered while building up an effective overall control strategy.

Scenario 1—Solar Insolation abundant, Fuel available, SOC full. SPV produces enough power to supply majority of the load demand and FCS can supply remaining load demand. As the Battery is fully charged, it will operate in voltage mode control, acting as a voltage source to keep the bus voltage constant while supplying bare minimum amount of current.

Scenario 2—Solar Insolation reduced, Fuel available, SOC low. Here, as insolation is reduced, SPV is not able to fulfill entire load demand and FCS has to supply more portion of the load. At the same time, as battery SOC is low, it will not supply any power and instead look for an opportunity to charge. Therefore, FCS has to maintain the bus voltage and also supply a significant portion of the load.

Scenario 3—Solar Insolation unavailable, Fuel available, SOC full. Considering operation during night time, where output of SPV will be zero, entire load demand has to be managed by the FCS and Battery. The battery is assumed to be charged by excess SPV generation throughout the day. In this case, the higher demand from evening to night (for illumination) has to be supplied primarily by FCS and additionally by the battery. Battery SOC should not fall below a minimum value, slightly above the absolute minimum in order to keep backup for the next morning.

4 Simulation of System

PSIM platform was used for the simulation and troubleshooting of the local level control of Boost Converter for the FC. In addition, power sharing models were also built to investigate the parallel operation of microgrid sources. Figure 4 shows Inner Current—Outer Voltage Control Loop implementation for FC boost converter.

4.1 Local Control of FC Boost Converter

The FC Source is represented by a current controlled voltage source using a simple line equation that approximates the input voltage of Fuel Cell based on the input current drawn. The boost converter design parameters are summarized in Table 1.

For an output voltage of 48 V, full load of approximately 1 kW is drawn by load resistor of 2.3 Ω—based on this fact, a variable load is designed with switches to trigger various loading conditions during simulation time. The two PI loops were tuned by trial and error process to obtain the following results shown in Fig. 5.

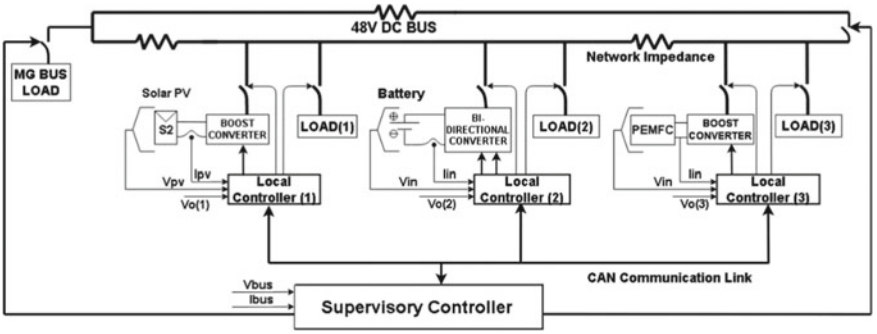

Fig. 4 System block diagram of the proposed DC microgrid setup

Table 1 Local control of FC boost converter—simulation details

S. No	Parameter	Values
Converter details		
1	FC input	48 V (no load) to 24 V (full load)
2	Bus voltage (output)	48 V
3	Switching frequency	15 kHz
4	L and r_L	500e−6 L, 30e−3 Ω
6	C and r_{ECR}	2200e−6 F, 0.5e−3 Ω
Inner PI loop		
7	Gain	7
8	Time constant	0.5e−3
Outer PI loop		
9	Gain	3.5
10	Time constant	15e−3
Load variation		
11	Time—0 to 0.25 s	2.33 Ω (full load)
12	0.25 to 0.5 s	4.63 Ω (half load)

4.2 Power Sharing

In this model, using two units of the same source and converter developed in the previous section, power sharing among the two parallel sources is observed by setting various reference values. One of the sources is under voltage control mode, whose job is to maintain the bus voltage and the other source is under current control mode, which will allow control over the current pumped into the load and thus the power. which should draw a total current of around 10.5 A from the sources. As shown in Fig. 6, the bus voltage is maintained at 48 V and the current share of source 1 and 2 can be varied depending on the current reference given to source 2.

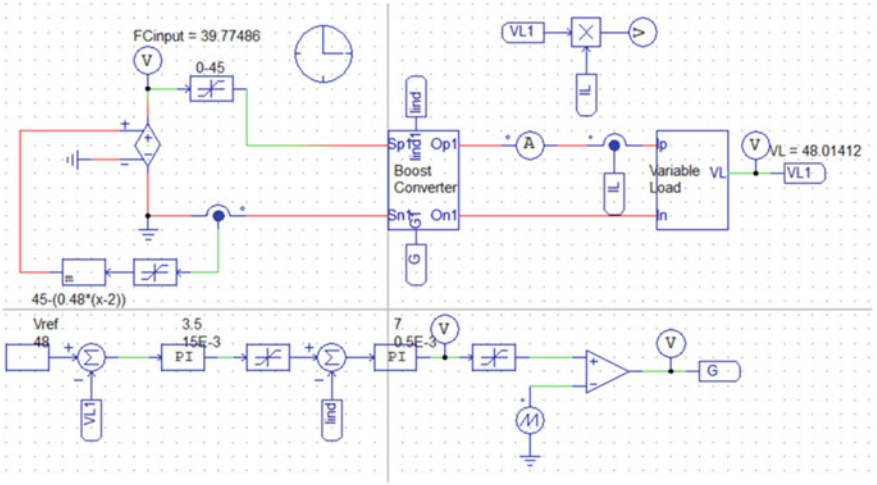

Fig. 5 PSIM simulation model: inner current—outer voltage control loop

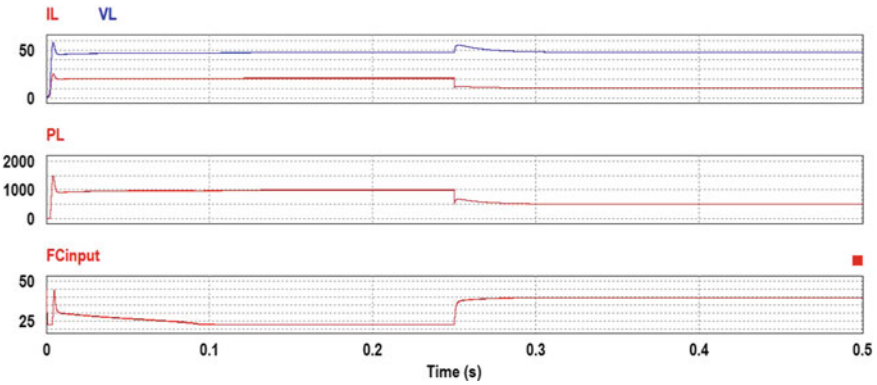

Fig. 6 Local control of FC boost converter—simulation results

Power Sharing with Two Sources: VMC and CMC

In the proposed setup as shown in Fig. 7a, Solar PV, Battery and Emulated Fuel Cell sources are used. The power sharing is decided by considering few important factors like capacity of each source, the time taken to deliver the power, for how long the power can be delivered by that source, availability of power in each source etc. Considering all these factors, scenarios were made where different sources are used in combination to power the load, such that power sharing is achieved in optimal manner.

The Solar PV source serves as the main source of power, whereas Fuel Cell can serve as backup source supply some base load, during fall in SPV output or periods of increased loads. The local controller helps to decide the amount of power

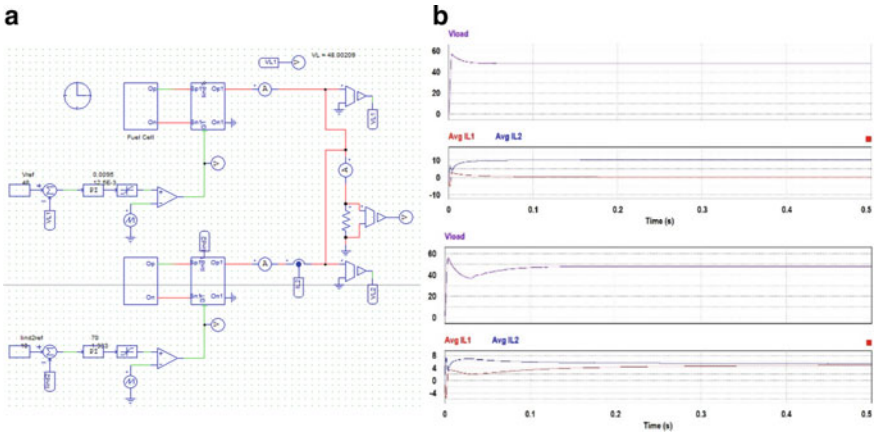

Fig. 7 **a** Power sharing model **b** simulation results **a** source 2 for 50% load current **b** source 2 with full load current

transferred from its respective source and the supervisory controller is responsible for communicating between the local controllers to make each of them aware of the status of other source and their attributes to optimize power sharing while maintaining the bus voltage.

The microgrid stability was tested with two sources—Fuel Cell and Battery assumed to power the load. The system was loaded up to roughly 20% of its capacity to observe power sharing between the emulated FC and battery source. For this, the FC was configured with VMC and Battery was configured with CMC. The VMC reference set to 48 V and the CMC reference was varied to emulate the decision given by the Hierarchical control. The results obtained are as shown in Fig. 8.

In scenario 1, the battery SOC is assumed to be sufficiently high and therefore it can share greater amount of load current. This behavior can be achieved by increasing the current reference for CMC source which will cause the current supplied by battery to increase and the current share of VMC source will reduce accordingly as per net load requirement. Conversely, in scenario 2, it is assumed that the battery SOC has fallen

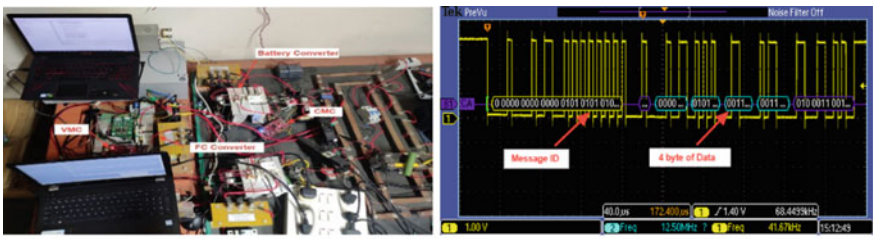

Fig. 8 **a** MG hardware setup with two sources **b** CAN communication pulses

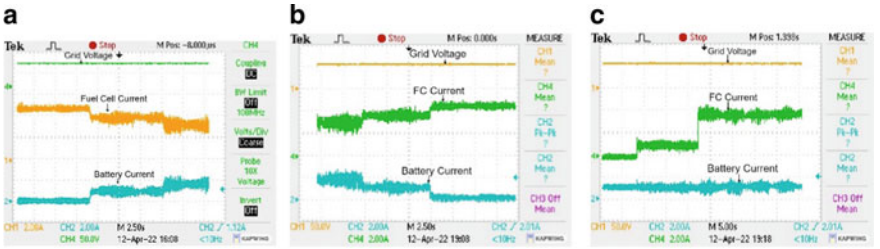

Fig. 9 Control over power share by variation in current reference **a** scenario 1: increase current reference, **b** scenario 2: decrease current reference **c** scenario 3: no change in current reference

below a certain threshold and the current drawn from battery needs to be reduced. Decreasing the current reference will relieve the CMC source and the majority of load current will once again be supplied by the VMC emulated FC source. In scenario 3, there is no change in the current reference and so the CMC source will supply constant share of power. For this situation, if the load demand increases, additional power required will be supplied by the VMC source. This behavior is apparent in the following waveform obtained, as the current supplied by emulated FC source increases as more load is added. During the test, according to the given load, the VMC Fuel Cell maintained 48 V and the CMC Battery supplied current according to the reference set at that time, rest of current being supplied by the other source (Fig. 9).

5 Conclusion

The paper presents details of design of a Hierarchical Controlled DC Microgrid. The simulation models in PSIM and Hardware setup validates the results of building blocks used in DC Microgrid. The emulated FC integrated with the existing DC Microgrid through the Boost Converter improves the stability of Microgrid as witnessed in the simulation and hardware results carried out under different operating scenarios.

References

1. Muchande S, Thale S (2020) Design and implementation of autonomous low voltage dc microgrid with hierarchical control. In: 2020 IEEE first international conference on smart technologies for power, energy and control (STPEC). IEEE, pp 1–6
2. Kumar J, Agarwal A, Agarwal V (2019) A review on overall control of dc microgrids. J Energy Storage 21:113–138
3. Hasaneen B, Mohammed AAE (2008) Design and simulation of dc/dc boost converter. In: 2008 12th international middle-east power system conference. IEEE, pp 335–340

4. Thakur S, Patil P, Agarwal V (2016) Design and development of controller area network based communication architecture for power sharing in a dc microgrid. In: 2016 IEEE 1st international conference on power electronics, intelligent control and energy systems (ICPEICES). IEEE, pp 1–6
5. Muchande S, Thale S, Wandhare R (2020) Integrated solar pv-battery and micro-hydro based low-voltage autonomous dc microgrid for rural electrification. In: 2020 47th IEEE photovoltaic specialists conference (PVSC). IEEE, pp 2612–2618
6. Prabhakaran P, Goyal Y, Agarwal V (2017) A novel communication based average voltage regulation scheme for a droop controlled dc microgrid. IEEE Trans Smart Grid 10(2):1250–1258
7. Guerrero JM, Vasquez JC, Matas J, De Vicu~na LG, Castilla M (2010) Hierarchical control of droop-controlled ac and dc microgrids—a general approach toward standardization. IEEE Trans Ind. Electron 58(1):158–172

Development of Integrated Test Set for SoC-SoH Estimation of Lithium-Ion Battery

U. B. Mujumdar and U. N. Jibhkate

1 Introduction

In recent times lithium-ion batteries (LiB) are being widely used as an energy storage solution in electric vehicles, consumer equipment, power backup inverters, drones, computers, phones, etc. This is due to the higher energy density, better cycle life capability, lower self-discharge rate, and higher current discharge capabilities offered by lithium batteries. The development of LiB technology has improved the performance, reduced the cost, and made the applications safer. This has resulted in an increased market size of the LiB. Lead–acid and nickel–metal hydride is the most prevalent battery chemistries utilized to date, and are increasingly being replaced by batteries containing lithium [1]. With the increased proliferation of LiB in various application segments, it has become essential to accurately estimate the two important battery parameters i.e., State of Charge (SoC) and state of health (SoH) for the safe operation and longer life cycles [2]. Most of the methods discussed in the available literature require the database of battery parameters like voltage, current, and temperature during the charge–discharge cycles.

Various types of battery test sets have been used in the literature for the generation of the LiB charge/discharge cycle database [2–8]. A test bench with a fully programmable power supply, programmable load, and data acquisition system has been used in ref [2]. Setup at Stanford energy control laboratory for collecting the data includes (i) host computer used to program test profiles and real-time data monitoring through the MITS Pro- and Data Watcher software, (ii) Arbin measurement system, (iii) Arbin LBT21024 with a programmable power supply, (iv) the IncuMax IC-500R thermal chamber and (v) a battery cell positioned in a cylindrical cell holder

U. B. Mujumdar · U. N. Jibhkate (✉)
Department of Electrical Engineering, Shri Ramdeobaba College of Engineering and Management, Nagpur, India
e-mail: ujwaljibhkate@gmail.com

S. Doolla et al. (eds.), *Advances in Renewable Energy and Its Grid Integration*,
Lecture Notes in Electrical Engineering 1041,
https://doi.org/10.1007/978-981-99-2283-3_6

[3]. Use of a battery testbed along with a set of sensors and temperature controller is referred to in ref [4]. Set up similar to [3] has been used in [6, 7]. Battery set with the facility to perform Cycling, HPPC, ICA, and GITT tests has been referred to in [5]. A Dual H bridge converter based system with zero voltage discharge capability has been discussed in [8].

This work is an attempt to develop an integrated hardware setup for the accurate estimation of SoC and SoH of LiB using low-cost generic hardware. As shown in Fig. 1, the proposed battery test setup comprises a bidirectional DC–DC converter, electronic load, DC power supply, various sensors, and a data acquisition system. USB Serial communication interface is provided to transfer the real-time parameters to a PC or a flash drive. The charge–discharge profile can be programmed using the PC interface. The control is implemented using a general-purpose microcontroller and generic hardware for easy implementation. The system is designed to have low complexity hardware, and relatively low-cost components, while offering several high-end battery management options like flexible data storage, communication, automatic state of charge (SOC) detection, and capacity. Though the data generated by the test set can be used for SoC and SoH estimation, the scope of analysis of this work is restricted to SoC estimation only. This paper is organized as follows: Section 2 details the fundamentals and common terms of the LIB, the configuration of the set-up is discussed in Sect. 3, design of the circuit is given in Sect. 4, the control structure is given in Sect. 5, experimentation and results are discussed in Sect. 6. Conclusion is done in Sect. 7.

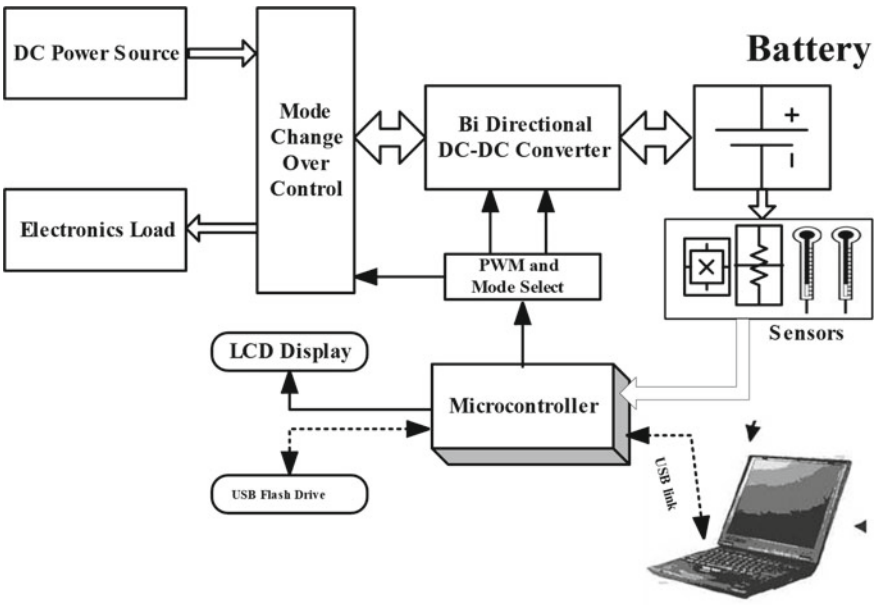

Fig. 1 Block diagram of proposed battery test-set

2 Fundamentals of SoC Estimation

The SoC of LiB is defined as the rate of available capacity to its maximum capacity when the battery is completely charged and describes the remaining percentage of battery capacity [1]. SoC is an important parameter used for the estimation of the state of health (SoH) of a battery, which is a measure of the battery's ability to store and deliver electrical energy, compared with a new battery. Various methods used for the SoC estimation are based on three main approaches; coulomb counting method, voltage method, and Kalman filter method [9].

2.1 Coulomb Counting (CC) Method

This most commonly used SoC estimation method is based on the measurement and time integration of charging and discharging currents. Mathematically, it is expressed in Eq. (1) as:

$$SOC(t) = SOC(t_0) + \frac{1}{C_{rated}} \int_{t_0}^{t_0+\tau} (I_b - I_{loss}) \mathrm{d}t \tag{1}$$

where $SoC(t_0)$ is the initial SoC, C_{rated} is the rated capacity, I_b is the battery current, and I_{loss} is the current consumed by the loss reactions. The coulomb counting method then calculates the remaining capacity simply by accumulating the charge transferred in or out of the battery. Accuracy of this method is decided by the preciseness of battery current measurement and information of accurate initial SoC.

2.2 Open Circuit Voltage (OCV) Method

This method uses OCV-SoC mapping curve for the estimation of SoC for a given value of OCV. This approach is comparatively simple to implement as it requires only voltage sensor for the estimation. The accuracy of estimation is better as compared to CC method as this method does not require the noisy current sensors. Since the battery OCV has strong relationship with temperature and load, estimations based on only OCV method has relatively lower accuracy during the online estimation. Another drawback of OCV method is that it takes long rest time to reach equilibrium condition.

2.3 Kalman Filter (KF) Method

The Kalman filter is an algorithm to estimate the inner states of any dynamic system, it can also be used to estimate the SOC of a battery [3]. As the estimation result is independent of any initial value, KF method has better accuracy than CC and OCV method. The KF gives the sets of mathematical equations, which predicts and corrects a new state repeatedly as the charging/discharging progresses. The method compares the measured input data and output data to calculate the minimum mean squared deviation of the true state as expressed by Eqs. (2) and (3).

$$State\ Equation : x_{k+1} = A_k x_k + B_k u_k + w_k \tag{2}$$

$$Measurement\ Equation : y_k = C_k x_k + D_k u_k + v_k \tag{3}$$

where x presents the system state, u is the control input, w is process noise, y is measurement input, v is measurement noise, A, B, C and D are the covariance matrixes which are time varying and describe the dynamics of the system. As the static and dynamic characteristics of LiB are nonlinear one, extended Kalman filter (EKF) has been used to address the issue.

3 Configuration of Battery Test Set-Up

The arrangement of the proposed battery charger test set is shown in Fig. 2. It is divided into three blocks, (i) Bidirectional DC–DC converter (BDC) (ii) Power supply and electronic load, (iii) LiB and sensors. BDC has two power switches S1 and S2, inductor L1, and the filter capacitors C1, and C2. Both the power switches are composed of MOSFET with a body diode, which also work as a freewheeling diode. A fixed voltage DC power source is used for charging the battery. PWM-controlled electronic load (EL) is used to obtain the load variation to achieve different discharge rates. Depending on the mode of operation i.e., charging or discharging, Electromechanical Relay (Relay-1) connects the BDC to the power source or EL. To completely isolate the LiB from the remaining part of the circuit during the rest period, Relay-2 is provided in the arrangement. Charging mode is facilitated by connecting the BDC input to the power supply and operating it as a buck converter. During the discharge mode, BDC is operated in boost mode with LiB as input and the EL to the output terminals. To facilitate the arrangement, Relay-2 is energized making the connection of the BDC terminal to EL. In conventional BDC, duty ratio of S1 and S2 controls the direction of power flow. In this work, the switches S1 and S2 are independently operated. During the charging, the PWM signal is given to S1 only, keeping S2 off all the time. This makes the BDC operate as a normal buck controller and the duty ratio can be varied from 0 to 100%. In a buck converter, the battery load is connected to the power source through a switch. During the off

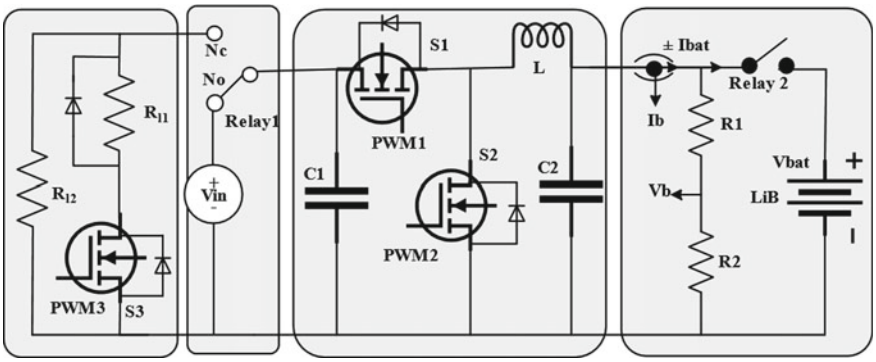

Fig. 2 Configuration of battery test-set

period of the switch, the input current becomes discontinuous and energy stored in the inductor and capacitor is supplied to the load. Ripple in output current can be minimized by selection of C and L. On the contrary, in boost mode, the input current is continuous and the inductor acts as an input filter keeping the input current ripple at a small value. Also on the output side, the control is smooth, especially at a lower duty ratio.

For these reasons, buck mode of BDC is used for charging the battery while boost mode is used for the discharge. To optimize the performance of BDC during charging and discharging mode, inductor is designed as per the boost circuit requirement and capacitor as per the buck. The component design considering two cell battery charger specifications is discussed below.

4 Design of Test-Set System

4.1 Design of BDC

The inductor is one of the crucial components in the BDC circuit since in boost mode it works as an energy storage element and in buck mode, it is a part of the filter circuit. In this setup, the value of the inductor is calculated considering it as a boost converter component given in Eq. (4) as,

$$L = \frac{V_{in}(V_o - V_{in})}{f_s * \Delta I * V_o} \tag{4}$$

where V_{in} and V_o represent the boost converter input and output voltage, f_s is the switching frequency, ΔI is the current ripple. Considering voltage and current requirements as per the rapid discharge cycle, the value of the inductor is $L = 560\,\mu H$. The filter capacitor is calculated using the expression in Eq. (5) as:

$$C = \frac{I_o(V_o - V_{in})}{f_s * V_o * \Delta V_c} \tag{5}$$

Substituting the value gives $C = 1000\ \mu$F.

4.2 Electronic Load

In practice, LiB loading varies over a wide range from no-load to a few times the full load capacity. To get a higher load current, the boost output required is excessively high as the load resistance is fixed. A parallel combination of fixed resistance (R_{l2}) and MOSFET controlled resistance (R_{l1}) referred to as electronic load (EL) is used as the load to address the issue. Fixed resistance (R_{l2}) avoids the open circuit condition on the output of the boost converter that occurs during the off-time of MOSFET connected in series with resistance R_{l1}.

Figure 3 shows the simplified arrangement of the boost converter and the EL. Let D_3 be the duty of electronic load, the equivalent resistance offered by the EL can be given in Eq. (6) as:

$$R_{el} = \frac{R_{l1}}{D_3} \tag{6}$$

The parallel combination offers the load resistance R_l given in Eq. (7) by,

$$R_l = (R_{el} \| R_{l2}) = \frac{R_{l1} R_{l2}}{(D_3 R_{l2} + R_{l1})} \tag{7}$$

With Boost converter operating at a duty ratio of D_2, the equivalent load resistance seen from LiB side is given in Eq. (8) as,

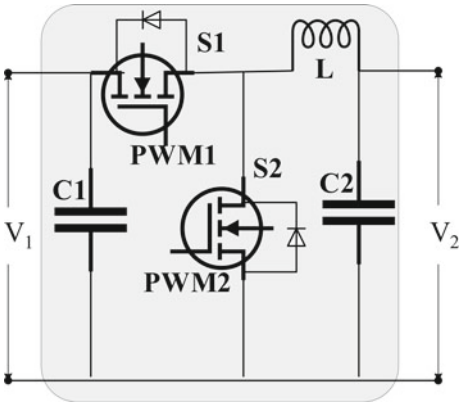

Fig. 3 Basic BDC arrangement

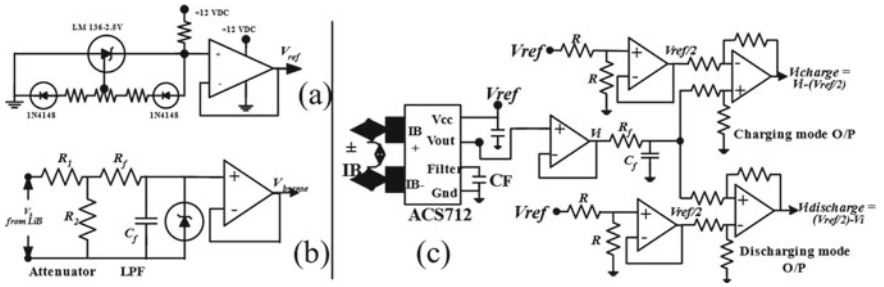

Fig. 4 **a** Precision voltage reference circuit, **b** voltage sensing circuit, **c** current sensing circuit

$$R_{equi} = \left(\frac{R_{11}R_{12}}{(D_3R_{12} + R_{11})}\right)(1 - D_2)^2 \tag{8}$$

4.3 Design of Sensing Circuit

Battery current, voltage, and temperature are the three main parameters required to be monitored during the charge and discharge cycles.

4.3.1 Battery Voltage Measurement

The battery voltage is suitably attenuated using a resistance divider arrangement as shown in Fig. 4b. High-value precision resistors are used in the network to minimize the loading effect and drift due to temperature rise.

4.3.2 Battery Current Measurement

Hall effect based, single polarity, bidirectional linear current sensor by Allegro Semiconductors is used for the battery charge–discharge current measurement. The sensor has a sensitivity of 100 mV/Amp with an output voltage of $V_{cc}/2$ at zero current where V_{cc} is the supply voltage. Output has a positive or negative slope depending on the direction of the current. Arrangement for the sensing of charge–discharge current using a single sensor is shown in Fig. 4c.

4.3.3 Temperature Measurement

To record the temperature, simple temperature sensor based on the LM35 from National semiconductors is used. Suitable mechanical arrangement has been made to protect the temperature sensor and mounted on the front side of the individual cell.

5 Control Structure

The main objective of control structure design is to accurately charge and discharge the test battery as per the specified parameters. Constant Current/Constant voltage (CC/CV) is the most commonly used charging technique referred to in the literature and the same is used in this work [10]. CC/CV charging cycle refers to the use of C rate and upper thresholds voltage (Vu) for CC charging and cut-off current for CV charging. The discharge cycle is normally specified by the discharge rate and the lower cut-off voltage (V_l) to avoid the deep discharge and potential damage to the battery system. Use of complementary PWM pulses with duty ratio regulation for switching MOSFET S1 and S2 has been referred to in the literature for controlling the magnitude and direction of power flow through a bidirectional converter [11]. To avoid the simultaneous conduction of two switches, a delay is added between the turn-off of one MOSFET and the turn-on of the other MOSFET. For a duty ratio below 50%, the ontime of MOSFET S2 is more than that of S1, the energy is exchanged from right to left of the circuit as shown in Fig. 4. For the duty ratio above 50%, the situation reverses and the energy is exchanged from left to right of the circuit. This switching technique has limited regulation of duty ratio. Also, with an active power source on either side of BDC, (charging mode), exceeding the boundary limit of duty ratio, reverses the direction of power flow with the input voltage tends to rise more than the input side power source rating. This can severely damage the power source used for the charging. To avoid this, both the switches are controlled using independent signals in this work. In Buck mode i.e., battery charging mode, switch S1 is controlled by regulating the duty ratio from 0 to 100% and MOSFET S2 is off. The body diode of S2 works as the freewheeling diode. In boost mode operation, MOSFET S2 is controlled using a PWM signal with a variable duty ratio of 0–100% and MOSFET S1 is off. Body diode of S1 freewheels the energy stored in the inductor.

5.1 Battery Charging Mode

The control structure for battery charging mode is shown in Fig. 5a. There are two separate loops for CC and CV control along with a CC/CV mode selector block. In the CC loop, I_{ref} is the reference current i.e., specified CC charging rate, I_b is the battery current, and V_{ref} is the voltage reference signal generated by the PI block

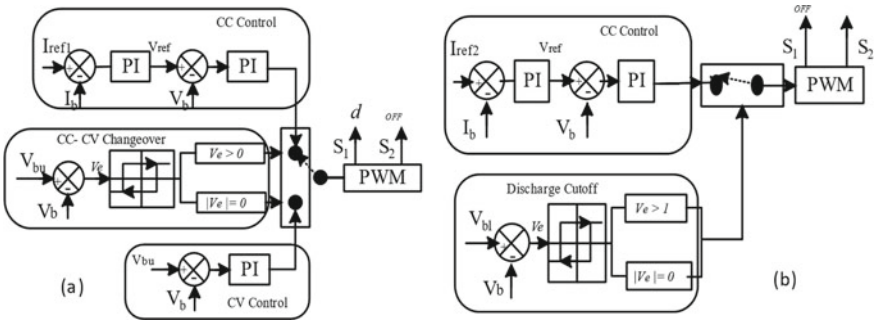

Fig. 5 Control loop structure for **a** CC–CV charging, **b** CC discharging

based on the error between I_{ref} and Ib. Another PI controller is used for tracking the V_{ref} for obtaining the required charging rates. Upon reaching the CC/CV threshold voltage, the mode selector block transfers the charging to CV mode. In this mode, battery voltage is maintained at a constant level using a PI controller, till the charging current drops to the end current value.

5.2 Battery Discharging Mode

The control structure for the discharge mode is shown in Fig. 5b. Here, I_{ref} denotes the specified discharge rate. A PI controller is used for maintaining the discharge rate equal to I_{ref} over the entire discharge cycle. The discharge cycle ends when the battery voltage reaches to lower threshold voltage.

6 Experimentation and Results

As mentioned in Sect. 1, the entire battery test system has been built around the microcontroller ATMega32A. Voltage, current, and temperature measurement is done using 10-bit resolution on-chip ADC. 16-bit timer-based PWM peripheral is used for controlling the switching of S1 and S2. Another PWM with the 8-bit resolution is used for controlling the electronic load. A real-time clock is used for keeping time and providing the timestamp to charge and discharge cycles. Long endurance EEPROM is used to keep the track of charge/discharge cycle number, which is a crucial information for SoH estimation. A standard report format providing the basic information about time, cycle no, charging/discharging rate is developed. Test data is the collection of voltage, current, and cell temperature.

Fig. 6a and b shows the photographs of the battery test set prototype and the switching signals, battery voltage, and current profile during the discharging mode.

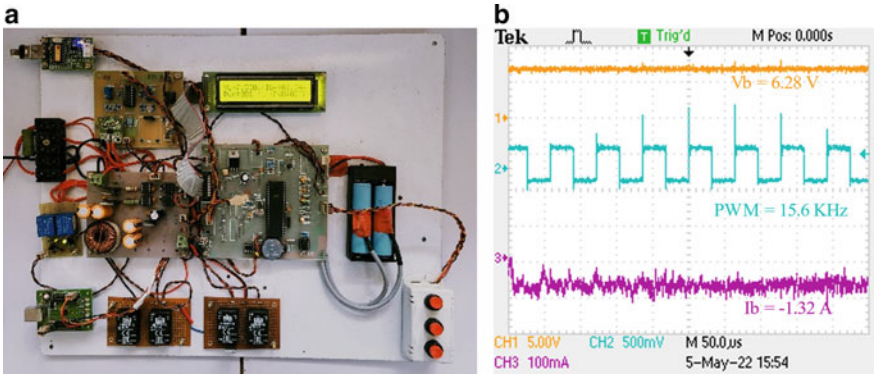

Fig. 6 **a** Laboratory prototype, **b** output waveforms

To verify the effectiveness of the proposed test set, a two-cell battery system has been assembled using LG18650 MH1 3200 mAh, 10 A, 3.7 V cell. The charge/discharge profile is set according the datasheet specifications.

The battery system has been successfully tested for several charge-discharge cycles.

The discharge profile of the fresh battery (Cycle 0 data) is used as a reference for OCV SoC mapping.

Python is used as a tool for normalization. Figure 7a and b show the voltage and current profile of the OCV test conducted on the battery set for SoC estimation.

The different OCV-SoC models for SoC estimation referred in [12] have been implemented on the generated database and the comparison results over the linear range are shown in Fig. 8a and b.

Using normalized OCV-SoC mapping, a look-up table is generated and stored in the microcontroller flash. This database is used for the calculation for initial SoC estimation and the real-time SoC during discharge is calculated using the CC method. To verify the accuracy, SoC has also been estimated by OCV and KF method using the data transferred to PC. Figure 9 (a) shows the estimated SoC using the OCV and KF methods while (b) shows the same using CC method. The analysis of both curves shows that the RMS error between estimated and calculated SoC is less than 1.038%.

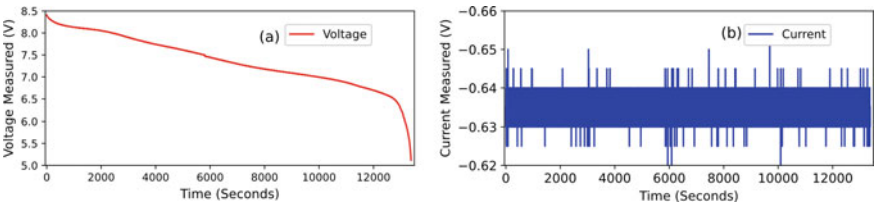

Fig. 7 OCV test profile of **a** voltage and **b** current

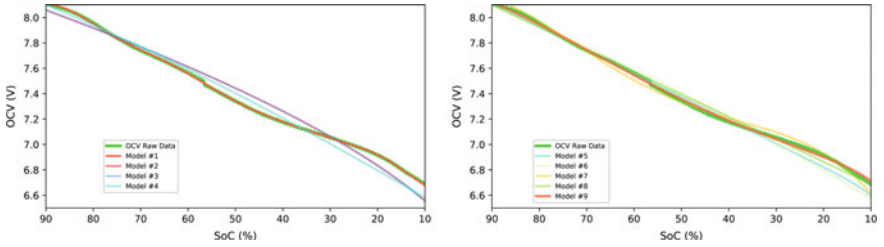

Fig. 8 Comparison of different OCV models on setup datasets

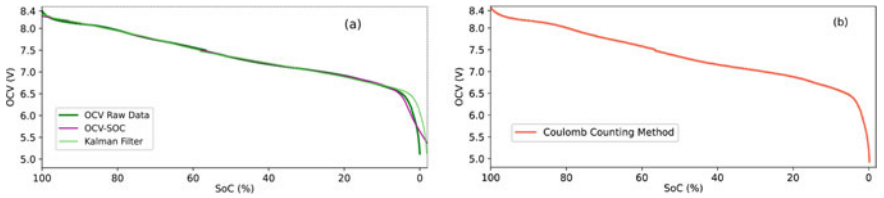

Fig. 9 **a** OCV and KF method and **b** CC method on setup dataset

7 Conclusion

This paper deals with the development of a LiB battery test setup for the estimation of SoC and SoH. A bidirectional power converter, wherein power flow can be regulated in either direction has been used for the charging and discharging of LiB. Modified switching scheme with independent control of BDC MOSFETs has been used for precise control of current through the converter. Duty radio-controlled electronic load with a combination of fixed and variable load resistance has been used to test the discharge profile of the battery under practical conditions. The performance of the test set is validated by conducting several charge-discharge cycles of the LiB battery system and estimating the SoC using different methods. As shown in result section, the SoC estimated using CC, OCV, and KF methods have minimal error.

The setup can be used to generate a database under different operating conditions over the entire life cycle of the battery set which can be used for the further analysis, training, and testing of different machine learning methods for estimating SoH.

Thus, it can be concluded that the battery test set developed in this work can be used as a reliable tool for conducting the experimentation and further research work on LiB.

References

1. Horiba T (2014) Lithium-ion battery systems. Proc IEEE 102(6):939–950
2. Catenaro E, Onori S (2021) Experimental data of lithium-ion batteries under galvanostatic discharge tests at different rates and temperatures of operation Data Brief 35:106894
3. Spagnol P, Rossi S, Savaresi S (2011) Kalman filter soc estimation for li-ion batteries, in Control Applications (CCA). In: 2011 IEEE International conference on Sept., pp 587–592
4. Jinhao M, Ricco M, Guangzhao L, Swierczynski M, Stroe DI, Stroe AI, Teodorescu R (2017) An overview of online implementable SOC estimation methods for Lithium-ion batteries. In: ACEMP 2017 International conference on, pp 573–580
5. Weng C, Cui Y, Sun J (2013) en, On-board state of health monitoring of lithium-ion batteries sin incremental capacity analysis with support vector regression. J Power Sources 235:36–44
6. Soares R, Bessman A, Wallmark O, Lindbergh G, Svens P (2018) An experimental setup with alternating current capability for evaluating large lithium-ion battery cells. Batteries 4:38
7. Zhang R, Xia B, Li B, Cao L, Lai Y, Zheng W, Wang H, Wang W, Wang M (2018) A study on the open circuit voltage and state of charge characterization of high capacity lithium-ion battery under different temperature. Energies 11:2408
8. Abu-Sharkh S, Doerffel D (2004) Rapid test and non-linear model characterisation of solid-state lithium-ion batteries. J Power Sour 130(1–2):266–274. ISSN 0378-7753
9. Pyo YH, Choi SY, Choi YJ, Kim RY (2016) A low cost lithiumion battery tester with a zero voltage discharge capability. In: IECON 2016 - 42nd annual conference of the IEEE industrial electronics society, pp 3135–3140
10. Rachid A, Fadil HE, Giri F (2018) Dual stage CC-CV charge method for controlling DCDC power converter in BEV charger. In: 2018 19th IEEE mediterranean electrotechnical conference (MELECON), pp 74–79
11. Nguyen TL, Guerrero JM, Griepentrog G (2020) A self-sustained and flexible control strategy for Islanded DC nanogrids without communication links. IEEE J Emerg Sel Top Power Electr 8(1):877–892
12. Jibhkate UN, Mujumdar U Development of low complexity open circuit voltage model for state of charge estimation with novel curve modification technique. Available at SSRN 4129826

A Novel Hybrid Islanding Detection Technique in Multi DG Microgrid System

Shashank Gupta, Santosh Kumar Singh, and Mahiraj Singh Rawat

1 Introduction

The best option for supplying the continuous energy of world needs is the solution as green energy (GE) source as opposed to burning fossils. The continuous degrading of fossil fuels has detrimental effects on the ecosystem and accelerates temp of environment lead to globally wide spread warming. For such of these cause, the world is looking to renewable energy sources (RES), VU/THD, and bilateral reactive power variation to satisfy future energy demands [1]. Therefore, the green energy generating units like solar with wind and hydro refers to small-scale power generating projects that are most likely to be integrated to the grid. The most serious issue with DG systems, though, is islanding. From the standards referred by IEEE 1547 [2], "An island represents a state where segment of an area aka electric power system (EPS) is powered by one or more locally supported EPSs with their associated PCCs and that segment of EPS is electrically isolated from rest of the left out EPS". Term islanding can be mainly categorizes in according to state of act ion i.e.: happened unintentionally and next is done for any particular purpose also known as intentional islanding. During intentionally isolating a microgrid from the main grid, it continues to reliably provide power energy support to local loads. It's a controllable mode of operation. When microgrids are cut off from the main grid, inadvertent islanding happens as a result of line tripping, failure, and human error. Some disrupting utility infrastructure on the main grid are major highlighted drawbacks of islanding which accidently or unintentionally occurred includes danger to working personal at work. Identification for non-intendant islanding, many islanding detection techniques (IDTs)

S. Gupta (✉) · S. K. Singh · M. S. Rawat
Department of Electrical Engineering, National Institute of Technology, Uttarakhand, Srinagar (Garhwal), India
e-mail: mt20eee012@nituk.ac.in

S. Doolla et al. (eds.), *Advances in Renewable Energy and Its Grid Integration*,
Lecture Notes in Electrical Engineering 1041,
https://doi.org/10.1007/978-981-99-2283-3_7

are categorizes and proposed by researchers in literature. IDTs can further classified: local and remote techniques. Communication between a utility and DGs has been supported by remote IDTs. The reliability of these techniques performs better than local methods, but they are not much economical. For the most of instances at distributed generation (DG) side, the locally evaluated parameter calculative techniques applied. These detection terminologies are further divided in three different modes i.e.; Active parameters based, passive parameters based, and hybridization of two or more techniques. In Passive parameter based detection, mostly the voltage, current, and frequency parameters locally available at the coupling bus are employed to detect islanding. Strong non-detect zone (NDZ), however, is one of the main shortcomings of this method. We refer to these load combinations as the NDZ because they frequently result in the failure of observation for islanded site. A steady ongoing lower-frequency injected signal gets monitored with variations incorporated in the observation, the active parameters based active IDT are evaluated. Design complexity with some negative impact on power quality are drawbacks of such procedures. At the bus of coupling point, ROCOF is measured using the phase locked loop (PLL) in [3–5]. Since the IDTs based on ROCOF is sometimes gets vulnerable to many different varying loads, setting a threshold is difficult. The VU-dependent passive IDT can locate islands by calculating the sequences of negative and positive voltages. The discrete fractional Fourier transform was developed and is utilised by many academics [6]. A HID utilising ROCOF over reactive power and d-axis current injection was employed to increase islanding detection time. In a mixed DG environment, this HID performs well [7]. To address the shortcomings of the first two methods, hybrid IDTs were proposed. Hybrid IDTs combine the advantages of active and passive or two passive/active IDTs, increasing their potency. Grid-connected PV systems have made up the majority of installations during the last few decades. Therefore, having solar PV systems that are connected to the grid is necessary to prevent islanding. This research suggests an improved hybrid IDT based on VU and ROCOF. Due to their simplicity of execution and lack of impact on power quality or detection time, the two PIDs are combined. According to the literature survey, some hybrid IDTs are: In [8] variation in reactive power with Q-f droop analysis; signal processing with controlling by power loop control [9]; voltage phase angle gets evaluated with observing the unbalance in voltages [10]; neural network based performance with wavelet transformations [11]; shift attaining voltage and actual real utilizing power [12]; changes observed by rate in frequency gets observed with sandia shift of frequency [13]; neural networking probabilistically with transformations employing wavelet packets [14]; interfacing the grid network system adaptive with neuro fuzzy [15, 16] analyze the factor of unbalancing in voltage patterns; rate of changes incorporated with reactive and active powers [17]; recognizing the patterns [18]; This paper suggests a combined hybrid improved solution with conclusive VU-ROCOF IDT.

With the combined evaluation of such two locally voltage frequency based available algorithms are merged which further have an additional advantage over no-effect on system-power quality concerns with detection time.

1.1 Prevailing Islanding Technique (PIT)

Before based on the imbalance found in the voltage profile and frequency set points in this paper, a recently developed method has been employed to enhance hybrid IDTs. The VU is measured for each DG and three-phase voltages seen at DG connected bus terminals are reported using the current IDT. The authors [19] preferred the technique based on imbalance spikes detected in voltage over the one based on THD in their suggested hybrid IDTs due to its great sensitivity to external disturbance. The frequency of the DG drops from 60 to 59 Hz when the recorded spike of unbalanced voltage exceeds the limit threshold value, which is communicated using the hybrid technique. Continuous voltage frequency measurements are made from the DG output. If the frequency drops below 59.2 Hz within 1.5 s of the shift, the circuit breaker at PCC trips, disconnecting the microgrid from the main grid. The hybrid technique sends a signal to the DG's frequency setpoint, forcing the frequency to drop from 60 to 59 Hz, if the recorded Vu spike exceeds the threshold value. The DG output voltage's frequency is continuously observed. A trip signal is sent to the circuit breaker at PCC to cut off power to the microgrid if the frequency drops to 59.2 Hz within 1.5 s of the shift. To enable the microgrid to operate on its own, the frequency setpoint is set at 60 Hz. Even after lowering the frequency setpoint to 59 Hz, the frequency at the DG terminal voltage stays near to 60 Hz. The conclusion that islanding has never occurred can be reached. This common strategy is explained using a flowchart in Fig. 1.

2 Proposed technique

The HID that is suggested combines the ROCOF and VU methodologies. In the event of a main grid separation, the DGs installed on the microgrid must be able to handle the load requirements. As a result, voltage imbalances are apparent at the DG terminals. Each DG's VU is measured, and voltage of all three phases gets scrutinize at the DG terminals. Any disturbances, like a sudden shift in the load or a main grid failure, could be detected as an increase in VU. The three-phase voltage imbalance at PCC is described using this PID method, which depends on the VU. This process is known as islanding, and it measures the ratio of the negative sequenced voltage (NSV) to the positive sequence voltage (PSV). The expression below in Eq. (1) can be used to calculate the voltage unbalance at any moment t.

$$VU_t = \frac{V_{NSt}}{V_{PSt}} \tag{1}$$

The voltage components in the negative and positive order at the DG output port are displayed. Only when the device is connected to ground do the zero sequence

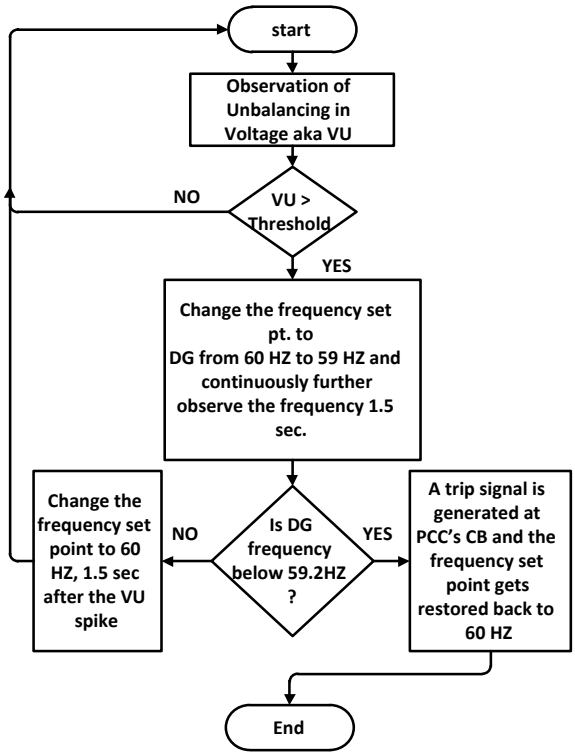

Fig. 1 PIT chart

components appear. With the calculation of sequence analyzer based Positive, Negative, and Zero components for voltage and current sequence at PCC are eavluated. There are negative sequence components throughout the islanding process [20]. The sequences for voltages given using the expression below in Eqs. (2, 3, 4).

$$V_{a1} = \frac{1}{3}(V_a + \alpha V_b + \alpha^2 V_c) \tag{2}$$

$$V_{a2} = \frac{1}{3}(V_a + \alpha^2 V_b + \alpha V_c) \tag{3}$$

$$V_{a0} = \frac{1}{3}(V_a + V_b + V_c) \tag{4}$$

Va0, Va1, and Va2 represents the zero, positive, and negative series voltages, respectively [21]. Where $\alpha = 1\angle 120°$. The ROCOF approach was used to differentiate between the load shift and the mains power failure. Once the VU spike following islanding surpasses a certain threshold, the ROCOF relay tracks the degree of changing frequency for the subsequent 2–50 cycles before transmitting it to the low pass filter (LPF) circuit. LPF is used to lessen high-frequency transients caused

by devices connected to the power system. The threshold value (TV) for a VU spike is 35 times the VU's average value over the just-past second [19]. After numerous simulations, an empirical decision was made to use a one-second duration. If the length is too short, it may be difficult to identify the spikes since the average values that were produced closely resemble the instantaneous values. Only when instantaneous readings are much higher than average levels may spikes be recognised. If the span is excessively lengthy, such as if an electronically controlled load is applied, there would be an immediate increase in VU. On the other hand, it will take some time for the average value to rise to a greater level. As a result, even a slight surge could cause false tripping. The ROCOF, df/dt, is recorded across several cycles at the PCC. The circuit breaker can cut off the power output if the df/dt value is higher than the TV. The ideal TV for the ROCOF approach, according to the literature, is 0.3 Hz/s with 0.7 s for islanded mode limits of detection. ROCOF can be determined [3], using Eq. (5).

$$\frac{\mathrm{d}f}{\mathrm{d}t} = \frac{f(t_k) - f(t_k - \Delta t)}{\Delta t} \tag{5}$$

where $f(t_k)$ is the frequency at the time of the kth sample, $f(t_k - \Delta t)$ is the frequency value determined before the time of the kth segment, i.e. $t_k - \Delta t$. If ROCOF continues to exceed the TV, a trip signal is delivered to the circuit breaker of PCC. Figure 2a displays the flowchart for the suggested approach.

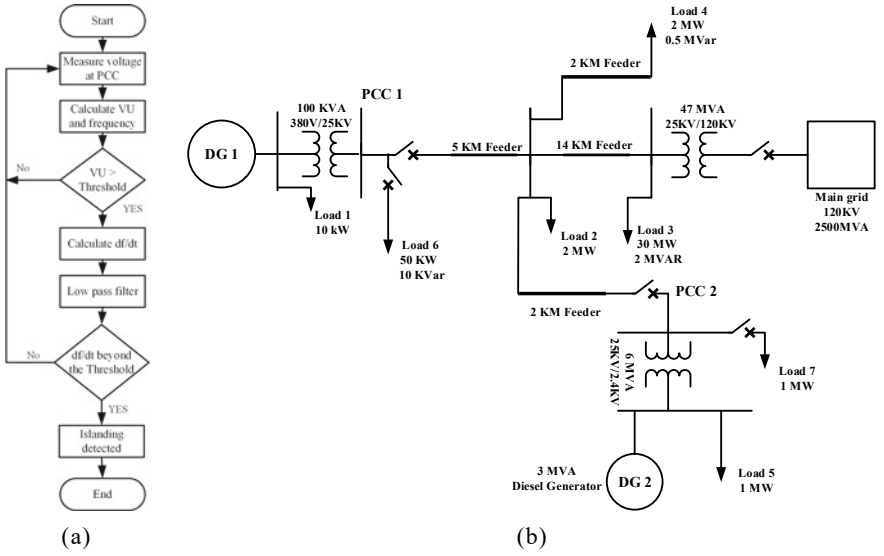

Fig. 2 **a** Proposed technique's flow chart, **b** single line diagram for test system

3 Simulation Results

The suggested method has been tested on the test system shown in Fig. 2b. In order to connect a 10 KW PV (DG1) array to a 25 kV feeder at PCC1, a universal bridge and 100 KVA 380 V/25 kV star-delta transformer are utilised. At PCC2, a 3 MVA Synchronous Diesel Generator (DG2) is connected to a 25 kV feeder using a 6 MVA, 25/2.4 kV star-delta transformer. The lengths of four feeder systems are respectively 14 km, 5 km, 2 km, and 2 km, with a combined total of 25 kV. Start the simulation. A 47 MVA 120/25 kV star-delta transformer connects this 25 kV feeder to a 120 kV and 2500 MVA short circuit level main grid. The PV system used was 10 KW. Standard test conditions of 25°C and 1000 W/M^2 are used to launch the simulation. Several disturbances were caused in the PCC1 lab, including 50 kW at 10 kVAR Microgrid 1's (MG1) load number six turns on after two seconds and shuts off after 2.5 s. Switching a 1 MW load 7 in the microgrid 2 at PCC2 at t = 3 s (MG2). At time t = 4 s, Microgrid 2 (MG2) is unplugged. These disruptions result in VU spikes and frequency changes at the corresponding DG terminals. The main grid terminal's circuit breaker opens at t = 4.5 s, which leads to unintentional islanding. A VU spike and ROCOF are thus seen at the terminals of both DGs. Figure 3a–f depicts the results of simulation for the above system at PCC1 (25 kV, 10 MVA base value).

At t = 2–2.5 s, load 6 in MG1 is shifted, but as can be seen in Figs. 3 and 4, this transition does not significantly affect the loading of DG1 and DG2 (d, e). Because they fall below the limit established by Eq. (1), spike prompt of VU and RO-COF detected by DG1 with DG2 are disregarded. At t = 3 s, MG2 switches to load 7. The loading for both DG-1 and DG2 will not gets effected by this change-over. As a result, the VU spike displayed by DG1 and DG2 is observd less than the value and is once again disre- garded. The changes are only visible in ROCOF, but the recommended technique does not classify them as accidental islanding. MG2 is deleted with primary grid at t = 4 s. The transition causes a ROCOF spike and a VU spike in PCC1. As demon- strated in Fig. 3, at PCC1, the ROCOF spike reaches the TV but the VU does not (d, e). This implies that the recommended algorithm would not see unintended islanding (UI) as occurring even the microgrid gets disconnected from the central main-grid for repair. UI occurs as a result of the main grid terminal's circuit breaker (C.B.) opening at t = 4.5 s. As a result, the unexpected VU surge occurred at PCC1, as seen in Fig. 3d. Additionally, as seen in the Fig. 3e and f, the ROCOF surpasses the threshold value, causing a trip signal to be transmitted to PCC1 at t = 4.515 s. Islanding may therefore be efficiently monitored in a short amount of time (about 15 ms). The lab at PCC2 had the following disruptions: In microgrid 1 (MG1), load 6 (10 kVAR, 50 kW) switches on after 2 s and shuts off after 2.5 s. Switching a 1 MW load 7 in microgrid 2 at PCC2 at t = 3–3.5 s (MG2). At t = 4 s, Microgrid 1 (MG1) is unconnected. These disruptions result in spikes and disturbances for VU and frequency respectively at the corresponding DGs. The main grid terminal's circuit breaker opens at t = 4.5 s, which causes UI. A VU spike and ROCOF are thus seen at the terminals of both DGs. The simulation output for the mentioned system at PCC2 (25 kV, 10 MVA base value) is shown in Fig. 4a–f.

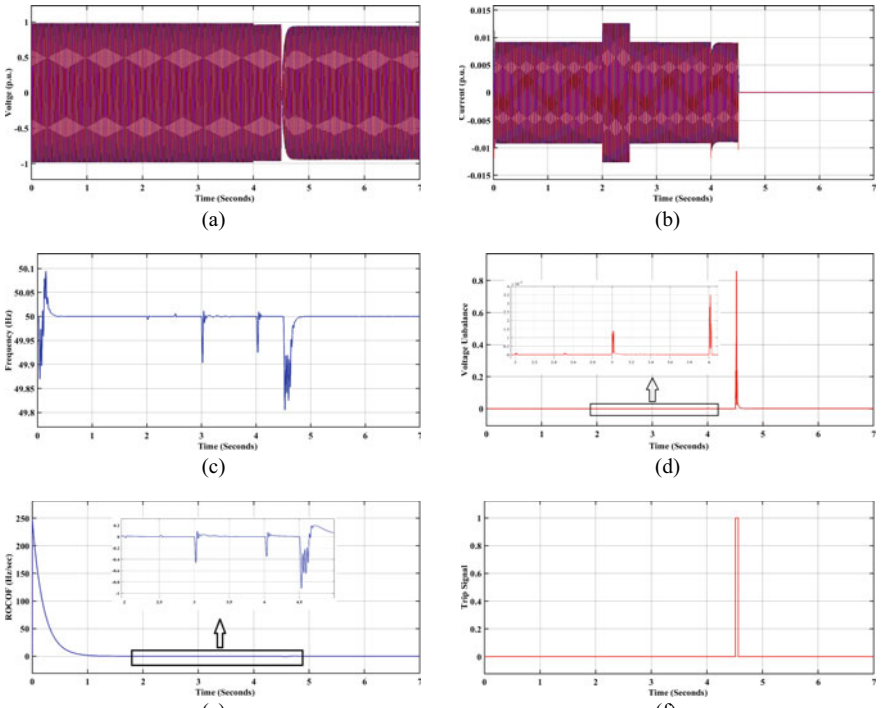

Fig. 3 PCC1 results, **a** voltagev(V) (in p.u.) versus time (T) (in sec), **b** current (I) (in p.u.) versus T (in sec), **c** frequency (F) (in Hz) versus T, **d** VU w.r.t T, **e** ROCOF w.r.t T, **f** trip signal indication to PCC-1 station's CB

As seen in Fig. 4, when load 6 in MG1 is switched at t = 2–2.5 s, it has no discernible impact on the loading of DG1 and DG2 (d, e). Due to the fact that they are below the TV established by equation, the VU spike and ROCOF that DG1 and DG2 detected are ignored (1). At t = 3–3.5 s, MG2 switches to load 7. This changeover does not substantial impact on the load charging distribution for DG-1 and DG2. Thereafter, the spike for the VU is visualized at DG1 and DG2 station which will be below the control value that resulted in disregarded once again. The changes are only visible in ROCOF, but the recommended technique does not classify them as UI. MG-1 gets obsoleted from the grid at t = 4 s. The transition causes a ROCOF spike and a VU spike in PCC2. At PCC2, as demon- strated in Fig. 4, ROCOF and VU spikes do not exceed the TV (d, e). This is predicated on the notion that the approach not take UI into account, even microgrid were isolated from the main grid for maintenance. UI occurs when the main grid terminal's circuit breaker (C.B.) opens at t = 4.5 s. As a result, PCC2 saw the unanticipated VU increase, as illustrated in Fig. 4d. A trip signal is provided to PCC 2 at t = 4.517 s as a result of the ROCOF exceeding the threshold value in the Figs. 4e and f, respectively. Therefore, islanding may be efficiently seen in a short amount of time (about 17 ms).

4 Conclusion

This study provides a unique HID approach for microgrids with inverter-based diesel generators employing VU and ROCOF.

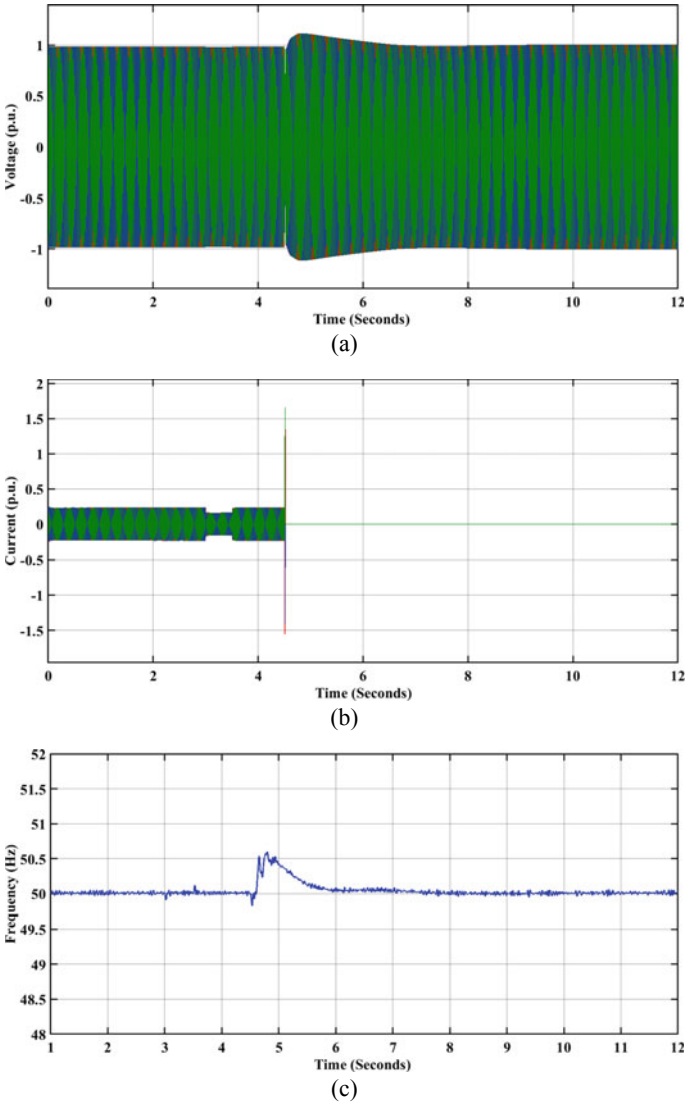

Fig. 4 PCC-2's results at, **a** V (in p.u.) versus T (in sec.), **b** I (in p.u.) versus T, **c** F (Hz) versus T, **d** VU w.r.t T, **e** ROCOF w.r.t T, **f** trip signal indication generated at PCC-2's station CB

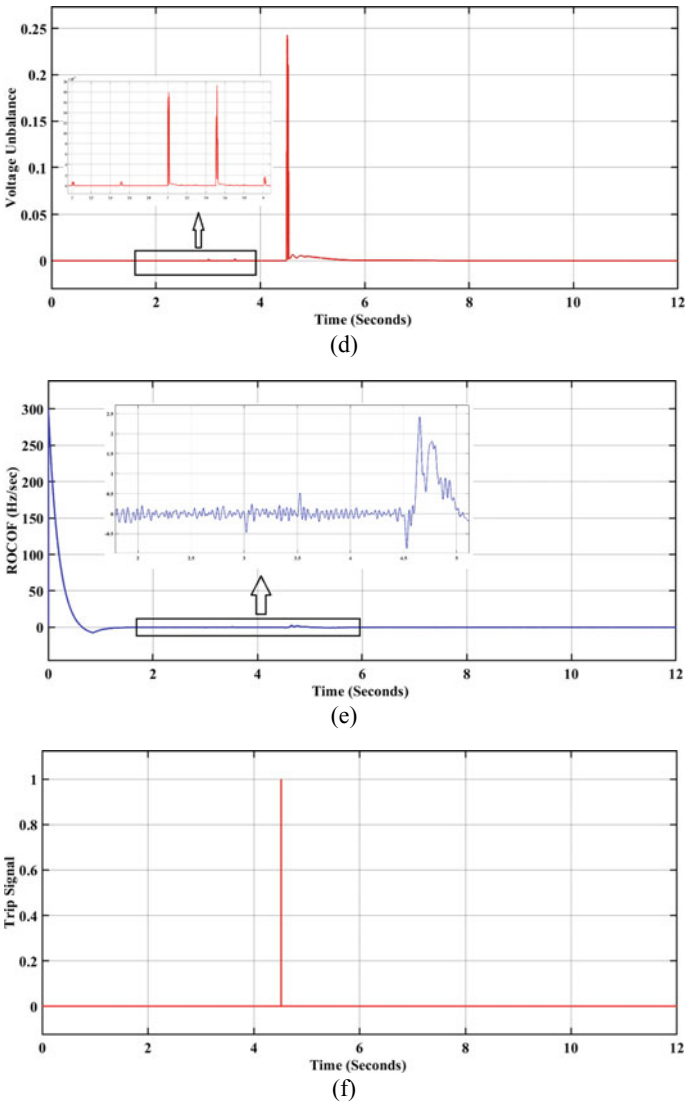

Fig. 4 (continued)

The proposed hybrid approach is contrasted with the hybrid IDT based on the literature's frequency setpoint (FSP) and VU. This technique can distinguish between islanded situations and load switching conditions, preventing spurious trips in the event of load switching. When used with a multi-DG system, this method works as intended. As a result, the suggested IDT performs better than PID methods with huge NDZ and active methods with poor power quality and no potential for autonomous operation in islanded mode. According on the simulation results, the suggested hybrid

method's islanding detection time is between 15 and 25 ms. The hybrid approach employing VU and frequency setpoint was also shown to have an islanding detection time of 0.21 s. MATLAB/Simulink is used to produce the simulation results.

References

1. Wang G (2020) Design consideration and performance analysis of a hybrid islanding detection method combining voltage unbalance/total harmonic distortion and bilateral reactive power variation. CPSS TPEA 5:86–100
2. Rawat MS, Vadhera S (2021) Evolution of islanding detection method for microgrid systems. Adv Comput Electric Eng 221–257
3. Marchesan G, Muraro MR, Cardoso G et al (2016) Passive method for distributed-generation island detection based on oscillation frequency. IEEE Trans Power Deliv 31:138–146
4. Guha B, Haddad RJ, Kalaani Y (2015) A passive islanding detection approach for inverter-based distributed generation using rate of change of frequency analysis. Southeast Con
5. Tzelepis D, Dysko A, Booth C (2016) Performance of loss-of-mains detection in multi-generator power Islands. In: 13th international conference on development in power system protection 2016 (DPSP)
6. Dutta S, Olla S, Sadhu PK (2021) A secured, reliable and accurate unplanned island detection method in a renewable energy based microgrid. Eng Sci Technol Int J 24:1102–1115
7. Nougain V, Prakash S, Mishra S (2018) Hybrid islanding detection method based on ROCOF over reactive power and d-axis current injection. In: 2018 8th IEEE India international conference on power electronics (IICPE)
8. Raipala O, Makinen A, Repo S, Jarventausta P (2014) A novel anti-islanding protection method based on the combination of a Q-f droop and RPV. In: IEEE PES innovative smart grid technologies. Europe IEEE, pp 1–6
9. Zamani R, Hamedani Golshan ME, Haes Alhelou H, Hatziargyriou N (2019) A novel hybrid islanding detection method using dynamic characteristics of synchronous generator and signal processing technique. Electric Power Syst Res 175:105911
10. Seyedi M, Taher SA, Ganji B, Guerrero JM (2019) A hybrid islanding detection technique for inverter-based distributed generator units. Int Trans Electr Energ Syst 29
11. Kumar SA, Subathra MSP, Kumar NM et al (2020) A novel Islanding detection technique for a resilient photovoltaic-based distributed power generation system using a tunable-Q wavelet transform and an artificial neural network. Energies 13:4238
12. Mahat P, Chen Z, Bak-Jensen B (2009) A hybrid Islanding detection technique using average rate of voltage change and real power shift. IEEE Trans Power Deliv 24:764–771
13. Khodaparastan M, Vahedi H, Khazaeli F, Oraee H (2017) A novel hybrid islanding detection method for inverter-based DGs using SFS and ROCOF. IEEE Trans Power Deliv 32(5):2162–2170
14. Ahmadipour M, Hizam H, Lutfi Othman M, Amran Mohd Radzi M (2018) An anti- Islanding protection technique using a wavelet packet transform and a probabilistic neural network. Energies 11:2701
15. Hashemi F, Ghadimi N, Sobhani B (2013) Islanding detection for inverter-based DG coupled with using an adaptive neuro-fuzzy inference system. Int J Electr Power Energy Syst 45:443–455
16. Nayak AM, Mishra M, Pati BB (2020) A hybrid islanding detection method considering voltage unbalance factor. In: 2020 IEEE international symposium on sustainable energy, signal processing and cyber security (ISSSC). IEEE, pp 1–5
17. Jhuma UK, Mekhilef S, Mubin M et al (2021) Hybrid islanding detection technique for distribution network considering the dynamic behavior of power and load. Circuit Theory Apps 50:1317–1341

18. Marín-Quintero J, Orozco-Henao C, Velez JC, Bretas AS (2021) Micro grids decentralized hybrid data-driven cuckoo search based adaptive protection model. Int J Electr Power Energy Syst 130(106960):106960
19. Menon V, Nehrir MH (2007) A hybrid islanding detection technique using voltage unbalance and frequency set point. IEEE Trans Power Syst 22:442–448
20. Kumar KM, Naresh M, Singh NK, Singh AK (2016) A passive islanding detection approach for distributed generation using rate of change of negative sequence voltage and current. In: 2016 IEEE Uttar Pradesh section international conference on electrical, computer and electronics engineering (UPCON)
21. (2018) An efficient passive islanding detection method for integrated DG system with zero NDZ. IJRER

Life Cycle Assessment of a Hybrid Solar Based Electric Vehicle Charging Station Using SimaPro

Shaifali Sood, Rajesh Kumar, and N. K. Tiwari

1 Introduction

Electrification of the transport sector is an important step toward decarbonizing the mobility sector since transportation is still largely dependent on fossil fuels. With India looking to be carbon neutral before 2070, electrification of hard-to-abate industries will be required. Transportation is one such sector which needs to control greenhouse gas (GHG) emissions in order to improve the air quality of the cities. Electric vehicles (EV) replacing the internal combustion engine vehicles will help to control the direct emissions from the fuel combustion in the engine. Yet it must be noted if the charging of EVs is grid-dependent and the grid has a high-carbon content, and it will turn out to be harmful instead of being environment friendly [1]. India should choose renewable energy sources as the alternative to the grid for charging purposes and solar energy is the easiest to deploy for charging purposes [2].

The cost competitiveness of renewables can be exploited at charging stations, and India's goal of establishing 450 gigawatts of renewable energy installed capacity by 2030 is vital in this too. The national electricity capacity still has 53% [3] electricity from coal, of this, about 60% is from fossil fuels.

In this study, a charging station energy system is designed and analyzed based on its technical, economic and environmental performance. To evaluate the environmental performance of energy sources used in charging, the lifetime assessment (LCA) should be carried out [4]. The LCA of the energy sources is carried out using

S. Sood (✉)
School of Renewable Energy and Efficiency, National Institute of Technology, Kurukshetra, India
e-mail: ms.shaifalisood@gmail.com

R. Kumar
Department of Mechanical Engineering, National Institute of Technology, Kurukshetra, India

N. K. Tiwari
Department of Civil Engineering, National Institute of Technology, Kurukshetra, India

S. Doolla et al. (eds.), *Advances in Renewable Energy and Its Grid Integration*,
Lecture Notes in Electrical Engineering 1041,
https://doi.org/10.1007/978-981-99-2283-3_8

the Indian codes [5, 6]. Similar studies [7, 8] have been conducted to understand the effect of electricity mixes of the countries and the energy sources using well-to-wheel and cradle-to-grave types of LCA for the EV charging in the past as well.

The objective of this study is to design an energy system to be used at an EVCS for placement inside the city at office parking space so that EVs can be charged without travelling for long distances. The charging pattern is also synonymous with the sunlight hours and the usage hours of the workspace parking. The energy source is hybrid (grid-based). In case of unavailability, it can draw power from the grid instead of relying on generators. The study intends to cover the following objectives:

- To carry out technical and economic study for the energy source used in a charging station which makes use of a hybrid system
- To understand the implication of deploying charging station inside city space and maximizing solar integration into that
- To conduct an LCA of the energy sources to understand the environmental impacts of choosing renewable sources over grid electricity
- To conduct sensitivity analysis for various scenarios of solar PV plant to understand its impact on economics and the environment.

2 Methodology

2.1 Modelling a Microgrid for a Charging Station

Study region. The optimal location for a charging station depends on its placement in the area and overall functioning. Additionally, one should consider the charging time and the availability of sufficient space. This study primarily takes into account daytime charging at office parking. The EV charging points at locations where people tend to park their vehicles can save the time and effort of travelling to access public EVCS. For renewable energy based charging stations, while selecting a site, the space constraint are to be considered. The installation of solar PV panels will require ample rooftop area. The selected office parking is in Noida at 28.45° northern latitude and 77.51° eastern longitude; the details are shown in Table 1.

Table 1 The details of the study region for the charging station

Particulars	Details
City	Noida
State	Uttar Pradesh
Country	India
Latitude and longitude	28.45° N 77.51° E
Maximum temperature	42.5 °C

Load Assessment. The charging station is intended to charge at least ten four-wheeled EVs in a day that are parked in an office building. The EV load demand is modelled in HOMER Pro from an available study [9]. To forecast the daily demand, the data from the study were taken using the GetData software and procured data was extrapolated for charging ten EVs at the EVCS. The resulting load profile, as shown in Fig. 1 peaked around 1 p.m., making a strong case for utilizing solar energy at the EVCS to maximize the usage of renewable energy in charging applications and decreasing the CO_2 emissions from the new system.

The electric load is AC in the system as the EV batteries are charged using AC current by the chargers. Also, the daily load was found sufficient for the ten cars parked at the charging station, assuming their battery capacity to be 30 kWh. The total daily demand and the peak demand can be seen in Fig. 2.

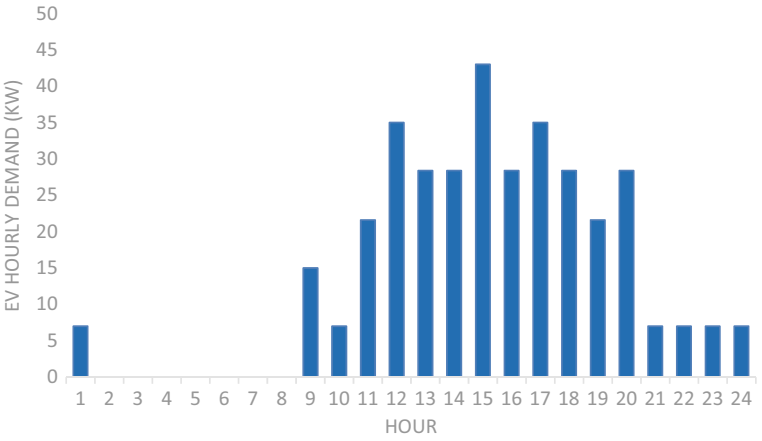

Fig. 1 The load profile used for designing an energy system for the charging station is extrapolated from a previous study

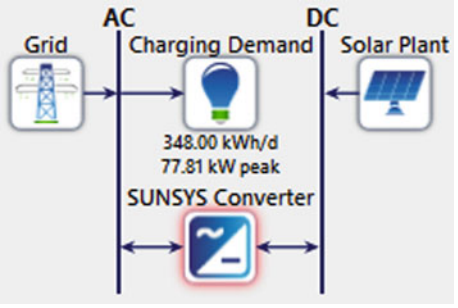

Fig. 2 The system architecture of one of the designs in HOMER

Table 2 The cost for various components according to market prices including the government subsidies

Component	Capital	Replacement	O&M	Unit
Solar	₹28,000	₹28,000	₹500	kW
Converter	₹5000	₹3800	₹115	kW
Battery	₹5000	₹5000	₹200	kWh

System components. *Solar PV.* The system utilizes a LONGi LR6-72HV-350 M with 350 Wp capacity with 72 Mono-crystalline cells offering 18.1% efficiency of module efficiency, as well as temperature coefficients and maximum operating temperature of 0.410 and 45°C, respectively. The solar PV modules are to be placed on the top of the roof of the charging station, which will be an office building. The interaction of the various components in the system is shown in Fig. 2.

Converter. The converter for the energy system is SUNSYS PCS^2 IM. This can feature solar PV input, battery connection, grid or generator input, including the load output. The efficiency for conversion from PV module to the load is 98% and from the grid to load is 99%. The converter converts the solar PV plant DC to AC, as shown in Fig. 2.

Battery storage. A lead-acid battery is featured in the preliminary system architecture as the backup storage system at the charging station. The battery is from BAE Secure PVS Solar 1.8 kWh whose round trip efficiency is 85%. But since most of the charging load is spread across the daytime very less backup is needed and there was cost escalation due to including batteries, so it was not included in the winning system.

Economic assessment. The lifetime of the designed charging station energy, which includes a solar PV plant is assumed to be 25 years as most PV manufacturers suggest. For the study, the nominal discount rate of 12% [10], an expected inflation rate of 4.6% [11] and then an actual discount rate of interest of 7.07% was obtained, which is used in the cost calculation of the software. As per the Central Electricity Authority, the electricity rate is ₹6.5 and the grid sell-back rate for those supplying electricity back to the grid is ₹2.25. In the study, additionally, the cost of various components was taken into account according to the prevailing market prices in the country and this is shown in Table 2.

2.2 Life Cycle Assessment of Microgrid

Goal, scope and functional unit. SimaPro 9.2.0.2 [12] software was used to perform the LCA to understand the effect of choosing the proposed case over other scenarios. The functional unit is 1 kWh of charging electricity used to charge EVs at the charging station. The scope of the study was gate-to-gate, where only the operational stage

of the energy systems was taken into account. The working stage for the solar PV hybrid system also included installing the solar system in the study area. The scenarios considered in the LCA are the same as shown in Table 3.

Life cycle inventory. The HOMER model was used as input at SimaPro primarily for the life cycle inventory stage. The two cases, one with grid and the other with a renewable energy system, were input into the software. To model the LCI for both the energy sources, Indian grid and the solar PV plant, additional help was taken from an earlier publication [13]. And the life cycle inventory of the electricity grid

Table 3 Life cycle inventory data used in SimaPro for conducting the LCA

	Unit	Quantity
Energy, electric vehicle charging	kWh	1
Inputs from technosphere		
Energy Source, grid	kWh	0.277[a]
Energy Source, solar PV	kWh	0.723[a]
Energy Source, grid	kWh	1
Inputs from technosphere		
Electricity, hard coal	kWh	5.32×10^{-1}
Electricity, natural gas	kWh	6.30×10^{-2}
Electricity, oil	kWh	1.29×10^{-3}
Electricity, hydro, reservoir, alpine region	kWh	6.81×10^{-2}
Electricity, hydro, reservoir, non-alpine region	kWh	4.96×10^{-2}
Electricity, hydro, run-of-river	kWh	1.21×10^{-2}
Electricity, nuclear, pressure water reactor	kWh	1.71×10^{-2}
Electricity, photovoltaic	kWh	1.27×10^{-1}
Electricity, wind	kWh	1.01×10^{-1}
Electricity, biomass, solid	kWh	2.57×10^{-2}
Electricity, from municipal waste incineration	kWh	1.08×10^{-3}
Energy source, solar PV	kWh	1
Inputs from nature		
Energy, solar, converted	MJ	3.850
Inputs from technosphere		
Tap water	kg	0.00296
Photovoltaic plant installation	p	6.70×10^{-6}
Emissions to air		
Water vapors	m^3	4.44×10^{-2}
Output to technosphere		
Wastewater	m^3	1.96×10^{-6}

[a] Values correspond to scenario 1 in the energy system

was from the year 2014 in the earlier publication, so it was adjusted to the year 2022 using data from Central Electricity Authority, India renewable dashboard [3]. The dashboard includes that data on the total installed electricity generation capacity in the country. Similarly, the life cycle inventory of solar PV was adjusted according to the components identified as necessary in the HOMER system architecture of the proposed case. The LCI data used in the software is shown in Table 3.

Life cycle impact assessment. One of the goals of this hybrid solar charging station design is to address the environmental impacts coming from the operational phase of the carbon-intensive grid in the country. The IMPACT 2002 + method from the SimaPro software was chosen to carry out the analysis. This method has 15 midpoint categories transformed into four endpoint categories, including human health, ecosystem quality, climate change, and resources. The human health category has the unit of Disability-Adjusted Life Years (DALY), which shows the number of years reduced from the average human lifetime indicating the reduced life quality. The ecosystem quality indicates the effect on species other than humans. Its unit PDF.m^2.year shows terrestrial biodiversity loss where PDF is potentially disappeared fraction. The climate change category is the most commonly used to understand the impact of any new system or process. It converts all the gaseous emissions with global warming potential into kg CO_2 eq. The resources damage category indicates the depletion of the resources.

3 Results and Discussions

3.1 Techno-economic Analysis Using Homer Pro

HOMER Pro simulations resulted in choosing the 84 kW solar PV system with a 65.8 kW converter. The proposed case indicated that a more significant amount of energy is being used from the solar PV plant. When the sunlight goes out, the electricity purchased from the grid starts at the charging station. The energy generation and purchase throughout the year can be seen in Table 4. The proposed case has excess electricity of 1121 kWh per year.

Table 4 The summary for electricity generated, purchased and sold in a year

Component	Production (kWh/year)
Solar PV	157,693
Grid purchases	56,942
	Consumption (kWh/year)
Grid sales	80,544
AC load	127,020

Table 5 The comparison of energy systems simulated in the Homer pro software

Scenario	Base case	Winning case
Solar PV Plant (kW)	0	84
Converter (kW)	0	65.8
NPC (million rupees)	9.56	5.00
Initial capital (million rupees)	0	2.68
O&M (million rupees)	0.82	0.20
LCOE (₹/kWh)	6.50	2.10
Renewable fraction (%)	0	72.3

The economic assessment involves comparing the base case and the winning case, which involves a solar PV plant. HOMER PRO provides the lowest NPC for 84 kW solar PV system from the search space after performing the calculation. This is the system which can be employed at least amount of investment and it will give the LCOE of ₹2.10 as compared to the LCOE of ₹6.50 in the base case. The comparison of the two systems is given in Table 5.

The economics of the winning case suggests that it will have a simple payback period of 4.19 years where as the discounted payback will be 5.15 years that suggests that in the remaining 19.85 years it will bring benefit to the charging point operator. The internal rate of return (IRR) of 23.5% is obtained for the system. A greater IRR % indicates that the system will deliver better returns and is, therefore, an economically preferable choice. Also, the return on investment (ROI) of 19.3%. So, it can be concluded that the system is both economically and technically feasible. The lifetime of the designed charging station energy will have an annual worth of Rs. 393,663. And for sending the renewable energy into the grid it will achieve maximum renewable penetration of 123% in its lifetime.

3.2 Environmental Analysis Using SimaPro

The interpretation stage of LCA presents the result in favour of the proposed case. The usefulness of EVs is only if the carbon intensity of the grid is brought down and with a small amount of renewable energy integration, this can't be done. This can only be achieved if there is the higher amount of renewable penetration in the grid. The results from LCA indicate that the proposed case has a climate change 0.274 kg CO_2 eq per kWh energy produced as compared to the base case with climate change value of 0.881 kg CO_2 eq. It can cut down the total carbon dioxide emissions from 111,904 to 34,803 kg every year during the operation period of the charging, which translates to 77,101 kg CO_2 eq prevented from going into the atmosphere.

The LCA was not limited to the carbon dioxide emission but ranged to various other damage categories of the IMPACT 2002 + method as shown in Table 6. The damage categories help to understand the result and implication of the winning case

Table 6 The LCIA results obtained for the two scenarios of energy system in SimaPro

Damage category	Human health	Ecosystem quality	Climate change	Resources
Unit	DALY	PDF * m^2 * yr	kg CO_2 eq	MJ primary
Base case	8.00E-07	0.1008	0.881	10.37
Winning case	2.70E-07	0.0481	0.274	3.33

better. The ecosystem quality improved by 52% in the winning case as compared to base case. The human health damage category decreased 66% in the winning case compared to the base case. Finally, the resource damage category that shows the depletion has decreased by 7 MJ on choosing the winning system.

4 Conclusion

The requirement for electric vehicles will increase as efforts to decarbonize the transportation sector grow. And the increasing use of electric vehicles will ramp up the energy demand for the grid. In this study, a hybrid energy-powered charging station is designed for Greater Noida. The system proposed for the location has a renewable penetration of 72.3% and the difference in the NPC for the base and the proposed case is Rs. 4.59 million, which shows its economic value. Such stations can be utilized in any city parking whose rooftop has an ample amount of sunlight. The amount of carbon dioxide that can be slashed by choosing the proposed case is 77 tons in a year. It can be concluded that the hybrid solar system will be beneficial both economically and environmentally. Also, such a system will be useful in the coming years for energy security in the nation as the fossil fuel prices in the international market continue to grow. The NITI Ayog has already proposed to have a dense charging station network powered by renewables that are high power or ultra-high power for the inclusion of EVs in the mobility ecosystem. The charging station located within the city will be particularly useful to work class travelling within the city. Additionally, greater solar integration will bring and economic benefits. The results clearly indicate that greater renewable integration brings down the overall impacts on the energy system.

References

1. Onn CC et al (2018) Greenhouse gas emissions associated with electric vehicle charging: The impact of electricity generation mix in a developing country. Transp Res Part D: Transp Environ 64:15–22. https://doi.org/10.1016/j.trd.2017.06.018
2. Pareek S, Sujil A, Ratra S, Kumar R (Feb. 2020) Electric vehicle charging station challenges and opportunities: a future perspective. In: Proceedings - 2020 international conference on

emerging trends in communication, control and computing, ICONC3 2020. https://doi.org/10.1109/ICONC345789.2020.9117473
3. CEA dashboard (2022) Dashboard - central electricity authority. https://cea.nic.in/dashboard/?lang=en Accessed 12 Jun. 2022
4. Rapa M, Gobbi L, Ruggieri R (Dec. 2020) Environmental and economic sustainability of electric vehicles: life cycle assessment and life cycle costing evaluation of electricity sources. Energies (Basel) 13(23). https://doi.org/10.3390/en13236292
5. B. of Indian Standards (2006) IS/ISO 14044: Environmental management-life cycle assessment-requirements and guidelines
6. B. of Indian Standards (2006) IS/ISO 14040: Environmental management - life cycle assessment - principles and framework
7. Cox B, Bauer C, Mendoza Beltran A, van Vuuren DP, Mutel CL (Jul. 2020) Life cycle environmental and cost comparison of current and future passenger cars under different energy scenarios. Appl Energy 269. https://doi.org/10.1016/j.apenergy.2020.115021
8. Querini F, Dagostino S, Morel S, Rousseaux P (2012) Greenhouse gas emissions of electric vehicles associated with wind and photovoltaic electricity. Energy Proc. 20:391–401. https://doi.org/10.1016/j.egypro.2012.03.038
9. al Wahedi A, Bicer Y (Mar 2022) Techno-economic optimization of novel stand-alone renewables-based electric vehicle charging stations in Qatar. Energy 243. https://doi.org/10.1016/j.energy.2021.123008
10. Commercial Property Loan Interest Rates- HDFC, ICICI, SBI & Other Top Bank. https://www.iservefinancial.com/commercial-property-loan-interest-rate Accessed 25 Jun 2022
11. India inflation rate - May 2022 Data - 2012–2021 Historical - June Forecast - Calendar. https://tradingeconomics.com/india/inflation-cpi Accessed 25 Jun 2022
12. SimaPro (2022) Manual: SimaPro tutorial. https://support.simapro.com/articles/Manual/SimaPro-Tutorial. Accessed 12 Jun 2022
13. Itten R et al. (2014) Life cycle inventories of electricity mixes and grid version 1.3 on behalf of the title life cycle inventories of electricity mixes and grid

Potential Assessment for Repowering of Solar Projects in India

Saurabh Motiwala, Sudarshan Kumar, Ashish Kr. Sharma, and Ishan Purohit

1 Introduction

India has recently achieved 100 GW of installed capacity of power generation through renewable energy technologies (RETs) in which solar power (~44 GW) and wind power (~39 GW) segments were the key contributors [1]. The country has ambitious plan of implementing 175 GW RE capacity for power generation by the end of year 2022. However, the target has also been upscaled 450 GW by 2030 [2]. This is one of the largest expansions plans globally for renewable energy-based power generation. In the meantime, Solar PV-based 'clean power' has also become the 'cheapest power' in India with the lowest tariff of 1.99 per kWh discovered in recent auctions [3]. It is interesting to mention here that, the normative solar tariff during the inception of National Solar Mission in India (2010) was around 17.91 per kWh. Even the Government has to supported the solar power generation through various financial and fiscal benefits. Similarly, the wind power sector has also shown strong southward movement of tariffs ever since the competitive bidding process was adopted by the Solar Energy Corporation of India (SECI) Ltd. Presently, levelized tariffs for solar and wind power are seen to be in the close range of 2.0–2.50 per kWh.

Operational history of utility scale (MW capacity) solar power projects is about 10 years old, whereas the wind projects have been operating since 90's in the country. By the end of August 2021, the installed solar capacity in India has reached 44.3 GW (38.8 GW utility scale ground mounted and 5.5 GW of rooftop solar) whereas wind

S. Motiwala · S. Kumar
Department of Aerospace Engineering, Indian Institute of Technology Bombay, Powai, Mumbai 400076, India

A. Kr. Sharma (✉) · I. Purohit
International Finance Corporation, World Bank Group Wordmark 3, 6 th Floor, Aerocity, New Delhi, Delhi 110037, India
e-mail: aksharmanith@gmail.com

S. Doolla et al. (eds.), *Advances in Renewable Energy and Its Grid Integration*,
Lecture Notes in Electrical Engineering 1041,
https://doi.org/10.1007/978-981-99-2283-3_9

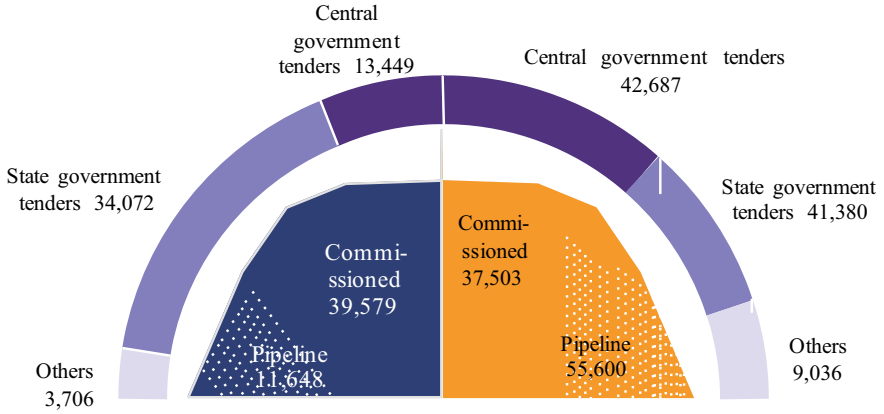

Fig. 1 Status of wind and solar installations in India

power installations stand at 39.7 GW capacity. It is further reported that around 55 GW solar projects are in the pipeline. The Fig. 1 presents the infographics of solar and wind power sector of India both for operational and pipeline capacities [4].

At present, the share of RE (solar and wind) in overall installed capacity5 (i.e., > 388 GW) is more than 20% contributing to 8.5% share in overall energy generation in the country [5]. It is further known that most of the RE resources are intermittent in the nature and therefore the power is not available at all times of the day. This is the biggest difference between RE power and the conventional power. However, the Government of India is trying to make RE power available 24 × 7 through several policy and technology interventions, viz., competitive procurement of round-the-clock (RTC) power, hybridization of wind and solar with battery storage, large scale battery storage systems with grid, etc. The cost of battery energy storage system (BESS) is gradually decreasing and, it is expected that the RE power can soon become competitive to conventional thermal power with quite high level of dispatchability.

The allotment of RE projects in India has been largely based on the auctions, which are called by several central and state agencies The intermediary procurement agencies sign 25-years power purchase agreement (PPAs) with the Solar Project Developers (SPD) at fixed tariff discovered through the auction process, and Power Sale Agreements (PSAs) with the buying clients/DISCOMs at this tariff escalated by the trading margin. Post 2016, wind power projects are also being procured through competitive process as that for solar through SECI.

In the solar PPAs, the maximum and minimum energy generation and energy feeding to grid is defined and accordingly SPDs design their projects in terms of MWp. The projects which were installed in the initial phase, the nameplate allowed capacity was relatively small and moderate (5–50 MW) the tariffs were high. On the other hand, initial wind PPAs were not constrained in terms of such energy generation perspective and as such there was no such limit for the amount of energy fed to the

grid. With the introduction of procurement through competitive process, the wind power contracts also saw cap for minimum and maximum energy generation.

As per the data published by Central Electricity Authority (CEA), from year 2016 onwards he average CUF for solar projects is in the range of 20–24%; however, for wind projects it has been reported below 18% consistently [6].

Lower value of CUF compare to anticipated value, is directly related to the performance of the power project and it's a serious concern not only to the project developers but also to respective lenders. Also, it means the underutilization of the evacuation infrastructure especially dedicated to transport the energy. This situation has necessitated to explore ways to enhance the energy generation of the operational solar PV and wind power projects installed in India through re-powering This article deals with the repowering scope of solar and wind projects in India, through assessing the potential.

2 Scope of Solar Repowering in India

Through review of the portfolio of several project developers and reports available in public domain, it has been observed that there is significant gap in the estimated vs actual energy generation in the solar PV projects in India. Projects above 50 or 100 MW capacity are underperforming as compared to smaller capacity projects. The projects implemented in early phases of NSM (from 2010–2013) have been analyzed by collecting energy generation data from several sources [7] As an example, Figs. 2 and 3 present the energy generation pattern of few representative projects under the National Solar Mission Phase-I Batch-I2 and Phase II Batch I3 from commissioning.

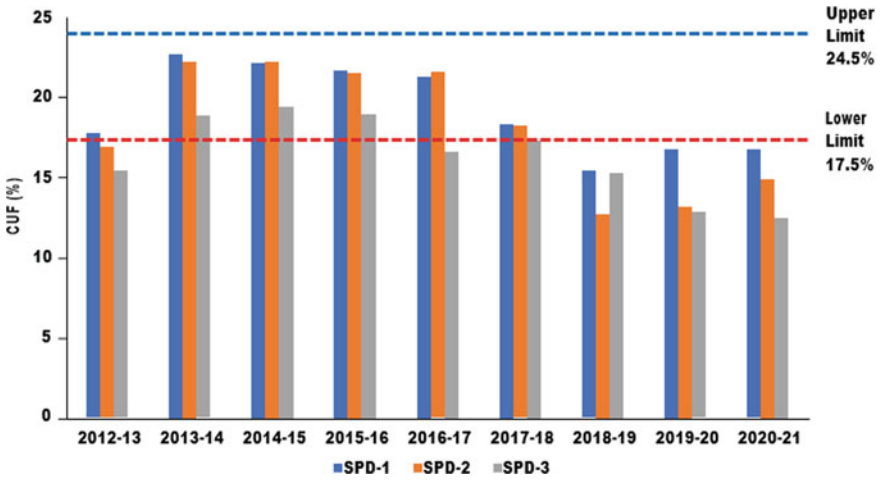

Fig. 2 Energy generation of representative projects under NSM Phase I

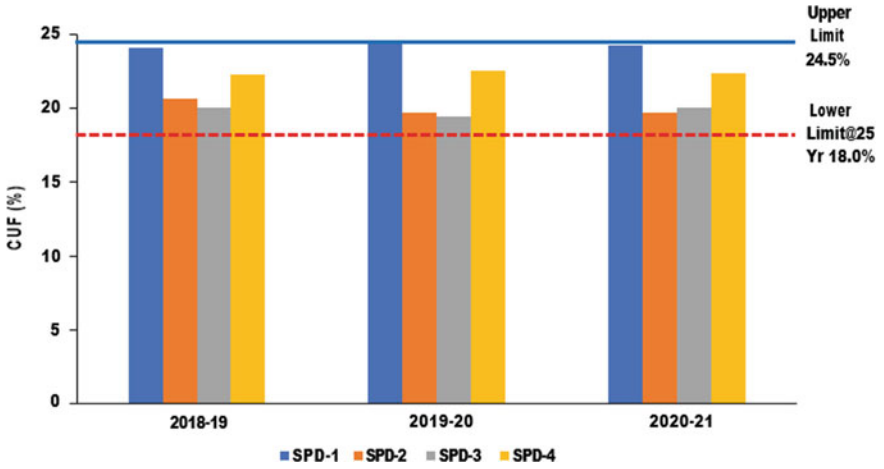

Fig. 3 Energy generation of representative projects under NSM Phase II (VGF)

This might be due to limitation of developers to manage operation and maintenance of larger capacity projects or even their inability to source finance for re-powering of those projects.

Thus, instead of replacing old technologies with new ones, the energy yield of a utility-scale solar or wind power project could be increased and optimized by adding a solar PV capacity up to a certain range. The nameplate capacity of solar PV modules is essentially the capacity at standard test conditions (STC), despite it is well established that the modules inherently possess a quality of degradation [8]. Thus, every year there is a deration in the solar plant capacity due to degradation and other operational factors. To overcome this issue, it is suggested that since the ground conditions are different than STC conditions, it is possible to install additional solar capacity (DC) behind the inverters (AC) to make up for the reduced energy generation.

Re-powering is an approach that addresses operational RE projects under performance-related issues. Besides, it optimizes land use through more efficient technologies and adequately utilizes power evacuation and transmission infrastructure of the operating projects as per the existing PPA requirements. In this context, present study exploring the market potential of re-powering utility-scale solar PV power projects in India. Once completed, the study could potentially be applied to assess the techno-economic feasibility of such approach.

In India, utility-scale solar PV projects have power purchase agreements (PPAs) at a fixed tariff for 25 years. This tariff is determined through competitive bidding by off-takers (such as SECI, NVVN, Discoms, etc.). Repowering potential of solar projects could be assessed through two approaches (i) Repowering up to PPA limit and (ii) Repowering up to technical limits.

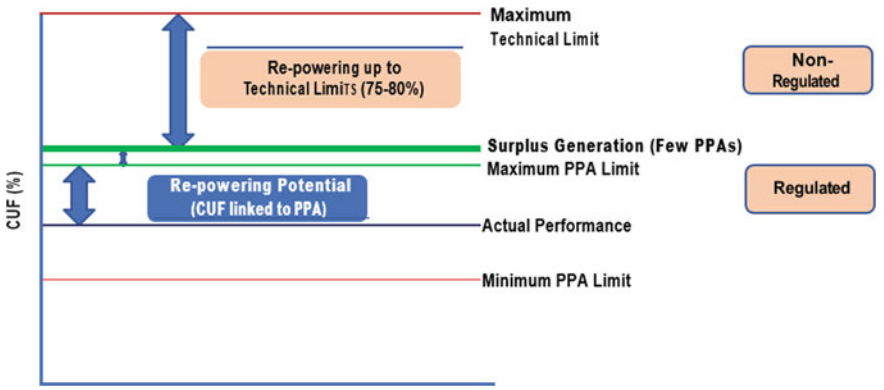

Fig. 4 Approaches of repowering

2.1 Re-powering Within PPA Limits

This approach is mainly for solar PV projects in which the capacity gap (and energy as well) due to degradation and plant unavailability could be fulfilled by installing additional DC capacity. In the approach of repowering, the additional capacity would be in line with the maximum allowed limit of energy generation as per the PPA (Fig. 4).

2.2 Re-powering up to Technical Limits

In case of solar PV projects, since the inception of their commercial deployment there have been several technological advancements especially in solar PV modules (crystalline to PERC, higher efficiency, and Wp rating) and inverters (central to string). For instance, about DC and AC, project developers have gradually increased their overloading capacities 12. By 2016, overloading of solar projects was in the range of 25–30%, and at present, several developers design projects with 55–60% overloading. Since 2019–20, mostly the industry has adopted at least 50% overloading. The reasons to increase the overloading capacity include lower tariffs, technical flexibility, reduced cost, higher upper limit of energy sale as per PPAs, etc.

Based on the discussions with Tier-1 solar PV module suppliers and inverter manufacturers, it was observed that it is possible to overload solar PV projects up to 75–80% in India with optimization of clipping losses and respective techno-economic parameters. For re-powering, operational projects with 0–30% overloading could be targeted to enhance energy generation to the best possible extent.

Up to the maximum PPA energy limits, the re-powered energy could be sold at a fixed tariff to off-takers, however, selling re-powered energy above PPA limits would require a separate (or amendment in the existing PPAs) regulatory framework.

3 Methodology Adopted for Assessing the Repowering Potential

Solar energy projects performed on variable energy resource, which comprises inherent intermittency and operational challenges. It has been observed through the technical assessment of a large capacity of utility-scale solar projects that there, is considerable difference between estimated energy (at project design stage) and actual generation, which might be caused by several reasons such as resource inadequacy, inter-annual variability, technical and design issue, operation and maintenance issue, grid availability, etc. In industrial practices, solar PV projects are financed at P50 level of energy generation; however, wind projects are at P 90 level of probability. The project life of solar PV is essentially considered as 25 years. There is inherent property of degradation in solar PV technology, which derates the capacity of the plant continuously and reduces the energy generation accordingly. Similarly, in wind projects wind resource makes maximum impact on energy generation. Considering the latest portfolio of utility-scale solar PV (36.8 GW) in the country by second quarter of year 2021 the potential of re-powering of solar has been estimated. The methodology adopted for the same is illustrated in Fig. 5.

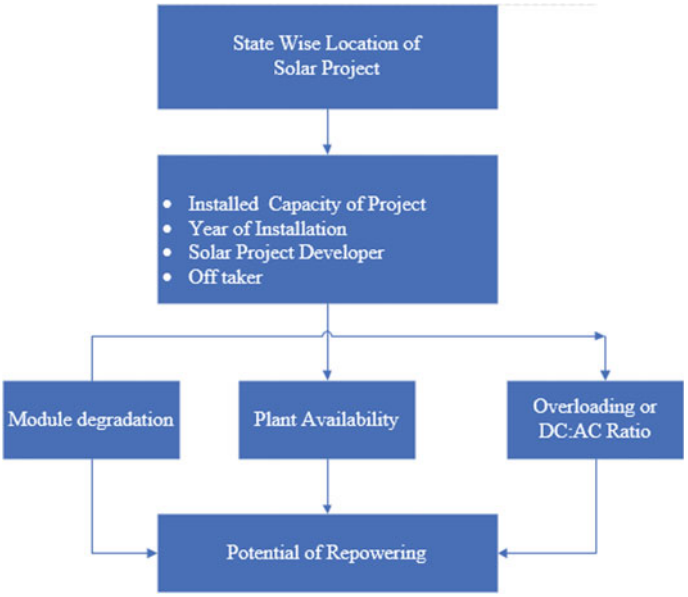

Fig. 5 Methodology adopted for estimating the repowering potential

3.1 Identification of State Wise Locations and Data of Solar PV Projects in India

To begin with, state wise locations of solar power projects in India have been identifies and validated through multiple sources. Further, data on the installed capacity of these projects, year of installation, name of solar project developers, off takers etc. have been collected. The other key aspects considered have been taken for estimating the potential of re-powering of solar projects in India are listed below.

3.2 Module Degradation

Degradation is an inherent property of solar PV modules made of any technology crystalline or thin film). This may involve either a gradual reduction in the output power of a PV module over time or an overall reduction in power due to failure of an individual solar cell in the module.

Degradation depends on several manufacturing, meteorological and operational parameters hence no manufacturer essentially guarantees it. However, there is warrantee associated with the solar PV modules, which reflects how this parameter may impact plant performance (Fig. 6). For potential estimation, in line with the technical datasheet of TIER-1 solar PV modules and best industry practices the following considerations have been made to incorporate degradation [8] in potential assessment:

- 2.5% at the end of the first year (which includes LID + first year module degradation)
- 0.8%/year up to first 10 years
- 0.7%/year for the next 15 years (i.e., 11th year onwards).

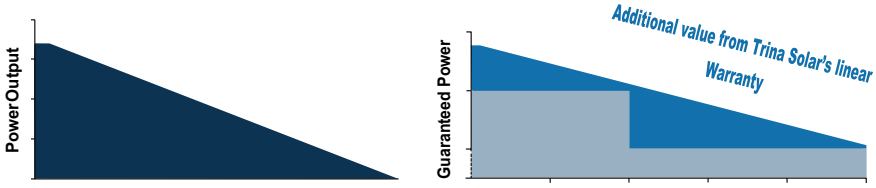

Fig. 6 Impact of module degradation on plant performance

3.3 Plant Availability

Plant availability depends on a lot of O&M parameters and protocol/practices of preventive and operative maintenances. For older projects (say from 2010–14)—even if the guaranteed plant availability by the O&M contractor is more than 96% and up to 98.5%, the key issue lies with the availability of spare parts. As of today, in these projects, it makes more sense to replace the entire equipment rather than looking for spare parts (e.g., replacing an existing inverter with the latest one instead of using substandard spare parts for existing inverters). The developers comprising in-house EPC offer very aggressive plant availability guarantees. Based on the review of various O&M contracts and guaranteed plant availability by the O&M contractors, the following plant availability values have been considered:

- 96.5% for 2010–12 (means 3.5% loss)
- 97.0% for 2013–14 (means 3.0% loss)
- 98.0% for 2015–16 (means 2.0% loss)
- 98.5% for 2017–2018 (means 1.5% loss).

Apart from plant availability, grid-availability also makes significant impact on annual generation from the projects especially, the projects connected to grids with STUs (33–220 kV level), where grid availability is 97–99.5%. We have not considered grid availability for estimation of the potential as this is beyond the control of the developer or O&M contractor.

3.4 Overloading (DC-AC Ratio)

In inception phase of 2010–12, most of the solar projects have been implemented with equal or minimum (~5%) DC to AC ratio due to higher cost of panels, policy restriction, PPA limitations, technology limits, etc. With the increased limits of salable energy to off-taker, technological advancements, and reduced cost of solar PV modules, etc., the developers have gradually increased DC to AC ratio from 10–30% to 50–55% or more. The key reason for high DC capacity is due to the fact that standard test conditions of solar PV modules, which are essentially laboratory conditions and not actual ground conditions. In the assessment, the DC capacity has been quantified through tracking of multiple utility scale solar PV projects from 2010 to 2021 of various capacities.

3.5 Sensitivity Assessment

From an investment and bankability perspective, utility-scale solar projects are structured and financed at P50 level of energy generation.6 There are several uncertainties associated (resource, design, operation, etc.) with the projects which cause an error of around 6–9% w.r.t P50 values. Solar resource database comprises maximum uncertainty in energy yield estimation. It has been observed that projects developed in India are not based on the long-term ground (measured) data. Mostly, their energy yields have been assessed using long-term average satellite databases, viz., Meteonorm7.1/7.2, and SolarGIS, etc. It has been observed that the projects commissioned till the year 2015–16 are mainly based on Meteonorm 7.1 and 7.2 database, which has an inherent uncertainty of 7–8%. From 2016 onwards, most of the developers are using Solar GIS satellite data, which has comparatively lower uncertainty in the range of 4–5%. Boundaries for sensitivity analysis have been considered in the range P50 (best case scenario) to P90 (worst case scenario). Most of the solar PV projects are currently operating in between P50 and P99 range.

- Total uncertainty 8.75% has been considered for the projects of 2010–2016 w.r.t. Meteonorm
- Total uncertainty 6.35% has been considered for the projects of 2017–2021 w.r.t. Solar GIS.
- The difference between P50 and P99 values are in the range of 15–20% depending on the database. Considering the above range of P values the re-powering potential has been estimated.

4 Results and Discussion

Using the methodology adopted in Sect. 3, repowering potential of solar energy projects in India has been estimated. Table 1 presents year-wise potential of re-powering solar PV projects in India.

It has been observed that the potential of re-powering solar PV projects is around 2.89 GWp capacity in the country till 2021; however, it is around 973 MWp till the year 2016. However, considering the input parameter's of sensitivity analysis mentioned in Sect. 3.5. The difference between P50 and P99 values are in the range of 15–20% depending on the database. Considering the above range of P values the re-powering potential has been estimated and presented in Fig. 7.

From the assessment of annual capacity growth and key considerations of the derating of the capacity the potential of re-powering of solar power projects in India has been estimated from 2.9 to 3.4 GWp in the range of P50–P99. From the performance assessment of several operational projects, it has been found that mostly the projects perform in between P50 and P75, hence around 3.0 GWp potential could be considered to proceed.

Table 1 Potential of re-powering of solar projects in India

CoD year	Cumulative capacity (MW)	Annual Inst. capacity (MW)	Overloading (DC:AC)	Annual inst. capacity (MWp)	Re-powering potential (MWp)	PPA tariff range (INR/kWh)
2010	64	5	5	5	1	10.95–12.76
2011	260	196	5	206	26	7.49–9.44
2012	1251	991	10	1090	132	7.00–12.45
2013	2303	1052	15	1210	131	5.50–8.01
2014	3032	729	20	875	88	6.46–6.71
2015	4609	1577	25	1971	164	5.00–7.02
2016	8885	4276	30	5559	422	4.34–5.20
2017	17,586	8702	30	11,312	715	2.44–3.47
2018	23,946	6360	40	8904	495	2.33–3.48
2019	31,371	7424	45	10,765	461	2.48–3.02
2020	33,986	2616	50	3923	118	1.99–3.99
2021	37,900	3914	55	6066	133	2.20–2.47
Total		37,900		51,948	2894	

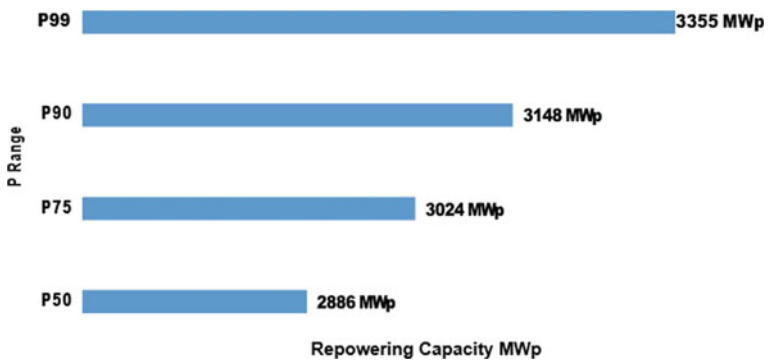

Fig. 7 Re-powering potential variation from P50 to P90 levels

State wise potential of solar repowering has also been presented in Table 2. For which latest installed capacity data (end of July 2021) of various states have been considered. This data provides AC capacities installed in each state. A weighted average overloading ratio has been calculated on the entire installed AC capacity based on the yearly overloading ratio values presented in Table. A weighted average overloading ratio of 40% has been obtained from the above analysis and same value has been applied to arrive at installed capacity (MWp) for each state. Table 2 presents

Table 2 Potential of re-powering of solar projects in Indian states—Top 10

S. no	State	Inst. capacity (MW)	Inst. capacity (MWp)	Re-powering potential (MWp)
1	Karnataka	7377	10,328	537
2	Rajasthan	6557	9180	477
3	Andhra Pradesh	4178	5849	304
4	Tamil Nadu	4003	5604	291
5	Telangana	3616	5062	263
6	Gujarat	3429	4801	250
7	Madhya Pradesh	2497	3496	182
8	Maharashtra	1939	2714	141
9	Uttar Pradesh	1795	2512	131
10	Punjab	930	1302	68

the 10 states for re-powering arranged in descending order of their respective potentials. Based on the analysis, Karnataka has the highest re-powering potential in India.

Further, in the perspective of potential tapping and implementation of repowering at ground level off-taker and SPD wise potential has also been assessed. To assess the same from the available database of commissioned solar PV projects, DISCOM-wise cumulative AC capacity data has been consolidated as presented in Table 3.

SECI and NTPC projects are spread across several states. For example, in the state of Rajasthan more capacity has been installed under Central schemes and less through the state policy. The rating of the Discom may give clarity for decision makers to develop bankable project considering minimum off-taker risk (Table 4).

Table 5 presents a case of overload commissioned projects up to 55%, which is the current practice in India. This table suggests a huge potential for DC capacity addition.

It has been determined that if the existing solar capacity of India could be repowered till the best technical limits (as per current practices) the cumulative potential of re-powering is above 6.5 GWp.

5 Concluding Remarks

- Using most conservative approach the potential of re-powering of solar PV projects has been estimated around 3 GWp in India just to meet the gap of PPA. In case the re-powering is targeted till the technical limits (or as per the recent practices) of the equipment the potential may be 6–9 GWp.

Table 3 Potential of re-powering of solar projects w.r.t. primary off-takers—Top 10

S. no	Primary off-taker	Inst. capacity (MW)	Inst. capacity (MWp)	Re-powering potential (MWp)	Rating	Rating agency
1	SECI	5010	7014	365	AAA	
2	NTPC	4040	5656	294	AAA	
3 (etc.)	Karnataka, BESCOM	3845	5384	280	B+	ICRA
4	Tamil Nadu, TNGDC	3439	4815	250	C	ICRA
5	Gujarat, GUVNL	2821	3950	205	A+	ICRA
6	Telangana, SPDCTL	2635	3689	192	B	CARE
7 APL	Andhra Pradesh, SPCD	1778	2489	129	B	CARE
8	Maharashtra, MSEDCL	1573	2203	115	A	ICRA
9	Uttar Pradesh, PVVNL	1457	2039	106	B+	CARE
10	Madhya Pradesh, MPPMC	1241	1737	90	B+	CARE
11	Rajasthan, RVPNL	1128	1579	82	C+	CARE
12	Punjab, PSPCL	906	1268	66	A	ICRA

- The potential project developers for solar re-powering are Adani/Total, ReNew Power, Azure Power, Tata Power, Acme, and SECI, NTPC, and the discoms of Karnataka, Tamil Nadu and Gujarat are the key off takers.
- In case of solar PV projects—the repowered energy up to the limits of PPAs is possible to sell power to the existing off taker at same PPA rate. However, the surplus/excess energy above the PPA cap requires separate provisions in PPAs to sell in the third parties/merchant market.
- Lots of business models could be explored considering the present regulatory regime and required amendments, which may open the sector of re-powering solar PV and wind power projects.

Table 4 Potential of re-powering of solar projects—Top 12 project developers

S. No	Solar project developer (SPD)	Inst. capacity (MW)	Inst. capacity (MWp)	Re-powering potential (MWp) at			
				P50	P75	P90	P99
1	ReNew	2546	3564	185	194	202	215
2	Adani	2410	3374	175	184	191	204
3	Adani-total JV	2373	3322	173	181	188	201
4	Azure power	2027	2838	148	155	161	172
5	Tata power	1880	2632	137	143	149	159
6	Acme	1803	2524	131	138	143	153
7	Greenko	1484	2077	108	113	118	126
8	NLC	1349	1889	98	103	107	114
9	Avaada	1152	1613	84	88	91	97
10	NTPC	964	1350	70	74	77	82
11	Hero future energy	838	1173	61	64	67	71
12	Sprng energy	714	1000	52	54	57	60
13	Mahindra	650	910	47	50	52	55

Table 5 Potential of re-powering—maximum technical limits

CoD year	Annual inst. capacity (MW)	Annual inst. capacity (MWp)	Overloading (DC:AC)	Add. DC overloading	Additional DC capacity (MWp)
2010	5	5	5	50	3
2011	196	206	5	50	98
2012	991	1090	10	45	446
2013	1052	1210	15	40	421
2014	729	875	20	35	255
2015	1577	1971	25	30	473
2016	4276	5559	30	25	1069
2017	8702	11,312	30	25	2175
2018	6360	8904	40	15	954
2019	7424	10,765	45	10	742
2020	2616	3923	50	5	131
Total	33,928	45,820			6767

References

1. Details available at https://mnre.gov.in/the-ministry/physical-progress. Accessed on 5 Oct 2021
2. Details available at https://unfccc.int/process-and-meetings/the-paris-agreement/the-paris-agreement/key-aspects-of-the-paris-agreement. Accessed on 5 Oct 2021

3. Details available at https://www.saurenergy.com/solar-energy-news/solar-tariffs-new-low-rs-1-99-kwh-latest-gujarat-auction. Accessed on 5 Oct 2021
4. Details available at https://bridgetoindia.com/report/india-renewable-map-june-2021/. Accessed on 5 Oct 2021
5. Details available at https://powermin.gov.in/en/content/power-sector-glance-all-india. Accessed on 5 Oct 2021
6. Details available at https://www.renewablesindia.in/. Accessed on 5 Oct 2021
7. Bridge to India. RE Navigator. Accessed on Nov 2021
8. NREL. https://www.nrel.gov/state-local-tribal/blog/posts/stat-faqs-part2-lifetime-of-pv-panels.html. Accessed on 10 Oct 2021

Modelling and Economic Optimization of Residential Load Based Microgrid in HOMER Pro by Dispatch Strategy

Smruti Ranjan Behera, Jyoti Ranjan Baral, and Twinkle Kisku

1 Introduction

Renewable energy investment and adoption of microgrids are surging in the recent years. Countries like China is investing in the renewable sector which is the world's highest and followed by United States and Japan. In this regard, a hybrid renewable energy system will be a cost-effective and preferred method of supplying electricity. In a study by Miah et al. [1] a stochastic method is used to achieve the least expensive configuration. The strategy's efficacy is determined by comparing the model's results to those of a green-house where an enhancement model isn't applied to it under the same experiment parameters.

Swarnakar et al. [2] considered a technical university in Rajasthan, India and optimized the microgrid within the university using HOMER Pro also performing several sensitivity analyses.

Singla et al. [3] studied the HOMER Pro software for designing micro-grids using various energy resources. The author briefs about the methodology used by HOMER Pro software including resource extraction, addition of components and sensitivity analysis of the design.

Dutta et al. [4] modelled and performed cost optimization on an existing micro-hydro and other renewable sources available for a locality in Nepal.

The microgrid design is being done in HOMER. This software is developed by NREL, United States. Softwares like HOMER, RETScreen, HYBRID2 and iHOGA are widely used for hybrid energy resources optimization. Other software tools used for HES either have some limitations in the range of component, compute slow or do not provide efficient economic optimization. HYBRID2 unsuitable for economic and multi-objective optimization. iHOGA is a hybrid optimizer written in C++ that is

S. R. Behera (✉) · J. R. Baral · T. Kisku
Odisha University of Technology and Research, Bhubaneswar, India
e-mail: rsmruti16@gmail.com

S. Doolla et al. (eds.), *Advances in Renewable Energy and Its Grid Integration*,
Lecture Notes in Electrical Engineering 1041,
https://doi.org/10.1007/978-981-99-2283-3_10

used to determine the best size for hybrid renewable energy systems. Over all among these softwares, HOMER has the advantage that it provides the option to simulate wider range of components. HOMER is the most extensively used and useful. It provides a comprehensive list of components to optimize as well as findings in the form of technical, environmental, and cost—benefit analysis. It's simple to use and processes data quickly. Tables and graphs are used to display the results [5].

2 Methodology

The process is started with electric load estimation. Next, the resources for the particular region are collected and this data will be helpful during the optimization and analysis process. For the best hybrid energy system setup, a number of economic studies or optimizations are used. Using the HOMER Pro optimization tool, the micro-grid design is simulated and results are generated. Optimum use of available resources helps to keep production costs of energy generation as low as possible as shown in Fig. 1.

2.1 Micro-grid Design

Here, the sizing of the micro-grid for a residence in a city on considering an annual load increment using HOMER Pro. In this work, the components of micro-grid taken into consideration are AC load (residential), PV modules, diesel generator and battery energy storage system. The selected location is Bhubaneswar, Odisha, India (20.2961° N, 85.8245° E). The synthetic data for residence group load profile available in the software was taken into account. There is a 20.47 kW peak load linked to this location's residences, and daily usage is 110.26 kWh.

2.2 Collecting Resources

Temperature data: The temperature data is downloaded from HOMER Pro under the resources tab. HOMER gets the data from NASA prediction of Worldwide Energy Resources (POWER) database. The data consists of monthly average air temperature

Fig. 1 Process flow

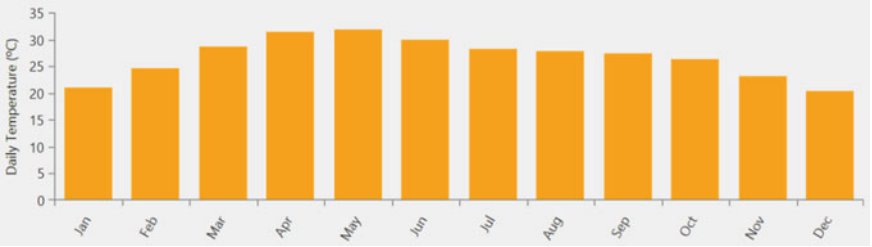

Fig. 2 Monthly average air temperature for the proposed location

Fig. 3 Monthly average solar global horizontal irradiance

over 30-years period (Jan 1984–Dec 2013). Based on their introduction site, PV modules are evaluated at 25°C (STC), higher temperatures can adversely affect yield by 10–25% [6]. As a result, while deciding on a site and solar panel configuration, temperature is a critical consideration as shown in Fig. 2.

The annual average (°C) is found to be 26.69.

Solar GHI data: HOMER gets the solar irradiance data from National Renewable Energy Laboratory database. The data consists of monthly average solar global horizontal irradiance data. Keeping all parameters constant, higher the irradiance, higher the PV output current, thus more power is generated as shown in Fig. 3.

2.3 Load Profile

Additionally, HOMER Pro provides us with a daily and annual load profile for our chosen area. The month of June is predicted to be the peak in this study. Evenings are considered the peak hours of the day in the daily load profile as shown in Fig. 4.

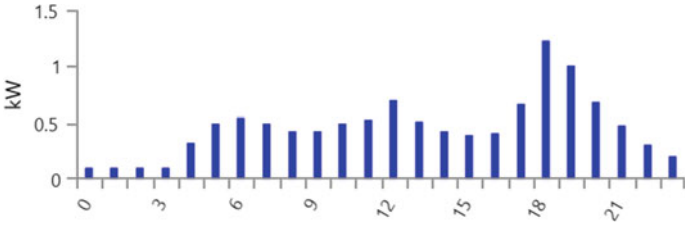

Fig. 4 Daily load profile

2.4 Simulation Software

When utilizing HOMER Pro to model a solar-powered system, inputs on the technological alternatives, costs of the components, and available resources must be given. Every year, the program calculates the energy balance between the potential quantity of energy generated and demand by simulating a huge number of various framework configurations. HOMER pro then calculates the flow of power between the architecture components. It is possible to configure HOMER such that it optimizes the system based on a variety of factors, including the size of the system.

2.5 Dispatch Strategies

Cycle charging

When a generator is needed, it runs at maximum capacity, and any excess power is used to recharge the battery bank. When renewable energy sources are few or nonexistent, the most effective charging strategy is to use cycle charging. In the table of results, "CC" stands for "cycle charging" [7].

Load Following

When a generator is required, it generates just enough electricity to fulfil the demand under the Load Following method. In systems with a large amount of renewable energy, load following is usually the best option.

MATLAB Link

An algorithm for HOMER Pro dispatch may be written using the HOMER Pro MATLAB Link. During the simulation, HOMER communicates with the MATLAB program to execute the specified MATLAB functions [7].

MATLAB Link controller is implemented in the work and a custom dispatch strategy is written. List of simulation parameters [8] are used to write the MATLAB script. According to the strategy, first the load requirement is fulfilled by the power available from PV. If excess power is left, it is utilized in charging the battery. If there is any unmet power, it is tried to be fulfilled by battery. If battery is unable to fulfill

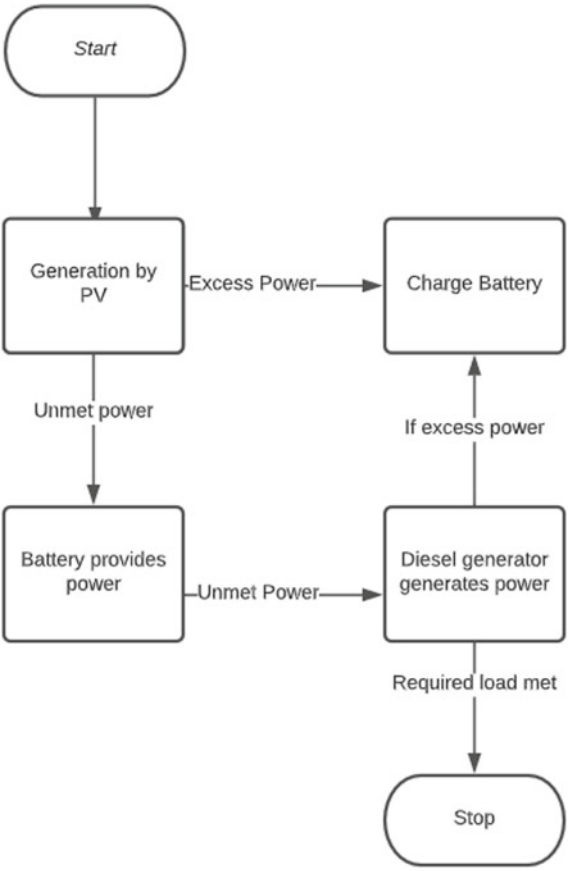

Fig. 5 Dispatch strategy flowchart

the demand, the diesel generator comes into play and meet the required demand as shown in Fig. 5.

3 Model and Simulation

A hybrid microgrid is modelled in HOMER Pro consisting of diesel generator, battery, PV and converter. The DC bus is used to link the battery and PV, whereas the AC bus is used to connect the load and diesel generator. The converter is connected to both AC and DC bus. Batteries and diesel generator will be used as reserve elements. The cost of each component is given as input to HOMER Pro. The microgrid system taken into consideration is shown in Fig. 6.

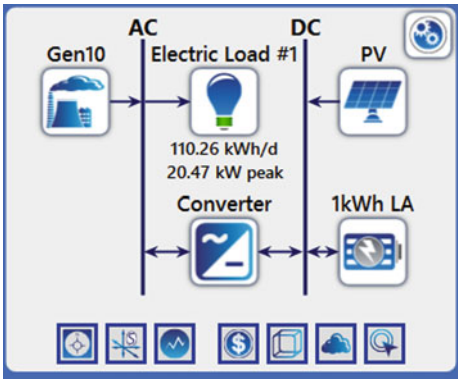

Fig. 6 Micro-grid connection schematic model

Table 1 Comparison of results from different controllers

Dispatch	PV (kW)	Battery (kWh)	Converter (kW)	Gen10 (kW)	NPC (₹)	COE (₹)	Ren frac (%)	Fuel (L/yr.)
MATLAB link	14.3	14	9.10	10	1,82,32,060	35.46	38.1	9878
Load following	14.8	15	10.00	10	1,81,52,682	35.69	35.0	10,087
Cycle charging	14.2	15	9.95	10	1,81,00,691	35.38	30.1	10,166

4 Results and Discussions

4.1 Optimization Results Using Different Controllers

From Table 1. it is noted that the price of energy is ₹35.46 for MATLAB link, ₹35.69 using Load Following and ₹35.38 using Cycle Charging. In Cycle Charging, the fuel used is more than that of Load Following because it uses Generator at full power.

Whereas MATLAB Link provides the option to go with a custom dispatch strategy with near about similar cost of energy.

4.2 Optimization Results of MATLAB Link Controller

Figure 7 shows the hourly details from all power sources against the load. During the day time, when the PV output is good enough, it is used to serve the load. During night, when there is no PV output, battery and diesel generator are used together to

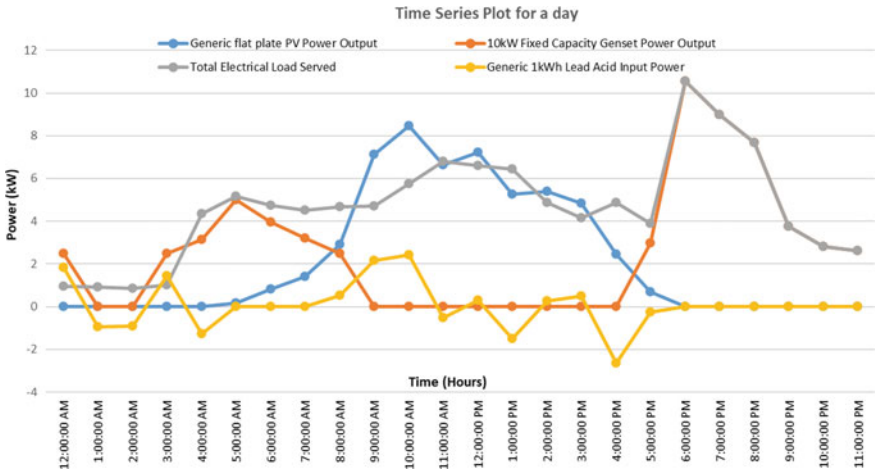

Fig. 7 Time series plot for a day

meet the load demand. As it is a residential load, the load is peak during the evening. As there is no PV output in the evening, most of the load is met by diesel generator.

4.3 SOC of the Battery

Figure 8 shows the state of charge of the battery in a day for a whole year. The graph clearly shows that the battery is being used least during peak months (i.e., around 180th day of the year) at the peak hours (10.00–14.00 h). The state of charge of battery during these hours is maximum indicating least usage further indicating that most of the load requirement is met by the solar PV system. This makes the system efficient.

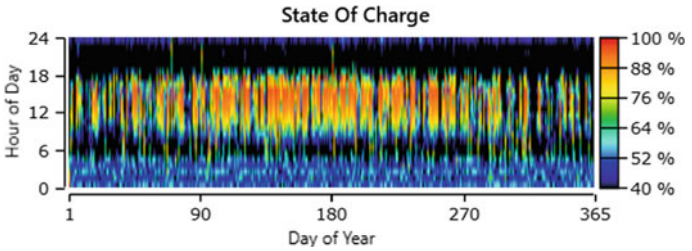

Fig. 8 SOC data throughout the year

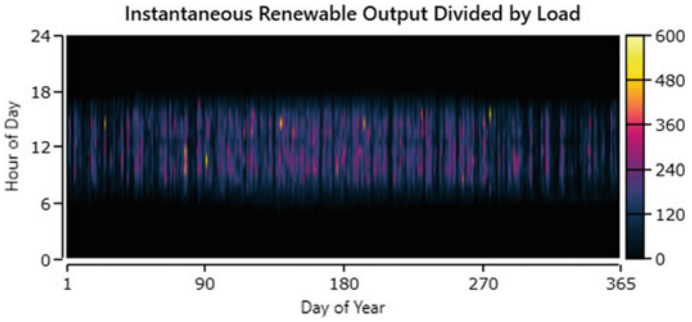

Fig. 9 Renewable penetration throughout the year

4.4 Renewable Energy Sources Output

Figure 9 shows the amount of load met by renewable energy (i.e. renewable output divided by load) in a day over a year. The graph clearly shows that the value of renewable output/load is greater than 100% during the day time which means the load is completely met by renewable sources. For the rest of the day, it is less than 100 percent. It implies that renewable resources are not able to meet the load. Other sources contribute to the production of energy to meet the demand.

From Table 1 the renewable energy resource penetration in our proposed system is around 38%.

5 Conclusion

The aim of this paper is to design a sustainable and economical micro-grid for residential purpose in Bhubaneswar, Odisha using HOMER PRO software. The renewable resource used in this paper is solar energy. It can vary depending upon the location and availability of resources over there. The total load demand is 40,245 kWh, production of energy is 43,282 kWh and cost of the proposed system is ₹1,82,32,060 while that of base system is ₹2,17,26,659. We are able to mitigate the load demand using the design proposed under a reasonable budget. This makes our system efficient and practically usable. Three dispatch strategies have been explained which includes cycle charging, load following and MATLAB link. We can write our own dispatch strategies and make the design more feasible and sustainable.

References

1. Miah MS, Momen Swazal MA, Mittro S, Islam MM (2020) Design of a grid-tied solar plant using homer pro and an optimal home energy management system. In: IEEE INOCON, pp 1–7
2. Swarnkar NM, Sharma R, Gidwani L (2016) An application of HOMER Pro in optimization of hybrid energy system for electrification of technical institute,. In: 2016 International conference on energy
3. Singla MK, Nijhawan P, Oberoi AS (2021) Cost–benefit comparison of fuel cell–based and battery-based renewable energy systems. Int J Energy Res 46:1736–1755
4. Dutta S, Qian A, Adhikari A, Yue W, Yufan Z, Zhaoyu L (2019) Modelling and cost optimization of an Islanded microgrid with an existing microhydro using HOMER software. In: 2nd ACEEE, pp 74–78
5. Kaur D, Cheema PS (2017) Software tools for analyzing the hybrid renewable energy sources: -a review. In: ICISC, pp 1–4
6. NASA power. Retrieved from: https://power.larc.nasa.gov/. Accessed 15 April 2022
7. Aziz A, Tajuddin MFN, Zidane TEK, Su CL, Alrubaie AJ, Alwazzan M (2022) Techno-economic and environmental evaluation of PV/diesel/battery hybrid energy system using improved dispatch strategy. Energy Rep 8:6794–6814. https://doi.org/10.1016/j.egyr.2022.05.021
8. Listing of simulation_parameters. Available on: https://www.homerenergy.com/products/pro/docs/latest/index.html. Accessed 16 April 2022

Conductance Factor-Based Control of Solar Photo-Voltaic Fed Shunt Active Power Filter

Ravi Kumar Majji, Jyoti Prakash Mishra, and Ashish A. Dongre

1 Introduction

In recent times, the development and deployment of solar photo-voltaic (SPV)-based microgrids are gaining significant attention particularly in rural electrification [1]. However, in practice, the power generated from the SPV-based microgrids is intrinsically unreliable due to unpredictable environmental and site conditions [2]. It is known fact that the power electronic converters plays a vital role in the effective control of SPV-based microgrids for reliable and stable operation along with appropriate maximum power point tracking (MPPT) algorithms [3]. These power conversion systems, however, are classified as nonlinear loads for the utility system. They produce significant harmonics and reactive currents, which interact with the line impedance, resulting in harmonic voltages and affecting other loads connected to the same point of common coupling (PCC) [4]. Shunt active power filter (SAPF) has been considered to overcome these issues since it offers a higher capacity of filtering and control flexibility. Indeed, SPV fed SAPF's are widely used as better choice since they are designed to fed the real power into the utility system while providing the multi-functional services at PCC [5]. Hence, SPV fed SAPF's may be termed as multi-functional-SAPF's (MF-SAPF's). Furthermore, MF-SAPF's can be operated in grid-injection or grid supplying mode of operation.

R. K. Majji (✉) · J. P. Mishra · A. A. Dongre
Electrical Engineering Department, National Institute of Technology Silchar, Silchar, Assam 788010, India
e-mail: ravimajji@ee.nits.ac.in

J. P. Mishra
e-mail: jpmishra@ee.nits.ac.in

A. A. Dongre
e-mail: ashish_rs@ee.nits.ac.in

S. Doolla et al. (eds.), *Advances in Renewable Energy and Its Grid Integration*,
Lecture Notes in Electrical Engineering 1041,
https://doi.org/10.1007/978-981-99-2283-3_11

It is essential to design a flexible and effective control strategy for the appropriate operation of MF-SAPF [6]. The MF-SAPF's control strategy includes the reference current estimation and current tracking controller for the converter. In the literature, various reference current estimation techniques are reported to improve the control flexibility of the MF-SAPF. The conservative power theory [7], synchronous reference frame (SRF) theory [8], instantaneous reactive power theory (IRPT), adaptive theory, unit vector template (UVT) controllers, and second-order generalised integrator (SOGI)-based theory have all been used to improve the characteristics of MF-SAPF. Low-pass filters (LPFs) and phase-locked loops (PLLs) for grid synchronization are essential components of SRF, IRPT, UVT controllers, and other classic controllers. Because of LPF and PLL blocks, the estimated signals are delayed [9]. Under a distorted utility voltage scenario with IRPT, the MF-SAPF's performance degrades. In [10], a conductance factor (CF)-based control is employed in three-phase utility with simplified computations. The supply current in the CF-based control is the sum of a fundamental active component of load current and the current required to maintain a constant dc-link capacitor voltage.

In the literature many studies has been devoted to the design and development of current tracking controllers employed for MF-SAPF's. Such controllers are proportional-integral (PI), hysteresis control, sliding mode, back-stepping [11], and Lyapunov function (LF) controllers with associated modulation stage. A major defect in the sliding-mode control method is the design of the sliding surface in a dynamic system. If the surface design is inadequate, the performance in dynamic situations suffers. As a result, this control method is ineffective in dynamic situations. The PI controllers are employed generally in the MF-SAPF applications because of their simplicity, readily available, and ease of implementation. However, the performance of such controllers has not acceptable under source-side variations and dynamic loading scenario. Further, PI controllers are designed and tuned based on the equivalent linear model [8], wherein the MF-SAPF's include nonlinear dynamics. Further, the modulation stage in conventional control strategy causes control delays. In recent years, several research efforts on a finite control set-model predictive control (FCS-MPC) have experienced rapid growth, and prove that this controller is effectively tracking the estimated reference current/voltage/torque in various power electronic converter applications [12–14]. This is because an FCS-MPC is simple to implement, incorporates model dynamics into the control algorithm, provides better dynamic and steady-state performance, and allows constraints to be easily incorporated into the cost function. In this context, in present work an FCS-MPC is employed for reference current tracking by the associated converters under solar irradiance variation and dynamic loading conditions. The following are the primary contributions of the present study:

- The SPV is connected to an MF-SAPF for improved power quality and active power injection into the distribution load connected at PCC.
- DC-link voltage regulation is analyzed with LF-based nonlinear controller.
- The performance of the SPV fed MF-SAPF is analyzed with CF-based FCS-MPCC under variation in solar irradiance and dynamic loading conditions.

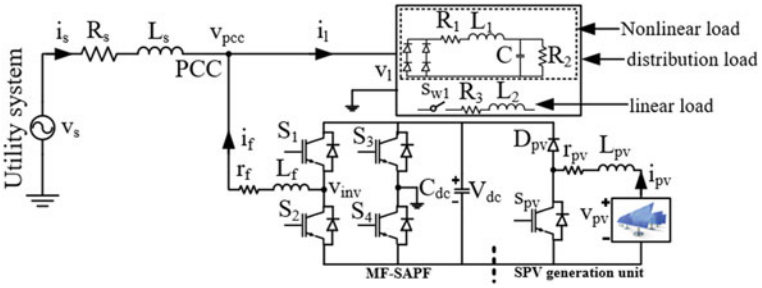

Fig. 1 SPV fed shunt active power filter in single-phase utility system

The rest of the paper is structured as follows: The system configuration is described in Sect. 2, followed by the MF-SAPF and SPVC dynamics in Sect. 3. The scheme of control strategy is described in Sect. 4. In Sect. 5, results and discussions under dynamic operating conditions are illustrated. Finally, the conclusions of the study are briefly summarized in Sect. 6.

2 System Configuration

Figure 1 depicts the configuration of solar photo-voltaic (SPV) fed shunt active power filter (SAPF) in single-phase utility system. The utility system voltage and current are represented with v_s and i_s respectively. The line impedance is represented with R_s and L_s. The SAPF is a H-bridge voltage source inverter connected at PCC through filter r_f and L_f. Since, SAPF can be controlled to provide multifunctional services, it is known as multifunctional-SAPF (MF-SAPF). The output current and voltage of the MF-SAPF are represented with i_f and v_{inv} respectively. The SPV generation unit is coupled at the common dc-link through dc-dc boost converter as shown, resulting in a double stage configuration. The filter parameters for SPV converter (SPVC) is represented as r_{pv} and L_{pv}. Similarly, V_{pv} and i_{pv} represents the voltage and current of the SPV unit. The dc-link capacitance is represented as C_{dc} with voltage V_{dc}. The distribution load considered at point of common coupling (PCC) is the combination of linear (R–L) and diode bridge rectifier (DBR), a nonlinear load. For the purpose of dynamic loading, linear load is connected using the switch s_{wl}. The voltage at PCC, voltage and current at distribution load are represented as v_{pcc}, v_l, and i_l respectively.

3 Converter Dynamics

The dynamics for MF-SAPF and SPVC are provide in the continuous and discrete-time domain as follows.

3.1 MF-SAPF Dynamics

From Fig. 1, owing to the MF-SAPF topology, the expression for the inductor current as a function of switching control variable (S) using Kirchhoff's voltage law is defined as follows:

$$L_f \frac{di_f}{dt} = S * V_{dc} - r_f i_f - v_{pcc} \tag{1}$$

where S depends on switching states of the MF-SAPF and following complementary action for converter-leg, thus, it can be defined as

$$S = \begin{cases} 1 & \text{if } S_1 \text{ and } S_4 \text{ is ON} \\ -1 & \text{if } S_2 \text{ and } S_3 \text{ is ON} \end{cases} \tag{2}$$

Similarly, using Kirchhoff's current law, the current at PCC is defined as

$$i_s + i_f - i_l = 0 \tag{3}$$

Based on Eqs. (1) and (3), the required discrete dynamics for the MF-SAPF at $t = k + 1$ instant with sampling-time T_s using forward-Euler approximation are expressed as follows:

$$i_f(k+1) \approx i_f(k) + \frac{T_s}{L_f}\left[v_s(k) - r_f i_f(k) - S * V_{dc}\right] \tag{4}$$

$$i_s(k+1) \approx i_l(k+1) - i_f(k+1) \tag{5}$$

Equation (5) is the predicted utility system current to implement the indirect current control approach.

3.2 SPVC Dynamics

The SPV generation unit consists of dc-dc boost converter integrated at the common dc-link of the system as shown in Fig. 1. The SPVC is used to regulate the SPV output with the help of a incremental conductance method-based maximum power point tracking (MPPT) algorithm [6]. The MPPT output current (i_{mpp}) according to variation in solar irradiance is considered as reference current (i_{pvref}) for SPVC. Now the expression for the inductor current as a function of switching control variable (S_{spv}) is defined as follows:

$$\frac{di_{pv}}{dt} = \frac{V_{pv}}{L_{pv}} - \frac{r_{pv} i_{pv}}{L_{pv}} - \left[1 - S_{pv}\right] * \frac{V_{dc}}{L_{pv}} \tag{6}$$

Then Eq. (6) in discrete form using forward Euler approximation for sampling time T_s at $t = k + 1$ instant can be expressed as

$$i_{pv}(k+1) \approx i_{pv}(k) + \frac{T_s}{L_{pv}}\left[V_{pv}(k) - r_{pv} i_{pv}(k) - \left[1 - S_{pv}\right] V_{dc}\right] \tag{7}$$

4 Control Strategy

4.1 Reference Current Estimation

In this study, the CF-based reference current estimation technique is realized to accomplish the indirect current control of MF-SAPF. Figure 2a depicts the CF based reference current estimation. Assume that the voltage at PCC is distortion free and sinusoidal. Thus, based on pq-theory [14], v_{pcc} is considered as α-axis component and the β-axis component is obtained by $\pi/2$ lag of v_{pcc}. Similarly, the α and β-axis components of load current are obtained as shown in Fig. 2a. Then the single-phase instantaneous load power is calculated as presented. However, for the purpose of indirect current control approach, the average load power (p_{lf}) due to the fundamental component is obtained using low pass filter (LPF).

LF-based dc-link voltage regulator: Generally, in conventional control approach PI controller is employed to generate the loss component for MF-SAPF. However, these are linear and the controlled system is nonlinear. Further, the performance of MF-SAPF is deteriorated under dynamic operating conditions with PI. The direct Lyapunov approach is widely used to determine the behavior of dynamic systems such as MF-SAPF about there equilibrium point, which is described by differential equations. Hence, the objective in this study is to develop a control method that ensures the global asymptotic stability of dc-link voltage of the MF-SAPF around its equilibrium. Now, a scalar energy-like function $V(x)$, called LF is constructed with the variables related to the energy stored (E_{dc}) in the dc-link capacitance as follows:

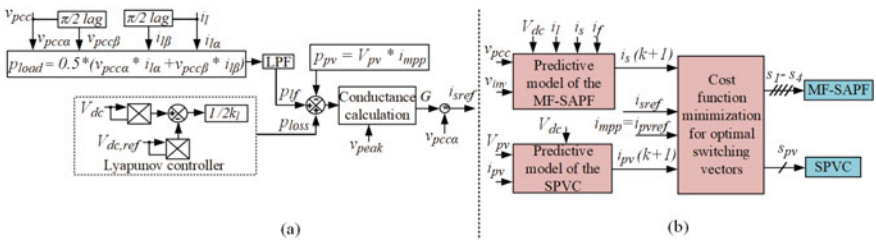

Fig. 2 Control strategy for SPV fed SAPF

$$E_{dc} = \frac{1}{2} * C * V_{dc}^2 \tag{8}$$

Theorem: A globally asymptotically stable system can be guaranteed using the direct Lyapunov approach if the LF satisfies the properties [15] such as $V(0) = 0$, $V(x) > 0$, for all $x \neq 0$, and $\dot{V}(x) < 0$ for all $x \neq 0$.

Proof: In order to ensure better performance from the LF-based controller, consider the squared error magnitudes of the actual and reference dc-link voltage as $\Delta\left(V_{dc}^2\right) = V_{dc}^2 - V_{dc_{ref}}^2$. Then Eq. (9) can be rewrite as

$$\Delta E_{dc} = \frac{1}{2} * C * \left(\Delta V_{dc}^2\right)^2 = \frac{1}{2} * C * \left(V_{dc}^2 - V_{dc_{ref}}^2\right)^2 \tag{9}$$

Now time-derivative of Eq. (9) result in the relation

$$\Delta \dot{E}_{dc} = \Delta p_{loss} = 2 * V_{dc}\left(V_{dc}^2 - V_{dc_{ref}}^2\right) * C * \dot{V}_{dc}$$

where, p_{loss} is the active power component needed to maintain the common dc-link voltage at reference.

$$\Delta \dot{E}_{dc} < 0 \Leftrightarrow 2 * V_{dc}\left(V_{dc}^2 - V_{dc_{ref}}^2\right) * C * \dot{V}_{dc} < 0$$

A constant k_l (strictly negative) is introduced to satisfy the condition $\dot{E}_{dc} < 0$ for $\dot{V}_{dc} \neq 0$, which yields

$$\Leftrightarrow 2 * p_{loss} = \frac{\left(V_{dc}^2 - V_{dc_{ref}}^2\right)}{k_l}$$

$$\Leftrightarrow p_{loss} = \frac{\left(V_{dc}^2 - V_{dc_{ref}}^2\right)}{2k_l} \tag{10}$$

Hence, according to direct Lyapunov approach, if $\Delta V_{dc}^2 = 0$, $\Delta E_{dc} \approx 0$, and $\Delta E_{dc} > 0$ for $\Delta V_{dc}^2 \neq 0$; and $\dot{E}_{dc} < 0$ for $\dot{V}_{dc}^2 \neq 0$. The realization of a LF-based nonlinear controller [16] is illustrated in Fig. 2a. The optimal value of k_l shows impact on the performance of the dc-link voltage regulation. In this study, k_l is equal to -2.75, that gives better performance of LF-based controller for dc-link voltage regulation.

Now, the requisite conductance factor (G) is defined and calculated as

$$G = \frac{p_{lf} + p_{loss} - p_{pv}}{v_{\text{peak}}^2} \tag{11}$$

where, p_{pv} is the power obtained from the SPV generation unit and v_{peak} of the fundamental voltage component of the utility system. The v_{peak} is expressed as

$$v_{peak} = \sqrt{v_{pcc\alpha}^2 + v_{pcc\beta}^2} \tag{12}$$

Finally, the expression for the reference utility system current for realization of indirect current control approach is defined as

$$i_{sref} = G * v_{pcc\alpha} \tag{13}$$

Algorithm 1 FCS-MPCC for MF-SAPF and SPVC

1: Measure required current and voltages of the MF-SAPF and SPVC.
2: Initialize $n_s \leftarrow 0$, $n_{pv} \leftarrow 0$, $S_1 - S_4 \leftarrow 0$, $S_{pv} \leftarrow 0$, $g_{ops} \leftarrow \infty$, $g_{oppv} \leftarrow \infty$.
3: Increase counter $n_s \leftarrow n_s + 1$, $n_{pv} \leftarrow n_{pv} + 1$.
4: Predict $i_s \rightarrow (S_1 - S_4)$ and $i_{pv} \rightarrow (S_{pv})$ at k + 1 instant using Eqs. (5) and (7) respectively. For SPVC: *If* $n_{pv} = 1$, $S_{pv} = 1$; *else if* $n_{pv} = 2$, $S_{pv} = 0$; end.
5: Retrieve i_{sref} from CF-based estimation of reference current unit, i_{pvref} from MPPT algorithm.
6: Cost-function minimization for optimal switching vectors using g_s and g_{pv}.
7: Check *If* $g_s < g_{ops}$, $g_{pv} < g_{oppv}$ *then* $g_{ops} \leftarrow g_s$, $g_{oppv} \leftarrow g_{pv}$.
8: Similarly, *if* $n_s < 4$, $n_{pv} < 2$ go to step-4, *else* $g_{ops} = min \cdot [g_s(n_s)]$; $g_{oppv} = min \cdot [g_{pv}(n_{pv})]$.
9: Apply $S_1 - S_4$ correspond to $min \cdot [g_{ops}(n_s)]$; S_{pv} correspond to $min \cdot [g_{pv}(n_{pv})]$.

4.2 Current Controller

Figure 2b illustrates the realization of current controller based on FCS-MPCC. As per the control logic of the FCS-MPCC, control objectives are framed in terms of cost function. Thus, a simple cost functions are adopted, considering the quadratic current errors of the MF-SAPF and SPVC as follows:

$$g_s = (i_{\text{sref}} - i_s(k+1))^2 \tag{14}$$

$$g_{pv} = \left(i_{\text{pvref}} - i_{pv}(k+1)\right)^2 \tag{15}$$

where, g_s and g_{pv} are the corresponding cost functions of MF-SAPF and SPVC. The minimization (close to zero) of above mentioned cost functions are subjected to obtain the optimal switching vectors for associated converters. The simplified FCS-MPCC algorithm steps for generating optimal switching vectors for MF-SAPF and SPVC are described in Algorithm 1. Since the algorithm is formulated with the finite control switching vector set and employed for reference current tracking control, it is known as finite control set model predictive current controller (FCS-MPCC).

5 Results and Discussions

The feasibility and effectiveness of the proposed control strategy is verified through MATLAB/Simulink simulation results under dynamic operating conditions. The system parameters for the simulation study are presented in Table 1. The dynamic operating conditions considered for the purpose of analysis are variation in solar irradiance (0–965 W/m^2) at standard temperature (27 °C) and sudden increase in distribution load. All dynamical operating conditions are verified for a simulation time of 1.25 s and analyzed for three operating modes as shown in Fig. 3.

Mode-1 (0–0.2 s): In this mode, a DBR load is connected at PCC and fed by the available SPV power and utility system. Since v_s and i_s are in-phase, this mode is known as grid supplying mode. The solar irradiance considered as 220 W/m^2. Thus, accordingly, MF-SAPF injects available SPV real power into the PCC along with harmonic compensation and reactive power support.

Table 1 System parameters for the simulation study

Parameters	Numerical values
v_s, f_s	220 V, 50 Hz
r_s, L_s	0.02 Ω, 0.2 mH
r_f, L_f	0.2 Ω, 30 mH
C_{dc}, V_{dc}	3500 μF, 400 V
SPVC: r_{pv}, L_{pv}	0.2 Ω, 5 mH
Linear load: R_3, L_2	25 Ω, 10 mH
DBR load: R_1, L_1, C, R_2	42.5 Ω, 10 mH, 3900 μF, 20 Ω

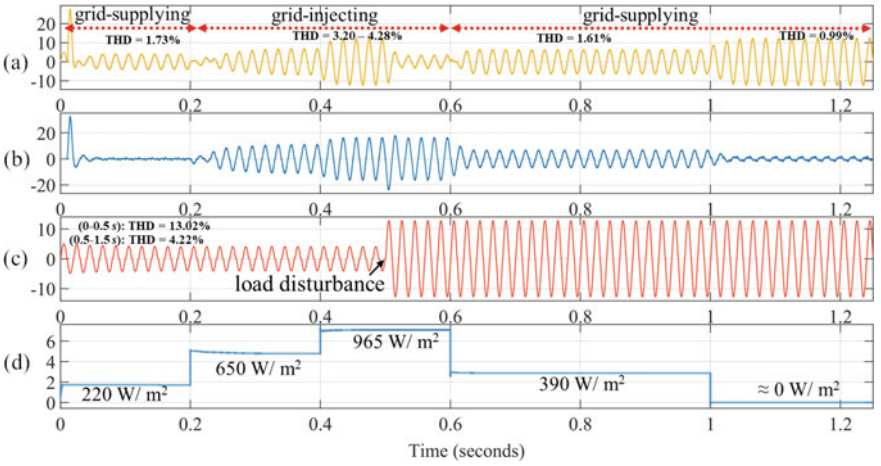

Fig. 3 Simulation results of **a** i_s, **b** i_f, **c** i_l, and **d** i_{pv} in SPV fed SAPF

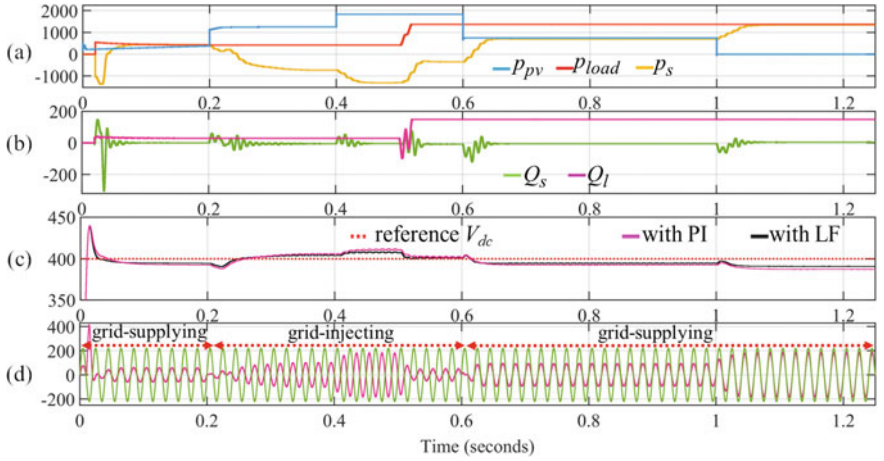

Fig. 4 Simulation results of under dynamic operating conditions

Mode-2 (0.2–0.6 s): In this mode, for analysis purpose, the solar irradiance is increased to 650 W/m^2 and 965 W/m^2 at $t = 0.2$ and 0.4 s respectively. Further, another linear load is connected to PCC at $t = 0.5$ s. Hence, the increased load demand is met by the SPV fed SAPF as observed. Since v_s and i_s are in phase opposition, this mode is known as grid injecting mode. The surplus power from SPV feeding into the PCC may be utilized to support other loads connected at PCC.
Mode-3 (0.6–1.25 s): In this mode, the solar irradiance is decreased to 390 W/m^2 at $t = 0.6$. Now the load demand is supported by the available SPV power through MF-SAPF and utility system. Since v_s and i_s are in-phase, this mode is also referred as grid supplying mode. Further, at $t = 1.0$–1.25 s, the solar irradiance is considered as ≈ 0 W/m^2 such that MF-SAPF performs only active power filtering for power quality improvement. Furthermore, the total harmonic distortion (THD) of i_s is improved at various operating scenario as presented in Fig. 4.

Figure 4a illustrates the power management in Watts among SPV (p_{pv}), load (p_{load}) and utility system (p_s), followed by the reactive power in vars of the load (Q_l) and utility system (Q_s) in Fig. 4b. The dc-link voltage is regulated better in terms of low steady state error with LF as compared to PI as shown in Fig. 4c. The simulation of v_s and i_s are presented in Fig. 4d under different operating modes. For analysis purpose, i_s is multiplied with a gain of 15 to its actual value.

6 Conclusion

The CF-based reference generation algorithm is implemented for MF-SAPF application. The computational burden is simplified as compared to conventional algorithms. Further, the application of FCS-MPCC is investigated for reference current track-

ing by the MF-SAPF and SPVC. The dc-link voltage regulation is realized using LF-based nonlinear controller. The performance of FCS-MPCC with CF approach is analyzed under variation in solar irradiance and dynamic loading conditions. From the presented results, it is evident that the control flexibility of the MF-SAPF is enhanced to provide the multifunctional services such as reactive power support, harmonic current compensation, and feeds the real power from the SPV generation unit into the utility system at unity power factor. The feasibility of the proposed control strategy is verified through the MATLAB/Simulink-based results.

References

1. Majji RK, Mishra JP, Dongre AA (2022) Model predictive control of solar photovoltaic-based microgrid with composite energy storage. Int J Circuit Theory Appl
2. Kabalcı E (2020) Review on novel single-phase grid-connected solar inverters: circuits and control methods. Sol Energy 198:247–274
3. Fekkak B, Menaa M, Boussahoua B (2018) Control of transformerless grid-connected PV system using average models of power electronics converters with MATLAB/Simulink. Sol Energy 173:804–813
4. Singh M et al (2010) Grid interconnection of renewable energy sources at the distribution level with power-quality improvement features. IEEE Trans Power Delivery 26(1):307–315
5. Echalih S et al (2022) A cascaded controller for a grid-tied photovoltaic system with three-phase half-bridge interleaved buck shunt active power filter: hybrid control strategy and fuzzy logic approach. IEEE J Emerg Sel Top Circuits Syst 12(1):320–330
6. Jain C, Singh B (2015) Single-phase single-stage multifunctional grid interfaced solar photovoltaic system under abnormal grid conditions. IET Gener Transm Distrib 9(10):886–894
7. Marafão FP et al (2015) Multi-task control strategy for grid-tied inverters based on conservative power theory. IET Renew Power Gener 9(2):154–165
8. Acuna P et al (2013) Improved active power filter performance for renewable power generation systems. IEEE Trans Power Electron 29(2):687–694
9. Babu N et al (2020) An improved adaptive control strategy in grid-tied PV system with active power filter for power quality enhancement. IEEE Syst J 15(2):2859–2870
10. Bonala AK, Sandepudi SR, Muddineni VP (2016) Variable conductance factor based control of multi-functional grid connected single stage solar PV system. In: 2016 IEEE 1st international conference on power electronics, intelligent control and energy systems (ICPEICES). IEEE
11. Hekss Z et al (2021) Advanced nonlinear controller of single-phase shunt active power filter interfacing solar photovoltaic source and electrical power grid. Int Trans Electr Energy Syst e13237
12. Vazquez S et al (2016) Model predictive control for power converters and drives: advances and trends. IEEE Trans Ind Electron 64(2):935–947
13. Cunha RBA et al (2019) Constant switching frequency finite control set model predictive control applied to the boost converter of a photovoltaic system. Sol Energy 189:57–66
14. Ye J et al (2018) A new flexible power quality conditioner with model predictive control. IEEE Trans Ind Inform 15(5):2569–2579
15. Golzari S, Rashidi F, Farahani HF (2019) A Lyapunov function based model predictive control for three phase grid connected photovoltaic converters. Sol Energy 181:222–233
16. Dellahi M et al (2020) Three-phase four-wire shunt active power filter based on the SOGI filter and Lyapunov function for DC bus control. Int J Circuit Theory Appl 48(6):887–905

Machine Learning Based Prediction of Solar Power Plant Performance Under the Impact of Natural Dust Accumulation

Sruthi Elaprolu and Ankur Bhattacharjee

1 Introduction

In recent years, with pollution levels reaching significant height and nonrenewable fuel sources running out exponentially, solar power can be a primary solution as green energy. Not only is it environment friendly, but it also has zero production cost and is a resource we can never exhaust. Solar Photovoltaic (PV) technology, has now drawn the interest globally to cater the sustainable development goals ensuring cleaner environment [1]. Eco-friendly sources offer abundant energy to meet the continuously increasing energy demand while significantly reducing the environmental hazards that could arise [2]. The increasing market of solar power as an alternate form of energy prompts interest in developing and operating PV systems to tap solar energy on a large scale to integrate it into society as a viable energy source.

Solar radiation is available in abundance around the equator region. However, most of these areas exhibit high ambient temperature and low-frequency rain, which aids dust accumulation. These environmental factors along with aging of the PV modules, can be detrimental to the performance of solar PV systems. The efficiency of solar power systems is influenced by many factors, such as weather conditions, topographic elevation, solar inclination, and seasonal changes etc. Their unreliability faces challenge in large-scale implementation. The accuracy of forecasting the power generation from the PV modules can influence the capability of stand-alone and/or power grid-connected solar PV systems. As the transmittance variation plays a major role in PV power generation, the position of solar PV modules need to be determined

S. Elaprolu · A. Bhattacharjee (✉)
Birla Institute of Technology and Science Pilani, Hyderabad Campus, Hyderabad, India
e-mail: a.bhattacharjee@hyderabad.bits-pilani.ac.in

S. Elaprolu
e-mail: f20190394@hyderabad.bits-pilani.ac.in

S. Doolla et al. (eds.), *Advances in Renewable Energy and Its Grid Integration*,
Lecture Notes in Electrical Engineering 1041,
https://doi.org/10.1007/978-981-99-2283-3_12

to trap maximum amount of photon energy [3]. Therefore, transmittance prediction is crucial for estimating the overall performance of solar PV plants.

Powerful Deep Learning techniques such as ANN and LSTM etc., are now being used in many studies in recent years to predict the power output of soiled PV modules [3–6] as they are accurate, interactive, and flexible. Such works are essential for efficient operation of solar power systems by applying optimal cleaning schedule and introducing novel material coating that can help self-cleaning of PV modules [7].

Considering the above-mentioned issues, in this paper, the prediction of transmittance (optical performance) for rooftop solar PV systems has been demonstrated under the impact of natural dust accumulation. ANN and LSTM tools have been utilized to predict the transmittance and thereby the performance of solar PV plants based on real experimental data set obtained over a period of one year (2020). The experimental setup has been established on the rooftop of the academic building at Birla Institute of Science and Technology (BITS) Pilani, Hyderabad campus for acquiring site specific data under seasonal variation throughout the year.

2 Experimental Setup

The data sets for predicting the transmittance have been obtained from an experimental setup at BITS Pilani (17° 32′ N, 78° 34′ E), Hyderabad campus, India. The wavelength and energy transmission for twelve months have been recorded using low-iron glass slides of 5 cm × 5 cm with a 4 mm thickness brought from the Renewable Energy Laboratory, University of Exeter, Penryn Campus, UK. These glass slides are primarily used to encapsulate the top layer of solar PV modules.

Suitable 3D printed stands were designed and fabricated to place the glass slides angled in three different ways; horizontal, vertical, and at the local tilt angle as shown in Fig. 1. Figure 2 shows the solar panels installed on the rooftop at the local tilt angle, in order to realize the actual power generation on field.

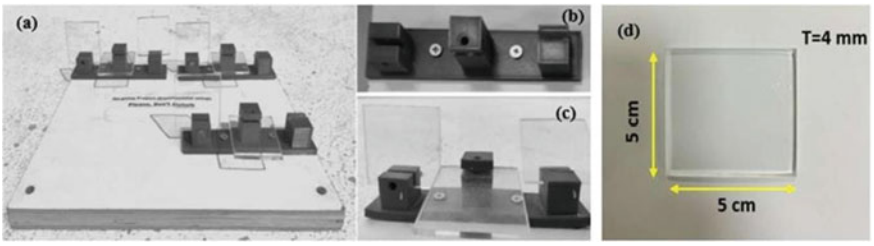

Fig. 1 **a** Low-iron glass slides kept in different positions for experimentation **b** 3D printed frames **c** different orientation of glass slides **d** bare glass slide as reference

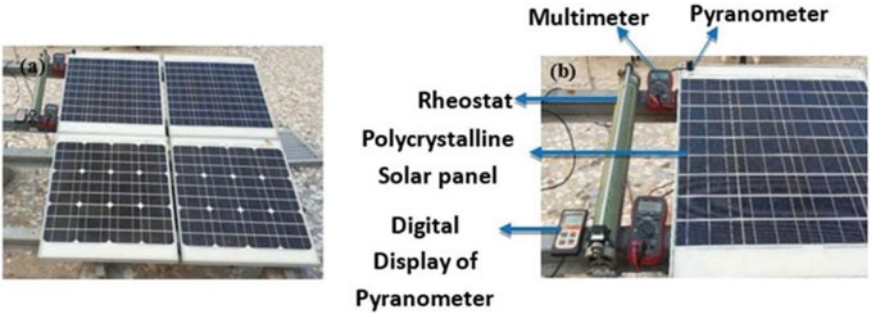

Fig. 2 **a** Solar PV installation set up and **b** solar PV power measurement unit

The optical performance measured using the glass samples are useful for corelating the impact of dust accumulation and power generation of PV panels installed at the same place.

The transmittance studies were performed using a UV–Vis spectrometer from Ocean optics (Custom Configured Maya2000 Pro Series) of wavelength ranges from 300 to 1100 nm. All these measurements were captured regularly and analyzed with the naturally accumulated dust particles on the glass slides without using any cleaning mechanism.

3 Proposed Prediction Models

In this work, the optical performance of solar PV modules under the impact of natural dust accumulation has been predicted by ANN and LSTM techniques based on practical site datasets.

ANN is a widely used tool for performance prediction where a network is created with a certain number of neurons that are interconnected, and data is fed to the network so that the network is trained as per the data input given after which the network is simulated with the testing data to predict the outcome.

The growing popularity has led to increased research comparing various forecasting techniques; auto-regressive models, neural networks, and optimized neural networks [8]. LSTMs are built with recurrent neural network (RNN) architecture with extended memory. Unlike Feedforward Neural Networks, RNNs cycle the data in loops, making the algorithm more suitable for sequential data like time series such as weather records and stock prices (Fig. 3).

A study [9] with data from a solar power plant in Tiruchirappalli, India worked with ANN models to forecast a 24-h (Day-ahead) solar power output; we are looking to predict the transmittance values using data recorded monthly throughout the year 2020. We use the data recorded across twelve months of 2020, containing transmittance percentages for just over eighteen hundred wavelengths ranging from three

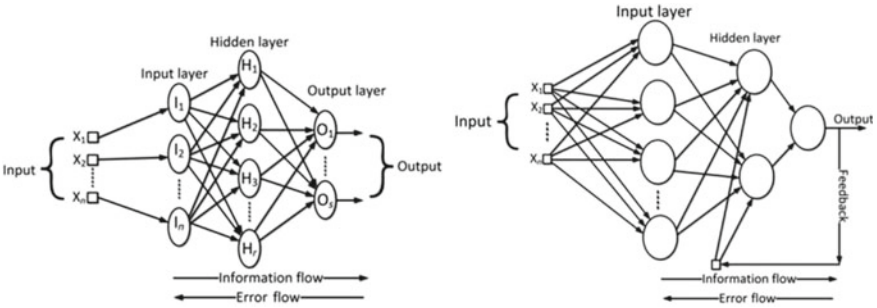

Fig. 3 Feedforward neural network and recurrent neural network (LSTM) architectures

hundred to eleven hundred. The angle of inclination (of the PV modules) significantly determines the radiation transmission. Each plant has a particular angle that maximizes the output (local tilt angle) depending on the region. Even though the generation of power from the PV modules is affected by various factors like irradiance, wind speed, ambient temperature, dust, snow, the orientation of the PV modules, maintenance, etc., [3, 10–12] these factors have not been considered.

Deep Learning models such as ANN, and LSTM are evaluated and compared in predicting the percentage transmittance of the PV modules for a given range of recorded wavelengths, as shown in Fig. 4. The accuracy of the prediction models was determined by computing error parameters such as; mean absolute error and percentage error (MAE/MAPE), root mean square error (RMSE), and the correlation coefficient (R^2) and plotting linear regression graphs.

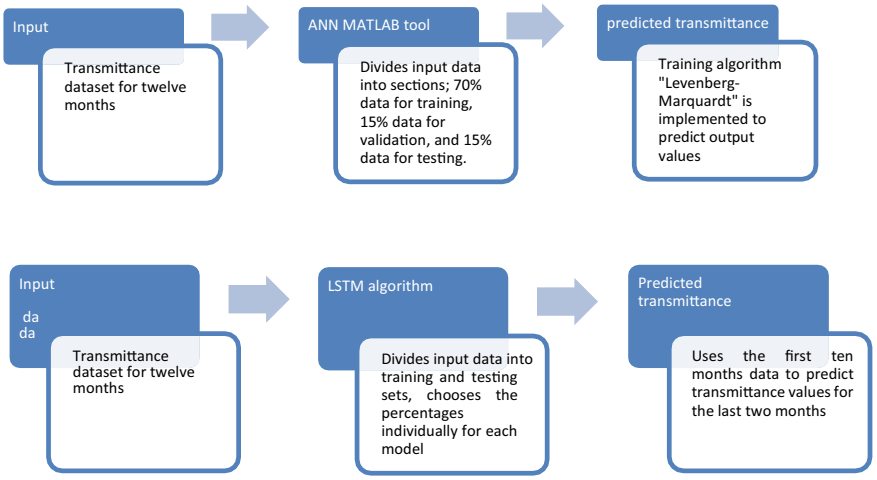

Fig. 4 Process flow for ANN and LSTM based prediction

The ANN model is created using a Neural Net Fitting Tool present in MATLAB. It allows for selecting the training algorithm and the number of neurons to be used. The ANN model automatically divides the data provided as 70% data for training, 15% data validation, and 15% data for testing. The training algorithm is "Levenberg–Marquardt," built into the tool. Note that this particular algorithm observed accuracy better than that of the other built-in algorithms present. The error has reduced as the number of data points used to train the ANN model is increased.

Two LSTM models are designed and compared in terms of the accuracy percentages; they work by recognizing a pattern, computing the data till time 't − 1' to predict the value at a time 't.' Both the models are coded in Python and predict transmittance values for the last two months.

4 Results and Discussion

4.1 Neural Network Model Based Analysis

The MATLAB/Simulink model based data driven prediction results are shown in Fig. 5.

The graphs indicate that the model has provided the horizontal output's predicted values with an accuracy of 99.19%, inclined with 99.01%, and vertical with 99.03%.

4.2 Long Short-Term Memory (LSTM) Algorithms

In the 'first algorithm', the model is trained with the data of the first 'eight' months, and values from the previous 'two' months are used to predict a value for this month. The accuracy of the model increases as the slope of the regression plot gets closer to 1. The analysis of error parameters is shown in Fig. 6 and Table 1.

In the 'second al', the data is split into 'ten' months for training and validation and 'two' months for testing and prediction. The transmittance data of the first 'ten' months is used to predict the value for the 11th month, and the data of months 'two to eleven' is used to predict the value for the 12th month. The algorithm code is run multiple times, with minimal training and validation losses has been chosen. The analysis of error parameters is shown in Fig. 7 and Table 2.

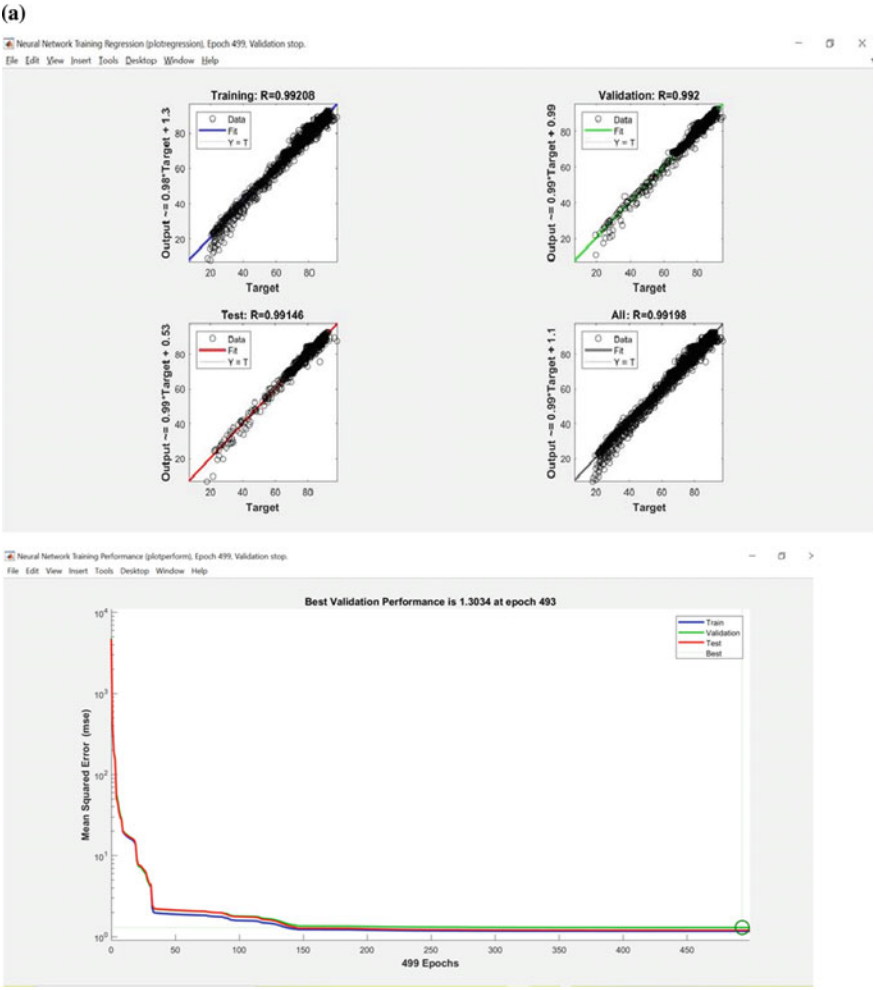

Fig. 5 The graphs show the mean square error (MSE) and regression plots for **a** horizontal, **b** inclined in local tilt angle, **c** vertical glass slides' transmittance prediction (optical performance study)

(b)

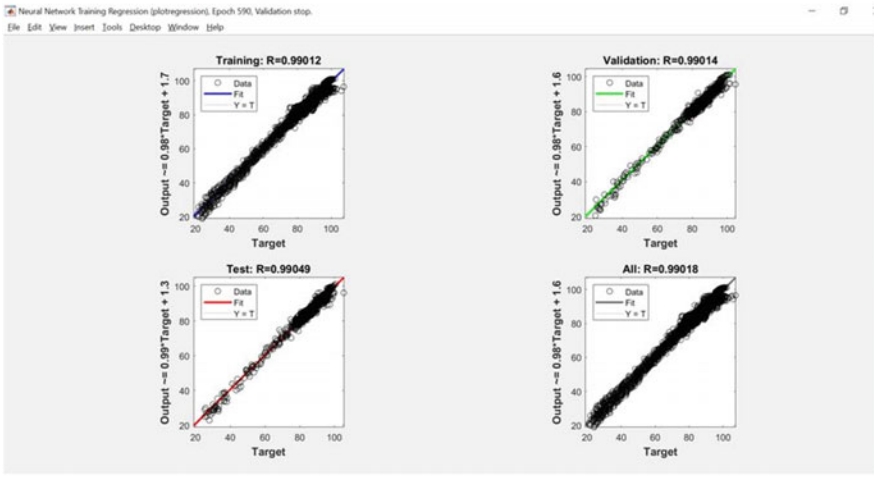

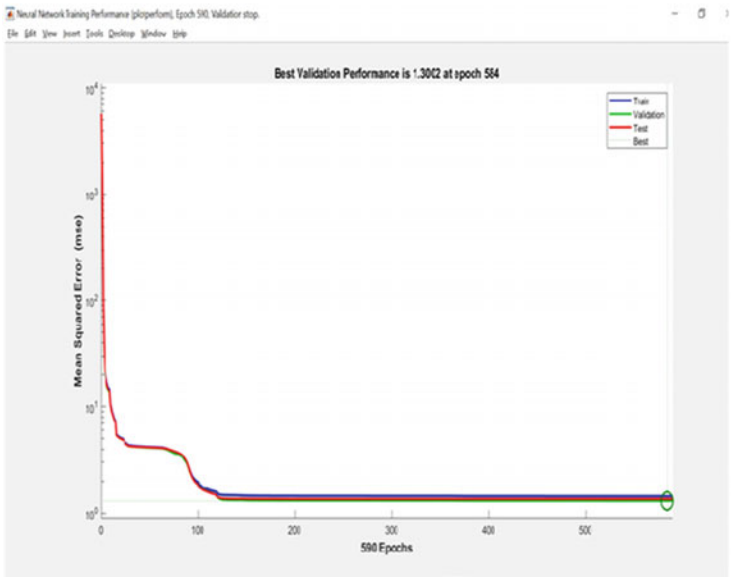

Fig. 5 (continued)

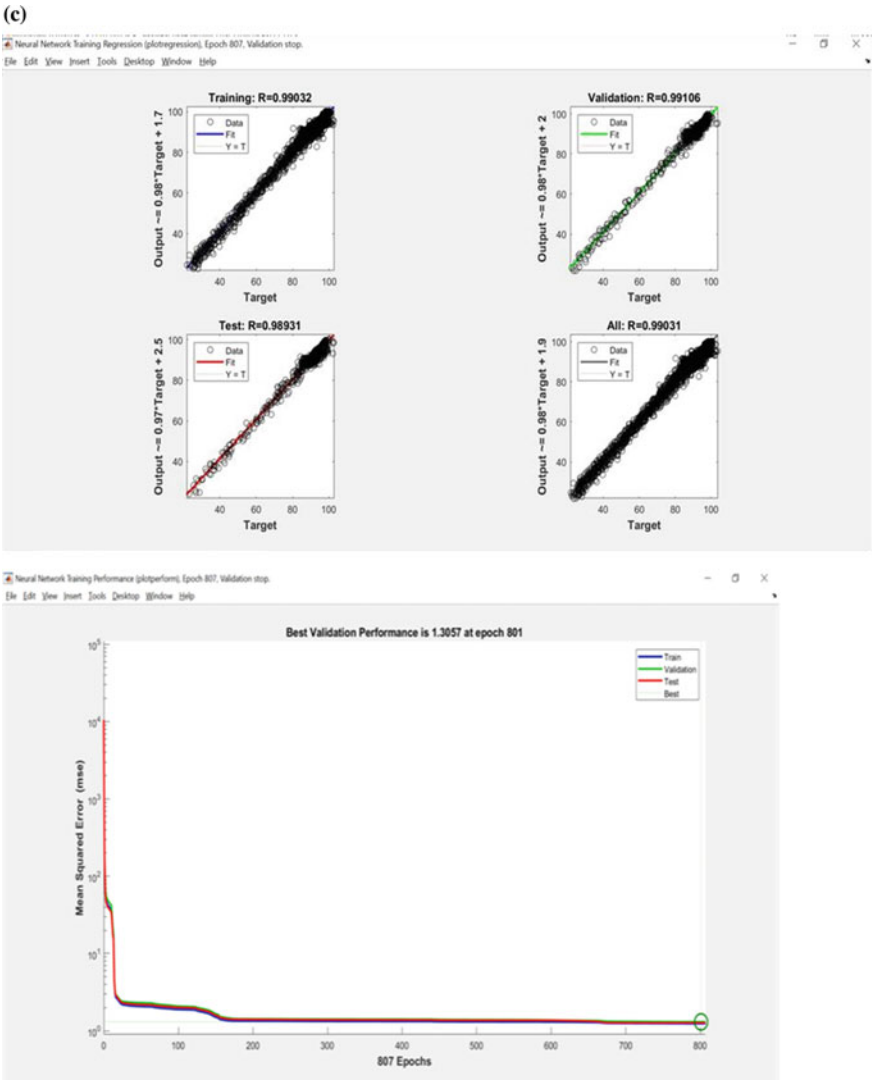

Fig. 5 (continued)

5 Conclusion

This work demonstrates a machine learning based prediction of solar PV power plant performance has been done using Neural Network in MATLAB/Simulink environment. The accuracy of the predicted data is around 99.01–99.19% for three different sets of input data, inclined at the local tilt angle, vertically, and horizontally positioned solar panels. The data from the three orientations provide with the information

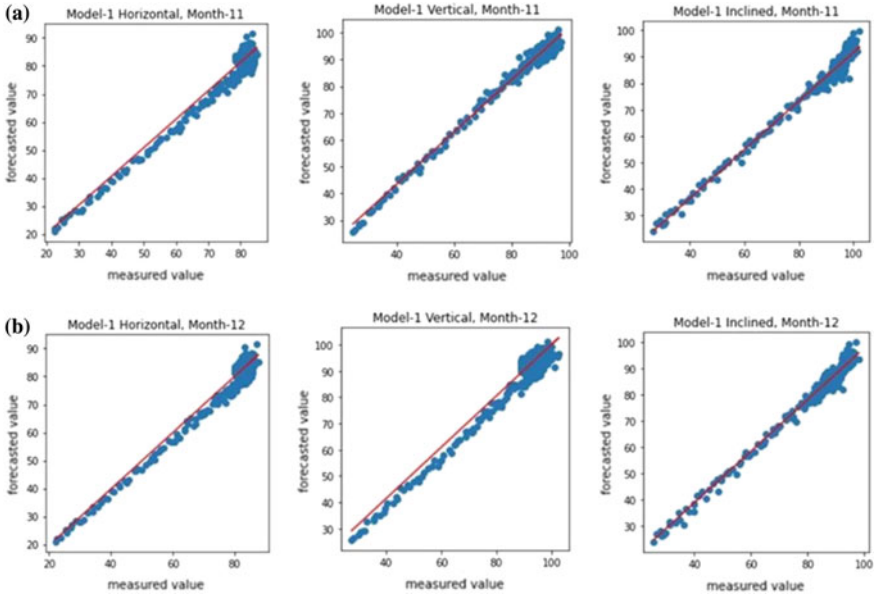

Fig. 6 Regression plot slopes of 1.02, 0.98, 0.92 for the month-11 (**a**) and 1.004, 0.976, 0.98 for month-12 (**b**) for horizontal, vertical and inclined in local tilt angle respectively

Table 1 Transmittance prediction error statistics for the first algorithm

Orientation of glass samples	MAPE	MAE	RMSE	R^2 Month 11	R^2 Month 12
Horizontal	2.488	1.977	2.308	0.907	0.918
Vertical	2.534	2.235	2.557	0.97	0.897
Inclined	5.386	4.92	5.81	0.97	0.966

to understand the effect of dust accumulation on the solar PV plant optical performance in terms of transmittance and thereby further estimation of power output. LSTM and ANN algorithms have been used to predict the optical performance of solar PV plant. Both the models show the highest accuracy in predicting data for the horizontally placed panels. As a validation of prediction work, The ANN model offers an accuracy of over 99%, whereas the LSTM model provides with an accuracy of over 92%. These prediction study will help in predicting the performance of the location specific solar power plants.

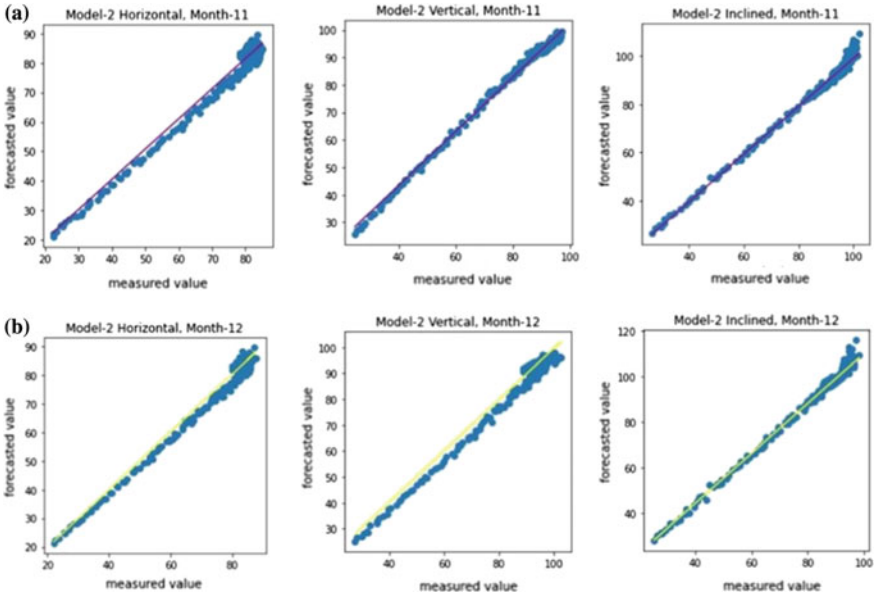

Fig. 7 Regression plot slopes of 1.023, 0.984, 0.988 for month-11 (**a**) and 1.008, 0.985, 0.987 for month-12 (**b**) for horizontal, vertical and inclined in local tilt angle respectively

Table 2 Transmittance prediction error statistics for the second algorithm

Orientation of glass samples	MAPE	MAE	RMSE	R^2 Month 11	R^2 Month 12
Horizontal	2.325	1.85	2.12	0.928	0.938
Vertical	2.498	2.195	2.47	0.985	0.925
Inclined	5.736	5.03	6.41	0.988	0.986

References

1. Lewis NS (2007) Toward cost-effective solar energy use. Science 315(5813):788–801
2. Singh GK (2013) Solar power generation by PV technology: a review. Energy 53:1–13
3. Ibrahim Reda AA (2004) Solar position algorithm for solar radiation applications. Sol Energy 76:577–589
4. Shapsough S, Dhaouadi R, Zualkernan I (2019) Using linear regression and back propagation neural networks to predict performance of soiled PV modules. In: The 9th international conference on sustainable energy information technology (SEIT), 19–21 Aug 2019
5. Yeom J-M, Han K-S (2010) Improved estimation of surface solar insolation using a neural network and MTSAT-1R data. Comput Geosci
6. Li Z, Mahbobur Rahman SM (2016) A hierarchical approach using machine learning methods in solar photovoltaic energy. Energies
7. Kumar S, Kamal N (2020) A radial basis function neural network based approach to mitigate soiling from PV module. J Phys: Conf Ser

8. Pedro HTC, Coimbra CFM (2012) Assessment of forecasting techniques for solar power production with no exogenous inputs. Sol Energy 86(7):2017–2028. https://doi.org/10.1016/j.solener.2012.04.004
9. Ehsan RM, Simon SP, Venkateswaran PR (2014) Day-ahead prediction of solar power output for grid-connected solar photovoltaic installations using Artificial Neural Networks. In: 2014 IEEE 2nd international conference on emerging electronics (ICEE), 2014, pp 1–4. https://doi.org/10.1109/ICEmElec.2014.7151201
10. Refaat SS, Nounou H, Abu-Rub OH (2018) ANN based prognostication of the PV panel output power under various environmental conditions. Texas A&M University
11. Babatunde AA, Abbasoglu S, Senol M (2017) Analysis of the impact of dust, tilt angle and orientation on performance of PV plants. Renew Sustain Energy Rev 90
12. Catelani M, Ciani L, Cristaldi L, Faifer M, Lazzaroni M, Rossi M (2012) Characterization of photovoltaic panels: the effects of dust. In: 2nd IEEE ENERGYCON conference & exhibition, 2012/Advances in energy conversion symposium

Application of Neural Networks in Reliability Evaluation of Distribution Networks Integrated with Distributed Generation

Meera Karamta and Matsiko Joshua

1 Introduction

Reliability is "the ability of a power system to perform the function it is designed for under the operating conditions encountered during its projected lifetime" [1]. Reliability is key in the power system today because of its immense impact on consumer satisfaction and electricity prices. The main purpose of the power grid is to uninterruptedly supply economical electrical energy to consumer loads. The distribution system as the final link between the bulk transmission and the customers did not previously attract reliability concern due to utilities only focusing on meeting demand within acceptable limits [2].

Distribution reliability has gained attention due to 80–90% of consumer reliability problems occurring within the distribution network. These failures are mainly due to the radial configuration of the distribution system, and partly due to the many constituents & devices within the distribution network. Reliability is represented basically as component failure rate and repair time and secondarily as statistical averages of a specific reliability attribute for a whole system or subsystem [2].

The onset of climate change has led to a proliferation of DERs such as solar PV systems, wind turbines and fuel cells within the grid, due to their renewability and zero greenhouse gas emissions. These are often connected to the distribution system to augment and backup supply from the grid. This enables the radial feeders to disconnect themselves from the grid in case of remote faults and continue meeting load demand using the DER supply, thereby improving distribution reliability. The

M. Karamta (✉) · M. Joshua
Department of Electrical Engineering, School of Technology, Pandit Deendayal Energy University, Gandhinagar 382007, India
e-mail: meera.karamta@sot.pdpu.ac.in

M. Joshua
e-mail: joshua.mmtee20@sot.pdpu.ac.in

S. Doolla et al. (eds.), *Advances in Renewable Energy and Its Grid Integration*,
Lecture Notes in Electrical Engineering 1041,
https://doi.org/10.1007/978-981-99-2283-3_13

conventional grid is therefore under drastic transformation from an inactive and mono-directional system to an active smart grid (SG). The SG has reliability and sustainability as key features and is expected to reduce interruption durations and associated losses due to faster power restoration, self-healing capabilities and optimal operation of the distribution system. The introduction of DERs close to the consumer loads is anticipated to ameliorate the voltage characteristic and decrease energy losses within the grid [1, 2]. The integration of numerous smart electronic devices into the grid, utilization of electric vehicles as storage devices, and the many prosumers could worsen power quality issues and consequentially deteriorate reliability. Additionally DER energy output is dependent on weather conditions such as solar irradiance, wind speed and tidal range, which greatly fluctuate, thereby making DER power stochastic. Therefore, this necessitates the need to evaluate DER impact on distribution reliability [3].

Reliability assessment techniques are either based on Monte Carlo Simulation (MCS) or analytical method. MCS relies on probability and samples component failure states for different scenarios to compute reliability indices whereas analytical methods rely on mathematical analysis. MCS is complex and intensive in terms of computing power and time. This constrains practical implementation of MCS and necessitates the need for pragmatic techniques such as ANN in reliability assessment. ANN are a dynamic ML techniques that mimic the interconnections and signals in the human brain to continuously learn [4, 5].

The impact of DERs on reliability in distribution networks is studied by Tawfiq and Aljohani [6] using MCS. DER optimal placement was studied and reliability benefits realized in by having DERs close to the load center. Memari et al. [7] applied various clustering algorithms in reliability assessment in a bid to improve accuracy and duration of MCS-related techniques. Fuzzy c-means technique was found to be superior to other algorithms. Gengfeng et al. [5] developed a novel machine learning based distribution network reliability assessment technique as a solution to the inefficiency, complexity and slowness of analytical techniques. A framework that coordinated ML and MCS was developed to improve pragmatic use of reliability assessment. Sanaullah et al. [4] assessed reliability gains with integration of DERs into the distribution network and found significant improvements. ANN was applied to optimally place the DER within the system for maximum reliability gains.

In this study we seek to assess the reliability gain with introduction of DERs into the distribution network and implement an ANN to predict reliability indices with DER integration. The paper is organized in five sections. Section 2 contains the system and simulation description. Section 3 contains the simulation results and discussion. Section 4 contains the conclusion.

2 Simulation

The Electrical Transient Analysis Program (ETAP) program is utilized for reliability evaluation of the IEEE-34 node system and MATLAB software utilized for ANN based prediction of reliability indices.

2.1 Base Case System

The IEEE 34 node test system in an existing distribution network with a nominal voltage of 24.9 kV and contains long and lightly loaded overhead transmission lines, numerous unbalanced loads summing to 2.063 MVA, a short low voltage section of 416 V, 2 inline voltage regulators and a pair of capacitor banks [8]. The base case of the study is attained by reliability evaluation of the IEEE-34 node feeder. The system parameters such as line lengths and material composition, regulator configurations and tap settings among others are obtained from [8] for input into ETAP. The intrinsic component average reliability statistics according to IEEE standards are obtained from [9] for input in ETAP.

2.2 DER Study Case

In case II, the base case is modified by inserting a 1 MW PV array at point 890 in the low voltage section of the system. Figure 1 represents case III, wherein the same DER is placed at node 838, the farthest node from the utility substation.

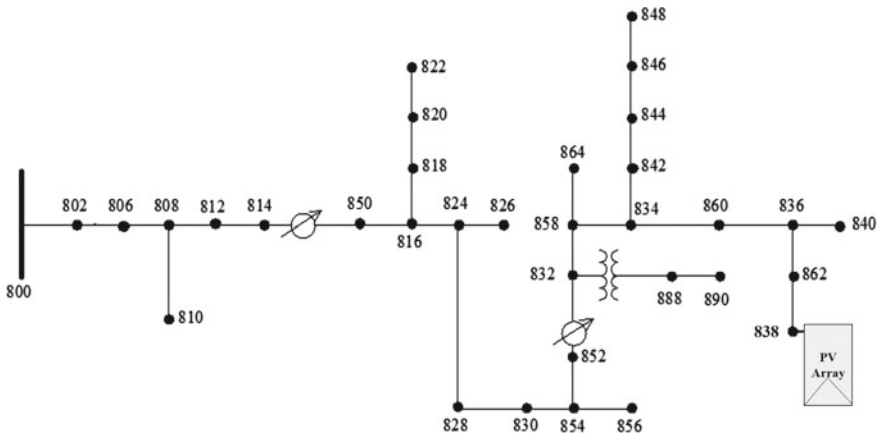

Fig. 1 Modified IEEE 34 node feeder with DER at node 838

All component reliability statistics, configurations and load ratings are maintained for all study cases. In order to study network dynamics for all cases, load flow analysis is performed using the load flow tool in ETAP and network parameters such as nodal voltages and branch currents studied and compared. The Newton–Raphson technique is used for the load flow analysis with error limit set to 0.1%.

2.3 Simulation Tools

ETAP is a state of the art computer program used to model and evaluate electrical systems. The ETAP modules used for the study are Reliability assessment and balanced load flow analysis [10]. This study relied on code written in MATLAB to implement the ANN for reliability index prediction [11]. The methodology adopted by the study for reliability evaluation in ETAP is shown in Fig. 2.

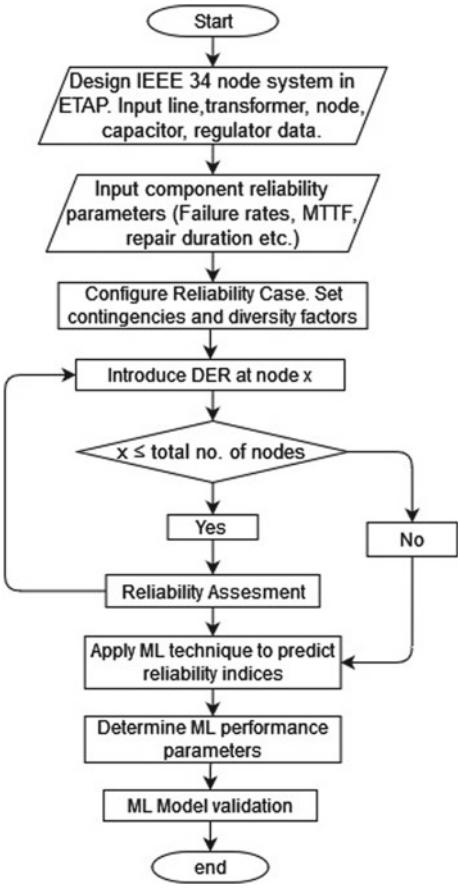

Fig. 2 Reliability evaluation flowchart

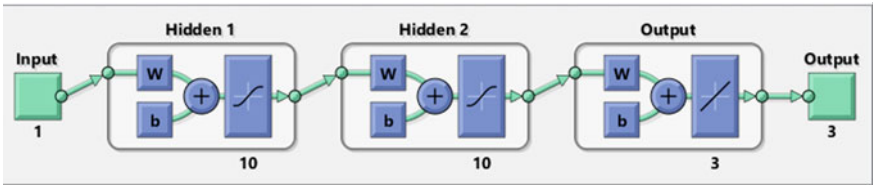

Fig. 3 Trained neural network layout

2.4 Scenario Generation and ANN Implementation

Various scenarios are generated by placing the solar PV system at each node in the system and the associated reliability indices noted according to the distance of the node from the utility substation. The dataset created is then input into the ANN. ANN is applied so as to predict the reliability gained when the DER is placed at a particular node within the system. A 4-layered feed-forward propagation ANN is developed by coding in MATLAB trained by Levenburg-Marquardt (LM) optimization. LM combines gradient descent and newton optimization methods. The distance of the DER from the utility substation i.e. node 800, is fed as the input and the actual reliability values fed as output. The LM algorithm maps them as a regression technique. Accuracy of ANN is measured in terms of Mean Square Error (MSE) by Eq. (1); where Y_i is the actual output and $\hat{Y}_i$ is the predicted output.

$$\text{MSE} = \frac{1}{n}\sum_{i=1}^{n}\left(Y_i - \hat{Y}_i\right)^2 \tag{1}$$

Figure 3 represents the trained neural network for the proposed reliability assessment.

3 Results and Discussion

3.1 Reliability Indices Calculation

System reliability indices commonly used include System Average Interruption Frequency Index (SAIFI), System Average Interruption Duration Index (SAIDI), and Expected Energy Not Served (EENS), among others [4]. These are computed as per the equations below;

$$SAIFI = \frac{\sum r_i * N_i}{\sum N_i} \tag{2}$$

Table 1 Comparison of reliability indices: base case versus case III

Reliability index	Base case	Case II	Case III
SAIFI (f/customer yr)	6.3029	5.4555	5.3997
SAIDI (h/customer yr)	199.2082	190.7629	190.3165
CAIDI (h/customer interruption)	31.606	34.967	35.246
EENS (MW h/yr)	354.781	337.675	337.177
AENS (MW h/customer yr)	14.1913	13.5070	13.4871

$$SAIDI = \frac{\sum U_i * N_i}{\sum N_i} \tag{3}$$

$$CAIDI = \frac{SAIDI}{SAIFI} \tag{4}$$

$$EENS = P_i * U_i \tag{5}$$

where r_i—failure rate, N_i—number of customers, U_i—outage duration per year and P_i—average load. Upon reliability evaluation in ETAP, the reliability statistics shown in Table 1 are attained for the base case, case II and case III.

Table 2 indicates the percentage improvement of each reliability index with integration of the DER at node 838. It is seen that all system reliability values improve with addition of a DER into the system. From Table 2, it is observed that there is a negative percentage change of CAIDI. As per Eq. (3), CAIDI is a fraction based on the SAIFI and SAIDI. The percentage improvement in SAIFI is much higher than that of SAIDI. The fractional improvement in the CAIDI comes out as negative. However, it can still be inferred from the results that overall for a customer the average interruption frequency reduces significantly in comparison to the reduction in the interruption duration.

Failure rates of power system components are dependent on their age, functional temperature and voltage strains among others. The component functional temperature is dependent on the line current [12]. The load flow results for all the study cases found a substantial reduction in branch currents on insertion of a DER, as shown in Fig. 4. This reduction is due to DER providing power to the loads and therefore offsetting a huge amount of current that was flowing through the lines from the utility.

Table 2 Reliability indices percentage improvements in study case III

Reliability index	Improvement (%)
SAIFI	14.33
SAIDI	4.46
CAIDI	− 11.52
EENS	4.98
AENS	4.96

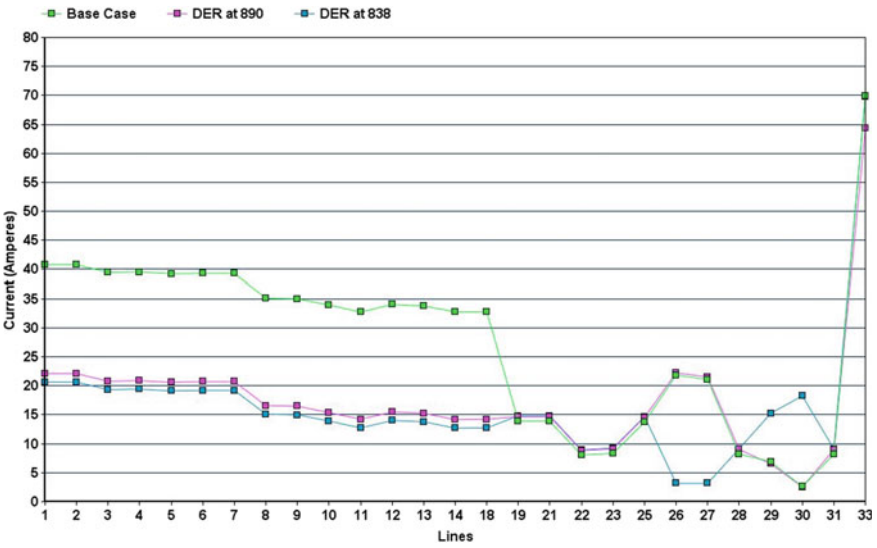

Fig. 4 Variation in line currents for IEEE-34 test system with DER located at node#890 and node#838

This reduction in branch currents results in a reduction of component temperatures due to reduction in ohmic losses. Voltage drops and energy losses reduce too and result into reduction in component failures and thus the improvement in reliability.

Figure 5 shows the per-unit (p.u.) nodal voltages within the system for all the study cases. It is clear that there is a substantial enhancement in the voltage profile with DER integration, particularly farther away from the utility. The under voltages registered in the base case are improved to about 1 p.u., the nominal voltage.

3.2 ANN Based Reliability Indices Prediction

On scenario generation, reliability values are attained for all the locations in the IEEE-34 node system. The variation in the actual values for SAIFI plotted against different DER location is shown in Fig. 6. It can be seen that reliability improves the farther the DER is placed within the system or closer to the load centers.

A plot of the actual and ANN predicted values in-terms of SAIFI, SAIDI and EENS are shown in Figs. 7, 8 and 9. It can be seen that nearly all the actual reliability values are accurately predicted by the ANN algorithm in all 3 cases.

On simulation, the performance of the ANN in terms MSE is found to be as low as 0.1256 and the average regression value found to be 1. These reflect a high prediction accuracy by the ANN.

The regression plots from the training, validation and testing of the ANN are shown in Fig. 10. The ANN accuracy is further indicated by all the points lying

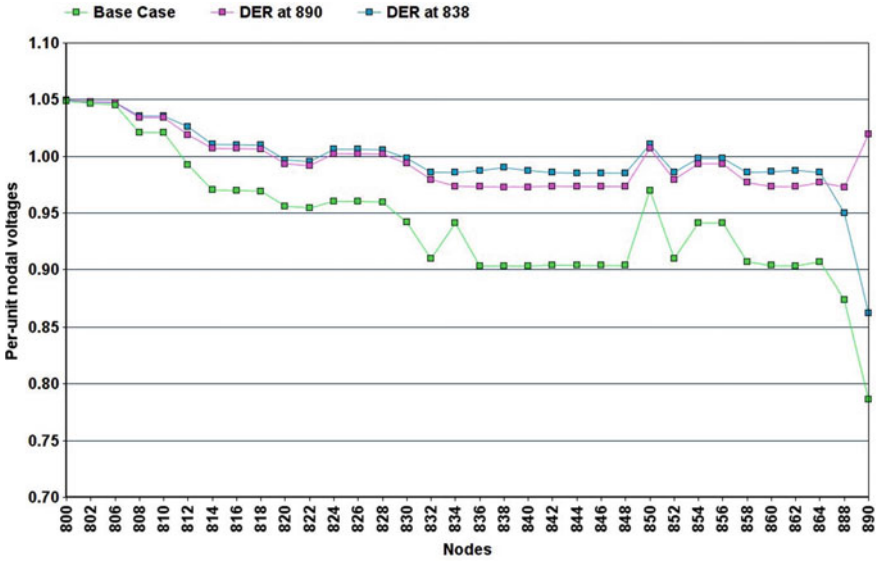

Fig. 5 Variation in per unit voltages for IEEE-34 test system nodes with DER located at node#890 and node#838

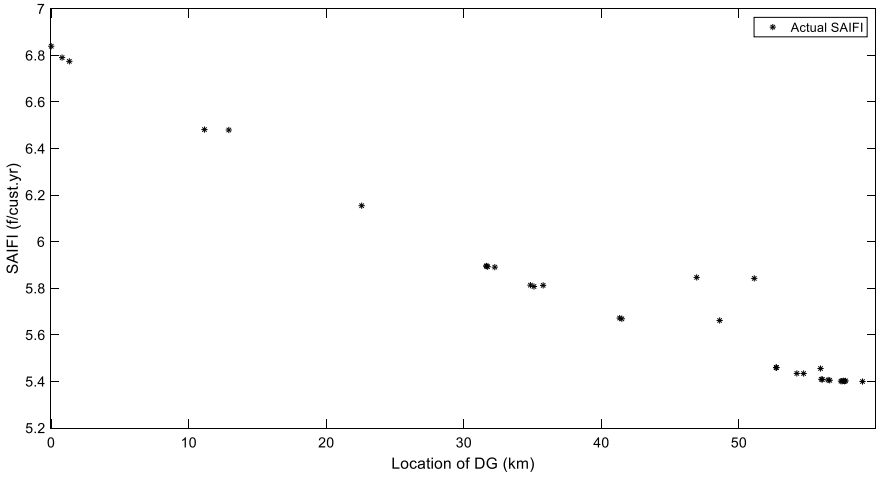

Fig. 6 SAIFI variation against DER location for test Case III: 1 MW PV placed at different system nodes

along the respective regression lines showing a positive correlation between input and output data.

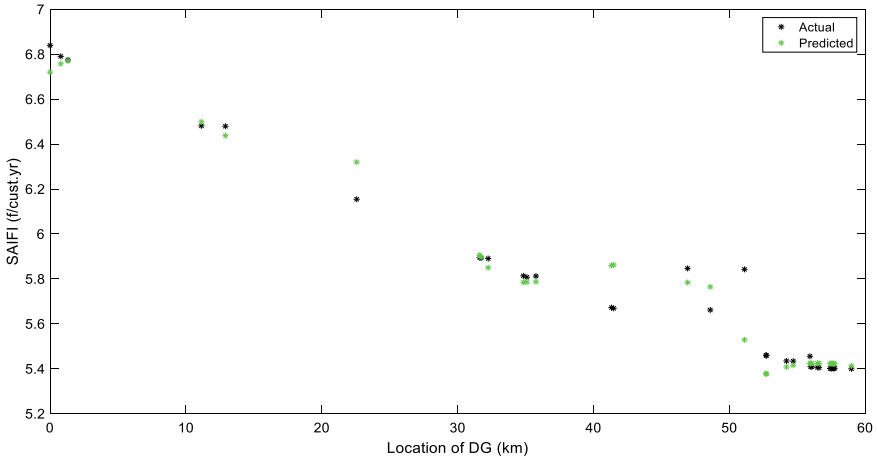

Fig. 7 Prediction results of SAIFI variation against DER location for test Case III: 1 MW PV placed at different system nodes

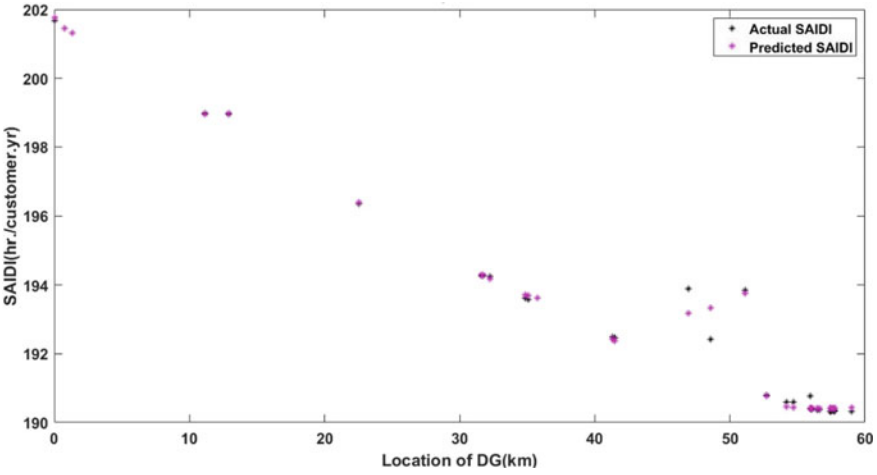

Fig. 8 Prediction results of SAIDI variation against DER location for test Case III: 1 MW PV placed at different system nodes

3.3 ANN Model Validation

The ANN model was further validated by creating a random node perfectly in-between nodes 828 and 830 at a distance of 38.20973 km from node 800. The distance was fed into the ANN model and corresponding results noted. The DER is then placed at the same point in ETAP and the corresponding reliability results noted. The results of both cases are compared in Table 3. The ANN prediction accuracy is

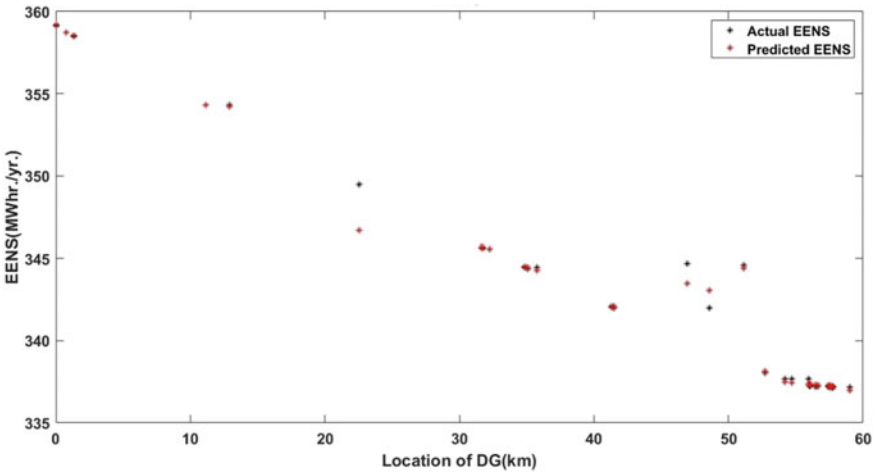

Fig. 9 Prediction results of EENS variation against DER location for test Case III: 1 MW PV placed at different system nodes

shown by calculating the MSE for all the three reliability indices. It is found to be 0.03313, which validates the ANN model as nearly accurate.

4 Conclusion

This study evaluates the reliability gains within a distribution network with integration of a DER in contrasted with the base case system containing no DERs. A 1 MW solar PV array is introduced as the DER into the IEEE-34 node test feeder and ETAP software used for reliability assessment. Upon simulation, improvement in all reliability indices is registered. Load flow analysis is undertaken to study system dynamics for all the study cases. Given that power system component failures depend on operating temperature and voltage stresses, the reliability improvement is mainly attributed to significant reduction in line currents and improvement of the system voltage profile with DER integration. Line current is proportional to line temperature, ohmic losses and voltage drops. Various reliability scenarios are then generated in ETAP by placing the DER at all nodes in the network. Reliability is found to improve the closer the DER is to the load centers. The data is then fed into an ANN in MATLAB software so as to predict reliability indices depending on DER location within the system. The ANN accurately predicted the reliability values with a mean square error of only 0.1256. The algorithm's performance is further validated through ETAP and accuracy found to be high. The ANN model can be applied in power systems to predict reliability gains in the IEEE-34 system with solar PV integration or network extension.

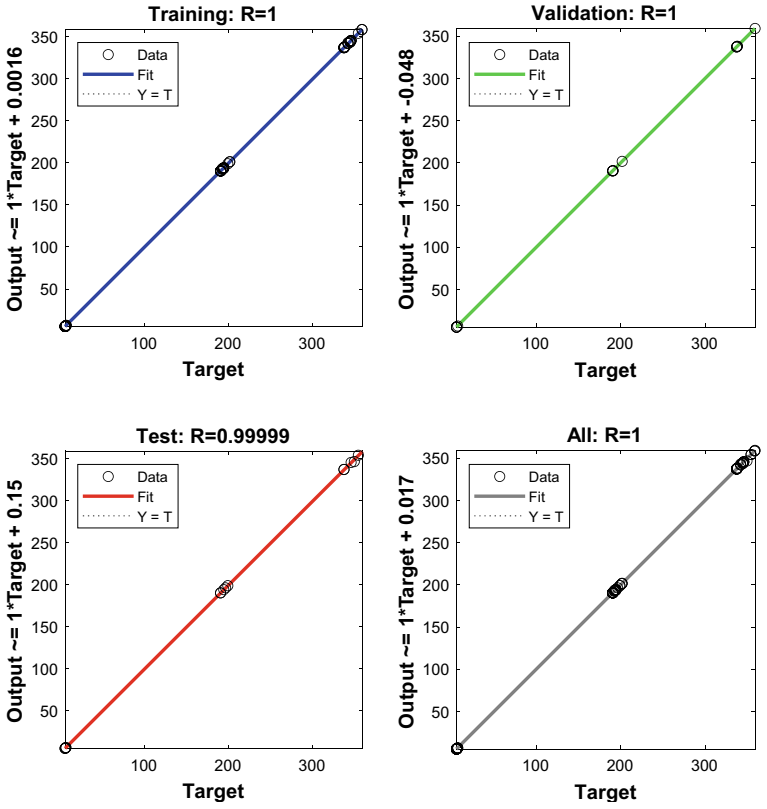

Fig. 10 ANN simulation regression plots

Table 3 Validation results of the ANN model

	SAIFI	SAIDI	EENS
ANN model results	5.8080	193.2592	343.4021
ETAP results	5.7379	193.0217	343.207
Error	− 0.0701	− 0.2375	− 0.1951
Squared error	0.00491	0.00564	0.03806

References

1. Chowdhury A, Koval D (2009) Power distribution system reliability. Wiley, New Jersey
2. Brown R (2002) Electric power distribution reliability. Marcel Dekker Inc., New York
3. Celli G, Ghiani E, Pilo FS, Giuseppe G (2013) Reliability assessment in smart distribution networks. Electr Power Syst Res 104:164–175
4. Ahmad S, Asar AU (2021) Reliability enhancement of electric distribution network using optimal placement of distributed generation. Sustainability 13(20)
5. Li G, Huang Y, Bie Z, Ding T (2020) Machine-learning-based reliability evaluation framework for power distribution networks. IET Gener Transm Distrib 14(12):2282–2291

6. Beshir TM, Mohammed A (2017) Matlab code to assess the reliability of the smart power distribution system using Monte Carlo simulation. J Power Energy Eng 5:30–44
7. Mehran M, Ali K, Hamed H-D (2021) Reliability evaluation of smart grid using various classic and metaheuristic clustering algorithms considering system uncertainties. Int Trans Electr Energy Syst
8. Kersting W (2001) Radial distribution test feeders. In: 2001 IEEE power engineering society winter meeting conference proceedings, Columbus, USA, 2001
9. IEEE (2004) IEEE guide for electric power distribution reliability indices. IEEE Std 1366-2003, pp 1–50
10. E. Inc. Energy management solutions. https://etap.com/. Accessed 19 Dec 2021
11. M. Works. MATLAB. https://www.mathworks.com/. Accessed 2 Apr 2022
12. Pabla AS (2011) Electric power distribution. Tata McGraw Hill, New Delhi, India

Feasibility Assessment of the Smart Grid in Uganda

Matsiko Joshua and Meera Karamta

1 Introduction

1.1 Challenges of Uganda's Power System

Uganda experiences incessant nation-wide power blackouts, with 17 incidents registered since 2016. The outages are more rampant at distribution level, with each customer encountering power outage for 16 h a month. Electricity reliability at household level is 36% [1]. Uganda's power system also faces high technical power losses, standing at 16% in the distribution system and 3.6% at transmission level. This is mainly due to congested and dilapidated transmission and distribution infrastructure [2]. Consequentially, this has led to poor power quality in relation to recommended voltages, frequency and wave shapes. Power in Uganda is occasioned by power surges, flickers, voltage instability and fluctuations [3].

Uganda also has high power tariffs, with electricity prices growing at 22% annually in the last 5 years. These high tariffs are why only 20% Ugandans have access to grid electricity [3]. There is also rampant power theft in Uganda, with the power utility reporting non-technical losses of 18%, translating to losses of $30 million annually. Power thefts are mainly attributed to the high cost of power [3]. Uganda also has an unfavorable monopolistic electricity market structure, with a sole power transmitter and 90% of the country served by a single distributor. This means there is no competition and the consumer has to accept the price set by the utility. This has

M. Joshua · M. Karamta (✉)
Department of Electrical Engineering, School of Technology, Pandit Deendayal Energy University, Gandhinagar 382007, India
e-mail: meera.Karamta@sot.pdpu.ac.in

M. Joshua
e-mail: joshua.mmtee20@sot.pdpu.ac.in

S. Doolla et al. (eds.), *Advances in Renewable Energy and Its Grid Integration*,
Lecture Notes in Electrical Engineering 1041,
https://doi.org/10.1007/978-981-99-2283-3_14

fostered high power costs and little re-investment. The sector regulator is also not independent [2].

Additionally, Uganda's power sector is at the risk of climate change due to 84% of electricity being generated from hydro resources. This heavy reliance is growing riskier, as temperatures are rising, rainfall is more unpredictable and occasional droughts. Recently, persistent drought led to hydropower production dropping from 340 to 140 MW due to low water levels in dams, which led to widespread power cuts. World-over, energy is a major contributor to climate change due to its production of greenhouse gases (GHG). Energy production is affected by climate change and the power supply affected in terms of reliability and costs. In Uganda, the energy sector contributes 10% of the GHG emissions, ranking 3rd [4].

1.2 The Smart Grid

Smart Grid involves integration of Information Communication Technologies (ICT) into the conventional power grid enabling bi-directional transfer of energy and information between the consumers and utility, plus introduction of Distributed Energy Resources (DER) in order to improve monitoring and control. The SG involves use of ICT for Wide Area Monitoring (WAM) of the power system, with visibility up to the load points, through advanced monitoring and metering infrastructure (AMI) such as PMUs, and smart meters. Benefits of the SG include efficient power transmission, faster power restoration, lower maintenance costs, active Demand Side Management (DSM), improved reliability, active customer participation, dynamic power pricing, power system self-healing, more accurate load forecasting and fault location [5].

Reference [6], undertook a feasibility evaluation of execution of the SG in Bangladesh as a solution to challenges of Bangladesh's inefficient grid. Reference [7] undertook SG feasibility assessment in India to solve their grid challenges. SG technologies were found to improve reliability, fault detection, and self-healing capabilities.

Reference [8] carried out a feasibility assessment of a SG in Nantucket as way to lower the tariffs, reduce aggregate demand and offset the huge investments needed. Reference [9] evaluated feasibility of a SG demonstration network in Panipat. The scope included smart metering and distribution automation etc. Reference [10] conducted feasibility assessment for a SG in Ufa in order to reduce losses, improve security, power quality and reliability, and introduce intelligent protection and communication in the power network.

The SG's capabilities underscore the SG as the solution to the challenges of Uganda's power system. However, no previous study has examined Uganda's power system to assess technical or economic viability of implementation of the SG. This study seeks to cover this literature gap. The remainder of the paper is organized in sections. Section 2 consists of the methodology and SG design. Section 3 consists of renewable resource mapping. Section 4 consists of the proposed system and Sect. 5 covers the CBA.

2 System Design

2.1 Methodology

The methodology used is adopted from [11] and is described stepwise below;

Project Definition

Under this, the project is explicitly defined, and technologies that could solve existing problems are surveyed. The renewables available for mapping are specified.

Specify Smart Grid Features

The SG features and their associated benefits are specified and how they solve the challenges. Overlapping functions are also highlighted.

Specify Benefits

The selected features are then matched to their benefits. Benefits are defined in terms of value gained by any stakeholder. Cross-cutting benefits are again highlighted.

Monetize Benefits

The specified benefits are monetized through estimation of their value in comparison to the base case and the cost offset from the present. The benefits are then discounted to their net present value (NPV). Benefits are quantified across the project lifetime.

Costing

This involved attaching monetary costs to project equipment, its installation, its operation and maintenance plus the qualitative benefits.

Cost and Benefit Comparison

NPV is used to quantify future costs and benefits to present value according to prevailing depreciation of money. NPV of costs and benefits is compared to assess whether the project is cost effective.

Sensitivity Analysis

Sensitivity analysis involves assessing how achieved results could change with changes in inputs and the challenges faced. Focus is put on uncertain inputs [11].

2.2 Major Smart Grid Components

Phasor Measurement Unit

PMUs Units are advanced devices that cyclically measure local estimates of current, voltage, phasor, frequency and its rate of change with a universal time stamp. PMU

use is justified by the need to capture system dynamics during unstable or faulty conditions to enable fast real-time control of the system [5].

Phasor Data Concentrator (PDC)

A PDC is "a function that collects phasor data, and discrete event data from PMUs and possibly from other PDCs, and transmits data to other applications." Values from PMUs are erratic and therefore PDCs carryout alignment and signal conditioning to transform the time-stamped phasor measurements into useful information [5].

Smart Meter

A smart meter is used as a measurement tool for hourly power usage and transmits it's readings to the centralized utility's system for system monitoring, control, invoicing and post-disturbance analysis. Smart meters are capable of real-time remote control of customer appliances and facilitate active DSM techniques [11].

Wide Area Monitoring System

WAMs are composed of remote PMUs, conveying time-stamped system parameters to PDCs that carryout signal handling and provide a high quality repository for the data before relaying the data to controllers for appropriate action [5].

Smart Grid Market

The smart market operates in synergy with the grid for optimal management, given the unpredictable events in a power system. DERs owners turn into active market players, continuously engaging in market scheduling and with the feed-in-tariff equal to market price. The smart market facilitates active DSM and integration of electric vehicles and virtual power plants [11].

2.3 Smart Grid Communication

Smart devices collect huge amounts of data which must be relayed in real-time, this requires a robust and quick communication system. The SG is made up of heterogeneous protocols, technologies and architectures which must be interconnected [11].

3 Renewable Resource Mapping

3.1 Solar Photovoltaics

Solar PV entails conversion of the sun's radiation and heat into electricity by solar PV cells. Solar PV has great potential due to being abundant, inexpensive and emission

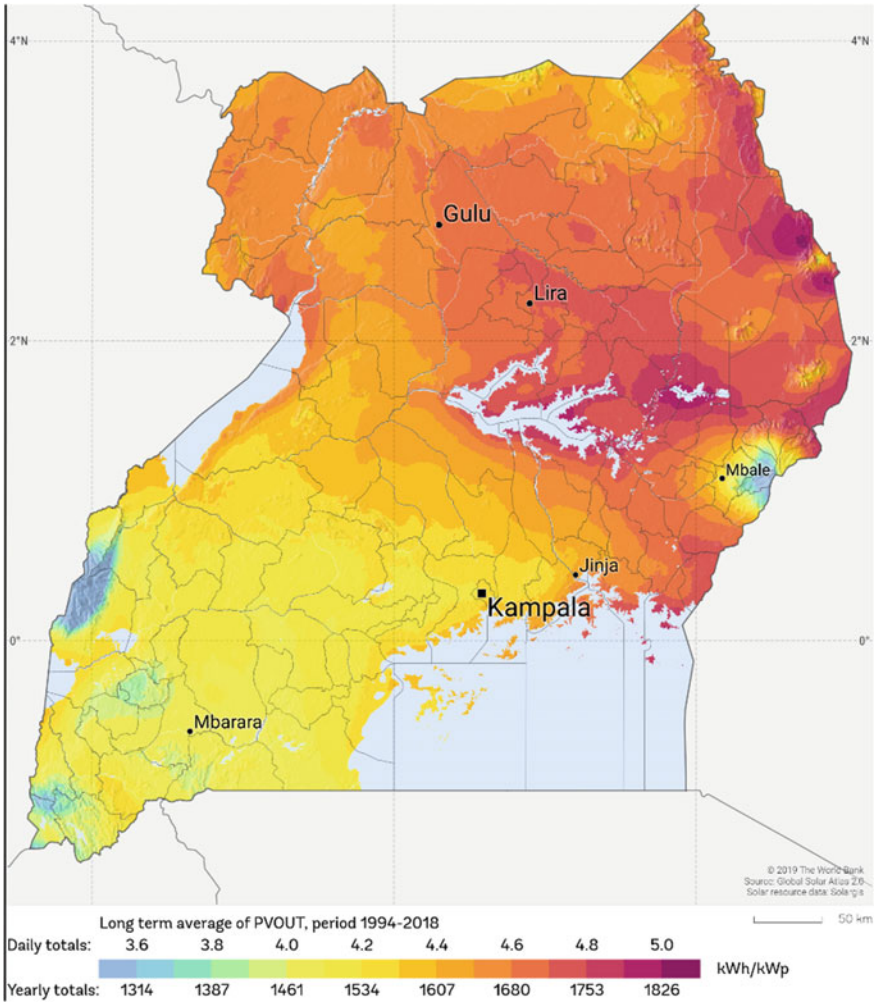

Fig. 1 Uganda's solar power potential [13]

free [12]. The solar PV potential of Uganda in kWh) per installed kWp per year is shown in Fig. 1. It is evident that the greatest potential for solar PV is in the North and Eastern regions of Uganda [13].

3.2 Wind Energy

Wind is air in motion from high pressure regions to lower pressure regions due to temperature imbalances on the earth's surface. Rotating wind turbines convert

the mechanical energy of wind into power, with output depending on wind speeds. Favorable wind speeds range from 2.5 to 25 m/s. In most of Uganda, wind speeds range from 2 to 4 m/s, which is insufficient for large scale wind generation [14].

3.3 Hydropower

Hydropower (HPP) involves conversion of the kinetic energy of running water which is motion due to difference in height. The running water rotates a turbine which is coupled with an electrical generator to produce electricity [15]. Large HPP production today stands at 855 MW in Uganda. Uganda's untested capacity is estimated to be 2000 MW. Uganda today boasts of 155 MW of small HPP with identified potential sites having estimated capacity of 274 MW [3, 14].

4 Proposed System

4.1 Substation Automation

Substation automation involves placing of PMUs and PDCs at both distribution and transmission substations along with ICT tools to enable WAM. This is essential because most equipment tasked with optimal functioning and protection of the grid is in substations. WAM of the grid enables faster location and identification of cascaded faults, which are responsible for Uganda's nationwide power outages. With proper fault location, appropriate relaying actions can be undertaken to avoid these outages [16].

4.2 Transmission Substation Automation

Installing PMUs at all substations of the network would be ideal for accurate monitoring. However, due to the high price of PMUs, this would make the system uneconomical, plus the communication technology availability constraint. Due to ohms law, a PMU at a particular bus is able to monitor adjoining buses, which makes it possible to use less PMUs than the number of system buses. This is known as the PMU optimal placement problem, an integer linear programming (ILP) optimization problem [16].

Uganda's transmission network shown in Fig. 2 is simplified into a 26 bus system, with integers assigned to each substation/bus as follows Lira (x_1), Opuyo (x_2), Tororo (x_3), Iganga (x_4), Bujagali (x_5), Isimba (x_6), Nalubaale (x_7), Lugazi (x_8), Namanve-South (x_9), Namanve (x_{10}), Mukono (x_{11}), Lugogo (x_{12}), Queensway (x_{13}),

Mutundwe (x_{14}), Kampala-North (x_{15}), Kawaala (x_{16}), Kapeeka (x_{17}), Kawanda (x_{18}), Masaka (x_{19}), Mbarara (x_{20}), Nkenda (x_{21}), Kabulasoke (x_{22}), Nkonge (x_{23}), Rugongo (x_{24}), Fort-Portal (x_{25}) and Hoima (x_{26}).

An ILP problem is formulated with 26 variables and 52 constraints, in order to optimally locate the PMUs within the system. Its equations are shown in (1)–(28) where x_i is a binary decision variable corresponding to bus *i*. The value x_i is assigned one if the PMU is placed at bus *i* and assigned zero if not.

$$\textbf{Objective Function}: \text{Min } Z = x_1 + x_2 + x_3 + x_4 + x_5 + x_6 + x_7 + x_8 + x_9 + x_{10} + x_{11} + x_{12} + x_{13} + x_{14} + x_{15} + x_{16} + x_{17} + x_{18} + x_{19} + x_{20} + x_{21} + x_{22} + x_{23} + x_{24} + x_{25} + x_{26} + x_{27} + x_{28} \quad (1)$$

Constraints: subject to bus monitoring constraints as below;

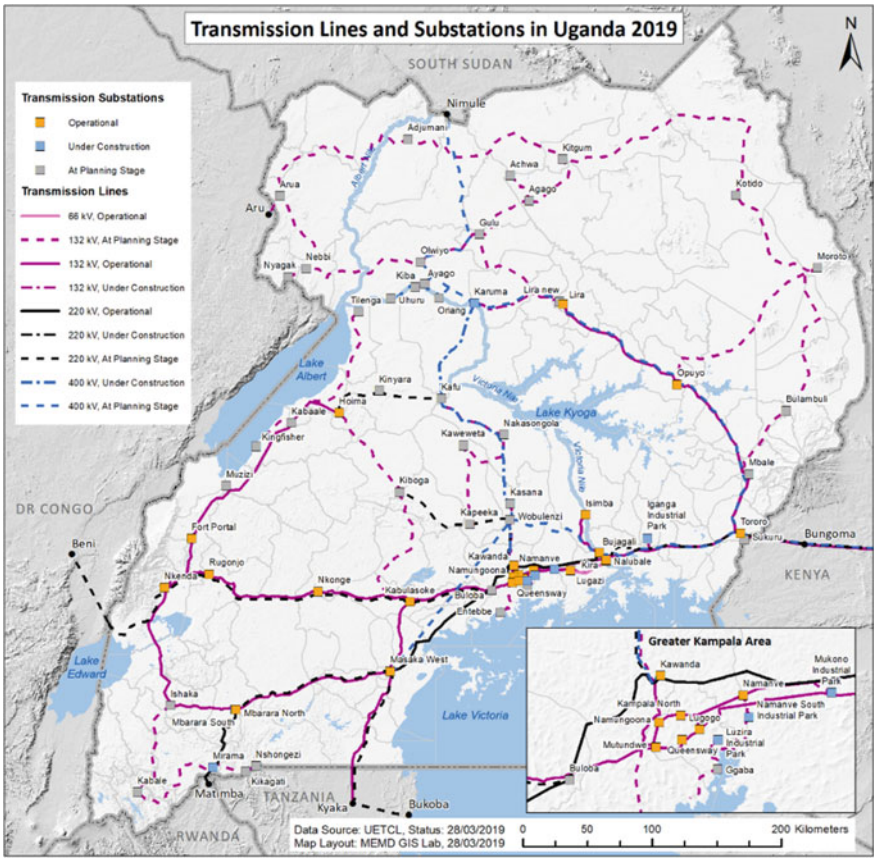

Fig. 2 Uganda's transmission network [2]

$$\text{Bus 1: } x_1 + x_2 \geq 1 \tag{2}$$

$$\text{Bus 2: } x_1 + x_2 + x_3 \geq 1 \tag{3}$$

$$\text{Bus 3: } x_2 + x_3 + x_4 + x_5 \geq 1 \tag{4}$$

$$\text{Bus 4: } x_3 + x_4 + x_5 \geq 1 \tag{5}$$

$$\text{Bus 5: } x_3 + x_4 + x_5 + x_6 + x_7 + x_{18} \geq 1 \tag{6}$$

$$\text{Bus 6: } x_5 + x_6 \geq 1 \tag{7}$$

$$\text{Bus 7: } x_5 + x_7 + x_8 + x_9 + x_{10} + x_{11} + x_{12} + x_{15} \geq 1 \tag{8}$$

$$\text{Bus 8: } x_7 + x_8 \geq 1 \tag{9}$$

$$\text{Bus 9: } x_7 + x_9 + x_{10} + x_{11} \geq 1 \tag{10}$$

$$\text{Bus 10: } x_7 + x_8 + x_9 + x_{10} + x_{15} \geq 1 \tag{11}$$

$$\text{Bus 11: } x_7 + x_9 + x_{11} \geq 1 \tag{12}$$

$$\text{Bus 12: } x_7 + x_{12} + x_{13} + x_{14} + x_{15} \geq 1 \tag{13}$$

$$\text{Bus 13: } x_{12} + x_{13} + x_{14} \geq 1 \tag{14}$$

$$\text{Bus 14: } x_{12} + x_{13} + x_{14} + x_{15} + x_{16} + x_{18} + x_{22} \geq 1 \tag{15}$$

$$\text{Bus 15: } x_7 + x_{10} + x_{12} + x_{14} + x_{15} + x_{16} \geq 1 \tag{16}$$

$$\text{Bus 16: } x_{14} + x_{15} + x_{16} \geq 1 \tag{17}$$

$$\text{Bus 17: } x_{17} + x_{18} \geq 1 \tag{18}$$

$$\text{Bus 18: } x_5 + x_{14} + x_{17} + x_{18} + x_{19} \geq 1 \tag{19}$$

$$\text{Bus 19: } x_{18} + x_{19} + x_{20} + x_{22} \geq 1 \tag{20}$$

$$\text{Bus 20: } x_{19} + x_{20} + x_{21} \geq 1 \tag{21}$$

$$\text{Bus 21: } x_{20} + x_{21} + x_{24} + x_{25} + x_{26} \geq 1 \tag{22}$$

$$\text{Bus 22: } x_{14} + x_{19} + x_{22} + x_{23} \geq 1 \tag{23}$$

$$\text{Bus 23: } x_{22} + x_{23} + x_{24} \geq 1 \tag{24}$$

$$\text{Bus 24: } x_{21} + x_{23} + x_{24} + x_{25} \geq 1 \tag{25}$$

$$\text{Bus 25: } x_{21} + x_{24} + x_{25} + x_{26} \geq 1 \tag{26}$$

$$\text{Bus 26: } x_{21} + x_{25} + x_{26} \geq 1. \tag{27}$$

$$x_1, x_2, x_3, x_4, x_5, x_6, x_7, x_8, x_9, x_{10}, x_{11}, x_{12}, x_{13}, x_{14}, x_{15}, x_{16}, x_{17}, x_{18}, x_{19}, x_{20}, x_{21}, x_{22}, x_{23}, x_{24}, x_{25}, x_{26}, x_{27}, x_{28} \geq 0 \tag{28}$$

On solution, the optimal solutions are x_1, $x_{5,}$ $x_{7,}$ $x_{14,}$ x_{21} and x_{22}. The proposed system therefore has 6 PMUs and PDCs at transmission level.

4.3 Distribution Substation Automation

For distribution automation, we make use of μPMU and μPDC. Uganda's distribution system is made of 33 and 11 kV lines, with 78 distribution substations. Adopting the same ILP technique used for the transmission system, 26 microPMUs and PDCs are found to be adequate for full visibility into the distribution system.

4.4 DER Integration

This is the ultimate phase of network modernization. For its effective operation, substation automation needs to be in place for real-time control of DERs, given with impulsive output [11]. From Figs. 1 and 2, it is evident that there is need for distributed generation in the North East and North West of Uganda due to non-availability of the power grid. This study therefore proposes 5 MW solar plants in each of the regions.

5 Cost Benefit Analysis

5.1 Cost Analysis

Installing a PMU at transmission level is $167,000 and $90,000 at distribution level. A PDC costs $135,000 at transmission level and $65,000 at distribution level. These PMUs measure up to 1000 V, have 40 inputs, capture 50 frames per second and sampling frequency of up to 16 kHz [17]. A kilometer of fiber optic cable is $1000. It is assumed that $2 million dollars are spent on using telecom infrastructure for the project lifetime. Meter Data Management Software (MDMS) costs $180,000 and server & database software costs $160,000 and PDC support software costs $4000 [7]. O&M costs are calculated as in [7] for the project lifetime of 15 years. According to [11] it costs $4000/kW for a PV solar power facility in initial capital expenditure and $20/kW for maintenance annually.

5.2 Project Costing

Table 1 details all costs excluding O&M costs. O&M costs are shown in Table 2.

It is to be noted that the value of money changes over time and therefore the O&M charges foreseen are not of the same value today. The Present Worth Factor (PWF) is used to estimate the present value [7]. PWF is calculated as per (29).

Table 1 Infrastructure project costs

	Item	Unit cost	References	Quantity	Total cost
1	Transmission PMU	$167,000	[17]	6	$1,002,000
2	Transmission PDCs	$135,000	[17]	6	$810,000
3	Distribution PMUs	$90,000	[17]	26	$2,340,000
4	Distribution PDCs	$65,000	[17]	26	$1,690,000
5	Fiber optical cable	$1000	[7]	39	$39,000
6	PDC software	$4000	[7]	1	$4,000
7	Meter data management software	$180,000	[7]	1	$180,000
8	Server OS database and antivirus software	$160,000	[7]	1	$160,000
9	5 MW PV power plant	$2,000,000	[11]	2	$4,000,000
10	Communication charges by telecoms	$2,000,000	[7]	1	$2,000,000
	Sub total				$12,225,000
	Taxes and installation charges	15%	[7]		$1,833,750
	Total after taxes				$14,058,750

Table 2 Annual operation and maintenance costs

Item	Unit cost	References	Quantity	Annual cost	Lifetime cost
Transmission PMU (2.5%)	$4175	[7]	6	$25,050	$375,750
Transmission PDCs (2.5%)	$3375	[7]	6	$20,250	$303,750
Distribution PMUs (2.5%)	$2250	[7]	26	$58,500	$877,500
Distribution PDCs (2.5%)	$1625	[7]	26	$42,250	$633,750
Fiber optical cable (2.5%)	$18	[7]	39	$683	$10,238
MDMS (5%)	$9000	[7]	1	$9000	$135,000
Server OS (5%)	$8000	[7]	1	$8000	$120,000
PV power plant	$20,000	[11]	2	$40,000	$600,000
Sub total				$203,733	$3,055,988

Table 3 Project cost summary

Item	Future value	Present value
Infrastructure costs	$14,058,750	$14,058,750
Operation and maintenance costs	$3,055,988	$1,986,392.2
Total	$17,114,738	$16,045,142.2

$$\mathrm{PWF} = \sum_{t-1}^{T} \left(\frac{1 + \mathrm{IF}}{1 + \mathrm{IR}} \right)^{t} \tag{29}$$

IF is inflation rate while IR is interest rate. At IF $= 6\%$ and IR $= 12\%$, PWF is 0.65. The project costs in present worth are summarized in Table 3.

5.3 Benefit Costing

The benefits rates are adopted from [11] and shown in Table 4.

5.4 Payback Period

The payback period is calculated by dividing the total investment cost by the annual benefits from the project.

$$\begin{aligned} \text{Payback} &= (\text{Total project costs})/\text{Benefits p.a.} \\ &= \$16{,}045{,}142/\$8{,}344{,}000 = 1.9229\text{years}. \end{aligned}$$

Table 4 Project benefit costs

Benefit	Present value	References	Annual Value
Reduced CO_2 emissions due to 10 MW solar plant	\$50/ton, and each MWh at 0.68 tons of CO_2	[11]	\$544,000
Reduced technical losses due to automation and distributed generation	Automation offsets 3% and DERs offset 4% losses	[11]	\$2,100,000
Annual savings due to reduction in outages	Estimated to reduce sustained outages by 1%	[11]	\$4,000,000
Offset investments in distribution	\$0 in year 1, growing to \$1.4 m by year 15	[11]	\$700,000
Decreased ancillary service cost	\$0 in year 1, growing to \$3.6 m by year 15	[11]	\$1,000,000
Total			\$8,344,000

5.5 Sensitivity Analysis

Uncertainties that arise in calculations of interest rates and payback duration of SG projects are largely based on utility tariffs and the implementation costs. In case of tariff increment, the envisaged growth in electricity demand can be matched by compensations from decreased technical losses or DSM techniques. The second uncertainty arises from economies of scale, whereby large scale implementation could significantly reduce SG investment costs and reduce payback duration.

Advances in SG technologies could also affect economic analysis by increasing benefits and reducing payback durations. The falling prices of DERs and more accurate metering could also be a factor. Climate change could reduce renewable outputs further and affect return rates due to reduced benefits. In Uganda's scenario, the other uncertainty today is the incompatible power market structure that does not support implementation of active DSM techniques. Lack of appropriate regulatory framework could lead to less return rates since full benefits are not attained.

6 Conclusion

This study aimed at assessing the technical ability of the smart grid as a solution to Uganda's power system's challenges mainly focusing on rampant nationwide blackouts. The SG components and features such as PMUs, WAM and DSM are found technically feasible to solve existing challenges in Uganda's power system. The study further maps possible renewable energy resources in Uganda and found solar PV the most feasible for implementation.

The study further proposes a SG system in which PMUs are optimally located within the transmission and distribution system to facilitate WAM. The economic

analysis focuses on estimating the cost of the proposed system and quantifying the benefits from implementation over the 15 year period project lifetime. The outcome of the cost–benefit analysis is a 2 year payback period which is minimal and confirmed the project economically feasible. Sensitivity analysis is also done to factor in uncertainties in the CBA analysis.

References

1. The Independent Magazine. Fourth nationwide blackout in five months! https://www.independent.co.ug/fourth-nationwide-blackout-in-five-months/. Accessed 26 Oct 2021
2. Electricity Regulatory Authority. Uganda's electricity sector overview. https://www.era.go.ug/index.php/sector-overview/uganda-electricity-sector. Accessed 23 Oct 2021
3. Tumwesigye R, Twebaze P, Makuregye N, Muyambi E (2011) Key issues in Uganda's energy sector. International Institute for Environment and Development, United Kingdom
4. Twinomuhangi R, Kato AM, Sebbit AM (2021) The energy and climate change nexus in Uganda: policy challenges and opportunities for climate compatible development. Open Access 5(121)
5. Antonova G, Paduraru S, Naccarino J, Price E (2010) Wide-area awareness: smarter power grid monitoring and analysis. ABB
6. Nayan F, Islam A, Mahmud S (2013) Feasibility study of smart grid in Bangladesh. Sci Res J Energy Power Eng 5:1531–1535
7. Kappagantu R, Daniel SA, Suresh N (2016) Techno-economic analysis of Smart Grid pilot project—Puducherry. Resour-Effic Technol 2(2):185–198
8. Sigety KC, Jaskolka SM, Hesler MP, Beliveau AM (2010) Feasibility of a smart grid on Nantucket. Worcester Polytechnic Institute, Nantucket, MA
9. Sreekumar N, Malik S (2019) Feasibility study for implementing smart community in India: a case study of Panipat Project. ISGT Latin America, Gramado, Brazil
10. Gemsjaeger B (2019) Proven feasibility study results in city of Ufa pilot project. Siemens AG, Nuremberg, Germany
11. Kempener R, Komor P, Hoke A (2015) Smart grids and renewables a cost-benefit analysis guide for developing countries. IREA, Colorado
12. Shaikh MRS, Waghmare SB, Labade SS, Fuke PV, Tekale A (2017) A review paper on electricity generation from solar energy. IJRASET 5(9)
13. W. B. Group. Solar resource maps of Uganda. Solar GIS [Online]. Available at: https://solargis.com/maps-and-gis-data/download/uganda. Accessed 12 Dec 2021
14. Fashina A, Mundu M, Akiyode O, Abdullah L, Sanni D, Ounyesiga L (2019) The drivers and barriers of renewable energy applications and development in Uganda: a review. Clean Technol 1(1):9–39
15. Energypedia. Hydro power basics. https://energypedia.info/wiki/Hydro_Power_Basics. Accessed 13 Dec 2021
16. Dua D, Dambhare S, Gajbhiye RK, Soman SA (2008) Optimal multistage scheduling of PMU placement: an ILP approach. IEEE Trans Power Deliv 23(4):1812–1820
17. Independent Electricity System Operator (2021) Estimated quantitative cost range analysis for installation of phasor measurement units (PMUs) in Ontario's power system. IESO, Toronto, Canada

Two-Stage Boost Inverter for Wave Energy Conversion

Souvik Datta and P. Sriramalakshmi

1 Introduction

1.1 Background

The modern world is much concerned about the excessive usage of conventional fossil fuel power plants. These fossil fuel power plants also cause greenhouse effect which is a prime reason for the climate change. Moreover, increasing power demand and the fast depletion of fossil fuels encourage the countries to find alternate solutions such as wind power, photo voltaic and ocean energy. Renewable energy sources will clearly play a vital role in reducing greenhouse gas emissions and ensuring a sustainable future for the entire globe. Development of renewable energy sources, including ocean, tidal and wave energy arises to reduce greenhouse effect and hence improves the production of electricity as well as reduces emission of carbon footprint. To address the aforementioned issues, wave energy has become more popular and various wave energy conversion systems are developed [1, 2]. Recently, ocean wave energy is emerging research area since it is considered as one of the cleanest and safest energy sectors. Hence it is gaining more attention among the researchers. Ocean waves are generated by numerous techniques such as through gravity, seismic tremors, solar energy etc. The wave energy potential is calculated theoretically as 16,000 TWh/year [3, 4], which is very much helpful in meeting the global energy demand. The wave energy resource with other renewable energy sources, such as wind and solar, can lead to positive synergies [5–7]. Wave energy systems can generate the power up to 90% power from the source, but wind and solar power

S. Datta · P. Sriramalakshmi (✉)
School of Electrical Engineering, Vellore Institute of Technology, Chennai 600127, India
e-mail: sriramalakshmi.p@vit.ac.in

S. Datta
e-mail: souvik.datta2019@vitstudent.ac.in

S. Doolla et al. (eds.), *Advances in Renewable Energy and Its Grid Integration*,
Lecture Notes in Electrical Engineering 1041,
https://doi.org/10.1007/978-981-99-2283-3_15

systems can generate only 20–30% [5–7]. Around 2% of the total energy demand of the globe is met by the ocean wave energy technology [8]. This is one of the cheapest among all other renewable resources, which is mostly rely on photovoltaic and wind power. A comprehensive review on the wave to wire model is presented in [6, 9–11] which reviews the various methodologies adopted for the conversion process of ocean wave energy to electrical energy using wave to wire model. A series of power electronic converters are essential to convert wave energy to electrical energy before feeding it to the load or grid. The detailed review of wave energy converter topologies is elaborated in [12]. Various electrical generators such as linear and rotary types used in the conversion process are elaborated in [13]. A direct-drive linear generator or rotary generators are used to convert the mechanical energy to electrical energy. The linear type system makes the overall system very economical. Different types of linear generators are available for converting the wave energy into electricity [13]. Based on the geometric and magnetic structures, various configurations of generators like linear and rotational types are available. Among all, the linear tubular generators are found to be highly efficient. The translator may be inside or outside of the generator stator. The power density is not similar for various generators. The linear generators produce the linear motion while the rotational one produces the rotary motion. There are various principles such as Oscillating Water Columns (OWCs), Wave-Activated Bodies (WABs) and Overtopping Devices (ODs), are associated with the wave energy conversion (WEC) technologies. Buoy Type WECs consist of various floating buoy. Very common type of WEC is the Heaving Point Absorber and it takes energy from any direction.

There are various power converter topologies used to convert the wave power to electrical power. There are many WECS technologies available in the literature. But the most promising method of conversion is still not definite for converting wave power to electrical power. The wave energy conversion techniques need to be chosen based on the location to achieve the highest efficiency of conversion. In addition, modeling and control techniques take main role in improving the efficiency of the WECS. Various configurations of wave energy conversion system (WECS) are presented in the literature and each one has adopted different converter topology. The power conditioning topologies are mainly used to adjust and condition the source voltage of the system to attain the desired output voltage. An appropriate combination of a diode rectifier and DC- DC boost converter is used as an interface between the PMSG and a single phase or three phase inverters [4].

In this research article, a wave energy powered zeta converter based two stage boost inverter is used to boost and invert the voltage availed from the wave energy powered rectified dc voltage. AC voltage is generated by a PMSG generator combined with the wave energy conversion system. The conventional boost converter cascaded with H bridge inverter is already available in the literature. In this article zeta converter based inversion is performed to obtain the constant magnitude of AC voltage from the variable AC voltage generated at the PMS generator. The grid integration aspects are well explained in [15]. A two-stage conversion system to convert variable AC voltage to a constant amplitude AC voltage with constant frequency is implemented using cascaded buck boost inverter system [16]. The complete article is arranged as

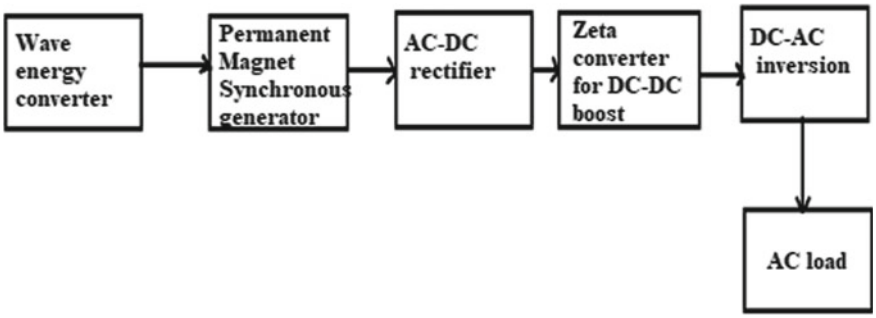

Fig. 1 Block diagram of wave energy powered boost inverter

follows: in Sect. 2, the proposed wave energy powered zeta converter-based boost inversion, and the design specification of wave conversion model, PMSG generator design specifications, zeta converter design specifications are tabulated. Section 3, discusses the operation of the zeta converter and modulation technique adopted to generate the pulses for the inverter. The simulation results of the completed wave energy based boost inverter are discussed in Sect. 4. The conclusions of the article and the future direction of research in the field of wave energy conversion is presented at the end of the article.

2 Circuit Analysis

2.1 Wave Energy Powered Boost Inverter System

The block diagram of the wave energy powered zeta converter based boost inverter is shown in Fig. 1. The wave power converted using the wave energy converter system is given to the permanent magnet synchronous generator as shown in Fig. 1. The electrical energy obtained from the PMS generator is rectified using the AC-DC rectifier and then the converted DC is given as the input to the zeta converter to boost the rectified DC voltage. Further the boosted DC if fed to the single-phase H-bridge inverter for inversion operation. The inverter output is supplied to the resistive load.

2.2 Zeta Converter to Boost the PMSG Output

The zeta converter used to boost the availed rectified DC voltage is depicted in Fig. 2. Zeta converter is similar as buck-boost converter. In addition, it has a wider range of duty ratio compared to any other conventional converters. Moreover, Zeta converter has low input current distortion and hence it has an improved power factor. In addition,

the output current has lower ripple and output-power range is wide. In this work, the duty ratio of Zeta converter is chosen to act as a boost converter. The boost converter is basically a DC-DC converter in which output voltage is greater than input voltage, while stepping down the current. It has two inductors (L1, L2), two capacitors (C1, C2), switch (TQ1), Diode (TD1). The circuit operation is explained in two modes considering that zeta converter is in Continuous Conduction Mode (CCM) and are presented in Figs. 3 and 4 respectively. The frequency of 100 kHz is used to produce the firing pulse for the zeta converter with the duty ratio of 0.697.

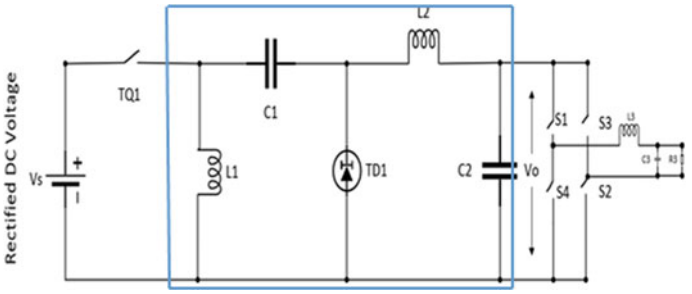

Fig. 2 Zeta converter based boost inverter topology

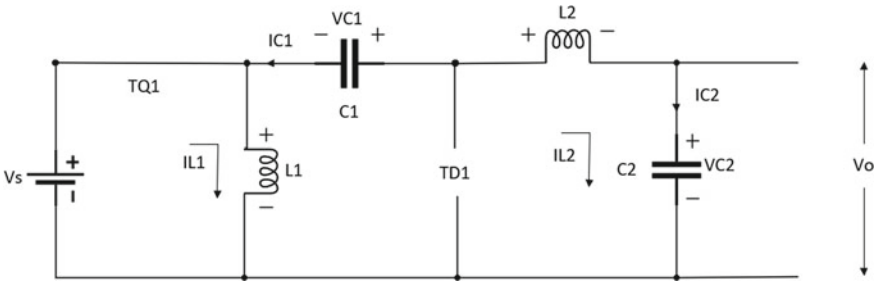

Fig. 3 Mode 1 of operation of zeta converter

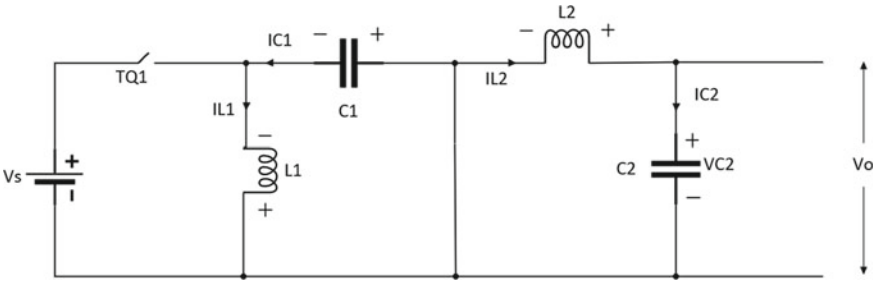

Fig. 4 Mode 2 operation of zeta converter

The topological structure of zeta converter-based boost inverter is depicted in Fig. 2. The Zeta converter operates in two modes

(1) *Zeta Converter in Mode 1*

During mode 1 as in Fig. 3, the MOSFET switch TQ1 is fired on and the diode T*D*1 is reverse biased. The source charges both the inductors L1 and L2. The inductor current *IL*1 and *IL*2 increases linearly. Also, C1 charges C2.

Inductor voltages (V_L) are obtained as

$$L1 * \frac{dI_{L1}}{dt} = V_s \tag{1}$$

$$\frac{dI_{L2}}{dt} = \frac{V_s}{L2} + \frac{V_{c1}}{L2} - \frac{V_{C2}}{L2} \tag{2}$$

The capacitor charging current is obtained as

$$C2 * \frac{dV_{c2}}{dt} = I_{c2} \tag{3}$$

(2) *Zeta Converter in Mode 2*

During mode 2 as in Fig. 4, the switch *TQ1* is switched off and the diode *TD1* is forward biased. Inductors *L*1 and *L*2 discharge through capacitors *C*1 and *C*2. Therefore, the inductor currents IL1 and IL2 decrease gradually.

Inductor voltage (L_1) is given as,

$$L_1 \frac{dI_{L1}}{dt} = -V_1 \tag{4}$$

Inductor voltage (L_2), is obtained by,

$$L_2 \frac{dI_{L2}}{dt} = -V_{L2} \tag{5}$$

Current through the capacitor C_1 is,

$$I_{L1} = C_1 * \frac{dV_{C1}}{dt} \tag{6}$$

$$\frac{V_0}{Vs} = \frac{I_{in}}{I_o} = \frac{D}{1-D} \tag{7}$$

where D is the duty cycle,

I_{in} is the input current through the zeta converter,

V_o and I_o are the output voltage across the zeta converter and current through the converter.

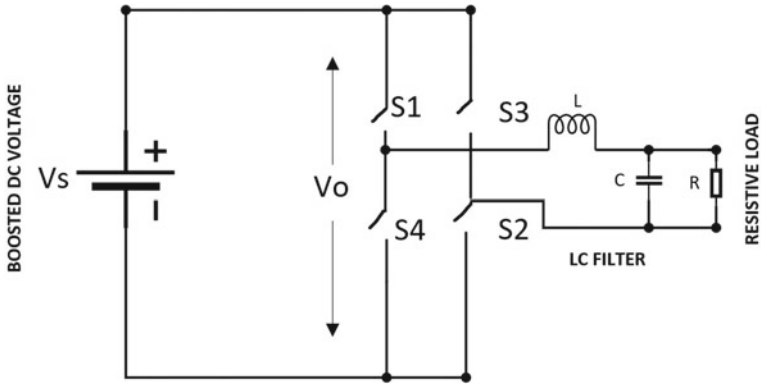

Fig. 5 H bridge inverter

3 Process of Converting Boosted DC to AC

The boosted voltage obtained from the zeta converter is fed to H bridge inverter as shown in Fig. 5. In this wave powered boost (Zeta) inverter, a resistive load is connected and ac power is delivered to the load. The conventional sinusoidal PWM strategy is used to produce the pulses for the MOSFET switches of the H-bridge inverter. The sinusoidal modulating signal is compared with the high frequency triangular waveform to produce the firing pulses of the inverter.

$$V_{acpk} = \frac{MBV_s}{\sqrt{2}} \tag{8}$$

where M is the modulation index,

B is the boost factor,

V_s is the DC output voltage across the rectifier.

4 Simulation Model of the Proposed System

The overall simulation model of the WECS powered boosted inverter system is depicted in Fig. 6 [17]. The wave energy conversion is modeled using the functional block with the parameters given in Table.1 and the specifications list of PMSG is listed in Table 2.

The proposed system is simulated using the specifications of Zeta converter [14] and H-bridge inverter as shown in Tables 3 and 4.

The switching pulse for the zeta converter is produced with the duty ratio (D) of 69.7% and at the switching frequency of 100 k Hz.

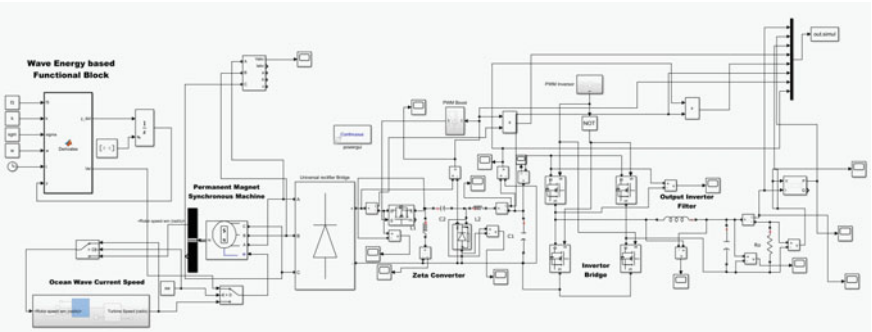

Fig. 6 Simulink model of the complete wave powered boost inverter system under study

Table 1 Wave energy conversion system parameters

Attributes	Values
Wave height (H)	1 m
Wave period (T)	10 s
Tidal current speed factor (K_{gc})	1.5
Wave angular frequency (ω)	2 * pi/T
Wave number	0.408

Table 2 Specifications of permanent magnet synchronous generator

Attributes	Values
Number of phases	3
Back Emf waveform	Sinusoidal
Rotor type	Round
Stator phase resistance (R_{ph})	0.0484 Ω
Armature inductance (L_a)	3.95×10^{-4} H
Flux linkage (λ)	0.1194
Pole pairs	8

Table 3 Specifications of the zeta converter

Attributes	Values
Input DC voltage (Vs)	30 V
Inductors (L1 and L2)	1.6 mH
Capacitance C1	0.159 μF
Capacitance C2	$4e^{-4}$ F
Duty ratio (D)	0.697
Switching frequency (fs)	100 kHz
Output voltage (Vo)	120 V

Table 4 Specifications of H-bridge inverter

Attributes	Values
Boosted DC voltage	120 V
Modulation index	1
Switching frequency	100 kHz
Output frequency	50 Hz
Output voltage	118 V
Resistive load	15 Ω
Filter inductance	3 mH
Filter capacitance	20 μF

5 Simulation Results

The simulated output AC voltage of PMSG is shown in Fig. 7. A three phase AC peak voltage of 30 V is obtained from PMS generator. The voltage from PMS generator is given to the diode rectifier for AC to DC conversion.

A rectified DC voltage of 30 V is availed from the rectifier circuit and is depicted in Fig. 8 and is given to Zeta converter for further boosting action.

The boosted voltage obtained from Zeta converter is shown in Fig. 9. It is boosted to 120 V DC.

The voltage stress across the diode (TD1) which presents in zeta converter is shown in Fig. 10. The current flows through the inductors L2 and L1 are shown in Figs. 11 and 12 respectively.

The voltage stress across the switch present in the zeta converter is shown in Fig. 13. It is similar to the voltage which is boosted at the zeta converter terminals. The same boosted voltage acts as the input voltage for the H bridge inverter.

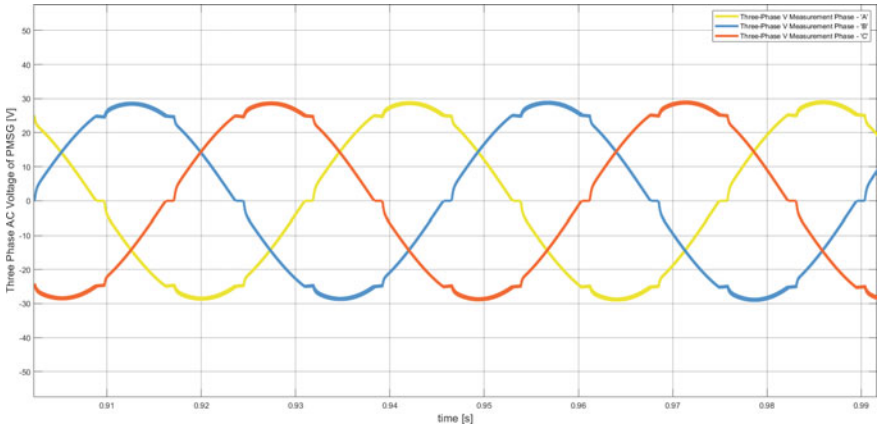

Fig. 7 Three phase AC voltage of PMSG (V)

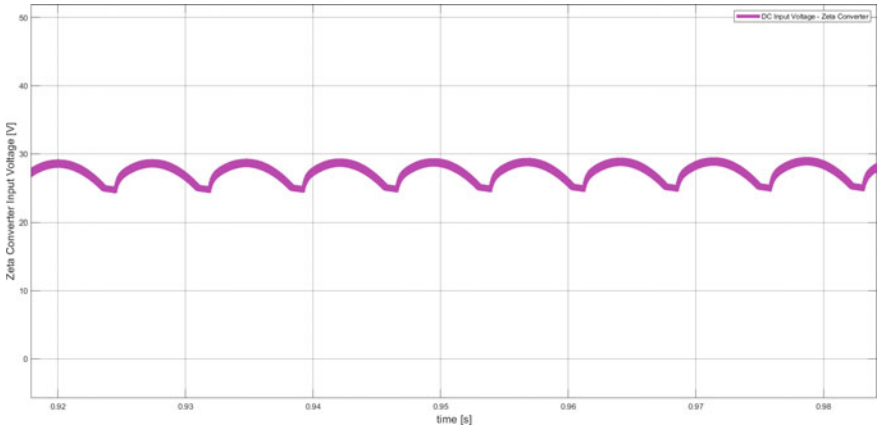

Fig. 8 Rectifier output (zeta converter input voltage)

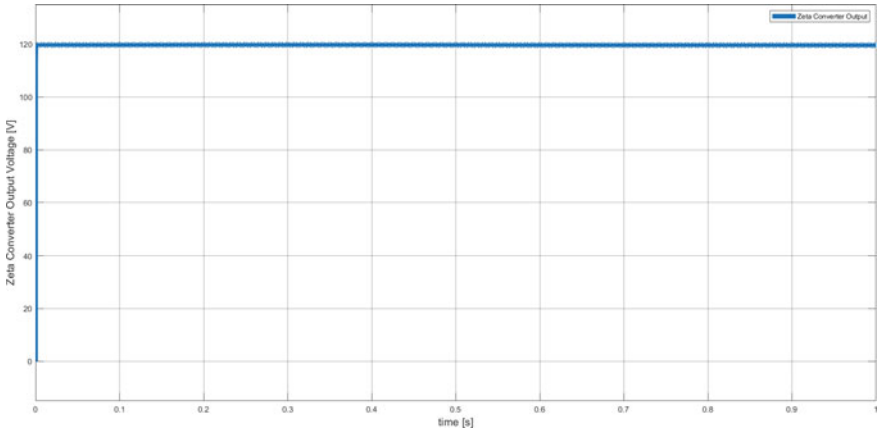

Fig. 9 Zeta converter output voltage (V)

Figures 14 and 15 depict the output voltage and output current at the inverter terminals before filter (Fig. 16).

The voltage stress across the switch S1 in the inverter bridge is shown in Fig. 17. The filtered AC inverted voltage obtained from the H Bridge inverter is given in Fig. 18. The filtered peak AC output voltage of 118 V is obtained across the resistive load terminals.

Figure 19a shows the relation between duty ratio and the voltage boost occurs in the circuit. For the same duty ratio, zeta converter can provide the higher boost compared to conventional boost converter.

By changing the value of duty ratio of the zeta converter, the conduction period of the switches can be controlled. With the rectified dc voltage of 30 V, zeta converter

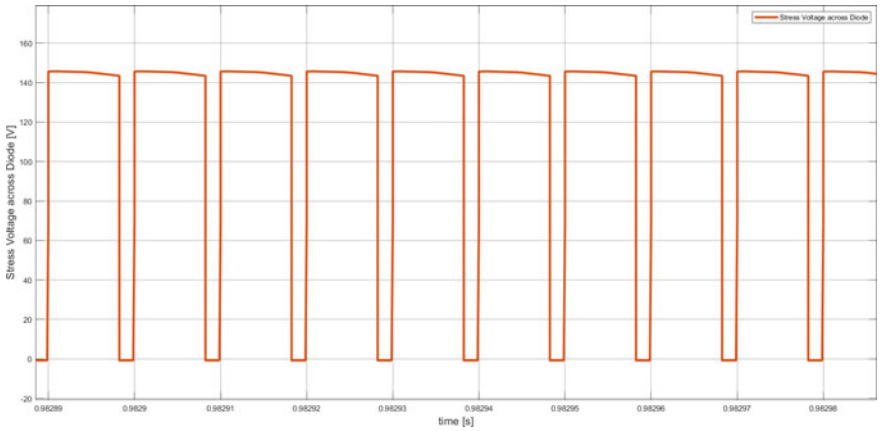

Fig. 10 Voltage stress across diode (V)

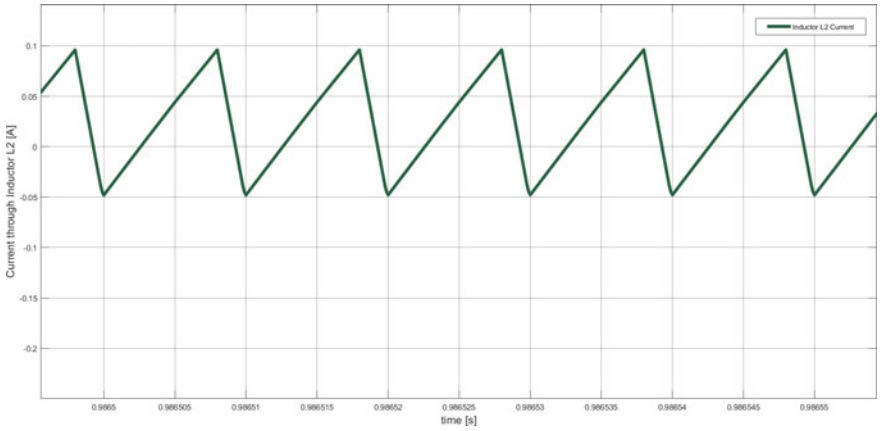

Fig. 11 Current through inductor L2 (A)

boosted the voltage to 120 V and with the modulation index of 1, the inverted ac voltage of 118 V is obtained at the efficiency of 98.33% keeping all the devices as ideal during the simulation. Figure 19b and c shows the harmonic profile of the output load current flowing through the load and voltage across the resistive load at fundamental frequency. The THD content meets the IEEE standards.

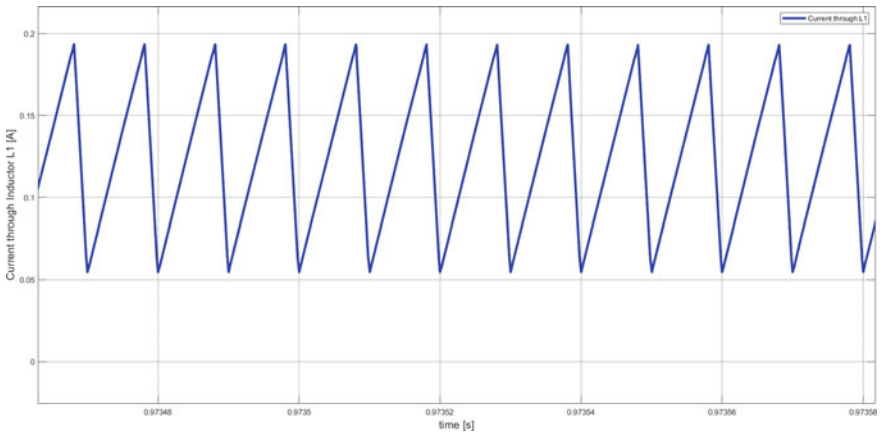

Fig. 12 Current through inductor L1 (A)

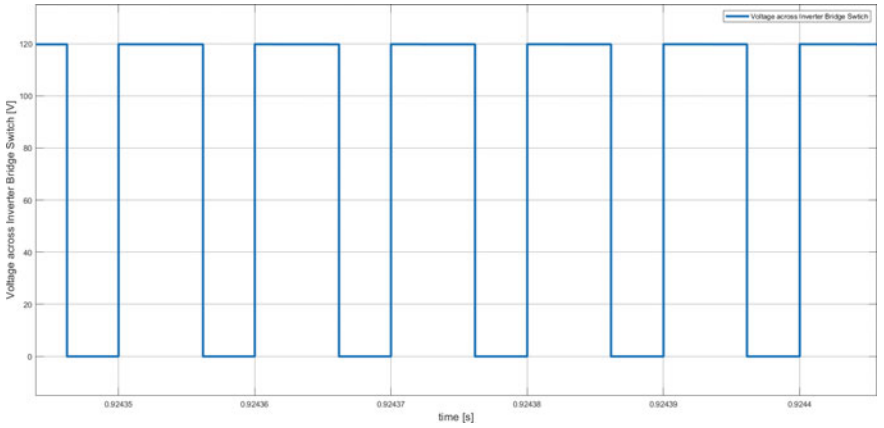

Fig. 13 Voltage across zeta converter switch TQ1 (V)

6 Conclusion

Wave energy technologies are going to be the better replacement and meet the shortage of fossil fuel in the near future. The wave energy is converted into electric energy using modern WECS technologies; but, they are not yet commercialized. And ocean technologies have great potential, but standard policies must be framed to support the research. Efficient WECS need to be developed in the upcoming years. More converter topologies and control strategies need to be developed for efficient conversion. Instead of two stage conversion, single stage boost conversion can be adopted to improve more boost and effective conversion.

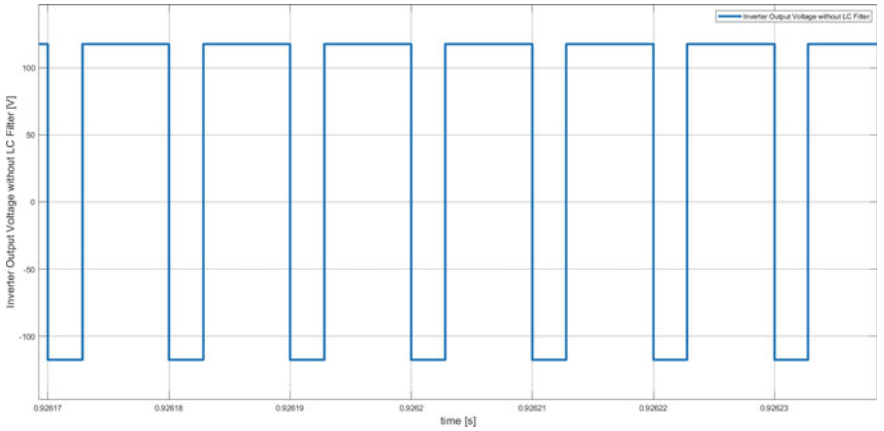

Fig. 14 Inverter output voltage without LC filter

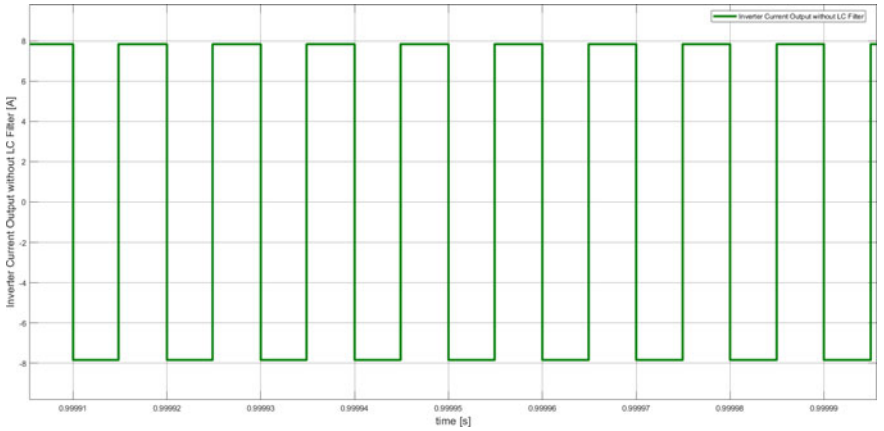

Fig. 15 Inverter output current without LC filter

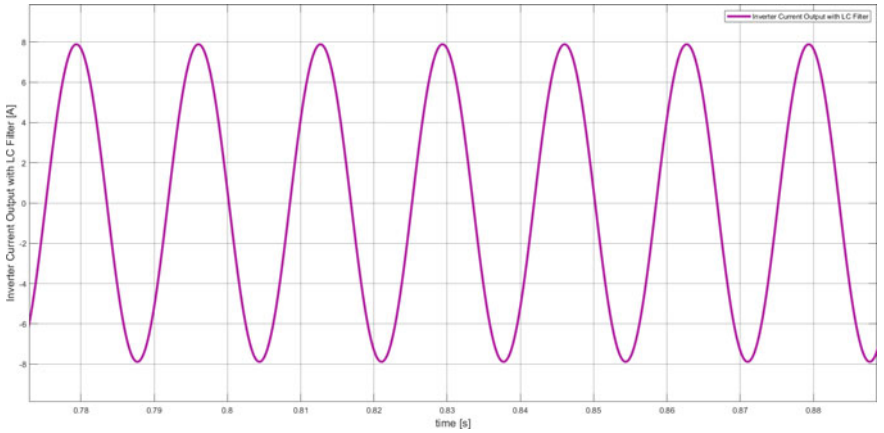

Fig. 16 Inverter output current with LC filter

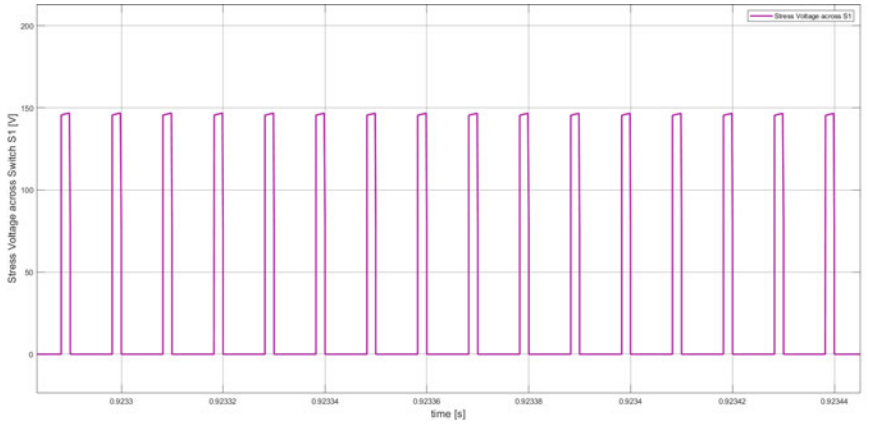

Fig. 17 Voltage stress across switch S1 (V)

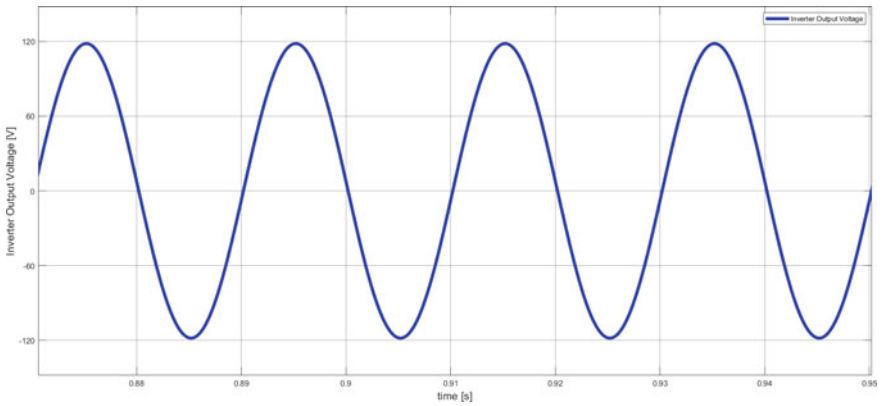

Fig. 18 Inverter AC output waveform (V)

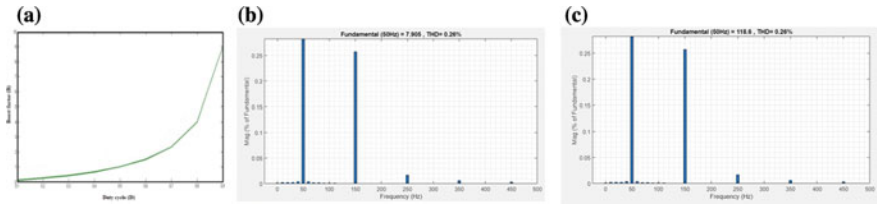

Fig. 19 **a** Graph between duty ratio and boost factor. **b** Harmonic profile of load current. **c** Harmonic profile of load voltage

References

1. Ozkop E, Altas IH (2017) Control, power and electrical components in wave energy conversion systems: a review of the technologies. Renew Sustain Energy Rev 67:106–115
2. Liu C, Yu H, Hu M, Liu Q, Zhou S, Huang L (2014) Research on a permanent magnet tubular linear generator for direct drive wave energy conversion. IET Renew Power Gener 8(3):281–288
3. Polinder H, Scuotto M (2005) Wave energy converters and their impact on power systems. In: 2005 international conference on future power systems. IEEE, p 9
4. Yan L, Zhang L, Peng J, Zhang L, Jiao Z (2017) Electromagnetic linear machines with dual Halbach array. Springer, Singapore
5. Czech B, Bauer P (2012) Wave energy converter concepts: design challenges and classification. IEEE Ind Electron Mag 6(2):4–16
6. Ahmed EM, Shoyam M, Dousoky GM (2012) On the behaviour of marine and tidal current converters with DC-DC boost converter. In: Proceedings of the 7th international power electronics and motion control conference, vol 3. IEEE, pp 2250–2254
7. Sinu KJ, Ranganathan G (2018) A novel hydro powered online power converter for marine lighting applications, vol9, pp 15–19
8. Da Y, Khaligh A (2009) Hybrid offshore wind and tidal turbine energy harvesting system with independently controlled rectifiers. In: 2009 35th annual conference of IEEE industrial electronics. IEEE, pp 4577–4582
9. Penalba M, Ringwood JV (2016) A review of wave-to-wire models for wave energy converters. Energies 9(7):506

10. Nielsen K, Kramer MM, Ferri F, Zurkinden AS, Alves M (2014) Overview of wave to wire models: deliverable D 4.10
11. Wang L, Isberg J, Tedeschi E (2018) Review of control strategies for wave energy conversion systems and their validation: the wave-to-wire approach. Renew Sustain Energy Rev 81:366–379
12. Ferri F (2014) Wave-to-wire modelling of wave energy converters: critical assessment, developments and applicability for economical optimisation
13. Prakash SS, Mamun KA, Islam FR, Mudliar R, Pau'u C, Kolivuso M, Cadralala S (2016) Wave energy converter: a review of wave energy conversion technology. In: 2016 3rd Asia-Pacific world congress on computer science and engineering (APWC on CSE). IEEE, pp 71–77
14. Vijay KO, Sriramalakshmi P (2016) Comparison between Zeta converter and boost converter using sliding mode controller. Int J Eng Res Technol (IJERT) 5(07)
15. Said HA, Ringwood JV (2021) Grid integration aspects of wave energy—overview and perspectives. IET Renew Power Gener 15(14):3045–3064
16. Maurya AK, Singh SP (2020) Analysis of cascaded buck–boost inverter for PMLG-based ocean wave energy converter. IETE J Res 1–11
17. MathWorks (n.d.) Wave currents and sea energy. Retrieved from https://www.mathworks.com/matlabcentral/fileexchange/80548-wave-currents-and-sea-energy. 17 May 2022

A Comprehensive Review for the Optimal Deployment of Plug-In Electric Vehicle Charging Station with Solution Techniques

Fareed Ahmad, Imtiaz Ashraf, Atif Iqbal, Irfan Khan, and Mousa Marzband

1 Introduction

This paper aims to aggregate and analyze the most recent studies on the optimal placement of electric vehicle charging stations (EVCS) during the last four years. The demand for plug-in electric vehicles (PEVs) has increased dramatically in the last decade, owing to the quick reduction in CO_2 emissions [20] and running charges compared to diesel-petrol base vehicles [27]. According to studies, EVs might reduced CO_2 by 28% by 2030 [1]. Nevertheless, two premium challenges could influence the broad society when moving to EVs, such as the increased price and the scarcity of charging establishments. The various enterprises and governments worldwide are expected to push the EV demand to USD 974,102.5 million by 2027, extending at a high compound yearly development rate from 2020 to 2027 [2]. The absence of facility for charging EVs is one of the most pressing concerns handled by the writers in this investigation. EVs are exponentially growing worldwide, posing a further issue for electrical distribution network operators (EDNO). Therefore, in this paper, the authors addressed the optimal siting problem for CSs in distribution networks by considering EDNO, EVs users, and CS owner perspectives.

F. Ahmad (✉) · I. Ashraf
Aligarh Muslim University, Aligarh, India
e-mail: fareed903@gmail.com

A. Iqbal
Qatar University, Doha, Qatar
e-mail: atif.iqbal@qu.edu.qa

I. Khan
Texas A&M University, College Station, TX, USA
e-mail: irfankhan@tamu.edu

M. Marzband
Northumbria University, Newcastle upon Tyne, UK
e-mail: mousa.marzband@northumbria.ac.uk

S. Doolla et al. (eds.), *Advances in Renewable Energy and Its Grid Integration*,
Lecture Notes in Electrical Engineering 1041,
https://doi.org/10.1007/978-981-99-2283-3_16

The authors of [17] studied the parking lots by increasing the income of the parking lot and using the cost related to power loss, electrical network reliability, voltage variation, and parking lot as the deciding factors. Furthermore, a mixed-integer programming prototype was produced to represent the challenge of optimizing total EV flows in the system, and the GA was employed to handle the presented problem. The authors developed a multi-objective mixed-integer nonlinear model, including the cost of FCS installation, the energy consumption of EVs, distribution system power loss, DGs, and bus voltage deviation in [25]. In [6], authors built a multi-objective mixed integer nonlinear problem including CS investment cost, EV traveling cost for charging, cost of power loss, DGs installation, and voltage variation. In this analysis, the non-dominated sorting genetic algorithm II was used to optimize the placement of CSs and DGs in the distribution network. According to [21], the power loss of a distribution system was offered as an objective for the location of CS, and the PSO algorithm was used to solve the specified optimization challenge. Power loss is taken as an objective for problem formulation and addressed by the PSO method, and CS and renewable energy sources are deployed at the optimal sites for the distribution network [11].

2 Evaluation of Problem Formulation

According to the literature, the writers have determined that CS owners must locate the CS to reduce installation costs while maximizing gain. Alternatively, EV owners want to locate the CS to reduce the cost of traveling, charging time, waiting time, charging for battery, access for charging, and so on, whereas EDNO want to install the CS to minimize the influence on distribution network parameters. Therefore, three studies for optimal CS placement are discussed, as seen in Fig. 1 which is also illustrated in Table 1.

2.1 Electrical Distribution Network Operator Perspective

Electricity is distributed to all connected power loads in the domestic, corporate, and industrial sectors through the electrical distribution network (EDN). In addition, the deployment of the new loads would impact the distribution network (DN) parameters. As a result, the EDNO perspective optimizes the cost for active power loss [5, 7, 19, 22], cost for reactive power loss, voltage deviation [5, 7, 9, 19], reliability cost [9], and distribution network stability for the of CSs.

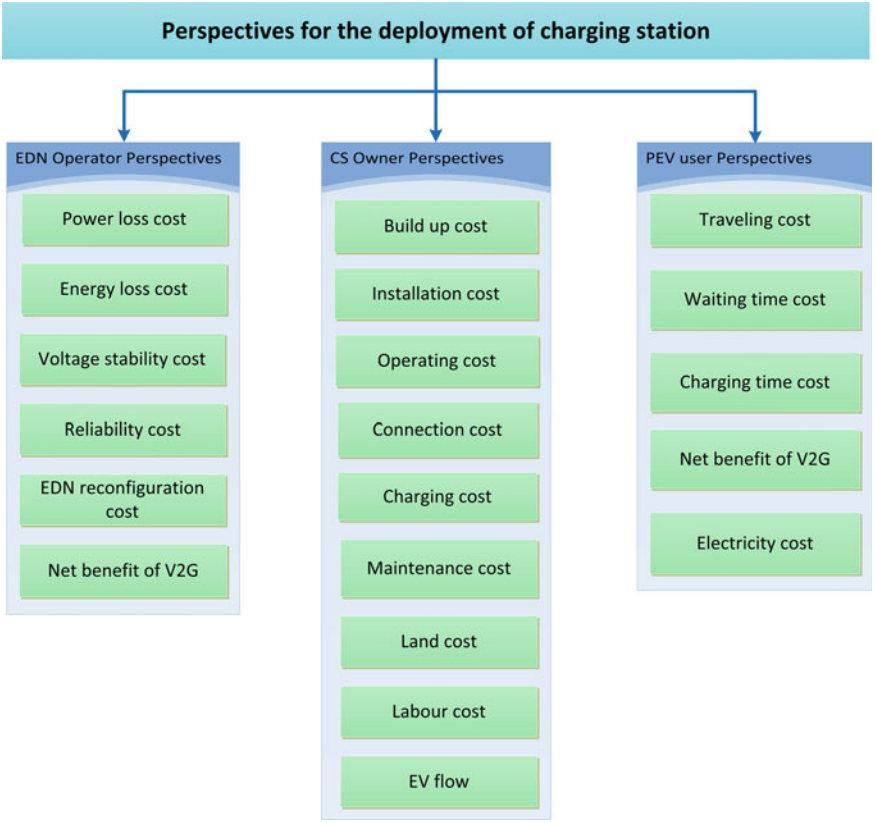

Fig. 1 Perspective for charging station deployment

Table 1 Different perspectives with references for siting of CS

Perspectives for optimal placement of CS	References
EDNO perspective	[11, 21]
CSO perspective	[10, 25]
EV user perspective	[18]
EDNO and CSO perspective	[5, 7, 9, 17, 19, 22]
CSO and EV user perspective	[13, 24, 28]
EV user and EDNO perspective	Not available
EDNO, CSO and EV user perspective	[6, 8, 15, 23]

2.2 Charging Stations Owner Perspective

The charging station owner (CSO) bears the total costs associated with installing EVCS to maximize income from the CS through charging. As a result, the CSO is looking for CS locations with the most income and the lowest investment. Therefore, the CSO perspective considers the investment cost [10, 23, 24], installation cost [5, 7, 9, 13], operating cost [9, 13], maintenance cost [7, 19], road construction cost, and land cost while determining the best CS site.

2.3 Electric Vehicle Users Perspective

The location of CS influences the behavior of EV charging. The cost for accessing the CS, traveling from energy required location to CS, time for waiting [24], and charging was evaluated as objective functions for CS deployment under the EV user's perspective.

In essence, when defining the optimal position of CS, the problem modeling of CS deployment in any specific zone is highly challenging. Recognizing objectives and constraints for modeling is a substantial research challenge for CS location, and recently four years of publication studies are expressed in Table 2.

2.4 Objective Function

This section delivers an overview of the miscellaneous objectives used to formulate the CS placement planning issue.

Cost Several research studies have addressed cost as an analytical function. As previously stated, cost functions may be created utilizing a variety of factors and methodologies. Infrastructure costs are a one-time expenditure involved with the construction of CSs and can be subdivided into cost of building, labor, land and charger. The cost of CS investment is specified in (1) as an objective function provided in various research articles [4, 5, 7, 9, 13, 15] for CS placement.

$$IC_i = C_{fix} + 25 \times C_{land} \times S_i + PC \times C_{con} \times (S_i - 1) \tag{1}$$

where C_{fix} is the fixed cost of CS, C_{land} is a cost for land, S_i shown the connectors installed at ith CS, and C_{con} is the cost for per connector.

Net benefit The CS might act as a link between the charging of EV batteries and the electricity network. Furthermore, the V2G enables EVs to contribute electricity to the electrical network via CSs during peak times. Net profit is used as the objective in the planning of V2G-enabled CSs. Furthermore, the profit raised by CSs in Eq. (2) by

Table 2 Analysis of CS placement problem in the perspectives of EDN operator, CS owner and EV user

Objective functions	Year	Method	Load modeling	DGs	V2G
Cost of voltage deviation, CS development and power loss [7]	2021	BMA	×	×	×
Cost of energy loss, voltage deviation and land [19]	2021	HHO	✓	×	✓
Cost of CS fixed and operating, traveling and for penalty [8]	2021	CSO, TLBO	×	×	×
Power loss cost [11]	2020	PSO	×	✓	×
Active power losses cost [21]	2020	PSO	×	✓	×
Traveling cost [18]	2020	EHDG	×	×	×
Cost of development, specific energy consumption and power loss [6]	2019	NSGA-II	×	✓	×
Power loss cost and EV flow [22]	2019	GWO	✓	×	×
Cost of installing EVCS [10]	2019	LP	✓	×	×
Construction and operational cost [13]	2019	Simulation	✓	×	×
Cost of CS development, EV user, power loss and voltage deviation [5]	2019	SFL-TLBO	×	✓	×
Reliability, cost for installation, operation and power loss [9]	2019	CSO-TLBO	×	×	×
Cost of power loss, reliability and voltage improvement [17]	2018	GA	×	×	×
Cost for investment for CS, traveling time and waiting time [24]	2018	SCE-UA	✓	×	×
Cost for connection, demand response, investment and power loss, demand response [23]	2018	PSO	×	×	×
Cost of transportation, sub-station power loss and CS development [15]	2018	BLSA	×	×	×
Cost of CS installing, users charging, CS access and waiting time [28]	2018	CPLEX	×	×	×
Plug-in electric vehicle flows [25]	2018	HA, GA	×	×	×

delivering energy to the network during peak time represents a benefit of supplying energy from the electrical network.

$$R(i) = Pr_p \times P_{park}(i) \times t_{dis}(i) \tag{2}$$

where $R(i)$ is the raised total amount from ith CS, $t_{dis}(i)$ is time in which battery of EV discharging through V2G perspective, Pr_p is the rate of energy during peak time.

Other cost functions Researchers consider power loss, distance, and covered trip as objective functions when addressing the CS placement challenges. Furthermore, installing a CS increases the burden on the existing network. Furthermore, the cost of power loss and voltage variation are the primary concerns for the deployment of CS under the EDNO concept. As a result, most researchers have included the cost of power loss [5, 7, 19, 22] and voltage variation [10, 24] as objective functions in (3).

$$P^c_{loss} = EC \sum_{i=1}^{B} \sum_{j=1}^{B} G_{ij} \left(V_i^2 - V_j^2 - 2V_i V_j \cos(\theta_{ij})\right) \tag{3}$$

where, EC is rate of energy in \$, B is the total nodes, G_{ij} is the conductance of branch between ith node to jth node, V_i is the ith node voltage, θ_{ij} is the difference of load angle, V_i^t, is the node voltage of ith.

2.5 Constraints

The CS placement issue is cracked under equality and inequality constraints. After installing CSs in the distribution network, the voltage restrictions at each bus, branch current limits, and temperature limits should be satisfied. The min. and max. CSs installed must also be specified. Furthermore, CSs should not be put too near together. The distance constraint considers the distances between CSs.

3 Review of the Solution Techniques for the Placement of CS

The solution methods minimize or maximize the objective functions to place the CS at an optimal location. The specified problems formulation for the deployment of EVCS, for instance, can be multi or single objective, it can be also non-linear also with concave or convex property. The problem model might be continuous, integer, discrete, or a mix of the variables utilized. As a result, selecting the appropriate

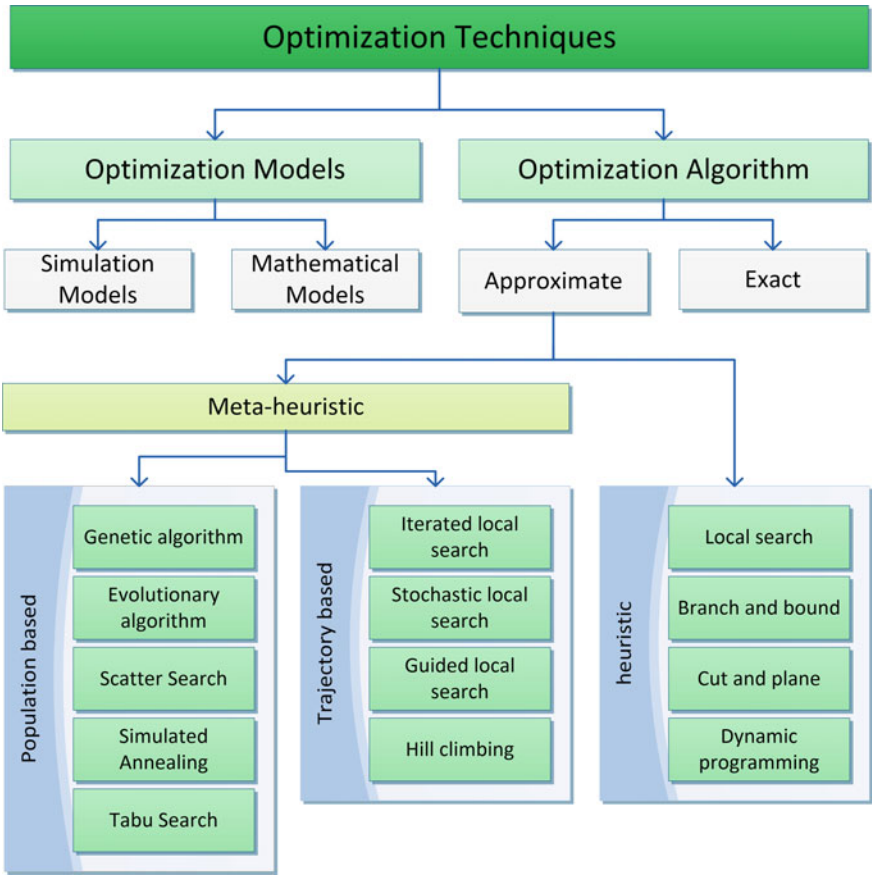

Fig. 2 Optimization techniques classification

strategies for the assigned issue is crucial. The paper provides a summary of different approaches for CS optimum position in this study, as depicted in Fig. 2. Furthermore, the two effective optimization techniques are classical and advanced optimization.

Classical optimization techniques can handle only differentiable and continuous problem. Moreover, most of the time formulated problem is not continuous and/or differentiable, therefore, this approach have limited applications.

Advanced optimization techniques Multi-modality, dimensionality, and differentiability are associated with optimizing large-scale issues, which traditional methodologies struggle to tackle. Because most classical approaches need gradient information, they are unsuitable for solving non-differentiable functions. Furthermore, traditional strategies frequently fail to address optimization issues with several local optima. On the other hand, advanced approaches devastate these obstacles to solving the optimization challenge.

3.1 Optimization Approach for Single Objective

In comparison to the multi-objective optimization problem, the handling procedures of the single-objective is straightforward. To address single-objective problems, conventional and advanced optimization methods are applied.

Genetic algorithm as the name indicates, imitate the genetic component of candidate populations to enhance the current set selection. When applying a GA, rigorous plan decisions should acclimate the algorithm. The gene-encoding procedure, crossover process, and fitness functions impact the technique's capacity to identify the correct output. A big pool of different data is also needed to prevent the technique from tangling in regional minima. This is often performed by randomly picking genes for a crossover, resulting in a slow convergence speed while ensuring exploration. According to [26], the target functions to frame the problem for EVCS deployment and problems handled by GA include traveling cost, installing cost for CSs, substation operating cost, and power loss cost.

Particle swarm optimization is a popular and efficient technique that optimizes execution using randomization and global particle communication. The swarm of potential solutions (particles) comb the investigation area for the most excellent solutions, continually trading and comparing personal and global bests. Recently, IPSO, several enhancements to the earliest PSO were created to improve computation time and deliver more exact results. CS and DER are put at an ideal RDS position in [3], and power loss is used as an objective for the model handled by the PSO method.

3.2 Multi-objective Optimization Techniques

The multi-objective functions have two main approaches: a **posteriori** and a **priori**. The priori technique reduces a multi-objective function into a single-objective function using weight coefficients. Furthermore, weights determine the objective's importance in the modeled problem. The major drawback of such a method is that technology should be performed numerous times to determine the Pareto optimal set. In addition, professional assistance is necessary, and this approach cannot identify some specific Pareto optimal fronts [16].

Non-dominated sorting genetic algorithm-II is a multi-objective meta-heuristic GA often used to tackle optimization issues with multi-objectives. The NSGA-II separates the population into numerous non-dominated chromosomal fronts, with the chromosomes in each group ordered in order of diversity [6].

3.3 Machine Learning Techniques

Without any explicit programming, the computer learns from prior experience in machine learning. The data-set that the algorithm utilizes to train itself is referred to as experience in this context. The models may effectively forecast trends with time and learning experience, offering predictive analysis [14]. Typically, machine learning techniques are divided into supervised and unsupervised learning, and reinforcement. Therefore, authors in [12] used hybrid version of GA and reinforcement learning algorithm to obtained the optimal placement of CS.

According to Table 2, researchers employ various techniques to solve the location problem of CS. GA and PSO are the two primary problem-solving approaches employed by researchers. Other methods used by the authors to handle the model include TLBO, ACO, LP, ABC greedy algorithm, GOA, GWO and branch and bound.

4 Conclusion

The placement of the CS may influence the characteristics and viability of the electrical system, the choice of the EV driver to charge the battery, and the decision of the investor to build the CS. As a result, this review paper approached the subject of optimal charging station location from three perspectives: electrical distribution system operator, CS owner, and EV user. Many studies in the review have investigated and assessed the problem modeling, perspectives, objective functions, and constraints to establish a strong position for the CS. Furthermore, this paper discusses objective functions and constraints for the problem, EV load modeling, renewable energy source integration, solution methodologies, and utilized perspectives.

References

1. Adnan N, Md Nordin S, bin Bahruddin MA, Ali M (2018) How trust can drive forward the user acceptance to the technology? In-vehicle technology for autonomous vehicle. Transp Res Part A Policy Pract 118:819–836
2. Ahmad F, Iqbal A, Ashraf I, Marzband M, Khan I (2022) The optimal placement of electric vehicle fast charging stations in the electrical distribution system with randomly placed solar power distributed generations. Distrib Gener Altern Energy J 1277–1304
3. Ahmad F, Iqbal A, Ashraf I, Marzband M, Khan I (2022) Placement of electric vehicle fast charging stations in distribution network considering power loss, land cost, and electric vehicle population. Energy Sources Part A Recov Util Environ Effects 44(1):1693–1709
4. Ahmad F, Iqbal A, Ashraf I, Marzband M, Khan I (2022) Placement of electric vehicle fast charging stations using grey wolf optimization in electrical distribution network. In: 2022 IEEE international conference on power electronics, smart grid, and renewable energy (PESGRE), pp 1–6

5. Battapothula G, Yammani C, Maheswarapu S (2019) Multi-objective optimal planning of FCSs and DGs in distribution system with future EV load enhancement. IET Electr Syst Transp 9(3):128–139
6. Battapothula G, Yammani C, Maheswarapu S (2019) Multi-objective simultaneous optimal planning of electrical vehicle fast charging stations and DGs in distribution system. J Mod Power Syst Clean Energy 7(4):923–934
7. Chen L, Xu C, Song H, Jermsittiparsert K (2021) Optimal sizing and sitting of EVCS in the distribution system using metaheuristics: a case study. Energy Rep 7:208–217
8. Deb S, Gao XZ, Tammi K, Kalita K, Mahanta P (2021) A novel chicken swarm and teaching learning based algorithm for electric vehicle charging station placement problem. Energy 220:119645
9. Deb S, Tammi K, Kalita K, Mahanta P (2019) Charging station placement for electric vehicles: a case study of Guwahati city, India. IEEE Access 7:100270–100282
10. Faridpak B, Gharibeh HF, Farrokhifar M, Pozo D (2019) Two-step LP approach for optimal placement and operation of EV charging stations. In: Proceedings of 2019 IEEE PES innovative smart grid technologies Europe, ISGT-Europe 2019, pp 1–5
11. Gupta K, Narayanankutty RA (2020) Environmental effects optimal location identification for aggregated charging of electric vehicles in solar photovoltaic powered microgrids with reduced distribution losses. Energy Sources Part A Recov Util Environ Effects 1–16
12. Ko YD (2019) An efficient integration of the genetic algorithm and the reinforcement learning for optimal deployment of the wireless charging electric tram system. Comput Ind Eng 128:851–860
13. Kong W, Luo Y, Feng G, Li K, Peng H (2019) Optimal location planning method of fast charging station for electric vehicles considering operators, drivers, vehicles, traffic flow and power grid. Energy 186:115826
14. Kotsiantis SB, Zaharakis ID, Pintelas PE (2006) Machine learning: a review of classification and combining techniques. Artif Intell Rev 26(3):159–190
15. Mainul Islam M, Shareef H, Mohamed A (2018) Optimal location and sizing of fast charging stations for electric vehicles by incorporating traffic and power networks. IET Intell Transp Syst 12(8):947–957
16. Mirjalili S, Jangir P, Saremi S (2017) Multi-objective ant lion optimizer: a multi-objective optimization algorithm for solving engineering problems. Appl Intell 46(1):79–95
17. Mohsenzadeh A, Pazouki S, Ardalan S, Haghifam MR (2018) Optimal placing and sizing of parking lots including different levels of charging stations in electric distribution networks. Int J Ambient Energy 39(7):743–750
18. Othman AM, Gabbar HA, Pino F, Repetto M (2020) Optimal electrical fast charging stations by enhanced descent gradient and Voronoi diagram. Comput Electr Eng 83:106574
19. Pal A, Bhattacharya A, Chakraborty AK (2021) Allocation of electric vehicle charging station considering uncertainties. Sustain Energy Grids Netw 25:100422
20. Parker N, Breetz HL, Salon D, Conway MW, Williams J, Patterson M (2021) Who saves money buying electric vehicles? Heterogeneity in total cost of ownership. Transp Res Part D Transp Environ 96:102893
21. Reddy MSK, Selvajyothi K (2020) Optimal placement of electric vehicle charging station for unbalanced radial distribution systems. Energy Sources Part A Recov Util Environ Effects 1–15
22. Shukla A, Verma K, Kumar R (2019) Multi-objective synergistic planning of EV fast-charging stations in the distribution system coupled with the transportation network. IET Gener Transm Distrib 13:3421–3432
23. Simorgh H, Doagou-Mojarrad H, Razmi H, Gharehpetian GB (2018) Cost-based optimal siting and sizing of electric vehicle charging stations considering demand response programmes. IET Gener Transm Distrib 12(8):1712–1720
24. Tian Z, Hou W, Gu X, Gu F, Yao B (2018) The location optimization of electric vehicle charging stations considering charging behavior. Simulation 94(7):625–636
25. Wang Y, Shi J, Wang R, Liu Z, Wang L (2018) Siting and sizing of fast charging stations in highway network with budget constraint. Appl Energy 228:1255–1271

26. Xiang Y, Liu J, Li R, Li F, Gu C, Tang S (2016) Economic planning of electric vehicle charging stations considering traffic constraints and load profile templates. Appl Energy 178:647–659
27. Zhou M, Long P, Kong N, Zhao L, Jia F, Campy KS (2021) Characterizing the motivational mechanism behind taxi driver's adoption of electric vehicles for living: insights from China. Transp Res Part A Policy Pract 144(2):134–152
28. Zhu Z, Gao Z, Zheng J, Du H (2018) Charging station planning for plug-in electric vehicles. J Syst Sci Syst Eng 27(1):24–45

After Lifetime Reliability and Performance Analysis of PV Modules

Mugala Naveen Kumar, Birinchi Bora, Arup Dhar, Deepak Yadav, Jai Prakash, and Chandan Banerjee

1 Introduction

As the fossil fuels are going to extinct in coming years, the entire world is looking for renewable energy sources as a step forward. Indian prime minister pledges in COP 26 that India aims to reach net zero emissions by 2070 and to meet 50% of the energy requirements from renewable energy sources by 2030. This shows the importance of renewable energy in coming decades. Generating electricity using solar PV is one of the major sources of energy production in India. One of the main challenges of using PV modules are cost effectiveness, lifetime and reliability. To enhance the usefulness of PV module, one of the solutions is to reuse the PV module for power generation after its lifetime.

By performing the degradation analysis of the PV modules which are in working condition for long duration, we can estimate the useful life time of the PV modules. People have reported about the degradation analysis of PV module for different climatic zones of India [1–3]. Withstanding for long period in harsh outdoor environment is one of the major technical strengths of the photovoltaic (PV) modules. Long term reliability and durability are the essential points not only for the manufacturers to determine the warranty period of the module but also for the consumers who can rely on the power generation from these PV modules.

In this study, monocrystalline modules from one of the Indian PV module manufacturers which are located in National Institute of Solar Energy (NISE), Gurugram, Haryana are considered. A study about these modules was already reported [4]. The PV modules which were installed and operational since 2000 are selected statistically. Various tests and characterization are performed to obtain the rate of degradation and understand the reliability of the module. The module reliable in terms of performance

M. N. Kumar (✉) · B. Bora · A. Dhar · D. Yadav · J. Prakash · C. Banerjee
National Institute of Solar Energy, Gurugram, India
e-mail: mugala.naveen@nise.res.in

S. Doolla et al. (eds.), *Advances in Renewable Energy and Its Grid Integration*,
Lecture Notes in Electrical Engineering 1041,
https://doi.org/10.1007/978-981-99-2283-3_17

and safety could be reuse for production of energy. The degradation rate measured for the module is used to estimate the energy generation in the coming years using the current power rating of the PV modules. This has been done on PVSyst by creating the '.PAN file' of the selected PV module and designing a Photovoltaic system of 1 kWp.

2 Methodology

Mono crystalline PV module from an Indian manufacturer which is installed in NISE outdoor test bed for 22 years are used for this analysis. The modules were statistically selected and various performance analysis were performed. The performance of the module measured in indoor conditions using solar simulator before installation, after 10 years of exposure and after 22 years of exposure. Degradation rates are determined after 10 and 22 years of exposure. The process flow chart used for module characterization after 22 years of exposure is given below:

(a) Visual inspection of the PV modules: PV modules are inspected visually as per IEC 61215-2021 to determine their physical conditions [5].
(b) Performance measurement of PV modules at STC: Initially the performance of the modules is measured at STC using A + A + A + solar simulator. Post STC performance, the effect of angle of incidence has been measured as per IEC 61853-2 [6]. After that, temperature coefficients of PV module are measured as per IEC 61853-1 [7]. These measurement data are necessary for creating a '.PAN' file in PVSyst using which energy generation from these PV modules are estimated.
(c) Once the electrical characterization of the PV modules is done, thermal imaging of these PV modules was performed using infrared (IR) thermal camera. Thermal imaging gives the insight on the heat signature of the PV modules which enable the understanding of the hotspot formation during operation, cell mismatch, shunt resistance and Potential Induced Degradation (PID) of the PV modules.
(d) EL imaging is a crucial testing for determining the health of the PV module by which the micro-cracks and the operational region of the PV cells can be determined.
(e) Insulation test of the PV modules has done as per IEC 61215-2021 to determine the leakage current and insulation resistance between the active circuit and the frame of the PV module.

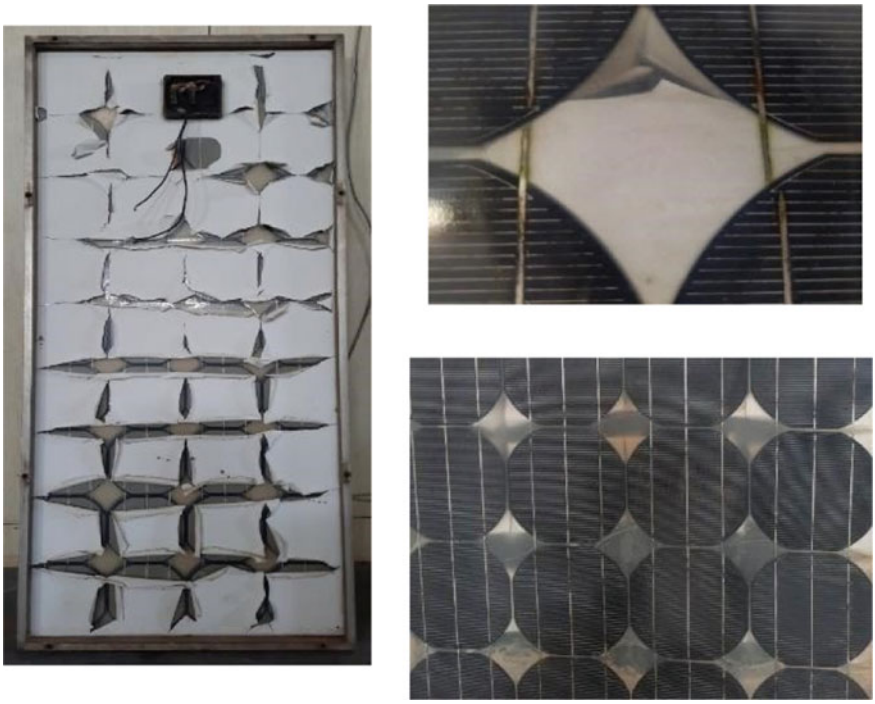

Fig. 1 Some of the observed visual defects during inspection

3 Results and Discussions

3.1 Visual Inspection

The visual inspection of 14 modules which are continuously exposed in outdoor condition for a long time are inspected under the illumination of 1000 lx. In this test it has been observed that many modules are severely affected in terms of back-sheet disruption, bubble formation due to moisture ingress, delamination and glass breakage. Figure 1 shows the visual defects of the PV module observed.

The results of the visual inspection are quantified in Table 1.

3.2 Performance Analysis at STC

To determine the degradation rate, electrical parameters such as Open circuit (Voc), Short circuit current (Isc), Voltage at maximum power point (Vmp), Current at maximum power point (Imp), Power at maximum power point (Pmax) and Fill factor (FF) of all the modules are performed at STC. These current results are compared

Table 1 Various defects observed during visual inspection of the PV modules operational for 22 years

S. No.	Visual defect	Percentage of modules effected (%)
1	Chalking	85
2	Corrosion in busbar, interconnection ribbon	85
3	Discoloration in the cells	71
4	Bubbles in the back sheet	14
5	Damage of back sheet	85
6	Damage of junction box	100
7	Corrosion of frame	0

with the STC results performed earlier on 2000 and 2010. With all these results the degradation rate is determined using the formula:

$$Degradation\,rate\,(\%) = \frac{Initial\,value - Final\,value}{Initial\,value \times Year\,of\,exposure} \times 100\%$$

A detailed annual degradation rate of all the electrical parameters of the PV module is shown in Fig. 2.

Detailed degradation rates (per year) of all the electrical parameters of the PV module are shown in Fig. 2, where last 12 years mean from 2010 to 2022, first 10 years replicate 2000–2010 and total 22 years is from 2000 to 2022. It can be

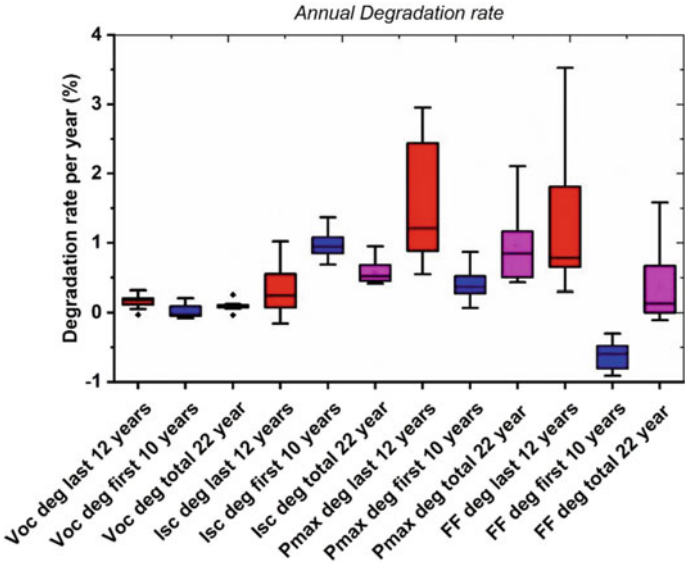

Fig. 2 Annual degradation rate of the electrical parameters

observed from Fig. 2 that the degradation in Voc after initial 10 years (2000–2010) and in last 12 years (2010–2022) consecutively is around 0.02% (per year) and 0.16% (per year). These results indicate that the junction quality and the shunt resistance of the of the PV modules has not degraded significantly. For Pmax, the initial 10 years' degradation is 0.4% (per year) and for last 12 years is around 1.2% (per year). The modules show power degradation of 0.85% per year The result of Voc and Pmax degradation signifies that the FF has degraded significantly in last 12 years as compared to the initial 10 years, which is evident from Fig. 2. Whereas in case of Isc, it has degraded to approximately 0.96% (per year) in first 10 years and then 0.24% (per year) in last 12 years. This points toward the fact that the Isc degradation has almost saturated in the first 10 years and very less degradation of Isc has happened in last 12 years. The possible reasons behind this can be the ARC degradation and reduction in transparency of the glasses happens in the initial 10 years only.

3.3 Insulation Test

To address the safety issues of the modules, insulation test is performed. The leakage current of a module increases with decrease in the insulation resistance, this comes under the safety concern of the PV modules. The insulation resistance tests of all the modules are performed using insulation resistance tester. For these modules insulation test is conducted under 2 conditions i.e., dry insulation test and wet leakage test. In dry insulation test the modules were tested by shorting the two terminals and applying 2200 V (1000 + 2 times the maximum system voltage of module) with respect to frame for two minutes. In wet insulation test (wet leakage test) the modules were tested by shorting the two terminals and applying 600 V (maximum system voltage of module) with respect to frame for two minutes. This procedure is performed as per the standard IEC 61215-2-2021. According to the standard, insulation resistance should be more than 400 Mega ohm (MΩ) for a module of area less than 0.1 m^2. It has been observed from the wet insulation testing that, out of 14 modules, 10 modules have insulation resistance value less than 400 MΩ. Therefore, it can be concluded that, only 4 modules have passed the Wet Leakage Test. In case of dry insulation test, 7 modules have insulation resistance value less than 400 MΩ out of 14 modules and therefore only 7 modules passed the dry insulation test. Only qualified module should be used for reusing. Before their deployment in the field, insulation test must be performed to ensure the safety.

3.4 IR Thermal Imaging

Due to poor contact between the cells and material degradation of a module, partial or complete solar cell may get heated locally and the temperature is not equally distributed throughout the entire module. As a consequence, hotspots may occur in

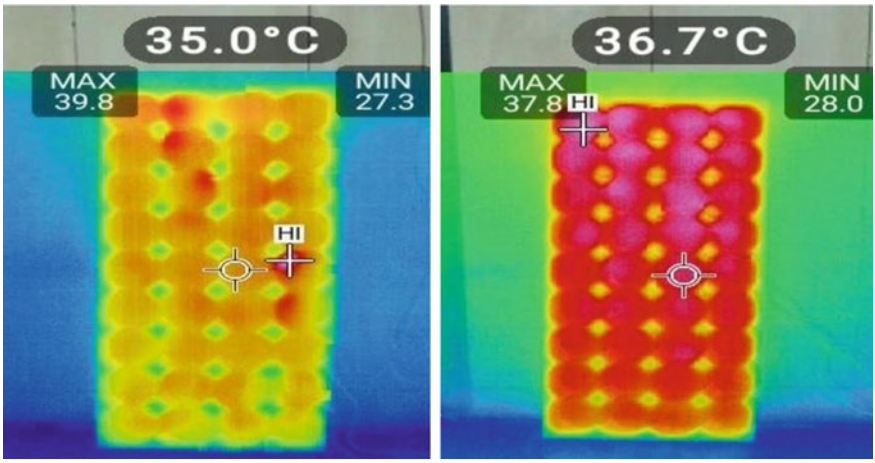

Fig. 3 IR images of the PV modules which were operational in field for more than 20 years

the PV modules. IR Thermal imaging has been performed using Fluke IR thermal imager and is presented in Fig. 3. For 14 modules IR images have been taken, and it has been observed that only in 4 modules hotspots are present. The reason for these hotspots is the corrosion of contacts which have increased the series resistance of the solar cells. This is also evident from the IV data of the particular modules when compared with their earlier IV curves.

3.5 Electroluminescence Imaging (EL Imaging)

Some cracks in the module is not visible with the naked eye, to have an insight of the electrical active area electroluminescence (EL) is performed where rated current and voltages are used to excite the solar cells and they emit light having wavelength near infrared region. To capture the higher wavelength light special IR camera are used and the picture obtained shows bright light from the electrically active area. Figure 4 shows the EL image of the particular module. If the brightness of the cells is uniform, there will be low series resistance. Almost all the modules have minor micro-cracks which can be clearly seen from the EL images shown in Fig. 4. Some solar cells of the modules also show degradation in terms of their shunt resistance. The cumulative degradation has resulted in the power losses over the time they were operational in the fields.

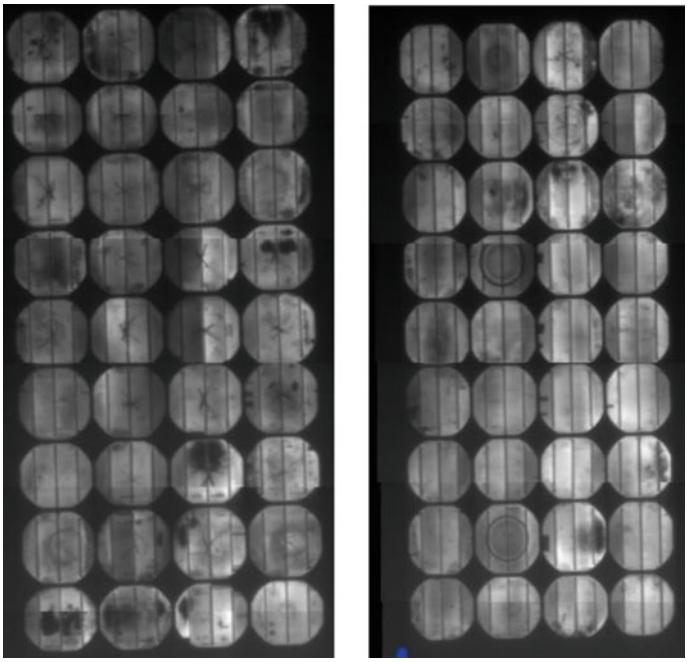

Fig. 4 EL images of the PV modules which were operational in field for more than 20 years

3.6 Estimation of Energy Generation of the PV Modules After 22 Years

The module with no visual defects or with reparable defects, no safety issues and low degradation rates could be reuse for the energy production after its lifetime as declared by the manufacturer. "PAN" file for PVSyst has been designed for the initial and current rating of the PV module and energy yield were estimated. The PAN file contains specifications of photovoltaic modules in text form. The designed plant capacity is of 1 kWp AC which consists of 15 PV modules of 78.4 Wp each according to their initial STC data in the year 2000. The energy estimation using the initial STC value of the module projected the generation of around 1730 kWh in the year 2022 as shown in Fig. 5a. During this energy estimation annual degradation of PV modules were considered as 0.4% (per year). After 22 years the same plant is designed with current STC data of the module i.e. 67.2 Wp and it was observed from Fig. 5b that the energy generation in the 1st year (2022) is around 1360 kWh. Therefore, it can be clearly observed that there is a significant deviation in the energy yield from the previous PVSyst energy estimation as compared to that of the current state of the PV modules. The reason behind the deviation is the rate of degradation which was predicted as 0.4% (per year) but in actual the yearly degradation happened to be around 0.95% (per year). With this new degradation rate PVSyst energy estimation

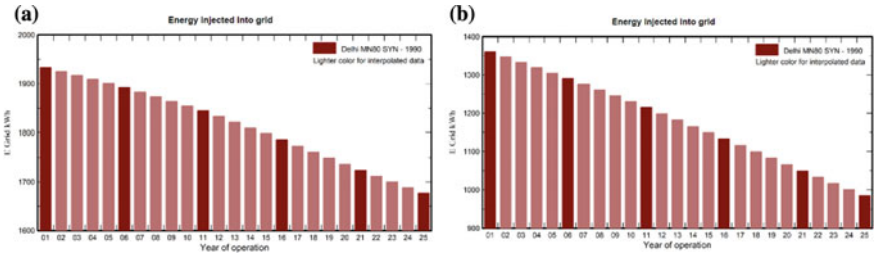

Fig. 5 **a** Energy estimation of the power. **b** Energy estimation of the power plant using the initial data of the PV modules plant using the current performance data of in 2000 the PV modules in 2022

was again performed and it is observed that the solar PV plant having 22 years old modules can generate 1000 kWh of energy after 25 more years. This is somewhere around 50% of the energy which the power plant was generating at its initial state.

This energy yield estimation after 20 years concludes that the PV modules which are installed in PV power plants for more than 20 years can still be used for power generation for various low power solar PV applications. For calculating the energy yield, one should use the current degradation rate and some crucial test should be performed to ensure the safety and performance of these refurbished PV modules. The visual inspection, EL imaging, IR imaging and the insulation test can predict the expected performance and safety of the modules. Reusing the PV module will maximize their utilization and reduce the electronics waste which will be generated from targeted use of solar PV modules.

4 Conclusion

In this work, the PV modules which were operational in outdoor field since 2000 are tested after 10 and 22 years of exposure. During visual inspection of theses PV modules, some defects like chalking of back sheet, metal corrosion, discoloration in the cells and damage of Junction box was observed. Although they seemed visually damaged, some of the module could be repaired and they were generating power with overall degradation of around 0.85% (per year) in terms of power. The performance analysis of all the PV modules were performed and it was observed that the maximum degradation is due to the fill factor losses. Therefore, it has been concluded that the shunt resistance has degraded significantly which is also evident from EL images. To reuse this PV modules, insulation and IR imaging has been performed which gives insight on the safety of the PV modules. Those PV modules which passes the criteria of 400 MΩ for both the dry and wet insulation test can be considered safe for further use after 20 years. Finally, with the current performance data and the degradation rate of the PV modules after 22 years the energy generation is estimated for another 25 years and it has been observed that it can still generate energy. Through this work, it is concluded that the PV modules which are in operation for more than 20 years

can be further used for power generation with few necessary testing, which ensures the precise power estimation and safety of the PV module. This exercise can be used make cheaper PV modules available for low power solar applications and can help in reducing the e-waste which is being produced due to discarding of PV modules post lifetime. However, to estimate the reliability of the module post lifetime, it is required to do reliability testing as per IEC 61215: 2021, which is a future scope of this study.

References

1. Chattopadhyay S et al (2016) All-India survey of photovoltaic module reliability: 2016. IIT Bombay, National Institute of Solar Energy, Gurugram. https://nise.res.in/public-information/technical-reports-resources/
2. Bora B, Sastry OS, Kumar R, Dubey R, Chattopadhyay S, Vasi J, Mondal S, Prasad B (2021) Failure mode analysis of PV modules in different climatic conditions. IEEE J Photovoltaics 11(2):453–460. https://doi.org/10.1109/JPHOTOV.2020.3043847
3. Rajput P, Tiwari G, Sastry O, Bora B, Sharma V (2016) Degradation of mono-crystalline photovoltaic modules after 22 years of outdoor exposure in the composite climate of India. Sol Energy 135:786–795
4. Sastry OS, Saurabh S, Shil SK, Pant PC, Kumar R, Kumar A, Bandopadhyay B (2010) Performance analysis of field exposed single crystalline silicon modules. Sol Energy Mater Sol Cells 94(9):1463–1468. https://doi.org/10.1016/j.solmat.2010.03.035
5. IEC 61215: 2021 (2021) Terrestrial photovoltaic (PV) modules—design qualification and type approval—part 1: test requirements. https://webstore.iec.ch/publication/61345
6. IEC 61853-2:2016 (2016) Photovoltaic (PV) module performance testing and energy rating—part 2: spectral responsivity, incidence angle and module operating temperature measurements. https://webstore.iec.ch/publication/25811
7. IEC 61853-1:2011 (2011) Photovoltaic (PV) module performance testing and energy rating—part 1: irradiance and temperature performance measurements and power rating. https://webstore.iec.ch/publication/6035

Financial Viability of Rooftop PV Systems in Residential Housing Societies in India

Pratik Joshi, Anand B. Rao, and Rangan Banerjee

1 Introduction

In 2015, India set a target of installing 100 GW of solar PV capacity under the National Solar Mission by 2022 to promote solar energy and reduce its dependency on fossil fuels [1]. The target was split between two categories; 60 GW of capacity was planned from ground-mounted large-scale PV installations, whereas the rest of the 40 GW was planned from rooftop PV systems.

Since the launch of the national solar mission, the states and the central government of India have aligned their policies by implementing various policy mechanisms such as reverse auction, capital subsidy, generation-based incentives, electricity bundling, tax incentives (such as a rebate on property tax, accelerated depreciation), and research grants. Renewable portfolio obligations, renewable energy certificates, and access-based regulatory policies such as net metering and net billing are adopted. Renewable power plants have been awarded a 'must-run' status to maximize energy yield and safeguard capital investment. India's solar PV industry has significantly grown in the last seven years. The supply chain for PV modules, inverters, and balance of components is emerging, and the number of engineering

P. Joshi (✉) · A. B. Rao · R. Banerjee
Ashank Desai Centre for Policy Studies (ADCPS), Indian Institute of Technology Bombay, Mumbai 400076, India
e-mail: pratikjoshi@iitb.ac.in

A. B. Rao · R. Banerjee
Centre for Technology Alternatives for Rural Areas (CTARA), Indian Institute of Technology Bombay, Mumbai 400076, India

R. Banerjee
Department of Energy Science and Engineering (DESE), Indian Institute of Technology Bombay, Mumbai 400076, India

S. Doolla et al. (eds.), *Advances in Renewable Energy and Its Grid Integration*,
Lecture Notes in Electrical Engineering 1041,
https://doi.org/10.1007/978-981-99-2283-3_18

procurement and commissioning companies engaged in the PV plant installation business have increased multifold.

The country has installed 53.9 GW of PV capacity by the end of March 2022 [2]. It includes 45.79 GW of ground-mounted large-scale installations and 6.65 GW of rooftop systems. Around 1.56 GW of capacity is reported from Off-grid systems. Only 16.6% capacity addition has been achieved in the rooftop category against 76% in the ground-mounted category. The rooftop category is lagging behind its target compared to the ground-mounted systems, which makes it imperative to study the reasons behind the modest deployment of rooftop PV systems and measures to accelerate the same. Understanding barriers and driving forces related to rooftop systems under the present policy scenario can help re-align future policies to accelerate the deployment.

This paper discusses the financial viability of rooftop PV systems under prevailing electricity tariffs and capital subsidies for various capital cost conditions. This paper aims to understand the conditions under which the rooftop PV project becomes financially viable for investment.

1.1 Background

The electricity sector in India is regulated as per the Electricity Act 2003. State electricity regulatory commissions annually revise electricity tariffs based on aggregate revenue requirement proposals submitted by electricity distribution companies (Discoms). The net electricity bill amount is inflated as discoms levy surcharges and state government taxes on consumed electricity in addition to fixed and energy charges mentioned in the electricity tariff schedule. From an economic point of view, consumers are looking for a cost-effective alternative to reduce the burden of high electricity bills. Rooftop PV systems are considered a natural solution due to their low maintenance, stationary structure, and environment-friendliness.

Around 75% of rooftop PV installations come from the commercial and industrial (C&I) segments [3]. Domestic consumers' reluctance to install PV systems can be attributed to lower electricity tariffs (than C&I consumers), high capital costs for small plant capacity, and limited access to capital.

The total technical rooftop PV potential of thirteen cities in India is estimated at around 17.8 GWp, indicating adequate capability to achieve set rooftop PV targets if implemented nationwide [4]. In order to achieve the target of 40 GW, government intervention is necessary to make PV systems profitable for a broad range of consumers. This paper focuses on assessing the economic feasibility of rooftop PV plants installed in residential housing societies (for common services such as lift, water pumping, and street lighting) in four Indian cities, namely Mumbai, Chennai, Kolkata, and Delhi.

Rodrigues et al. have discussed the economic feasibility analysis of 1 and 5 kW systems in 13 countries [5]. Ghosh et al. and Fuke et al. have presented a case for 5 kWp for Bangalore using actual site data and Delhi using a simulation study,

respectively [6, 7]. Similar studies by Mukherji et al., Shukla et al., and Saxena et al. have been reported in the literature [8–10].

The analysis chooses the residential housing society over the individual house as cities will have more multi-storey buildings than individual houses. Moreover, system sizes with a wide capacity range can be considered in the case of housing society as the range of required PV capacity will be broad. The required PV capacity for a particular society will broadly depend on the number of families in it and the availability of shade-free rooftop areas. In the next section, a detailed methodology is explained with the help of a techno-economic framework, followed by data collection and assumptions.

2 Methodology

This paper uses a cash-flow model approach to study the effect of location and size on the Simple Payback Period (SPP) and Internal Rate of Return (IRR) under different compensation scenarios and various capital cost conditions. SPP and IRR are used to assess the economic feasibility of a project. SPP indicates the time (in years) required to recover the initial investment cost. A lower payback period shows that investment is recovered earlier, ultimately reducing investment risk. This metric is easy to calculate and understand. However, it does not consider the time value of money and ignores cash flows beyond the payback period. In the present study, each year's cumulative cash inflows are calculated to arrive at the payback period, as annual cash inflows are uneven. The following formula is used to calculate SPP;

$$Simple\ Payback\ Period = E + \frac{B}{C} \tag{1}$$

In the above equation, E represents the year immediately preceding the year when cumulative cash flows become more than or equal to zero, B represents the residual recovery amount, whereas C stands for cash inflow during the final recovery year.

The IRR is the discount rate value at which the investment's net present value becomes zero. IRR is compared with investors expected minimum rate of return. It is determined by setting the net present value equal to zero and iteratively solving for the discount rate value. The following formula is used to calculate IRR;

$$IRR_{k+1} = \frac{Annual\ return}{\text{Initial investment}}\left(1 - \frac{1}{(1 + IRR_k)^n}\right) \tag{2}$$

In the above equation, k indicates iteration, and n indicates the project's economic life. The step-by-step calculation process is explained with the help of a techno-economic framework in the following section.

2.1 Framework

A techno-economic framework is shown in Fig. 1. The framework uses the System Advisor Model (SAM) developed by the National Renewable Energy Laboratory to simulate the monthly electricity generation of a solar PV plant in Mumbai, Chennai, Kolkata, and Delhi for three system sizes (10, 50, and 100 kWp).

Four compensation scenarios (25, 50, 75, and 100% of monthly electricity consumption) are created. Compensation scenarios use compensation ratio (CR) to factor in a temporal mismatch in the generation and consumption of electricity over a billing period. For a perfectly designed grid-tied system, the compensation ratio is the ratio of self-consumed units compensated at the retail electricity tariff rate to the total number of units generated by the PV system in a specific billing period. The compensation ratio can also accommodate regulatory conditions requiring the loss of specific grid-injected units against distribution grid balancing and management expenses. It allows the investor to compare PV system performance under such regulatory restrictions.

During simulation in SAM, Trina solar 335 Wp multi-crystalline PV module is selected. The inverter selected for this study is Fronius Symo Advanced 10.0 kW for 10 kWp system, ABB Trio 50 kW for 50 kWp system, and Solis 100 kW for 100 kWp system. The number of modules in a string and the total number of strings are chosen such that DC/AC ratio for the PV system remains 1 for the 10 kWp system, 1.07 for 50 kWp, and 1.08 for 100 kWp. The average capacity utilization factor (CUF) of all three system sizes at four locations is shown in Table 1. Under the given assumptions, the capacity utilization factor across four locations varies in the range of 1.83%.

Monthly bill savings are obtained by applying the electricity bill calculation methodology of respective Discom to each compensation scenario. The monthly electricity bill calculation methodology is determined from electricity bills and tariff schedules. The bill calculation consists of calculating energy charges, wheeling

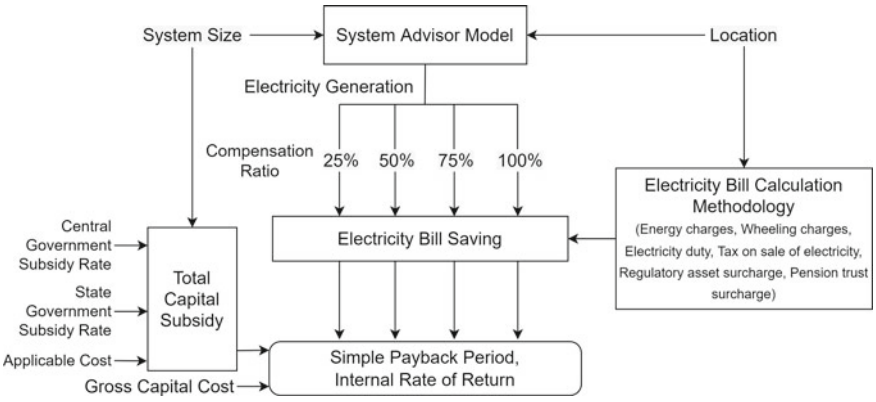

Fig. 1 The techno-economic framework used in the present study

Table 1 Related information on all locations (applicable cost in INR)

City	Mumbai	Chennai	Kolkata	Delhi
Electricity distribution company	Tata Power	Tamil Nadu Generation and Distribution Corporation Ltd	West Bengal State Electricity Distribution Company Ltd	BSES Yamuna Power Ltd
Tariff category	LT I (B)	LT I-A	A(DM-U) for < 50 kW and D-ID for ≥ 50 kW	Domestic
Applicable cost for 10 kWp	40,000	39,770	44,640	37,000
Applicable cost for 50 kWp	37,000	36,170	41,640	37,790
Applicable cost for 100 kWp	37,000	36,170	41,640	37,790
Wheeling charges (INR/kWh)	1.88			
Regulatory asset surcharge (% of energy charges)				8
Pension trust surcharge (% of energy charges)				7
Electricity duty (% of energy charges)	16			
Electricity tax	0.2604 INR/kWh			5% of energy charges and surcharges
Average CUF (%)	18.47	18.27	16.64	17.04

charges, electricity duty, tax on the sale of electricity, regulatory asset surcharge, and pension trust surcharge wherever applicable. The only variable component of bill calculation is considered to determine monetary savings as fixed charges are required to be paid even after installing the PV system.

The central government provides a 20% capital subsidy for residential housing societies up to a capacity of 500 kWp [11]. The subsidy is calculated on applicable cost, the lowest rate between rates discovered for rooftop systems by different states/union territories in that year, or MNRE benchmark cost [12]. The government of Tamil Nadu provides INR 20,000/- per kW under Chief Minister's Solar Rooftop Capital Incentive Scheme [13]. The total capital subsidy (central + state) is calculated to determine the net capital cost. To see the cost effect, the gross capital cost is changed from INR 40,000/kWp to INR 90,000/kWp in the INR 10,000/- step. The system is assumed to be maintenance-free. A simple payback period and internal rate of return are calculated to arrive at the results. The framework is used for three

system sizes in four cities under six capital cost scenarios. The results are discussed in the results section.

2.2 Data Collection

The name of Discom, tariff category, applicable cost, and various charges used in monthly electricity bill calculation are shown in Table 1. The electric distribution company (Discom) is assigned to each city based on location. The electricity connection category for housing societies and associated tariff schedule is accessed from the websites of Tata Power for Mumbai [14], Tamil Nadu Generation and Distribution Corporation Limited for Chennai [15], West Bengal State Electricity Distribution Company Limited for Kolkata [16], and BSES Yamuna Power Limited for Delhi [17].

2.3 Assumptions

During simulation in SAM, the system with a fixed tilt mechanism with a tilt angle equal to latitude is selected. The azimuth angle is kept at 180°. An average annual soiling loss of 5% is assumed, which causes a reduction in total irradiance. An annual DC degradation rate of 1.84%/year accommodates module degradation under Indian climatic conditions over its lifetime [18]. The project's lifetime is assumed to be 25 years for this study. It is assumed that the electricity tariff and electricity consumption remained unchanged. Any rise in electricity tariff will make the economic parameters (SPP and IRR) favor investors, whereas the probability of a significant fall in the long term is low. The electricity consumption of a housing society is not expected to change significantly as most of the loads are constant in nature.

3 Results

The SPP and IRR for 10, 50, and 100 kWp systems in Mumbai, Chennai, Kolkata, and Delhi under four compensation scenarios with the capital cost at INR 40,000/- and INR 50,000/- are shown in Fig. 2. It can be observed that Mumbai has a higher rate of return than the rest of the cities under all compensation scenarios.

Systems become financially viable at a capital cost of INR 40,000/kWp and INR 50,000/kWp in all cities for a compensation ratio of 0.75 and one, with a payback period ranging from 1.7 to 6.2 years (average SPP of 3.7 years) and with IRR ranging from 14.14 to 57.6% (average IRR of 28.9%). It shows that systems become economically feasible at low capital cost provided that an adequate compensation mechanism is in place.

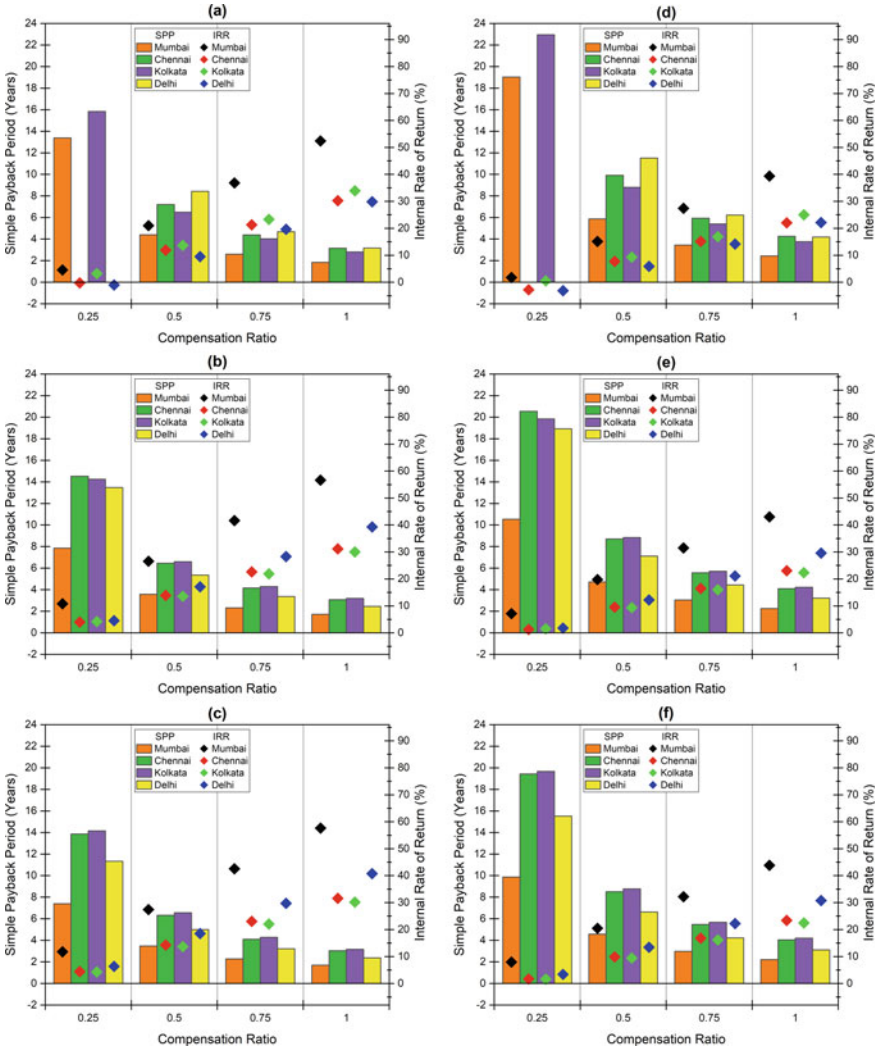

Fig. 2 SPP and IRR at INR 40/Wp capital cost for system size of **a** 10 kWp, **b** 50 kWp, **c** 100 kWp and at INR 50/Wp capital cost for system size of **d** 10 kWp, **e** 50 kWp, **f** 100 kWp

SPP and IRR for 10, 50, and 100 kWp systems in Mumbai, Chennai, Kolkata, and Delhi under four compensation scenarios with the capital cost at INR 60,000/kWp and INR 70,000/kWp is shown in Fig. 3. IRR for all system sizes for compensation ratio of 0.75 and one range from 8.08 to 35.17% (average IRR of 17.56%). Mumbai remains the most favorable location, with the highest IRR of 35.17% for a 100 kWp system size for a compensation ratio of one. A compensation ratio of 0.25 is unviable for all system sizes across all locations.

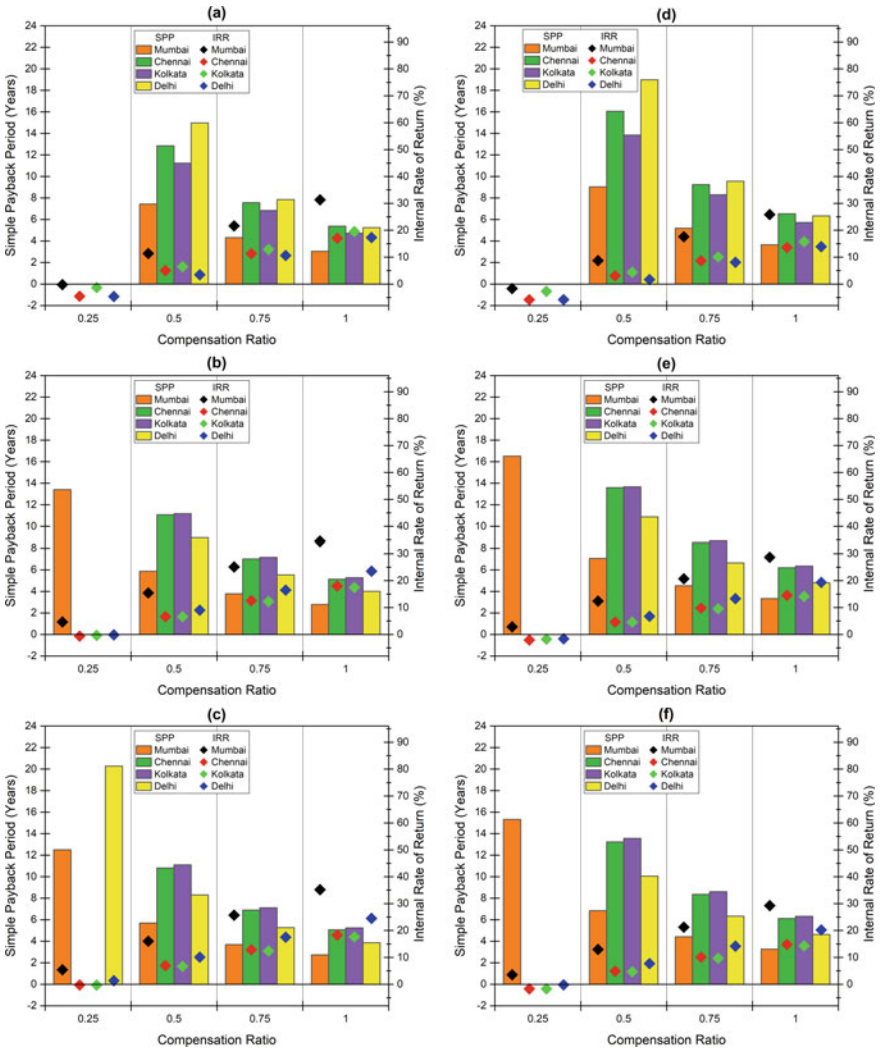

Fig. 3 SPP and IRR at INR 60/Wp capital cost for system size of **a** 10 kWp, **b** 50 kWp, **c** 100 kWp, and at INR 70/Wp capital cost for system size of **d** 10 kWp, **e** 50 kWp, **f** 100 kWp

Under prevailing conditions, systems with a 10 kWp size with capital cost equal to or higher than INR 60,000/kWp are marginally viable and require case-specific details to comment on economic feasibility. Figure 4 shows SPP and IRR for 10, 50, and 100 kWp systems in Mumbai, Chennai, Kolkata, and Delhi under four compensation scenarios with the capital cost at INR 80,000/kWp and INR 90,000/kWp. At a capital cost of INR 90,000/kWp, for a compensation ratio of one, the average SPP in four cities remains at 7.5 years for 10 kWp, seven years for 50 kWp, and 6.8 years for 100 kWp. The average IRR values are 12.05% for 10 kWp, 13.69% for 50 kWp,

and 14.05% for 100 kWp. Systems with 0.25 and 0.5 compensation ratios are not financially viable. The system finances deteriorate as system cost increases.

In the case of Mumbai and Delhi, IRR increases as system size increases from 10 to 50 kWp above, which shows modest changes. IRR's rate of change in the case of Kolkata and Delhi is low. In Kolkata, for a compensation ratio of one, IRR decreases as system size increases. In Mumbai, the average IRR of a 10 kWp system reduces from 52 to 21% as capital cost increases from INR 40,000/kWp to INR 80,000/kWp.

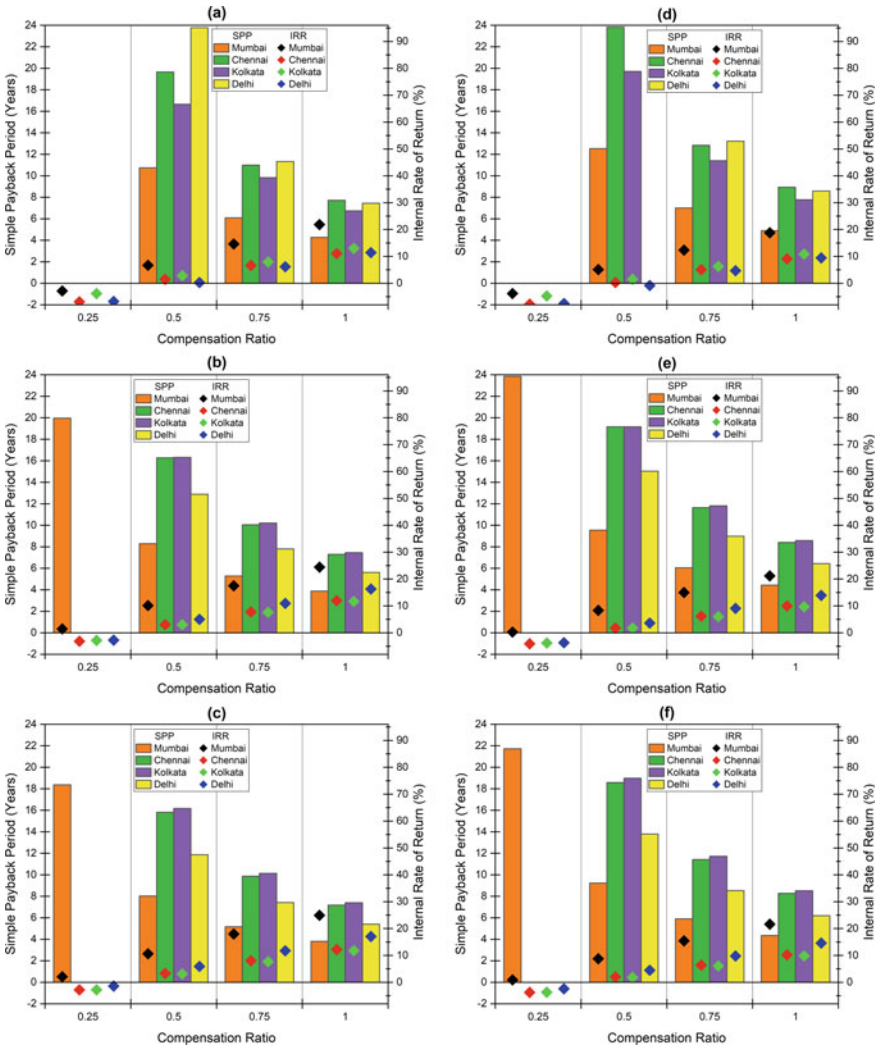

Fig. 4 SPP and IRR at INR 80/Wp capital cost for system size of **a** 10 kWp, **b** 50 kWp, **c** 100 kWp, and at INR 90/Wp capital cost for system size of **d** 10 kWp, **e** 50 kWp, **f** 100 kWp

The results presented in this study are validated by comparing SPP and IRR with similar studies. Rodrigues et al. have reported an IRR of around 20% for a 5 kW system located in Jaipur, India, for an initial cost of INR 46,834/kWp [5]. Ghosh et al. assessed a 5 kWp system in Bangalore and found SPP of 8 years and IRR of 10% for a capital cost of INR 67,400/kWp, degradation factor of 0.5% per year, and a plant load factor of 19% [6]. In a 2020 study, Fuke et al. reported an SPP of 9.73 years for a 5 kW grid-connected system in Delhi at the cost of INR 67,240/kWp [7].

For the capital cost of INR 79,690/kWp, 20% capital subsidy, and CUF of 14.64%, Mukherji et al. reported SPP of 5 years and IRR of 20% for a 50 kWp system in Jaipur [8]. A simulation study on a 110 kWp system on a hostel building in Bhopal resulted in an SPP of 8.2 years, considering the capital cost of INR 74,560/kWp [9]. In a recent study performed in 2021, an SPP of 5.78 years was achieved for a 100 kWp system in Delhi at a capital cost of INR 65,371/kWp and CUF of 20.66% [10]. While the uniqueness of the study design and variation in input parameters, including but not limited to location, time, initial cost, and tariff rate, restrict the direct correlation of SPP and IRR, the comparison shows that the findings in the present study are in line with previous studies.

4 Conclusion

The financial viability of rooftop PV systems largely depends on the effective electricity billing rate and capital cost. Under prevailing tariff and subsidy conditions, the economic parameters of rooftop systems in Mumbai are more favorable than in the rest of the locations due to the high electricity bill rate and higher capacity utilization factor.

The system's internal rate of return is sensitive to the capital cost, and it halves as the capital cost doubles. It signifies the importance of capital cost in decision-making for an investor. PV modules and inverters contribute more than half of the capital cost. Hence, government intervention is needed to protect the market from price shocks as PV manufacturing, and the associated supply-chain is concentrated in a few countries.

Systems with a compensation ratio equal to or lower than 0.5 are not viable irrespective of system size and location—a higher self-consumption results in notable improvement in the payback period and rate of return. Hence, efforts should be made to promote the self-consumption of electricity at the consumer end. The existing net-metering/billing mechanism can be replaced with a mechanism that promotes self-consumption and discourages consumers from injecting electricity into the grid within a specific billing period. It includes not carrying forwarding excess injected units into the successive billing cycle and depositing part of injected units to recover distribution grid balancing and management expenses.

References

1. Press Information Bureau (2015) Revision of cumulative targets under national solar mission from 20,000 MW by 2021–22 to 1,00,000 MW. Press Information Bureau, Government of India
2. Ministry of New & Renewable Energy (2022) Programme/scheme wise cumulative physical progress as on Mar 2022. MNRE, Government of India
3. Bridge To India (2021) India solar rooftop map, Dec 2021
4. Singh R (2020) Approximate rooftop solar PV potential of Indian cities for high-level renewable power scenario planning. Sustain Energy Technol Assess 42:100850
5. Rodrigues S, Torabikalaki R, Faria F, Cafôfo N, Chen X, Ivaki AR, Mata-Lima H, Morgado-Dias F (2016) Economic feasibility analysis of small scale PV systems in different countries. Sol Energy 131:81–95
6. Ghosh S, Nair A, Krishnan SS (2015) Techno-economic review of rooftop photovoltaic systems: case studies of industrial, residential and off-grid rooftops in Bangalore, Karnataka. Renew Sustain Energy Rev 42:1132–1142
7. Fuke P, Yadav AK, Anil I (2020) Energy performance and economic analysis of different PV technologies for grid connected rooftop PV system. In: PIICON 2020—9th IEEE power India international conference
8. Mukherji R, Mathur V, Bhati A, Mukherji M (2020) Assessment of 50 kWp rooftop solar photovoltaic plant at the ICFAI University, Jaipur: a case study. Environ Prog Sustain Energy 39:e13353
9. Shukla AK, Sudhakar K, Baredar P (2016) Design, simulation and economic analysis of standalone roof top solar PV system in India. Sol Energy 136:437–449
10. Saxena AK, Saxena S, Sudhakar K (2021) Energy, economic and environmental performance assessment of a grid-tied rooftop system in different cities of India based on 3E analysis. Clean Energy 5:288–301
11. Ministry of New & Renewable Energy (2019) Operational guidelines for implementation of phase-II of grid connected rooftop solar programme for achieving cumulative capacity of 40000 MW from rooftop solar projects by year 2022. Government of India, India
12. Ministry of New & Renewable Energy (2021) Amendments in implementation guidelines of rooftop solar programme phase II. Government of India, India
13. Tamil Nadu Energy Development Agency (2022) Chief minister's solar rooftop capital incentive scheme
14. Maharashtra Electricity Regulatory Commission (2019) Schedule of electricity tariff for FY 2020–21 to FY 2024–25 (India)
15. Tamil Nadu Electricity Regulatory Commission (2021) Provisional tariff subsidy for FY 2021–22 by the Government of Tamil Nadu (India)
16. West Bengal Electricity Regulatory Commission (2022) Tariff order of WBSEDCL for the years 2020–21 and 2021–22 (India)
17. Delhi Electricity Regulatory Commission. Electricity tariff schedule for FY 2021–22-BRPL, BYPL, TPDDL and NDMC (India)
18. Rao Golive Y, Zacharaiah S, Bhaduri S, Dubey R (2019) All-India survey of photovoltaic module reliability: 2018

Electricity Access-Development Linkages of Centralised and Decentralised Supply Schemes

Omkar Buwa and Anand B. Rao

1 Introduction

"Have you worked out the problem of electricity for every home? What is the cost?"[1] on 30th April 1945, Mahatma Gandhiji wrote a letter to Cambridge return economist Shri. Amiya Nath Bose expressing his concern about the electricity access to every home in India. These efforts were worth taking as in later years, the importance of electricity for development was acknowledged by the global community.

The electricity access to every end user may be realized through different supply schemes. They are categorized as centralised or decentralised. Centralised supply scheme is a grid network where bulk power stations supply electricity through transmission and distribution. Decentralised supply schemes are mini grids at community level or solar home systems (SHS) at household level.

These different supply schemes differ in terms of the attributes. The various models may also exist considering whether these supply schemes exist separately, compete, or integrate with each other. The choice of electricity supply scheme and the choice of supply model may impact the development.

The aim of this paper is "to understand the electricity access-development linkages of centralised and decentralised supply schemes". In particular, households' electricity access is considered. Following are the major contributions:

(a) Discussion on the attributes of the supply schemes and linkages to the development

[1] Quoted by Shri Chandra Kumar Bose (Son of Shri Amiyo Nath Bose); Available at http://www.dailyo.in/politics/mahatma-gandhi-indian-freedom-struggle-sarat-chandra-bose-partition-congress/story/1/6599.html; last accessed on March 25, 2022.

O. Buwa (✉) · A. B. Rao
Centre for Technology Alternatives for Rural Areas, Indian Institute of Technology Bombay, Mumbai, India
e-mail: onbphd@gmail.com

S. Doolla et al. (eds.), *Advances in Renewable Energy and Its Grid Integration*,
Lecture Notes in Electrical Engineering 1041,
https://doi.org/10.1007/978-981-99-2283-3_19

(b) Discussion on the relationship between supply schemes and relevant models.

Some future research work areas are also briefly described.

2 Electricity Access and Development Linkages

2.1 Electricity Access

There is no internationally accepted and adopted definition of electricity access. But some common important meanings are minimum level of household electricity, access to the services driving economic development and the public services like schools, hospitals etc. International Energy Agency (IEA) defines the energy access as "a household having reliable and affordable access to both clean cooking facilities and to electricity, which is enough to supply a basic bundle of energy services initially, and then an increasing level of electricity over time to reach the regional average" [8]. The definition talks about the household level electricity access.

On 25th September 2017, SAUBHAGYA-Pradhan Mantri Sahaj Bijli Har Ghar Yojana was launched in India. This scheme proposes either grid extension or providing SHS to unelectrified households [15]. There is no consideration of mini grids as source of electricity supply as per this scheme. On 28th April 2018, Government of India declared that every single village has access to electricity [14]. But the electricity access to every end user is still dream in India. As per latest available data of the World Bank in 2020, 1% population (around 1.4 crores) of India was still without electricity access [16].

2.2 Development

Impact of electricity access on economic growth is indicated by relationship between per capita electricity consumption and economic growth indicator—GDP in per capita. It is observed that GDP per capita increases with electricity access. Human development index considers three dimensions—a long and healthy life, knowledge, and decent standard of living. Electricity plays very important role in all the three dimensions for positive growth. Economic growth is considered with social and environmental impact analysis to define "sustainable development". Sustainable development goals (SDGs) were set by UN in 2015 with the 2030 agenda for sustainable development. Out of 17 SDGs, SDG 7 is "Ensure access to affordable, reliable, sustainable and modern energy for all".

2.3 Electricity Access and Development: Case Studies

The links between energy supply and income generation were empirically assessed. The region chosen for the same was Indian Himalayas. The impact of use of energy appliances on income generating activities was studied in this research [10].

The impacts of electrification on educational outcomes, gender and power relations, income generation, feelings of inclusion and exclusion and health in the village of Tsilitwa in the rural Eastern Cape, South Africa were studied. Complex nature of access development was observed in this work and ethnographic method is recommended to study the access development linkages. Authors concluded that the impact of electricity access will be different for different individuals and may be negative sometimes e.g. rising sense of income disparity [12].

When causal relationship between electricity consumption and HDI was analysed, it was observed that there is no major impact of electricity access on HDI in short run while long run shows positive co integration. Similar study was carried out to understand the causal relationship between electricity consumption and economic growth (GDP). The sensitivity of electricity-economic growth was observed to be very high for regional differences, countries' income levels, urbanisation rates and supply risks [9].

The effect of electricity on income, education, health, and labor productivity in Nepal was studied. Econometric approach was followed for the study. It was observed that a household electricity access has a very large and significant effect on income, educational attainment, and agricultural productivity while effect of electricity on health is not very significant [5].

In addition to household level, the impact of electricity consumption on environment in Cambodia was analyzed. Findings of this research are useful for SDG7 goal achievement and design the environment friendly policy [7]. Some more research is reported in the literature where the similar studies were conducted in India, Ghana, Côte d'Ivoire, and Africa [1, 2, 6, 13].

In Table 1, it is observed that different attributes, the types of electricity supply scheme, their relationship, and the impact of the different supply scheme models on the development are not explored in electricity access-development linkages studies.

3 Electricity Supply Schemes

3.1 Attributes of Electricity Supply Schemes

Availability of electricity supply in terms of electric wires and other required infrastructure is not sufficient to achieve the development. Electricity should flow as and when required by the different services. IEA definition of energy access consists of three attributes—reliability, affordability, and capacity to fulfill the electricity demand. Typical household electricity services are lighting, entertainment and

Table 1 Electricity access impact with various end uses [4]

End use	Impact of electricity access
Use of variety of electrical appliances	Improved standard of living and comfort levels
Activities like reading, watching TV, socialising	Increased length of the active day
Household activities for women	Time saving from laborious work, opportunity to take part in income generating activities, improved reading
Studying	Increased study time, improvement in the school enrollment and grade completion
Refrigeration	Positive impact on health, improved food conservation, enhanced nutrition
Electric lighting	Reduced likelihood of respiratory illness, reduced fire incidences due to candles and other fuel lamps

communication, space cooling and heating, refrigeration, mechanical loads, product heating and cooking. These services are impacted by the attributes of electricity supply.

Electricity services affect the socio economic development as they fulfill the requirements of household activities. Energy sector management assistant program (ESMAP) of the World Bank defines multitier matrix to measure access to household electricity supply. The attributes referred for the same are—Capacity, Availability, Reliability, Quality, Affordability, Legality, Health and Safety [4].

The attributes of electricity supply is the important link between electricity access and development. In Table 2, it is also observed that the expectation of the people have increased with the access of electricity. They seek improved electricity services and thus the assessment of the quality of services is necessary [3].

3.2 Types of Electricity Supply Schemes

Centralised electricity supply is the conventional electricity supply scheme. This is also called as a grid extension. The electricity is generated using fossil fuels (coal based plants), nuclear energy, and water (hydro power plants) in centralised power plants. The same is transferred through transmission and distribution network which is monitored by national and state level utilities. This is called as vertical structure of electricity supply.

Monopoly of centralised supply scheme ended due to various reasons like increased competition in the electricity industry, entry of private players, and technology development in renewable electricity generation. There are various environmental, economic, technical, political and social reasons for the development of small scale generation near the loads [11]. This small scale generation is called as decentralised electricity supply scheme. Decentralised electricity supply can be categorized

Table 2 ESMAP household electricity attributes [4]

Attribute	Meaning	Measure
Capacity	The ability of the system to provide a certain amount of electricity in order to operate different appliances	Watts or watt hours
Availability	The amount of time during which electricity is available	No. of hours per day, no. of evening hours
Reliability	Defined in terms of frequency and duration of scheduled outages	No. of disruptions, reliability indices
Quality	Electrical supply quality in terms of voltage	Power quality indices
Affordability	Whether households are able to pay for the electricity they use	Comparison with defined standard consumption package
Legality	Electricity connection following norms of the supplier	Household survey, bill payment
Health and safety	Wiring installation as per national standard set by regulation	The evaluation of electrocution risk

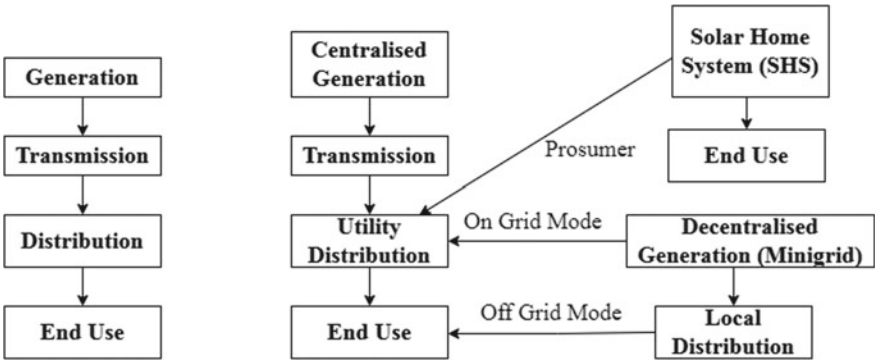

Fig. 1 Centralised and decentralised electricity supply schemes

as mini grids and solar home systems. Figure 1 shows centralised electricity supply (vertical structure at left) and decentralised electricity supply (horizontal structure at right).

4 Supply Schemes Relationship Models

Three possible models of relationship between centralised and decentralised schemes are—separated model, uncoordinated integration, and integrated development. In separated model, decentralised electricity supply is planned separately and those areas are focused where the centralised supply has not reached or unable to reach

due to various constraints. In uncoordinated integration, there is competition between centralised and decentralised electricity supply. This model may create some overlapping issues due to the lack of coordination between service providers. The strengths of both the models can be brought together in the integrated development approach. This model requires detailed policy and financial considerations [17].

5 ESMAP Electricity Supply Attributes and Models

The models and relevant ESMAP attributes are described in Table 3. In the analysis of decentralised supply systems, mini grids and SHS resemble in the attributes like availability, reliability, quality. Role as a prosumers (producer plus consumer) is possible for the SHS user. Prosumers can take benefit by selling electricity to the network as shown in Fig. 1.

It is observed that some of the attributes at household level like legality may not impact the development and the end user can choose any of the available choices. This is also applicable to health and safety attribute as national and international standards are mandatory in the processes independent of type of supply scheme and model. The attributes like capacity, availability, reliability, quality, and affordability are major drivers for the development.

6 Conclusion

To understand the linkages of electricity access and the development, there is need to look beyond the electricity access as physical connection. In state of the art literature, the electricity access—development linkages are studied without any special focus on the attributes, types of electricity supply, and their different realisation models. The attributes for the electricity supply schemes give different results for different models. The attributes of electricity supply and the supply scheme models are important linkage to the development.

7 Future Scope

The attributes may differ for other end users like agriculture, small scale industry. There is scope to understand the access-development linkages amongst the end user categories and measure the overall development. Future research can also study the linkages amongst the attributes. The changes in one attribute e.g. affordability may directly or indirectly impact the other attributes e.g. availability. This study can be extended to understand the dynamics of electricity access and development with computer simulations.

More options of electricity supply like energy storage, vehicle to home and vehicle to grid technology, and electricity generation by using biomass may be considered in the analysis. The end user may use electricity from multiple sources simultaneously in case of uncoordinated and integrated model. The linkages of this utilisation pattern to the development may be studied. There is scope to study the transition from one scheme or model to another and study the relevant impact on the development.

Table 3 Attributes and models linkage for different supply schemes

Attribute	Supply scheme	Model		
		Separated (centralised and decentralised supply separate)	Uncoordinated integration (centralised and decentralised supply in competition)	Integrated development (centralised and decentralised supply in coordination)
Capacity	Centralised	High	To be calculated considering demand closest to the generation	Appropriateness is decided by the detailed study, long term comprehensive policy
	Decentralised	Low (areas not covered by centralised grid are focused)	To be calculated considering remote area demand	
Availability	Centralised	Available for more time, Proper network planning can increase availability	Available for more time, Proper network planning can increase availability	Better compared to other two models due to detailed analysis for integration
	Decentralised	Seasonal fluctuations, required energy storage to ensure availability after sunset	More sophisticated model than 'separated' as decentralised supply is in competition with the grid	
Reliability	Centralised	High	High	Better compared to other two models due to detailed analysis for integration
	Decentralised	Low due to seasonal fluctuations	Impacted by seasonal fluctuations, energy storage must ensure the reliability, reliability expectation more than 'separated' model	

(continued)

Table 3 (continued)

Attribute	Supply scheme	Model		
		Separated (centralised and decentralised supply separate)	Uncoordinated integration (centralised and decentralised supply in competition)	Integrated development (centralised and decentralised supply in coordination)
Quality	Centralised	High power quality	High power quality	High power quality
	Decentralised	Power quality improvement actions are needed, power quality is impacted by seasonal fluctuations	Power quality improvement actions are needed, higher quality supply expected as area covered is larger compared to separated model	Power quality improvement actions are needed, higher quality supply expected and gets support from grid supply
Affordability	Centralised	Lower tariff which is decided by the regulatory commission	Tariff decided by the regulatory commission	Tariff decided by the regulatory commission
	Decentralised	Higher tariff which is decided by the operator and village energy committee	Tariff decided by the operator, but the investment depends on government policies	Tariff decided by the operator, but the government support is given in terms of subsidies
Legality	Centralised	Connection process is standardized, thefts are caught by dedicated vigilance department, regulatory commissions decide the rules		
	Decentralised	Connection process is decided by the operator and local committee, thefts are caught through complaints and local vigilance, the operator and local committee decide the rules		

	Positive points
	Drawbacks
	Floating points

References

1. Adusah-Poku F, Takeuchi K (2019) Determinants and welfare impacts of rural electrification in Ghana. Energy Sustain Dev 52:52–62
2. Agrawal S, Harish SP, Mahajan A, Thomas D, Urpelainen J (2020) Influence of improved supply on household electricity consumption—evidence from rural India. Energy 211:118544
3. Aklin M, Chindarkar N, Urpelainen J, Jain A, Ganesan K (2021) The hedonic treadmill: electricity access in India has increased, but so have expectations. Energy Policy 156:112391
4. Bhatia M, Angelou N (2015) Beyond connections: energy access redefined. ESMAP technical report 008/15. World Bank, Washington, DC. © World Bank. https://openknowledge.worldbank.org/handle/10986/24368. License: CC BY 3.0 IGO
5. Bridge BA, Adhikari D, Fontenla M (2016) Household-level effects of electricity on income. Energy Econ 58:222–228
6. Diallo A, Moussa RK (2020) The effects of solar home system on welfare in off-grid areas: evidence from Côte d'Ivoire. Energy 194:116835
7. Han P, Kimura F, Sandu S (2020) Household-level analysis of the impacts of electricity consumption on welfare and the environment in Cambodia: empirical evidence and policy implications. Econ Model 89:476–483
8. IEA (2020) Defining energy access: 2020 methodology. IEA. Retrieved 10 Mar 2022 from https://www.iea.org/articles/defining-energy-access-2020-methodology
9. Karanfil F, Li Y (2015) Electricity consumption and economic growth: exploring panel-specific differences. Energy Policy 82:264–277
10. Kooijman-van Dijk AL (2012) The role of energy in creating opportunities for income generation in the Indian Himalayas. Energy Policy 41:529–536
11. Mandelli S, Barbieri J, Mereu R, Colombo E (2016) Off-grid systems for rural electrification in developing countries: definitions, classification and a comprehensive literature review. Renew Sustain Energy Rev 58:1621–1646
12. Matinga MN, Annegarn HJ (2013) Paradoxical impacts of electricity on life in a rural South African village. Energy Policy 58:295–302
13. Njoh AJ, Ananga E, Ngyah-Etchutambe IB, Ricker F, Madosingh-Hector R, Rizutto V, Akiwumi FA (2022) The relationship between electricity consumption and improvement in women's welfare in Africa. Women's Stud Int Forum 90:102541
14. PTI (2018) All villages in India electrified: PM. Times of India
15. REC India (2017) Government schemes (Saubhagya). https://recindia.nic.in. Retrieved 15 Mar 2022 from https://recindia.nic.in/saubhagya
16. The World Bank (2020) Access to electricity (% of population)—India | 2020 data (worldbank.org). Retrieved 23 June 2022 from http://data.worldbank.org/indicator/EG.ELC.ACCS.ZS?locations=IN
17. Urpelainen J (2014) Grid and off-grid electrification: an integrated model with applications to India. Energy Sustain Dev 19:66–71

Optimal Allocation of Electric Vehicle Charging Station with Distribution Generation and D-STATCOM Using Grey Wolf Optimization

Udit Kumar and Shelly Vadhera

1 Introduction

EVs are an electric load to the already burdened Indian grid system. With the increase in number of electric vehicles there comes a variety of issues such as increased active power loss, generation-demand mismatch, voltage profile degradation, reduction of voltage stability margin. To address these issues, proper and optimal allocation of EVCS has to be done. Optimal allocation handles the rising electric load and manages the resources at hand with greater ease.

Optimal allocation of EVCS has been done in the past works using various algorithms minimizing the cost function. In the work [1], simultaneous optimal locating and sizing of EV and Renewable Energy System (RES) with the management of electric vehicle charging is achieved. To achieve the goal, a optimization problem with multi-purpose is created to procure objective variables for bringing a reduction in active power loss, fluctuation in voltage by reducing voltage deviation, EV battery cost, and charging and demand supply cost. The capacity and position of EVCS and RES are taken as objective variables. Once the problem is formulated, a hybrid algorithm combining to solve the optimization issue for the various situations, the Genetic Algorithm-Particle Swarm Optimization (GA-PSO) is used. The performance of the recommended methodology is examined on standard bus system (IEEE 33 RDS) to validate the capability of the hybrid algorithm for optimally locating and sizing RES and EVCS simultaneously. The result of hybrid algorithm shows that it outperforms algorithms such as Differential Evolution to achieve the desired objective. Many

U. Kumar (✉) · S. Vadhera
National Institute of Technology, Kurukshetra, Kurukshetra, Haryana, India
e-mail: udit_32014323@nitkkr.ac.in

S. Vadhera
e-mail: shelly_vadhera@nitkkr.ac.in

S. Doolla et al. (eds.), *Advances in Renewable Energy and Its Grid Integration*,
Lecture Notes in Electrical Engineering 1041,
https://doi.org/10.1007/978-981-99-2283-3_20

works such as [2] propose the hybrid algorithm implementing the Pareto dominance-based Chicken Swarm Optimization (CSO) along with Teaching Learning (TL) based algorithm to obtain pareto optimal solution inheriting the strengths of both CSO and TL. To extract the best option from a non-dominated pool of candidates, fuzzy decision making has been used. The Optimization framework desires to concurrently reduces the cost, increase grid stability, and getting access of feasible charging station easily. To compute the grid stability the composite index comprising of reliability, voltage stability, and power loss using VRP index. Multi-purpose objective function comprising single objective functions such as cost, VRP index, accessibility index is used. Grasshopper Optimization Algorithm (GOA) based fuzzy approach is also used for optimal allocation of EVs, DG, and Shunt Capacitors (SC) in DS [3]. The algorithm is executed in two stages. In the first stage, optimal allocation of DG and SCs is done using GOA based fuzzy approach to improve power factor, voltage profile, reduce active power loss. In the second stage optimal location of EVCS and number of EVs at charging station is found. GOA is found to be fast converging than PSO and GA techniques with simulations performed on 51 bus and 69 bus indicating the superiority of algorithm over the simultaneous optimization approach done conventionally. The advantage of integrated DGs and SCs is that they can effectively handle the load growth in distribution network while supplying EVCS with full capacity. DGs and SCs can maintain node voltages during steady-state battery charging. AI based approaches [4] has also been implemented for optimal allocation of EVCS and DGs. This work integrates AI based approach with hybrid particle swarm optimization along with grey wolf optimization (HGWOPSO) to find the suitable nodes for EVCS and DGs. The algorithm is tested on IEEE-33 and IEEE-69 bus system. To further validate accuracy of the algorithm the outcome of this algorithm is compared with the outcome of other approaches such as PSO and GWO optimizing individually. In comparison to GWO and PSO for the above bus system, HGWOPSO shows significant loss reduction. With fixed EVCS load incorporating current and voltage restrains optimal DG installation is carried out for loss mitigation in distribution system (DS). Reliability analysis on the distribution network is done to point out influence of DGs and EVs on its health. For different cases reliability indices are calculated. Result of the work shows that reliability indices decline when only EVCS are placed on the 33 and 69 bus system. However, an increase in the reliability indices is observed on incorporation of DGs into the grid along with EVCS. Several works [5] also measures reliability of distribution network when plug-in electric vehicles (PEV) are connected for varying penetration levels to investigate the impact on the grid. Few of the PEVs are integrated in vehicle-to-grid (V2G) mode to render aid during peak loads. Reliability of this type of network in accessed using multi-level coordinate search (MCS) along with minimal path method. The modification in this method is the arbitrary charging sites, driving distances, and initial PEV battery status generation and use of PVDG units as DG. Thus, EVCS are integrated with solar PV modules. In addition to the system reliability calculation, Expected Energy Not Charged (EENC) is presented to measure reliability of PEV's in the system. Three PEV penetration levels with and without DGs have been analyzed i.e., 35, 51, and 62%. An increased reliability of system with the use of PEVs can be observed

from this work. EENC showed great improvement with DG and PEVs. EENC is an energy index and plays a major role in deciding location for EVCS for suitable charging possibilities and preventing charging when the distribution network fails. In the event of failure of the network restoration can be performed by injecting power into the system via V2G mode.

DG may be used to provide energy closer to load centres, minimising line power losses and improving voltage profile. Renewable DGs such as PVDG and WTDG can help lessen CO2 emissions. As a consequence of DG employment, consumers turn prosumers by collaborating in energy generation in their dwellings [6]. DSTATCOM are hooked to the line to assist reactive power compensation, which leads to reduced power quality issues [7].

The GWO technique is proposed in this work for effective EVCS planning to diminish the impact of charging of EV by integration of DG. The recommended approach employs DG and D-STATCOM for improving reliability along with power loss reduction and voltage profile improvement. Load-oriented reliability indicators are used to investigate the influence on system reliability.

2 Problem Formulation

2.1 Objective Functions

$$\min(F_a(k), F_b(k), F_c(k), F_d(k)) \text{ k} \in \text{variable space} \tag{1}$$

Equation (1) is used for the optimal placement of EVCS.
Where $F_a(k)$ is the minimum value of TPL for variable space i.e. k
$F_b(k)$ is the minimum value of TQL for variable space i.e. k
$F_c(k)$ is the minimum value of voltage deviation index for variable space i.e. k
$F_d(k)$ is the maximum value of voltage stability index for variable space i.e. k

$$F_a = minTPL = \sum_{i=1}^{Nb} |I_i|^2 \cdot R_i \tag{2}$$

$$F_b = minTQL = \sum_{i=1}^{Nb} |I_i|^2 \cdot Q_i \tag{3}$$

where TPL and TQL are total active and reactive power losses
I_i: Current flowing in ith branch
R_i: Resistance of ith branch
Q_i: Reactance of ith branch.

Voltage Deviation Index (VDI)

The quality of the bus voltage is analyzed in respect of voltage deviation index. Voltage deviation index is expressed as:

$$F_c = min\left(\sum_{i=1}^{Nb}\left(V_n - V_{ref}\right)^2\right) \tag{4}$$

F_c is the minimum voltage deviation index
V_n is the node voltage
V_{ref} is the reference voltage.

Voltage Stability Index (VSI)

VSI of DS can be formulated as follows:

$$\begin{aligned} VSI_{n+1} = |V_n|^4 - 4 \cdot \left[P_{n+1}X_m - Q_{n+1}R_m\right]^2 \\ - 4 \cdot \left[P_{n+1}R_m + Q_{m+1}X_m\right] \cdot |V_n|^2 \end{aligned} \tag{5}$$

where, VSI_{n+1} depicted the VSI of $(n+1)th$ bus, P_{n+1} specifies the active power at $(n+1)th$ bus and Q_{n+1} shows the reactive power at $(n+1)th$ bus and, X_m and R_m expresses the reactance and resistance of *mth* branch joining the *nth* and $(n+1)th$ bus.

Throughout operation, voltage collapse at the node with the lowest voltage stability index. As a consequence, the objective function for maximising lowest VSI is given as:

$$F_d = min\left(\frac{1}{VSI_{n+1}}\right) \tag{6}$$

Load Orientate Reliability Indices

Indices for Reliability are also considered and the mathematical formulas of various types of load-oriented reliability such as EENS (Expected Energy Not Supplied) and AENS (Average Energy Not Supplied) are considered [4].

2.2 Constraints

Voltage Limit. Each bus voltage must lie within the range of [0.95–1.05 p.u.]

$$V_{mn} \leq V_n < V_{mx} \tag{7}$$

Line Current. Current carried within every line must not exceed the allowable line current limit.

$$I_m \leq I_m^{mx} \tag{8}$$

where, I_m represents the actual current flows in mth line.

Power Injection. The power injected both real and reactive must be within specified limits.

$$P_{dg_n}^{mn} \leq P_{dg_n} \leq P_{dg_n}^{mx} \tag{9}$$

$$Q_{dg_n}^{mn} \leq Q_{dg_n} \leq Q_{dg_n}^{mx} \tag{10}$$

Power Balance. The sum of TPL and added EVCS load must be equal to the active and reactive power injected by DG and substation (SS) combined.

$$P^{sub} + \sum_{n=1}^{N_{bus}} P^{dg}(n) = \sum_{n=1}^{N_{br}} P_{ls}^{m}(n, n+1) + \sum_{n=1}^{N_{bus}} P_{d,n} + P_{evcs}^{n} \tag{11}$$

$$Q^{sub} + \sum_{n=1}^{N_{bus}} Q^{dg}(n) + \sum_{n=1}^{N_{bus}} Q^{dstat}(n) = \sum_{n=1}^{N_{br}} Q_{ls}^{m}(n, n+1) + \sum_{n=1}^{N_{bus}} Q_{d,n} \tag{12}$$

where, P^{sub} and Q^{sub} are the active and reactive power supplied by SS subsequently, Q^{dstat} (n) is the reactive power injected by D-STATCOM at nth bus, $P_{d,n}$ and $Q_{d,n}$ are the power demand for active and reactive power at nth bus, $Q^{m}{}_{ls}$ and $P^{m}{}_{ls}$ represents the reactive and real power loss in the mth branch, Q^{dg} (n) and P^{dg} (n) are the total reactive and real power injected by DGs at nth bus, $P^{n}{}_{evcs}$ is the charging load at nth bus subsequently N_{br} and N_{bus} denotes the number of branches and buses, respectively.

Load Flow Analysis

Gauss Seidel and Newton Raphson techniques cannot be applied in case of DS (Distributed system) because of various problems arising due to the complex structure of distribution network thus the most prominently used Load flow analysis techniques in case of DS are forward backward sweep and direct load flow. In this analysis the direct load flow method is implied to find the required solutions because of its robustness [8].

2.3 Grey Wolf Optimization

In 2014, Mirjalili et al. [9], stated a population based meta-heuristic optimization approach called "Grey Wolf Optimizer" (GWO) which is influenced by hunting mechanism and social hierarchy shown by the grey wolves. Onward with this the wolves engage in aggregate hunting, which require pursuing, enclosing and eventually attacking which are also depicted in this technique.

Algorithm 1: Optimal placement of EVCS with DG and D-STATCOM
Input: Data of System, Customer information, Failure rate, Outage time, EVCS data
Output: Optimal allocation
1: DLF Load Flow
2: **while** Run GWO till $iter_{(Max)}$ reached
3: Initialize Search Agents
4: Objective Function
5: Calculate Power Loss by calling DLF
6: **if** (Power Loss defies constrains) **then**
7: Eliminate $Solut^n$
8: **else**
9: Update $posit^n$
10: **end if**
11: **if** (Obtained $Solut^n$ better than last run) **then**
12: Take new $Solut^n$
13: **else**
14: Replay GWO
15: **end if**
16: **end while**
17: **return** *Optimal allocation*

3 Results and Calculation

The implementation of the algorithm is presented in this section and then applied to IEEE 33-bus system with base values taken as 100 MVA and 12.66 kV with the total loading of 3715 kW and 2300 kVAr respectively. Every EVCS contains 30 charging outlets with each having capacity of 50 kW thus making the total capacity of unit EVCS as 1500 kW [4]. Now the total power loading becomes 1503.715 kW and 2300 kVAr respectively.

To test the algorithm several cases are defined which are as follows:

Case 1: Base Case (W/o the placement of EVCS, DG, D-STATCOM).
Case 2: Two EVCS placed at second and nineteenth node.
Case 3: Two EVCS and one DG with upf.
Case 4: Two EVCS and one DG with fixed power factor of 0.95.
Case 5: Two EVCS and one DG with optimal power factor of 0.89.
Case 6: Two EVCS and one DG with upf, one D-STATCOM.

Several indices such as VSI, VD, EENS, AENS, TPL, TQL are calculated to optimally place the EVCS for case 2 to case 6 and case 1 is the base case. In the base case the losses are 210.98 kW and 143.02 kVAr respectively with the minimum voltage and minimum VSI of 0.9038 p.u. and 0.6672 p.u. respectively.

Effect of Two EVCS with DG and D-STATCOM Integration

The power losses in case 2 are 234.20 kW and 156.54 kVAr respectively with minimum voltage being 0.9018 p.u. and minimum value of VSI being 0.6615 p.u. appearing at bus 18 and two EVCS is the optimally located at 2 and 19 bus. Subsequently in case 3 with DG valuing 3.703 MW with upf situated at bus 8 and two EVCS is the optimally located at 8 and 19 bus, the power loss is obtained as 130.32 kW and 94.85 kVAr respectively with the minimum voltage being 0.9479 p.u. and minimum value of VSI being 0.8073 p.u. appearing at bus 33. Therefore, with the addition of DG TPL, TQL reduces whereas the minimum voltage and minimum value of VSI is improved. Whereas in case 4 for DG valuing 4 MW 0.95 fixed power factor placed at 7 bus and two EVCS is the optimally located at 7 and 19 bus, the losses amount to be 78.65 kW and 65.4 kVAr, therefore TPL and TQL reduces with the addition of DG and for case 5 with DG valuing 4 MW with optimal power factor of 0.8905 placed at 26 bus and two EVCS is the optimally located at 2 and 26 bus, the losses accounted are 74.5572 kW and 58.4425 kVAr. With implement of D-STATCOM as stated in case 6 the active power loss and reactive power reduces to 80.77 kW and 57.9868 kVAr respectively, DG is placed at 10 bus, D-STATCOM is placed at 30 bus and two EVCS is the optimally located at 10 and 19 bus. DG and D-STATCOM are linked with EVCS to ensure the smooth operation of the DS, due to its positive impact on voltage profile as seen in Fig. 1. In the case 3, the min voltage of 0.9479 p.u. at bus number 33, whereas in case 6 the min voltage is improved to 0.9734 p.u. at bus 33. Thus, it can be implicated that voltage profile improvement can be seen with employment of D-STATCOM with VD (voltage deviation) being minimal in case 6 which is 0.077 p.u., it can be seen from Fig. 1. The inclusion of EVCS and DG units has an impact on both the VSI and the voltage profile. VSI for base case is 0.6672 p.u. and drops down to 0.6615 p.u. in case 2. It can be seen from Fig. 2, that optimal allocation of DG along with D-STATCOM enhances minimum VSI which is 0.8979 at 33 node. Figure 3 shows the convergence curve. Table 1 depicted all the cases with their optimal location. Optimal node for EVCS, DG and D-STATCOM placement is found by using GWO for loss reduction, from above algorithm.

Figure 3 graph show the convergence curve for different cases.

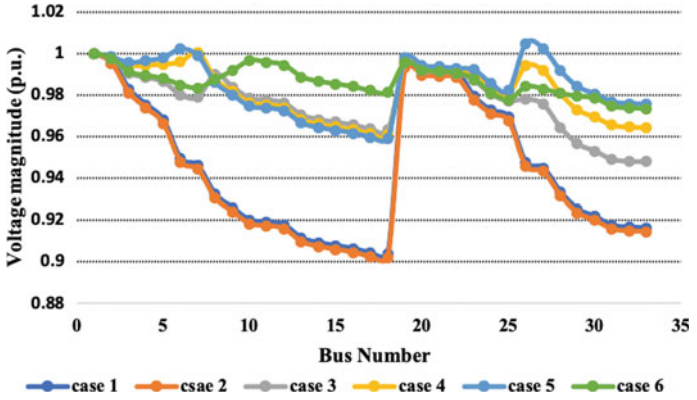

Fig. 1 Voltage profile of 33 bus system after integrating EVCS with DG and D-STATCOM units

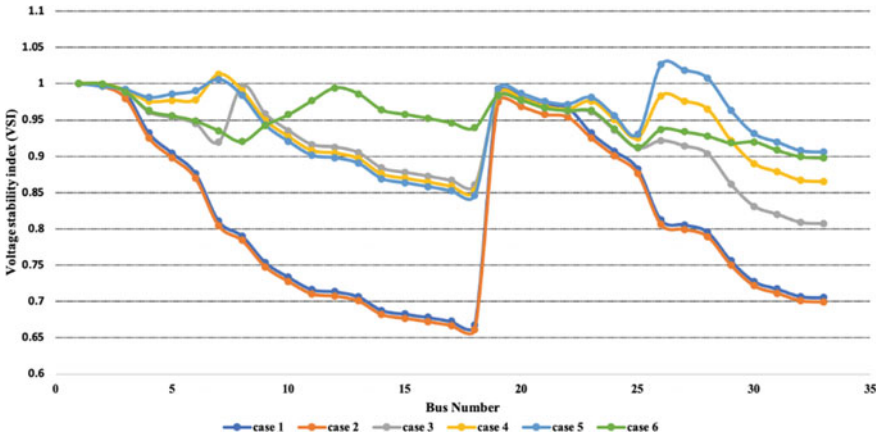

Fig. 2 VSI for 33 bus system for different cases

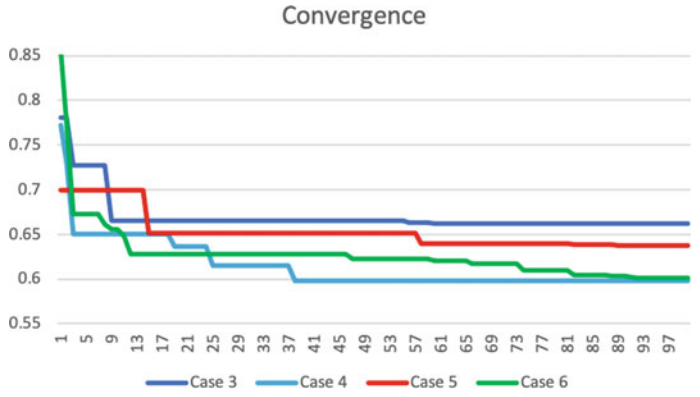

Fig. 3 Convergence curve for 33 bus system for different cases

Table 1 Values of different indices calculated for all the cases

Cases	EENS (MWh per year)	AENS (MWh per customer per year)	EVCS location	DG location		TPL (kW)	TQL (kVAr)
				Location	Size (MW)		
Case 1	1883.5	2.045	–	–	–	210.98	143.022
Case 2	2663.5	2.8656	2.19	–	–	234.20	156.54
Case 3	2063.5	2.2454	8.19	8	3.7037	130.3261	94.8523
Case 4	2063.5	2.2454	7.19	7	4	78.652	65.34
Case 5	2321.5	2.5261	2.26	26	4	74.5572	58.4425
Case 6	2171.5	2.3629	10.19	10	3.0771	80.7794	57.9868

Effect of EVCS Integration with DG and D-STATCOM on Reliability of 33 Bus Distribution Networks

On EVCS integration into the DS the power supplied is unable to meet the set load demand with inturn increases the indices associated with the energy not supplied which is not desirable form DS's perspective. On installation of EVCS a deterioration in the load-oriented reliability indices is observed with the AENS base value being 2.045–2.8656 MWh/customer/year after the EVCS integration. Whereas DG integration enhances these indices due to its effective voltage management thus improving power transfer capability while reducing power loss by governing power injected into the system which is realized from Table 1.

4 Conclusion

In this paper the authors have presented the impact of EVCS on the standard bus system with the addition of DG and DSTATCOM. The mechanism of EV charging requires additional grid power, leading to increased power losses. Consequently, DG with different power factor and D-STATCOM should be used to recompense the increased generated power losses due to EVCS. Optimal node for EVCS, DG and D-STATCOM placement is found by using GWO for loss reduction. The investigation shows that unit DG and D-STATCOM significantly increase the system's performance by voltage profile enhancement and loss reduction. Additionally, analysis on reliability is performed to assess the combined effect of loading due to EVCS and DG on the power quality of the DS with dependability indicators being studied for various circumstances. The installation of EVCS significantly reduces the network's reliability however on inclusion of DG increases the reliability indices.

References

1. Mozafar MR, Moradi MH, Amini MH (2017) A simultaneous approach for optimal allocation of renewable energy sources and electric vehicle charging stations in smart grids based on improved GA-PSO algorithm. Sustain Cities Soc 32:627–637. https://doi.org/10.1016/j.scs.2017.05.007
2. Deb S, Tammi K, Gao XZ et al (2020) A hybrid multi-objective chicken swarm optimization and teaching learning based algorithm for charging station placement problem. IEEE Access 8:92573–92590. https://doi.org/10.1109/ACCESS.2020.2994298
3. Gampa SR, Jasthi K, Goli P et al (2020) Grasshopper optimization algorithm based two stage fuzzy multiobjective approach for optimum sizing and placement of distributed generations, shunt capacitors and electric vehicle charging stations. J Energy Storage 27. https://doi.org/10.1016/j.est.2019.101117
4. Bilal M, Rizwan M, Alsaidan I, Almasoudi FM (2021) AI-based approach for optimal placement of EVCS and DG with reliability analysis. IEEE Access 9:154204–154224. https://doi.org/10.1109/ACCESS.2021.3125135
5. Galiveeti HR, Goswami AK, Dev Choudhury NB (2018) Impact of plug-in electric vehicles and distributed generation on reliability of distribution systems. Eng Sci Technol Int J 21:50–59. https://doi.org/10.1016/j.jestch.2018.01.005
6. Zeb MZ, Imran K, Khattak A et al (2020) Optimal placement of electric vehicle charging stations in the active distribution network. IEEE Access 8:68124–68134. https://doi.org/10.1109/ACCESS.2020.2984127
7. Gupta G, Fritz W, Kahn MTE (2017) A comprehensive review of DSTATCOM: control and compensation strategies
8. Teng JH (2003) A direct approach for distribution system load flow solutions. IEEE Trans Power Delivery 18:882–887. https://doi.org/10.1109/TPWRD.2003.813818
9. Mirjalili S, Mirjalili SM, Lewis A (2014) Grey wolf optimizer. Adv Eng Softw 69:46–61. https://doi.org/10.1016/j.advengsoft.2013.12.007